ADIPOSE TISSUE AND ITS ROLE IN MODULATING THE MAMMARY TUMOR MICROENVIRONMENT

A Dissertation

Presented to the Faculty of the Graduate School

of Cornell University

In Partial Fulfillment of the Requirements for the Degree of

Doctor of Philosophy

by

Bo Ri Seo

August 2014

ADIPOSE TISSUE AND ITS ROLE IN MODULATING THE MAMMARY TUMOR MICROENVIRONMENT

Bo Ri Seo, Ph. D.

Cornell University 2014

Targeting cancer cells has been the primary focus of most cancer therapies, and only recently has the interaction of cancer cells with host stroma been recognized as a driving force for cancer evolution. In the presence of tumor-derived physicochemical cues, the host stroma fails to fulfill its primary role – the maintenance of tissue or organ homeostasis – and in fact aids in shaping a pro-tumorigenic microenvironment, ultimately promoting tumor progression. This interaction of cancer cells with the host stroma often complicates conventional cancer therapy and ultimately leads to unfavorable outcomes.

The mammary stroma is largely composed of adipose tissue, and upon the onset of mammary tumors, the residing stromal vascular cells and adipocytes possibly partake in extracellular matrix (ECM) remodeling and blood vessel recruitment. Both tumor-associated ECM remodeling and neovascularization are typically mediated by myofibroblasts, which are known to be recruited or differentiated from other stromal cells. However, whether tumor-derived biochemical and mechanical cues can induce the conversion of adipose-derived stem cells (ASCs) or adipocytes into myofibroblastic cells is yet unknown.

Furthermore, obesity has been highlighted as a risk factor for breast cancer possibly due to its role in modulating the mammary microenvironment. Nevertheless, whether obesity influences the phenotype of host cells in the mammary stroma in a manner similar to tumors, thereby advancing tumorigenesis, has yet to be determined. The goal of this dissertation is to find answers to these aforementioned unanswered questions by leveraging *in vivo* and *in vitro* engineering techniques.

The results presented here demonstrate that implanted or host ASCs and adipocytes indeed possess pro-tumorigenic potential to stimulate breast tumor malignancy in part due to their ability to convert into myofibroblastic lineages upon tumor or obesity-associated microenvironmental cues. The

findings of this work emphasize the importance of contextual cues and their roles in inducing the participation of the host stroma in regulating mammary tumor progression. Finally, the conclusions of this work potentially provide new insight for the development of therapeutic approaches for cancer and tissue regeneration.

BIOGRAPHICAL SKETCH

Bo Ri Seo was born to Mu Kyoung Kim and Won Kyo Seo in Seoul, South Korea on May 1st, 1983 and grew up in Cheongdam-dong Gangnam-gu Seoul. She attended Daewon Foreign Language High School, and completed her secondary education at Cheongdam High School in January 2002. She then enrolled as an undergraduate student at Korea University in the Department of Life Science and Biotechnology. In the summer of 2004, she was chosen to study for one year at the University of California, Davis as part of a foreign exchange program. Upon her return, she graduated with a Bachelor of Science degree in Food Science and Technology from Korea University in February 2007. Before starting her Ph.D. program, she worked at the toxicological research division in the National Institute of Food and Drug Safety Evaluation and at the Korea University Medical College as research assistant. In September 2007, she moved to Ithaca to initially pursue a Ph.D. program in Food Science but decided after a year rotation to join Prof. Claudia Fischbach's lab in the Department of Biomedical Engineering. Her doctoral research focuses on investigating the role of the mammary microenvironment in modulating breast tumorigenesis and has resulted in a number of awards including the Gordon Research Conference 2013 Best Poster Award and a Mogam Fellowship. She also served as president of the Korean Graduate Student Association at Cornell from 2009 to 2010 for which her contributions and leadership were recognized by the receipt of the Graduate Student Leadership Award. After completing her doctoral training, she will continue to pursue her postdoctoral research in translational medical science.

To my beloved parents who have always supported and believed in me

ACKNOWLEDGEMENTS

First and foremost, I would like to sincerely thank my research advisor, Prof. Claudia Fischbach, for her support and patience during my pursuit of a doctoral degree. Personally, the initial adjustment to life in the U.S. and switching my Ph.D. program from Food Science to the Biomedical Engineering were quite challenging. These challenges also probably meant that it must have required much more effort and dedication for her to mentor me. However, I was able to overcome the initial hurdles thanks to her support and encouragement, and my doctoral work in BME at Cornell would not have been able to reach its current level without her guidance. I am looking forward to continuing our mentor-mentee relationship in the future.

I would also like to thank the members of my graduate committee – Prof. Alexander Y. Nikitin and Prof. Delphine Gourdon for their advice during my doctoral tenure. It has certainly been a joy to absorb their simultaneously deep and far-reaching breadth of knowledge. In particular, the constructive feedback from Prof. Nikitin helped me to focus my research efforts in the right direction. I am also extremely thankful for Prof. Gourdon and her willingness to answer any questions related to biomechanics with simple explanations that made everything easy to understand.

I would also like to acknowledge people in the Fischbach lab who made significant contributions to advancing my doctoral work. First of all, I would like to thank Emily Chandler for her training when I joined the lab. The complimentary work that she completed through her doctoral project helped me carry out this project. In addition, I would like to truly thank Jacqueline Gonzalez for her willingness and devotion to our many projects. Also, her wit and coolness truly made my Ph.D. life enjoyable and I am grateful that we developed such a friendship during my time. I am also indebted to Maureen Lynch and David Infanger for their mentorship. Maureen always provided me with wise advice and the way she was able to successfully switch fields from mechanical to biomedical engineering has always served as an

inspiration for me. David seemingly enjoyed providing me frank advice, most of which was unsolicited, but this advice helped me become an independent Ph.D. student. Also, I truly appreciate his English lessons, which I found quite useful in managing people who bothered me. I also would like to thank Young Hye Song for her great help to complete my last doctoral project. Her energetic and positive personality made our work time more joyful. Late night frozen yogurt, apple cider, and donuts that we shared together over the years will remain in our bodies as a rich souvenir for our friendship. I would like to acknowledge Peter DelNero for his tremendous help while we were writing a review paper together. I would like to thank Youjin Cho and her mother who have been caring for me. I am also thankful for the support of Fischbach Lab members: Daniel J. Brook, Nora Springer, Siyoung Choi, and Frank He.

I also would like to thank our collaborators, who supported me in completing my doctoral projects. In particular, I would like to acknowledge the Gourdon group members, Karin Wang and Roberto Andresen Eguiluz, both of whom were of great intellectual help to me and more importantly supported me as friends. I would also like to thank Prof. Rebecca M. Williams, Prof. Matthew J. Paszek, Le Chang in the Nikitin lab, and Haibo Sha in the Qi lab, Sunish Mohanan at Cornell as well as Dr. Andrew J. Dannenberg, Priya Bhardwaj in his lab and Dr. Linda Vahdat at the Weill Cornell Medical College. Also, I would like to thank Nakwon Choi for supporting me during my early years and technical assistance. In addition, I would like to acknowledge funding source, which has been supporting my doctoral research and my stipend: NYSTEM**,** NIH (R21CA161532, RC1 CA146065, 1U54 CA143876, 1R01CA185293-01) Mogam Biotechnology and Foundation Scholarship. Also, I would like to acknowledge people who helped to proofread my dissertation: Maureen Lynch, Nora Springer, Karin Wang, Young Hye Song, Peter DelNero, Eugene Hwang, Prof. Delphine Gourdon and Prof. Claudia Fischbach.

Moreover, I am thankful for the support and friendship of friends from the Cornell Catholic community, especially Fr. Daniel McMullin, Fr. Kim Yun Joon, my godmother Prof. HaeEun Helen

Chun. I would like to acknowledge the board members of the Korean Graduate Student Association at Cornell, who helped me while I was serving as president of the organization: : Prof. Yong Lak Joo, Sung A Kim, Nakwon Choi, Seung Keun Youn, Eugene Hwang, Jaesung Lee, Jungyoon Mo, Yumi Seo, Youngho Chung, Jai Kyoung Jung, and Paul Dongwoo Kim.

There are others who do not fit any of these categories but who I cannot thank enough. I am grateful for my family who provides me unconditional love and great support just with their presence. Also, I would like to thank Eugene Hwang, my best friend and soul mate for always being by my side and sharing bitter and joyful moments together. I am especially thankful for the fact that he likes cooking. Last but not least, I thank God for this life and all of the opportunities he has given me, especially this journey of the past years which have taught me an important life lesson:

"You are the sky. Everything else, it is just weather."

-Pema Chödrön

TABLE OF CONTENTS

LIST OF FIGURES

Chapter 1

Chapter 2

Chapter 3

Chapter 4

Chapter 5

Chapter 6

LIST OF TABLES

Chapter 4

LIST OF ABBREVIATION

2D	Two-dimensional
3D	Three-dimensional
ANOVA	Analysis of variance
α-MEM	Minimum essential medium (α-modification)
α-SMA	Alpha-Smooth muscle actin
ASC	Adipose-derived stem cells
ASVC	Adipose stromal vascular cell
BCA	Bicinchoninic acid
bFGF	Basic fibroblast growth factor
BMP	Bone morphogenetic protein
BrdU	5-Bromo-2´-Deoxyuridine
BRCA	Breast cancer susceptibility protein
BSA	Bovine serum albumin
CFA	Cancer-activated fibroblasts
CFM	Confocal reflectance microscopy
DAB	3,3'-diaminobenzidine
DAPI	4',6-diamidino-2-phenylindole
DIO	Diet-induced obesity
DMEM	Dulbecco's modified Minimum essential medium
DMTA	Dynamic mechanical thermal analysis
ECM	Extracellular matrix
EGF	Epidermal growth factor
ELISA	The enzyme-linked immunosorbent assay
ER	Estrogen receptor
ERK	Extracellular signal regulated kinases
FBS	Fetal bovine serum
Fn	Fibronectin
FRET	Förster resonance energy transfer
GAGs	Glycosaminoglycans
GPDH	Glycerol-3-phosphate dehydrogenase

HER2	Human epidermal growth factor receptor 2
HUVECs	Human umbilical vein endothelial cellS
HFD	High fat diet
IL-6, IL-8	Interleukin-6, -8
KRBH	Krebs-Ringer-HEPES
LF	Low fat diet
MAPK	Mitogen-activated protein kinases
MMPs	Matrix metalloproteinases
NADH	Nicotinamide adenine dinucleotide
ob/ob	Leptin deficient mouse
OVX	Ovariectomized
PBS	Phosphate buffered saline
PDMS	Polydimethylsiloxane
pFAK	Phosphorylated focal adhesion kinase
PPAR-γ	Peroxisome proliferating-activated receptor-gamma
RGD	Arg-Gly-Asp amino acid sequence
ROCK	Rho-associated protein kinase
SEM	Scanning electron microscope
SFA	Surface force apparatus
SHG	Second harmonic generation
TCM	Tumor-conditioned media
TFM	Traction force microscopy
TGF-β	Transforming growth factor-β
TNF-α	Tumor necrosis factor-α
VEGF	Vascular endothelial growth factor

CHAPTER 1

INTRODUCTION

1.1. Cancer

Cancer is one of the most life-threatening diseases, causing an estimated 7.5 million deaths and nearly $900 billion economic losses worldwide in 2008[1,2]. These socioeconomic impacts highlight the urgency of cancer research with the ultimate goal to aid in developing better therapeutic approaches to this disease. Cancer is a malignant mass of neoplastic cells, arising from a sequential process of transformation, selection, and uncontrollable expansion of a single or few cells[3]. A profound understanding of several oncogenes (i.e. *src* and *myc)*, tumor-suppressing genes (i.e.*TP53)*, and pro-tumorigenic molecules have contributed to advancing therapeutic approaches as well as improving clinical outcomes[4,5]. However, such therapeutic methods are effective only for limited types of cancer or primary cancer patients[6,7]. This is partially because i) cancer is an organ-, stage-, and patient-specific disease and ii) it often becomes resistant against any given therapies over time through its own surveillance system but also through an interaction with host stromal cellular and extracellular components[8,9].

In the healthy condition, host stromal cells maintain a fine balance in their microenvironment which constrains outgrowth of abnormal cancerous cells[10]. However, during the course of tumorigenesis host cells lose their phenotypic integrity upon prolonged exposure to tumor-derived cues and in turn contribute to constructing an increasingly pro-tumorigenic microenvironment that favors tumor progression, invasion, and metastasis[10]. The tumor microenvironment has tissue-specific features in accordance with the architecture, cellular, and extracellular composition of each tissue, and it also evolve during the course of tumor progression[11,12]. Therefore, understanding the dynamics of cancer cell and host stroma interaction in a specific cancer type will aid in developing better therapeutic approaches overall**.**

1.2. Breast cancer

Breast cancer is one of the leading threats to women's health worldwide[13]. The transformation of normal mammary epithelial cells (and/or myoepithelial cells) can be initiated by various risk factors including genetic mutation (*BRCA1*, *BRCA2* and *TP53*, etc.), menopausal status, aging, obesity, mammographic density, health complications, and lifestyle habits[13]. The aforementioned risk factors are quite important as they play critical roles in shaping a pro-tumorigenic microenvironment, which ultimately regulates tumor malignancy. In addition, breast cancer has various subtypes and each subtype is classified by its unique molecular and histologic patterns, which ultimately influence the tumor microenvironment. Since these unique patterns have a strong association with the etiology as well as clinical outcomes of cancer, accurate classification of breast cancer is prognostically and clinically important for choosing appropriate treatment strategies[14].

For molecular classification, estrogen receptor (ER), progesterone (PR), and epidermal growth factor-2 (HER2/neu) are key markers to delineate the 5 subtypes of breast cancers: Basal-like/triple negative (ER^-, PR^-, $HER2^-$), luminal A (ER^+, PR^+, $HER2^-$) luminal B (ER^+, PR^+, $HER2^+$), HER2-enriched ($HER2^+$, $PR^{+/-}$, $ER^{+/-}$), and normal breast-like breast cancer [15,16]. In the United States, luminal A (45%) occurs most prevalently but is relatively curable. In contrast, basal-like breast cancer patients (5 to 15%) are rare yet they exhibit the poorest clinical outcomes and survival rate[15]. Subtypes classified by the receptor status are treated through their respective receptor inhibitors. For example, Trastuzumab and Tamoxifen have been used for $HER2^+$ and for ER^+, respectively[17]. However, receptor-based treatment is not effective for all breast cancer subtypes. For example, triple negative breast cancer does not respond to receptor inhibitors or endocrine therapy[18]. Also, although the receptor-based treatments have been shown to positively affect their respective cancer types, what is often unaccounted for is the dynamic interaction

between cancer and host stroma and its resulting tumor microenvironment. This interaction complicates therapy by providing a niche where cancer cells can escape from the given cancer drugs[8].

In addition, histopathological analysis has also been used clinically to diagnose tumor stage and grade via characterization of morphological changes of cellular components as well as overall tumor stroma structure[16]. For example, breast tumor stroma progressively changes from in-situ, invasive, to metastatic exhibiting distinct features in each stage, so analysis by a trained pathologist is useful for a prompt diagnosis of tumor stage. However, the specific molecular mechanism underlying the development of unique histopathological pattern in each breast cancer subtype is not fully understood. Due to the lack of understanding, still there is a gap between diagnostic results from histopathological analysis and their corresponding treatment. In addition, as briefly stated, risk factors play pivotal roles in forming unique tumor microenvironment, so a better understanding of mammary tumor stroma dynamics in conjunction with breast cancer risk factors and the resulting impacts on tumor malignancy and recurrence will ultimately help to develop better diagnostic tools as well as therapeutic methods.

1.3. The tumor microenvironment: An emerging hallmark of cancer

Since Paget's "seed and soil" hypothesis, a growing number of studies supporting his seminal proposal have emphasized the significance of the tumor microenvironment[19,20]. The dynamic tumor microenvironment is modulated by key processes, which have been defined as hallmarks of cancer,: genomic mutation and instability, unlimited replicative capability, disrupted control of mitogenesis, cell death resistance, induced angiogenesis (blood vessel branching), activated invasion and metastasis, pro-tumoral inflammation, and anabolic metabolism[21]. Each of aforementioned processes occurs while affecting the other processes, and these interwoven processes require the collaboration of cancer cells with host stromal cells. For example, unlimited replication of cancerous epithelial cells leads to formation

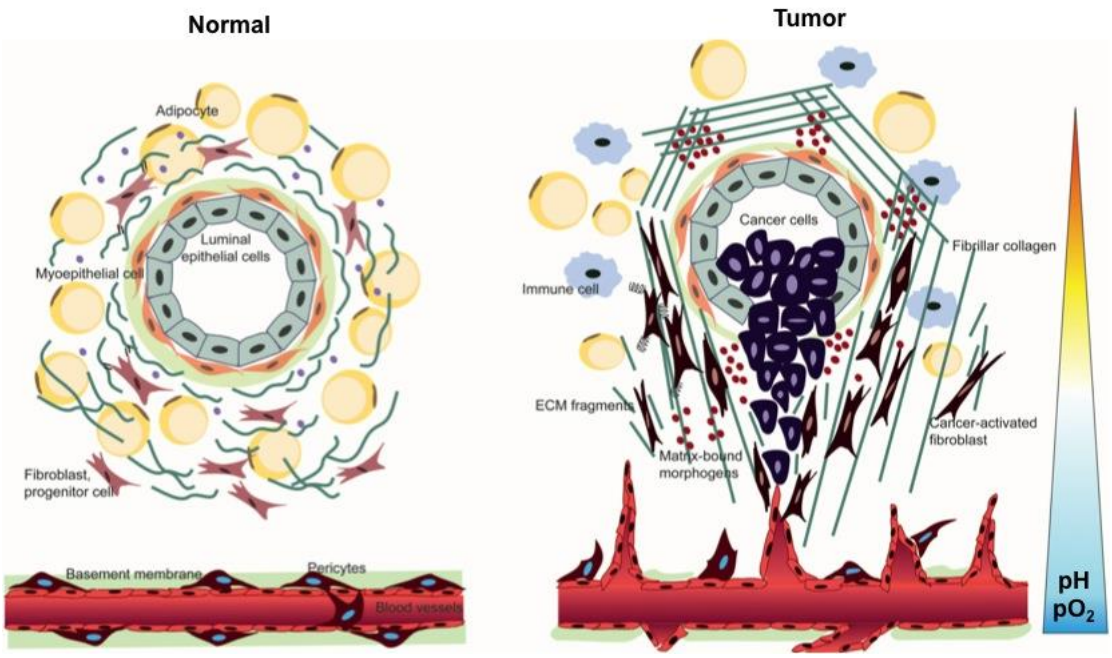

Fig. 1.1. Normal and tumor mammary microenvironment

of a tumor mass. The mass creates a hypoxic core where blood vessels are not able to reach out and stimulates chronic inflammation, which in turn recruits inflammatory cells into tumor stroma. The resulting inflammatory cell-mediated factors activate surrounding stromal cells such as fibroblast or progenitor cells to partake in fibrotic reaction, a part of innate wound healing process. The fibrotic reaction consequently densifies and then stiffens tumor stroma, which explains why tumors typically appear as rigid lumps, which are easily palpable. Thus, tumor stiffness has been recognized as a hallmark of cancer and often used as diagnostic marker. However, tumor stiffness is not just a passive outcome of tumorigenesis, but it, in turn, actively promotes tumor progression by stimulating cancer cell growth as well as promoting some of the aforementioned key processes such as angiogenesis[22-25].

Tumor desmoplasia

(Published in *Adv Drug Deliv Rev* (2014))[9]

As described briefly, one of the key features of tumor microenvironment is the dynamics of tumor stroma. As tumors progress from a benign to malignant stage, tumor stroma structure changes facilitate tumor growth, invasion and metastasis. The change is mediated by tumor-associated fibrosis, called as tumor desmolasia. Tumor desmoplasia is initiated by the recruitment of cancer-associated fibroblasts (CAFs). The recruited CAFs, which include myofibroblasts, deposit abundant amounts of fibrillar ECM molecules including collagen I and fibronectin[26]. These ECM compositional changes entail structural and mechanical alterations of the ECM[27-29]. For example, CAFs mediate the partial unfolding of fibronectin, which increases both the stiffness of individual fibronectin fibers[30,31] and their ability to bind other ECM molecules such as glycosaminoglycans (GAGs) and collagen[32]. Along with elevated collagen crosslinking (e.g., by lysyl oxidase, non-enzymatic glycation, or transglutamination[33,34]) and GAG concentration[28], these pronounced changes in ECM density and intermolecular interactions globally enhance tumor stiffness with direct consequences for tumor progression. Despite this overall increase in matrix deposition and cross-linking, tumor cells simultaneously mediate the degradation of the ECM, in part by secreting enzymes such as matrix metalloproteinases (MMPs). In addition to generating tumorigenic ECM fragments[35], elevated MMP activity affects the local (micro-scale) physical properties of the tumor ECM. For example, MMPs can govern degradation and reorganization of fibrillar collagen, while enhancing interactions with other ECM components through exposure of cryptic binding sites[36-38]. Nevertheless, it has to be kept in mind that non-proteolytic functions of MMPs may be similarly important. For example, MMP-9 has been associated with smooth muscle cell adhesion, migration, and cell-mediated collagen contraction, independent of its proteolytic function[38,39]. The diverse roles of MMPs in tumorigenesis have previously been reviewed by Egeblad[40] and Page-McCaw[41]. Such alterations of ECM composition, structure, and mechanics stimulate malignancy and drug resistance by inducing

manifold changes in cell signaling[42-45], which governs cell fate decisions, tumor angiogenesis, progression, and drug resistance (e.g., Rho/Rock, ERK/MAPK, and PI3K) [46-49]

Tumor angiogenesis

Angiogenesis is a multi-step process of new blood vessel formation from existing endothelial cells (ECs): EC activation, ECM remodeling, EC migration and branching and neo-vessel stabilization[50]. Angiogenesis requires collaborative efforts of surrounding stromal cells with ECs acting upon the pro- and anti-angiogenic signaling, which is typically well-balanced[50]. However, any induced imbalance between pro- and anti-angiogenic signals modulates the interaction between ECs, their neighboring cells, and ECM, consequently slanting the vasculature homeostasis toward avascularity or dysfunctional hypervascularity[51,52].

During tumorigenesis, tumor growth rate often surpasses the rate of regular vascularization, which remains quiescent during health[51]. Since blood vessels function as a path to deliver oxygen and nutrients as well as take away metabolic waste, the lack of blood vessels relative to tumor mass size ultimately results in a hypoxic (<1% O_2) and acidic (pH ~6.6-6.8) microenvironment, which in turn triggers angiogenesis by stimulating pro-angiogenic signaling [53-59]. In particular, hypoxia activates the transcription factor hypoxia inducible factor 1 (HIF-1), which is positively linked to up- regulation of pro-angiogenic factors such as vascular endothelial growth factor (VEGF), basic fibroblast growth factor (bFGF), Interleukin 8 (IL-8). In addition, biochemical and mechanical cues derived from ECM also modulate tumor angiogenesis through direct and indirect pathways, some of which include modulation of pro-angiogenic signaling, as described next.

Excessive matrix remodeling via desmoplasia generates stiff and denser stroma, which also ultimately stimulates angiogenesis. ECM-derived biomechanical cues stimulate proliferation, migration

and blood vessel branching of ECs as well as pro-angiogenic signaling of neighboring stromal cells. In addition, a dense matrix reduces the rate of diffusion of small molecules along the dysregulated transport during tumorigenesis, which ultimately creates uneven distribution of angiogenic molecules, thereby forming irregular blood vessels. Moreover, matrix degradation via matrix metalloproteinases (MMPs) is required to facilitate EC branching and blood vessel morphogenesis. For example, MT1-MMP is known to regulate precise matrix degradation to facilitate vessel sprouting from endothelial tip cells[60]. Likewise, seemingly-typical biochemical and mechanical cues derived from cancer cells, ECs, surrounding stromal cells, soluble factors, and ECM collectively promote tumor angiogenesis, yet these cues lead to blood vessels that are structurally and functionally different from normal ones, which in turn, hinder effective cancer therapy. Therefore, investigating how tumor angiogenesis is regulated in conjunction with tumor desmoplasia is necessary for improving therapeutic delivery.

Cancer-associated fibroblasts, myofibroblasts

As briefly described, tumor stiffening is mediated by CAF. CAF shares similar features with myofibroblasts, and thus the two terms have been used interchangeably. As a primary cellular mediator of wound healing, myofibroblasts are primarily involved in ECM deposition and facilitating new blood vessels formation for tissue repair. Thus, myofibroblasts deposit abundant matrices comprising thicker and linearized collagen type I and unfolded fibronectin, and secreted multiple pro-angiogenic morphogens such as VEGF, bFGF and IL-8[61]. Their pro-fibrotic and pro-angiogenic potentials also have been associated with disease progression such as fibrotic disease and cancer.

Myofibroblasts are recognized by their distinct morphology and α-SMA stress fibers, which trigger contractility[32]. The origin of myofibroblasts is controversial although various cell types including fibroblasts, both native or recruited bone-marrow mesenchymal stem cells, and endothelial cells exhibit

myofibroblastic potential upon the fibrosis-triggering chemical (TGF-β, and IL-8) and physical stimuli (substrate stiffness and shear stress)[32]. However, it has yet to be determined what the main cellular source of myofibroblasts is in mammary tissue during breast tumorigenesis.

1.4. Obesity and breast cancer

Obesity is a pathological condition resulting from unbalanced calorie uptake and energy expenditure[62]. The incidence of obesity in both adults and children has been progressively increasing over the past two decades worldwide[62,63]. This public health concern comes from the higher morbidity of obese patients with multiple diseases such as cardiovascular diseases, type 2 diabetes mellitus and several types of cancer including breast cancer[64]. In addition, childhood obesity increases the predisposition to develop these aforementioned diseases during adulthood[65], which may further expand the population affected by obesity-associated health problems.

Specifically, obesity has been link to a higher incidence of breast cancer, particularly in postmenopausal women[66]. This connection has been thought primarily due to the obesity-mediated increase in aromatase activity and thus, enhanced estrogen production[66]. However, recent studies showed that obesity has a strong correlation with the incidence of basal-like breast cancer (triple-negative) in pre-menopausal women, and triple-negative breast cancer typically exhibits higher histopathological grades while not responding to hormone-based therapies suggesting that the connection between obesity and breast cancer may result from more than dysregulated endocrine functions[67,68]. Thus, a better understanding of obesity-mediated features will aid in interrogating the mechanism underlying the link.

Obesity induces pronounced adipose tissue expansion upon the extra energy uptake, and this adipose tissue expansion results from hypertrophy as well as hyperplasia of adipocytes[62,69]. The abnormally expanded adipocytes also lose their functional integrity, which consequently dysregulates

leptin signaling, fatty acid synthesis, as well as insulin resistance, which are also known to modulate cancer cell growth as well as metabolism[64]. In addition, the abnormal growth of adipocytes consequently stimulates the infiltration of inflammatory cells, leading to chronic inflammation[64]. The infiltrating macrophages together with dysregulated adipocytes produce pro- and anti-inflammatory cytokines such as IL-6, IL-8, tumor necrosis factor-α (TNF-α), and TGF-β, all of which also are known to promote tumor growth, invasion and metastasis.[62,64,70] In addition, aforementioned inflammatory cytokines also induce interstitial fibrosis which might be similar to tumor desmoplasia[71]. Fibrosis results from a chronic wound healing process where myofibroblasts are recruited and deposit abundant ECM deposition, thereby stiffening tissue as seen during tumor desmoplasia[71,72]. Despite the similarity between obesity-associated fibrosis and tumor desmoplasia, whether obesity-associated fibrosis is functionally linked to tumor progression has yet to be determined. Therefore, simple extrapolation of fat mass to the predisposition of obesity-associated cancer might not be appropriate since not only adipose tissue expansion but also its resulting cascades such as metabolic dysfunction, inflammation, and fibrosis potentially regulate cancer development and progression.

1.5. Adipose tissue and its cellular source

Adipose tissue

Breast tissue primarily consists of compliant adipose tissue containing adipocytes, and adipose stromal cells (ASCs) including progenitor cells, fibroblasts, endothelial cells, pericytes, and immune cells (macrophages and mast cells). Adipose tissue (AT), specifically white adipose tissue, has been mainly considered an energy storage depot of our body. However, AT is also a secretory depot to produce a broad spectrum of bioactive morphogens such as adipokines (leptin, and adiponectin), inflammatory cytokines (TNF-α, TGF-β, IL-6, and IL-8) and chemokines (monocyte chemotactic protein-1)[73].

AT is broadly divided into two major depots, skin (subcutaneous) and abdominal-/organ-associated fat (visceral). This classification is seemingly simple yet AT develops very unique characteristics depending on its origin. In addition, their distinct features ultimately influence the development of specific diseases during obesity as well as its associated diseases[74]. For example, visceral AT exhibits metabolically active features with a higher level of lipolysis as well as lipid synthesis than subcutaneous fat, so visceral AT is positively correlated with type 2 diabetes and cardiovascular diseases while subcutaneous fat is inversely related to these metabolic diseases[75,76]. However, since visceral AT is directly connected with the liver through the portal venous system, all metabolites and soluble factors such as free fatty acids, hormones, and cytokines from visceral fat tissue have systemic effects, which may eventually influences subcutaneous fat[73]. In addition, architecture and cellular and extracellular components of fat tissue can be also organ-specific[77]. For example, mammary or breast AT exhibits unique architecture, cellular composition and molecular signaling profiles although anatomically it seems close enough to subcutaneous fat. In addition, its architecture changes signaling throughout a women's lifetime (i.e. pregnancy and menopausal status), which also might influence the incidence of breast cancer[11,78,79]. Therefore, precise classification of the features of AT from different locations is prerequisite when determining clinical relevance.

Mammary AT and its ECM remodeling

Mammary AT embraces the functional components of the breast, mammary gland epithelium[79]. In healthy individuals, mammary gland epithelium is highly organized by cellular bilayers and complex stroma. Mammary gland morphogenesis results from a well-programmed process directed by various stimuli including ECM-derived physicochemical cues, which provide an instructive guide to epithelial cells and their neighboring stromal cells[78]. During mammary gland morphogenesis, TGF-β mediated

ECM deposits at the tip of the gland endbuds and this ECM remodeling ultimately facilitates epithelial cells to grow and sprout for branching[80,81]. In addition, during involution, the mammary AT is completely restructured by stimulating epithelial cell apoptosis but protecting the stem cell niche for recovery[79].

Such deconstruction and restoration of mammary AT stroma are well coordinated with mammary gland functions. Therefore, perturbed mammary structure might facilitate tumorigenesis. For example, changes in mammary stroma structure and its molecular signaling during pregnancy have been also correlated with pregnancy-associated breast cancer[82]. Likewise, during obesity mammary fat may also go through fat expansion, inflammation as well as fibrosis, which modulate mammary microenvironment. However, it remains unclear whether obesity modulates the mammary microstructure. If this is the case, then the cellular mediators of this change are not well understood. Therefore, I will discuss possible cellular candidates that can contribute to ECM remodeling in (mammary) AT in the following section.

Adipocytes and adipose-derived stem cells

AT contains two major cellular groups, adipocytes and adipose stromal vascular cells (ASVCs), which includes progenitor cells, (myo-) epithelial cells, fibroblasts, endothelial cells and immune cells (macrophages and mast cells). Floating adipocytes and settling adipose-derived stem cells (ASCs) can be easily separated by simple centrifugation[83].

Adipocytes are mature fat-laden cells differentiated from pre-adipocytes or stem cells under the regulation of transcription factors such as CCAAT/enhancer-binding protein (C/EBP) gene family and peroxisome proliferator-activated receptor-γ (PPAR-γ)[84]. Adipocytes were believed to be terminally differentiated and rarely proliferative. However, recent studies indicate that not only can adipocytes change their functions, but also commit themselves to different lineages in response to microenvironmental cues[85]. This finding opens up the potential of adipocytes to contribute to the progenitor cell population as well as

myofibroblastic cell population which contribute to matrix remodeling and furthermore fibrosis in mammary AT during obesity or tumorigenesis.

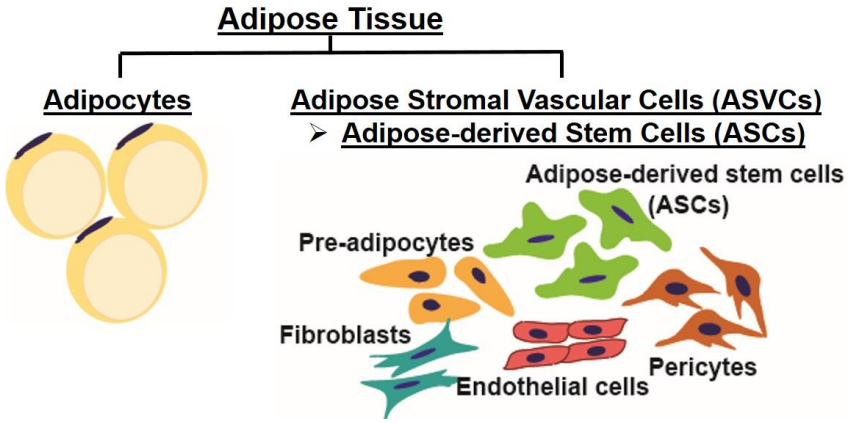

Fig. 1.2. Cellular components in adipose tissue

In addition, ASVCs contained ASCs, which are multi-potent adult stem cells isolated by various markers including integrin family members (i.e. CD9, ALCAM/CD16), CD44, CD90/Th1 and ICAM-1/CD54[83]. In healthy condition, the number of ASCs is maintained constant and if necessary, ASCs are differentiated to replenish other types of cells to maintain tissue homeostasis[83]. However, an abnormally larger population of ASCs in response to the microenvironmental cues of a host tissue might perturb tissue homeostasis as recent clinical reports showed controversial outcomes for implanted adipose tissue or ASC-based therapies[86]. Similarly, during obesity ASVC population including ASCs is enlarged either by their enhanced proliferation or dedifferentiation of adipocytes to progenitor-like cells[64]. However, whether obesity-associated changes of the microenvironment modulate the composition of ASVC remains unclear. Therefore, understanding pathological potentials of ASCs in diseases will be beneficial to developing adequate cancer therapy as well as tissue engineering approaches.

1.6. Mechanotransduction and extracellular matrix components

Mechanotransduction

Tensional homeostasis plays a critical role in maintaining organ, tissue and cell integrity[87]. Mechanotransduction, or cascade of transmitting outside-in and inside-out cues is mediated by the reciprocal interactions of 1) external-to-internal force, and 2) force sensory-to-responsive machineries. External forces such as shear, tensile or compressive stresses modulate contractility via integrin-mediated adhesion, actomyosin polymerization (source of internal force), and biochemical signaling [88].

In cells, mechano-sensing machineries have been suggested including integrin-mediated adhesion, cadherin-mediated junction and ion-channels[89]. In particular, integrin-mediated focal adhesion (FA) complex is the most established model. Integrin is a transmembrane modality to sense ECM-associated stimuli and send the signal inward[89]. Moreover, each ECM ligand recruits a specific combination of 18 α- and 8 β-integrin subunits, which consequently triggers distinct cascade signaling[90]. Then, the FA complex is formed with integrin clusters to interact with fibrillar ECM and actin filaments via adhesion complex proteins required for FA assembly such as talin and vinculin[90]. Mechanical forces activate FA complex assembly, and the fully activated FA complex then stimulates tyrosine kinase or phosphatase such as focal adhesion kinase (FAK), which activates small GTPase RhoA and subsequently its effector, Rho Kinase (ROCK)[90]. The activated Rho/ROCK signaling phosphorylates myosin light chain, which consequently induces stress fiber development and myosin-mediated contractility[90]. The pulling force is transmitted from actin, integrin, and to ECM, which initiates the whole process of cyclic mechanotransduction again[90]. Finally, the transduced signaling such as activation of Rho/ROCK signaling regulates cell proliferation, differentiation, and migration[90]. Also, the contractile force changes ECM structure and conformation which then can influence cellular behaviors including cell adhesion, proliferation, and the pro-angiogenic potential[90,91].

Collagen and its assembly

Collagen is one of the most widely used materials for tissue engineering material due to its biocompatibility, bioactivity, and ability to be remodeled[92]. Specifically, in the interstitial space, fibrillar collagen type I and III are the most abundant types and even further up-regulated during diseases[93]. In addition, dramatic changes in microstructure and organization of collagen matrix have been clinically associated with disease progression such as cancer and fibrotic diseases[42,94]. Therefore, many *in vitro* engineered systems utilize collagen to interrogate the role of collagen physicochemical properties in the regulation of cellular behaviors.

Collagen gelation or polymerization *in vitro* occurs through an enthalpy-driven self-assembly process which has three phases: lag phase, growth phase, and the plateau phase[93]. During the lag phase, when reaching a critical aggregation concentration, collagen monomers spontaneously start to form aggregates.. Afterwards, collagen fibrils grow both laterally and axially in accordance with collagen concentration, optimal temperature, neutral pH, ionic strength, salts, surfactant, and other macromolecules (cells, other proteoglycans, and glycosaminoglycan) during lag and growth phases, and the fibrils are assembled until available collagen monomers are depleted[93].

The microstructural changes of collagen fibers ultimately alter the biophysical properties of collagen fibers as well as the matrix as a whole, so modulating aforementioned parameters (temperature and pH, etc.) has been used to control collagen microarchitecture as well as the mechanical properties of collagen-based tissue constructs[93]. However, there is still a lack of understanding as to whether and how individual physical parameters of collagen matrix microarchitecture (i.e. collagen fiber diameter, length and alignment) modulate cellular behaviors.

Fibronectin and its mechanosensitive structure

Fibronectin (Fn) is a functionally important ECM protein due to its mechanosensitive structure[95]. Fn is a large dimeric glycoprotein present in both soluble (plasma Fn in blood) and insoluble forms (matrix Fn in various tissue stroma). Two 250kDa monomers are linked through disulfide bonding at their C-terminus. Each monomer contains three types of repeating modules (I, II, and III) and each module has specific functional binding domains for cells, adjacent Fn, growth factors, and other ECM proteins such as collagen, and fibrin[96].

Among the three types of repeating modules, type III is responsible for Fn's force-mediated conformational change and subsequent interaction with cells and other ECM proteins due to its mechanosensitive structure. The type III module consists of disulfide bridge-free β-sheets making itmore susceptible to tensile force such cell-mediated contraction, whereas β-sheets in type I and II modules are stabilized by two disulfide-bonds, respectively[97]. In addition, Type III modules contain cell binding sites such as RGD-loop site in III_{10}, multiple cryptic sites buried in the equilibrium state to bind Fn modules and integrins and the PSHRN site in III_9. The PSHRN site, also called 'synergy site,' is functionally coupled with the RGD-loop site due to its spatial proximity[96].

Upon mechanical strain such as tensile force from cell contraction, Fn is extended and then its tertiary structure becomes unfolded. The unfolding Fn subsequently exposes Fn-binding cryptic sites as well as separating the RGD and synergy sites. Specifically, the changes in distance and orientation of RGD and synergy site influence the interaction with $\alpha_5\beta_1$; $\alpha_5\beta_1$ has higher affinity to RGD when it remains close and faces the synergy site, while the separation of the two sites decreases Fn's affinity to $\alpha_5\beta_1$[96]. On the other hand, Fn binding to $\alpha_v\beta_3$ is unaffected by conformational changes. These altered integrin affinities of Fn directly influences cellular behaviors such as proliferation, differentiation, and pro-angiogenic activity. Moreover, the exposed cryptic sites enable Fn to Fn interactions for Fn fibrillogenesis, so contraction-mediated unfolding of Fn is required for Fn assembly[91,95]. Furthermore, the bioactivity of

Fn-bound biomolecules is modulated in a force-dependent manner[95,98]. For example, contraction-driven Fn unfolding releases latent TGF-β by exposing the buried binding site holding the TGF-β[99].

In tumors, Fn is as extensively up-regulated as collagen, but more importantly its "unfolded" conformation contributes to enhancing tumor growth, angiogenesis and invasion[100,101]. In addition, Fn aids collagen assembly and influences collagen fiber orientation (i.e., linearity), dysregulations of which are representative of tumor desmoplasia and fibrosis[102,103]. Therefore, evaluation of the conformational changes of Fn in diseases vs. healthy conditions will aid us in identifying and understanding the pathology of diseases such as cancer.

1.7. Biological and engineering approaches

Orthotopic xenograft of mammary tumor model

Mouse models of human cancer provide physiological relevance of the findings from *in vitro* tissue culture models[104]. Thus, we utilized an orthotopic xenograft tumor model where human cancer cells are injected into the cleared mammary fat pad with and without human stromal cells, and grown until tumor formation over 6 - 8 weeks[105]. This method allows us to evaluate human breast tumor progression with or without interaction with human stromal cells *in vivo*. Mammary fat pads provide implanted cells with a mammary-specific microenvironment as compared to subcutaneous xenografts[104]. However, the compromised immune system of this mouse model may influence the cancer-associated inflammation. In addition, mouse mammary gland structural changes during mice life cycles are different from that of human mammary gland structural changes, so the responses of mammary tumors grown in mouse mammary fat pad may differ from those in a native human mammary microenvironment[106], which might be a caveat for currently available mouse models.

Obese mouse models

The most widely used genetic mouse models of obesity are either those with the leptin-gene mutation (*ob/ob*) or the leptin receptor mutation (*db/db*)[107]. *Ob/ob* mice gain weight rapidly due to the loss of the leptin gene, and eventually develop obesity and insulin resistance with hyperinsulinemia. *Db/db* mice are leptin receptor-deficient so their perturbed leptin signaling causes hyperleptinemia. In addition, they develop insulin resistance, hyperinsulinemia, as well as hyperglycemia so this mouse model has been used for type 2 diabetes research[107]. However, human obesity is not just a monogenic disease but is affected by other genetic and environmental factors[62]. Thus, other polygenic mouse models as well as diet-induced obesity (DIO) models of obesity can complement the aforementioned monogenic mouse models. Especially given the fact that diet and sedentary life style rather than genetic mutation greatly influence the occurrence of human obesity, DIO models are useful to study human obesity. For DIO models, mice were fed with high-fat or low-fat diets for 6 to 8 weeks and naturally developed obesity[108].

Förster resonance energy transfer imaging technique

The unfolding process of Fn increase the distance between the type III domains.. Thus, the proximity between the type III domains can provide us with relative Fn conformation, and this average conformation can be measured by the Förster Resonance Energy Transfer (FRET) imaging technique[31,97]. Briefly, four specific cysteines and eight random lysines on the type III module are dual-labeled with Alexa Fluor 546 acceptor fluorophores and Alexa Fluor 488 donor fluorophores, respectively. Fn conformation determines the proximity of acceptors and donors within one Fn molecule, and the proximity enables non-radiative energy transfer from excited donors to acceptors via their dipole-dipole interaction. The donors are excited by a low intensity of laser light to prevent photo-bleaching and the

emitted signals from both donors and acceptors are collected by confocal fluorescence imaging. The ratio of the acceptor and donor intensities (I_A/I_D) is calculated as an indicator of Fn fiber conformation[31].

$$\text{Fn FRET intensity} = \frac{Intensity\ of\ Acceptor}{Intensity\ of\ Donor}$$

Fn conformation relative to its quantified FRET intensity is determined using pre-obtained calibration curves showing the FRET intensity of chemically denatured dual-labeled Fn as well as ii) its corresponding circular dichroism spectra as an indication of β-sheet content in chemically denatured dual-labeled Fn[95,97]. Low FRET intensity indicates unfolded Fn conformation and high FRET intensity implies a near-to-compact form of Fn. Similarly, the strain of Fn fiber relative to the FRET intensity can be obtained by referencing a pre-obtained calibration curve showing the FRET intensity as a function of real fiber strain, which were macroscopically measured using a strain device[95].

Surface forces apparatus

Surface Forces Apparatus (SFA) is a sensitive technique that allows to measure a wide range of surface-surface interactions by means of optical interferometry[109,110]. In particular, this technique is capable of measuring from very weak surface interactions (such as electrostatic and van der Waals forces) to indentation of bulk materials (extraction of ECMs elastic moduli). Semi-reflective surfaces (back silvered mica glued onto semi-cylindrical surfaces) are used to build an optical interferometer that traps white light, similar to two facing mirrors. The optical interferometer is used to obtain the absolute distance between the surfaces from the light that exits the optical interferometer, resulting in fringes of equal chromatic order (FECO). For measurements, two cylindrical discs containing the mica substrates are faced to each other and mounted in a crossed configuration (cylindrical axes positioned at 90°). One surface is mounted on a double cantilever spring of known spring constant. The other surfaces is mounted on a motorized micrometer. The FECO fringes are recorded while the surfaces are moved by a known

distance. If the surfaces start to displace in a nonlinear fashion, the spring is deflecting. It is this deflection what allows to calculate the force acting between the surfaces. The resulting force distance profile can be further analyzed to extract the compressive elastic moduli of a viscoelastic media using the Johnson contact mechanics model[111]. The compressive elastic moduli of cell-deposited matrices can therefore be measured by means of the SFA.

Imaging analysis of collagen fibers

1) Confocal Reflectance Microscopy (CRM)

To accurately characterize the collagen matrix, multiple imaging approaches have been established. Confocal reflectance microscopy (CRM) imaging has been the most commonly utilized technique to visualize the structure of fibrillar collagen network (fibril diameter, mesh size, pore size as well as orientation)[109]. CRM utilizes reflection, back scattering of light to visualize collagen fibers. A laser at 488nm is split through a beam splitter and the split laser illuminates collagen fiber. Subsequently the reflected light from collagen matrices is collected to construct a 3D collagen matrix. No specific chemical is required for this imaging technique, so it has been clinically used to examine the morphological features of melanocytic skin tumors. Moreover, reflectance is not affected by fluorescence imaging so it is possible to perform a dual imaging of collagen fibrils with fluorescently-labeled cells, or other proteins simultaneously[109]. However, one drawback of this technique is that collagen fibrils at certain angles cannot be visualized by CRM[110]. Therefore, additional techniques are necessary to complement CRM for accurate analysis.

2) Other collagen imaging techniques

Second harmonic generation (SHG) imaging technique also has been utilized to image collagen fibrils from *in vitro, ex vivo,* and *in vivo* systems. Second harmonic generation is an optical phenomenon where two photons from laser light illuminated to material like collagen are converted to a single photon of half the wavelength with a doubled energy. This is related to the structure of the material, so non-centric materials like collagen can be imaged via SHG[111].

Lastly, polarized microscopy has long been used to visualize the different size and orientation of collagen fibrils. While the refracted light from isotropic material shows unidirectional patterns regardless of the orientation of the material, the refracted light from anisotropic material such as collagen is diverged to two different directions and the split light travels at a different velocity. The orientation and structural factors of collagen fibrils determine the direction and velocity of the refracted light, which can then be visualized with different colors after being filtered through a polarizer[112].

1.8. Research objectives

Dynamic extracellular matrix (ECM) remodeling and angiogenesis – two well-known hallmarks of cancer – are functionally linked during tumorigenesis[61]. Excessive matrix remodeling and its resulting stiffening provide biochemical and mechanical cues at various (nano to micro) scales to promote tumor growth in part by regulating angiogenesis[113]. These processes are directly and indirectly regulated by stromal myofibroblasts during tumorigenesis[61]. Various sources of myofibroblastic cells have been reported, but it has yet to be determined whether host cells in mammary tissue also contribute to the myofibroblast population upon the regulation of tumor-derived biochemical and mechanical cues. Mammary tissue consists of adipose tissue, which contains adipose-derived stem cells (ASCs) and adipocytes[114]. The multi-potency of ASCs and the plasticity of adipocytes have been reported previously[85]. However, their potential to differentiate into myofibroblastic cells, thereby promoting tumor stiffening

and angiogenesis remains poorly understood. In addition, it is interesting to note also that the population of ASCs in adipose tissue increases during obesity, a key risk factor for breast cancer. Also, obesity shares similar features with cancer such as a low-grade chronic inflammation and fibrosis thus making it possible that the obesity-primed ASCs may play a pivotal role in bridging obesity with breast cancer in much the same way that cancer-associated ASCs do.

Thus, I hypothesize that ASCs and adipocytes promote breast tumor progression upon the regulation of pathological biochemical and mechanical cues during tumorigenesis as well as obesity. In particular, ASCs and adipocytes are committed to myofibroblastic cells, thereby partaking in dynamic ECM remodeling, and angiogenesis, all of which consequently promote tumor progression.

This hypothesis was addressed by investigating the following sub-hypotheses:

1. **Cancer-activated ASCs promote breast tumor progression**
2. **Cancer-activated adipocytes increase the myofibroblastic cell population, thereby stimulating ECM remodeling and angiogenesis**
3. **Obesity-associated interstitial ECM remodeling promotes tumor malignancy**
4. **Collagen fiber microstructure regulates the pro-angiogenic potential of ASCs.**

Further details of the studies completed to confirm or deny these hypotheses are described in the subsections below.

1. Cancer-activated ASCs promote breast tumor progression

In chapter 2, the pro-tumorigenic role of ASCs in the promotion of breast tumor progression will be discussed. For this study, both mouse and human cells were assessed as a model of progenitor cell components of adipose tissue. Well-characterized mouse preadipocytes 3T3L1 (ATCC) and adipose-

derived stem cells (Lonza) were utilized to examine the pro-tumorigenic potential of adipose tissue-derived progenitor cells upon tumor-derived biochemical and mechanical cues. To mimic tumor-derived morphogens, tumor-conditioned media (TCM) were collected from malignant breast cancer lines MDA-MB231 (ATCC). Additionally, the responses of the progenitor cells to soluble factors from a series of mammary epithelial cells (benign to malignant) as well as mouse mammary cancer cells (MCN1 and MCN2) were assessed. Tumor-associated mechanical cues were recapitulated by culturing cells on 2D and 3D scaffolds (alginate, collagen and polyacrylamide) with varying stiffness. Finally, orthotopic mammary tumor models were generated to confirm our in vitro studies and for the analysis of in vivo samples, various physical tools (e.g., imaging techniques and mechanical testing tools) were utilized.

2. Cancer-activated adipocytes increase the myofibroblastic cell population, thereby stimulating ECM remodeling and angiogenesis

In chapter 3, the impact of cancer-activated adipocytes on ECM remodeling and angiogenesis were addressed. To assess the matrix remodeling and angiogenic potential of adipocytes in the presence of tumor-derived soluble factors, adipocytes were cultured in both 2D and 3D *in vitro* systems with TCM. Adipocytes were obtained through adipogenic differentiation of ASCs and 3T3L1s and cultured by TCM in 2D culture plate and 3D collagen scaffolds. The phenotypic changes of cancer-activated adipocytes were determined by analyzing their adipogenic markers and myofibroblastic features. To address the clinical relevance of *in vitro* findings, the adipogenic features of adipocytes in mouse and patient-derived tumors were analyzed. Finally, the impacts of their enhanced pro-angiogenic signaling on endothelial cell sprouting – an indication of angiogenesis – were assessed.

3. Obesity-associated interstitial ECM remodeling promotes tumor malignancy

In chapter 4, I propose that obesity-associated interstitial ECM remodeling may provide a functional link between obesity and breast cancer. To investigate the role of obesity-associated interstitial fibrosis in the promotion of mammary tumorigenesis, pro-fibrotic features in the mammary fat of both mouse and human samples were separately extracted from cancer-free lean and obese subjects and analyzed. In addition, fibrotic characteristics of adipose tissue from obese and lean mice were also assessed as a function of fat depot (subcutaneous vs. visceral fat) and menopausal status (ovary intact vs. ovariectomized mice). To specifically look for the cellular mediators of obesity-mediated interstitial fibrosis, ASCs were isolated from age-matched lean and obese mice and characterized utilizing various physical oncological approaches. To understand the functional significance of fibrosis mediated by obesity-associated ASCs, the impacts of biochemical and physical cues of ECM derived from ASCs on tumor malignancy were examined. Lastly, clinical relevance of our findings was established by assessing human tumor specimens collected from normal and obese patients.

4. Collagen fiber microstructure regulates the pro-angiogenic potential of ASCs.

In chapter 5, I will discuss whether the microstructural changes of collagen fibers that were detected in the presence of tumors and obesity provide a feedback mechanism that regulates the phenotype of ASCs. To investigate whether microstructural changes of collagen fibers regulate the pro-angiogenic potential of ASCs, we generated 3D collagen scaffolds with different fiber microstructures. We assessed the phenotypic changes of ASCs as a result of changes in fiber thickness and in turn how they remodeled their surrounding matrices. In addition, we assessed the pro-angiogenic potential of the ASCs, which were altered by the fiber microstructure through the use of co-culture 3D models with human umbilical vein endothelial cells (HUVECs). Finally, we investigated whether changes in the microstructure of collagen fibers regulate cell behaviors in a mechanoregulation-dependent manner.

The findings of my doctoral work suggest that ASCs and adipocytes contribute to an increase of myofibroblastic cells, thereby promoting tumor stroma remodeling and progression. In addition, obesity-primed ASCs show a pro-tumorigenic potential similar to that of cancer-associated ASCs. Thus, microenvironmental cues including the change of collagen fiber structure, even at the micro-scale, potentially stimulate the phenotypic alteration of host adipose stromal cells favoring breast tumorigenesis.

These findings suggest great clinical implications in the field of cancer research and tissue engineering. Although adipose tissue has been greatly appreciated for regenerative applications such as breast reconstruction, our findings call for more careful consideration of the contextual cues, which could possibly activate the pathogenic potential of host or exogenous adipose tissue. In particular, the health conditions of tissue recipients as well as donors might play a pivotal role in the safety of implanted adipose tissue. Implanted or host adipose tissue in cancer patients might develop pathogenic potential due to the contextual cues, and obesity-associated ASCs might not exhibit the same characteristics as those from normal individuals and again highlight that caution must be exercised in such procedures. In addition, given the increase of obesity and its strong connection with both pre- and post-menopausal breast cancer, our findings will contribute to developing better diagnostic and therapeutic approaches. Finally, as our studies indicate that even micro-scale alterations to the tumor microenvironment can influence the behavioral changes of host cells, more careful consideration is required when designing tissue engineering approaches based on adipose tissue and biomaterials.

CHAPTER 2

IMPLANTED ADIPOSE PROGENITOR CELLS AS PHYSICOCHEMICAL REGULATORS OF BREAST CANCER

Published in *Proceedings of the National Academy of Sciences (2012)*

2.1. Contributors

Co-authors of this work made the following contributions: Emily M. Chandler (alumnus in the Fischbach lab) is a co-first author, and she made significant contributions to this project leading *in vitro* studies to investigate the roles of tumor-derived cues in regulating the differentiating potential of ASCs. Joseph P. Califano (alumnus in the Reinhart-King lab) performed traction force measurement via traction force microscopy (TFM). Roberto C. Andresen Eguiluz, a Ph.D. student in the Gourdon lab aided in measuring tumor stiffness via dynamic mechanical thermal analysis (DMTA), Jason S. Lee (alumnus in the Fischbach lab) assessed the pro-angiogenic signaling of ASCs in response to varying stiffness, Christine J. Yoon (alumnus in the Fischbach lab) performed phosphorylation of focal adhesion kinase (pFAK) analysis of ASCs in response to tumor-derived cues. David T. Tims (alumnus), master student and James X Wang (alumnus), undergraduate student at the moment in the Fischbach lab measured ASC-mediated collagen contractility and the resulting stiffness of collagen scaffolds. Le Cheng, a Ph.D student in the Nikitin lab at the moment aided in performing *in vivo* study. Sunish Mohanan performed histopathological assessment of tumor sections. Mark R. Buckley (alumnus), a Ph.D. graduate student in the Cohen lab and Prof. Itai Cohen aided in measuring the stiffness of ASC-embedded collagen gels with their custom-built tool. Prof. Alexander Yu Nikitin providing help us to design and pursue *in vivo* experiments. Dr. Rebecca M. Williams performed second harmonic generation imaging analysis of

collagen in tumor explants, Prof. Delphine Gourdon provided help to measure tumor stiffness via DMTA, analyze the data and prepare the manuscript, Prof. Cynthia A. Reinhart-King provided her technical and scientific advice on TFM analysis, and Prof. Claudia Fischbach primarily led this project providing guidance for the experimental design, data interpretation and preparation of the manuscript.

2.2. Abstract

Multipotent adipose-derived stem cells (ASCs) are increasingly used for regenerative purposes, such as soft tissue reconstruction following mastectomy. However, the ability of tumors to commandeer ASC functions to advance tumor progression is not well understood. Through the integration of physical sciences and oncology approaches we investigated the capability of tumor-derived chemical and mechanical cues to enhance ASC-mediated contributions to tumor stroma formation. Our results indicate that soluble factors from breast cancer cells inhibit adipogenic differentiation while increasing proliferation, pro-angiogenic factor secretion, and myofibroblastic differentiation of ASCs. This altered ASC phenotype led to varied extracellular matrix (ECM) deposition and contraction, thereby enhancing tissue stiffness, a characteristic feature of breast tumors. Increased stiffness, in turn, facilitated changes in ASC behavior similar to those observed with tumor-derived chemical cues. Orthotopic mouse studies further confirmed the pathological relevance of ASCs in tumor progression and stiffness *in vivo*. In summary, altered ASC behavior can promote tumorigenesis, and thus their implementation for regenerative therapy should be carefully considered in patients previously treated for cancer.

2.3. Introduction

Adipose-derived stem or progenitor cells (ASCs) are widely used in tissue engineering due to their multipotency, ability to enhance vascularization, and relative ease of isolation from the stromal

vascular fraction of adipose tissue[115,116]. In particular, ASCs are increasingly considered for reconstructive procedures following surgery for breast cancer, which compose the majority of the 93,000 breast reconstructions performed in the U.S. per year [117]. ASCs offer several advantages over commonly utilized silicone and saline implants including their ability to regenerate functional adipose tissue, which reconstitutes a large fraction of the breast[118,119]. However, malignantly transformed cells may be present in breast cancer survivors without manifest disease, and it remains unclear whether implanted ASCs may increase the risk of tumor development and relapse [120] by establishing a microenvironment conducive to nascent or recurrent tumorigenesis.

Mammary tumors are stiffer than normal mammary gland tissue [121,122], due in part to tumor-cell secreted morphogens that vary extracellular matrix (ECM) assembly. Altered ECM deposition and contraction not only enhances tumor rigidity [29], but further modulates tumor progression by perturbing epithelial morphogenesis [123] and vascular development [124]. Myofibroblasts regulate these outcomes by controlling the mechanical properties of the tumor-associated ECM and by functioning as a major source of host-derived pro-angiogenic factors (e.g., vascular endothelial growth factor [VEGF]) [29,125]. Generally, local fibroblasts are considered the primary origin of myofibroblasts and regulator of this desmoplastic reaction, but bone marrow- and tissue-derived mesenchymal stem cells may also contribute to this cell population. Specifically, ~20% of tumor-associated α-smooth muscle actin (α-SMA) positive myofibroblasts originate from bone marrow, whereas non-bone marrow tissues including adipose tissue contribute to the remainder[126,127]. However, the integrated effects of tumor-associated physicochemical cues on ASC-dependent tumorigenesis are not well understood.

Here, we applied a physical sciences-based approach to correlate tumor-mediated changes in ASC phenotype with tissue stiffness, vascularization, and growth. Our findings support that ASCs can develop into myofibroblasts in response to physicochemical factors provided by cancerous cells. This

phenotypic change not only enhanced angiogenesis, but also ECM rigidity, which further increased the tumor-promoting capacity of ASCs in a positive feedback loop. These findings support the role of ASCs as key regulators of mammary tumor progression and recurrence, which warrant review of current tissue engineering therapies following mastectomy and may be explored towards more efficacious therapies for breast cancer patients.

2.4. Materials and methods

Cell culture

3T3-L1, MDA-MB231, MCF-7 (all from ATCC), and MCN1 and MCN2 mammary tumor cells isolated from the mammary epithelium of MMTV-Cre, $p53^{L/L}$ and MMTV-Cre, $p53^{L/L}$ $Rb^{L/L}$, respectively [128], were routinely cultured in MEM (α-modification [αMEM], Sigma) containing 10% FBS (Tissue Culture Biologicals) and 1% antibiotic (penicillin/streptomycin, Gibco). MCF-10A (ATCC), MCF10AT1, and MCF10ACA1a (both from Barbara Ann Karmanos Cancer Institute [129]) were maintained in DMEM/F12 supplemented with horse serum, epidermal growth factor (EGF), hydrocortisone, cholera toxin, insulin, and penicillin/streptomycin (all from Invitrogen) as previously described [130]. ASCs and HUVECs (both from Lonza) were cultured in their corresponding growth media (ADSC-GM and EGM-2, respectively; Lonza). Lonza isolates ASCs from lipoaspirates based on expression of stem cell-associated surface markers [131], cryopreserves cells at passage 1, and does not pool cells from multiple sources. Here, ASCs from two separate, female donors were utilized at passages less than 7. ASC function in response to TCM and matrix mechanical properties was assessed as described in SI Materials & Methods. Additionally, the effect of 3T3-L1 derived matrices on MDA-MB231 cell growth was measured as documented in SI Materials & Methods.

In vivo studies

Media, ASCs and/or MDA-MB231 cells (1 x 10^6 in 20 μL of DMEM/ Ham's F-12, 10 % FBS, 1 % antibiotic) were injected into the cleared mammary fat pad of at least six 3 week-old female SCID/NCr mice (Charles River Labs, 01S11) (2 tumors per mouse) per condition in accordance with Cornell University animal care guidelines. Explants were harvested 6 weeks after implantation, imaged, weighed, and divided for subsequent formalin-fixation/paraffin-embedding and lysis in T-PER buffer (Pierce). H&E-stained sections were broadly evaluated for pathological features of malignancy. Cross-sections were characterized further via immunohistochemical staining for CD31, α-SMA, type I procollagen, collagen, and desmin. Staining procedures and image analysis methods are described in SI Materials & Methods. VEGF and IL-8 content in lysates was measured via mouse VEGF and human IL-8 DuoSets (R&D) and normalized to protein content as determined via BCA protein assay (Thermo Scientific). Tumor stiffness was determined using a Dynamic Mechanical Thermal Analyzer (DMTA) as further outlined in SI Materials & Methods.

Analysis of ASC proliferation, adipogenesis, pro-angiogenic capability, and migration

Conditioned media was collected from the different tumor and epithelial cell lines in αMEM (1% FBS, 1% antibiotic) over 24-hours, normalized to cell number, concentrated 10-fold in an Amicon centrifugal filter unit (Millipore, MWCO = 3kDa), and subsequently reconstituted with media containing 1% FBS, 1% antibiotic specific to the treatment cell type (SI Table 1). Control medium was incubated for 24-hours without exposure to cells and then processed similarly. Conditioned media was globally tested for cytokines using Human Cytokine Antibody Arrays (Affymetrix) and specifically for IL-8 using ELISA DuoSets (R&D). Following 3 days of treatment in control media or TCM, cell counting was performed using a Z2 Beckman Coulter counter. To assess proliferation, 10 μM BrdU (Sigma) was added

to cells 20 hours prior to fixation in 4% paraformaldehyde. Then samples were incubated in ice-cold 1N HCl, secondly 37°C 2N HCl, and then 0.1 M borate buffer prior to adding biotinylated mouse anti-BrdU. Subsequently, BrdU and nuclei were visualized by incubating streptavidin conjugated Alexa Fluor 555 (both from Invitrogen) and DAPI (4',6-diamidino-2-phenylindole). The percentage of BrdU positive nuclei was determined from 5 images per samples with 4 samples per condition. Adipogenesis of 3T3-L1s and ASCs was induced as previously described [132] and by using ADSC-GM SingleQuots® (Lonza), respectively. Differentiation into adipocytes was assessed by Oil Red O staining, immunofluorescence analysis of PPARγ, and by measuring glycerol-3-phosphate dehydrogenase (GPDH) activity. To this end, supernatants collected after lysing cells on ice in a buffer containing 50mM Tris, 1mM EDTA, and 1mM β mercaptoethanol (all from J.T. Baker) were mixed with dihydroxyacetone phosphate and oxidized nicotinamide adenine dinucleotide (NADH). The decrease in NADH absorbance at 340 nm was quantified on a spectrophotometer over a 7 min period. Enzyme activity was normalized to total protein content as measured by protein assay (Bio-Rad). To visually assess differentiation into lipid-rich adipocytes, cells were fixed in formalin prior to staining with Oil Red O (Sigma) for 2 hours. Samples were imaged with a bright field microscope. For analysis of pro-angiogenic activities, 3T3-L1s or ASCs were preconditioned in control or TCM for 3 days, then fresh media containing 1% FBS and 1% antibiotic specific to the treatment cell type (SI Table 1) was added, collected after 24 hours, and processed as described above. VEGF secretion of preconditioned ASCs or 3T3-L1s was analyzed via human or mouse Quantikine ELISA (R&D Systems), respectively. To assess the effect of altered VEGF secretion on HUVEC migration, ASCs and 3T3-L1 cells were preconditioned in 24-well plates for 3 days. Collagen-coated transwell inserts seeded with HUVECs were placed atop tumor-preconditioned 3T3-L1 or ASCs cells in 300 μL fresh αMEM (1% FBS, 1% antibiotic). After 24 hours, inserts were formalin fixed following a swabbing of the top of the membrane to remove non-migrated HUVECs. Cells on the

lower side of the membrane were stained with DAPI and nuclei were counted. The number of migrated HUVECs was then normalized to the number of progenitor cells within each well.

To determine the effect of tumor-derived soluble factors on adipose progenitor recruitment, 3T3-L1 cells were seeded on top of collagen I (PureCol, Inamed)-coated Nunc 10 mm Tissue Culture inserts (8.0 μm pore) with either 300 μL of TCM or control medium beneath the membrane. After 18 hours, 3T3-L1s were formalin fixed following a swabbing of the top of the membrane to remove non-migrated cells. Cells on the lower side of the membrane were stained with DAPI and the average number of nuclei was counted in 8-10 images per sample.

Analysis of myofibroblast differentiation and matrix stiffening

Differentiation into myofibroblasts was assessed by immunofluorescence analysis of α-SMA, procollagen I, and collagen I. TGF-β signaling was modulated by supplementing control or TCM with 2 ng/mL recombinant human TGF-β1 or 0.5 μg/mL anti-human LAP (neutralizing TGF-β1 antibody) (both from R&D Systems), respectively. IL-8 signaling was evaluated by supplementing growth media with 3-30 ng/mL recombinant human IL-8 (R&D). For contraction assays, ASCs were suspended in 15 mg/ml collagen (1×10^6 cells/ml) isolated from rat tails [133], cast into circular molds 0.5 mm thick and 4 mm in diameter [134], and cultured in TCM or control medium under free-floating conditions on an orbital shaker for 2 weeks, with media changes every other day. To inhibit proliferation, TCM or control medium containing 4 μg/mL mitomycin (Fisher Scientific) was added to gels when at the initially as an initial exposure has been shown to inhibit proliferation over long cultures [135]. Actin polymerization and pROCK signaling were inhibited by supplementing culture media with 1 μM cytochalasin D or 20 μg/ml Y-27632 (both from Tocris), respectively. Gel contraction was determined by measuring the surface area of each gel using the magnetic lasso tool in Photoshop (Adobe) to trace the apical surface circumference. For the

analysis of cell matrix stiffening, these same collagen gels were stained with dichlorotriazinylaminofluorescein (5-DTAF), sandwiched between two glass plates, and imaged with a Zeiss LSM 510 confocal microscope as previously described [136]. A shear stress was applied to the gel while a photobleached line in the sample was imaged. As described previously, a MATLAB algorithm was then used to calculate the gel modulus based on the displacement of the photobleached line [136].

Western Blot analysis

Cells were lysed in RIPA buffer (Thermo Scientific) containing protease inhibitor (Sigma), phosphatase inhibitor cocktail (Sigma), and 1mM phenylmethylsulfonyl fluoride (PMSF) in isopropyl alcohol. Equivalent quantities of protein were loaded as measured by BCA protein assay (Thermo Scientific). Proteins were separated by SDS-PAGE and transferred to a PDVF membrane (Bio-Rad). Primary antibody to α-SMA (Abcam) was incubated with the membrane overnight at 4°C, followed by a 1 hour incubation with HRP-conjugated anti-rabbit secondary antibody (Novus Bio) at room temperature. Chemiluminescence detection was performed to visualize probed protein using ECL kit (GE healthcare) based on manufacturer's protocol.

Analysis of ASC response to matrix mechanical properties

For TFM analysis, polyacrylamide gels 1, 5, and 10 kPa in stiffness were prepared with embedded fluorescent beads, and cellular traction stresses were measured using TFM as previously described [137-140]. Briefly, images of the gels in a stressed and relaxed state were taken pre- and post-removal of the cells with trypsin, respectively. The substrate strains were converted to traction stresses using the LIBTRC analysis library developed by Professor Micah Dembo of Boston University, who also invented the basic theory that underlies TFM. Polyacrylamide gels of the same stiffness were used for

immunofluorescence analysis of pFAK[Y397] as described in staining procedures section. For studies of the combined effects of stiffness and TCM, cells were seeded on 0.2-30 kPa stiff polyacrylamide gels and cultured in either control media or TCM for 10 days followed by staining and analysis as further outlined in the staining procedures section.

For studies using RGD-modified alginate substrates, alginate (Protanal LF 20/40, FMC) was modified with GGGGRGDSP (Peptides International) as previously described (1). 3%, 1.5%, and 0.75% (w/v) solutions of alginate in αMEM were cast between glass plates with 1 mm spacers and crosslinked in a solution of 0.1 M $CaCl_2$, 0.01 M HEPES (J.T. Baker) prior to punching out topographically flat disks 1 cm in diameter. The aggregate moduli of these gels were measured on a mechanical tester (ELF 3100, Bose) under radial confinement and uniaxial compression at 15 % strain. Cells were seeded on top of the gels and cultured in well plates. For analysis of cell proliferation and adipogenic differentiation, cells were harvested by dissolving these constructs in 50mM EDTA (J.T. Baker) in PBS and analyzed as described above. To analyze VEGF secretion, cell-seeded gels were transferred to a new culture dish (containing fresh media with 1% FBS, 1% antibiotic). After 24 hours, media and cells were collected and analyzed as described above.

Staining procedures

For immunocytochemistry, formalin-fixed cells were rinsed with 0.05% Triton-X in PBS (PBS-X) followed by incubation with 2% BSA in PBS-X (PBS-X/BSA) for blocking. Afterwards, the cells were incubated with the desired primary antibody diluted in PBS-X/BSA overnight at 4°C. Following two washes in PBS-X, samples were incubated with secondary antibodies diluted in PBS-X/BSA for 1 h at room temperature. The following primary antibodies were used: rabbit anti-mouse PPARγ (Cell Signaling), rabbit anti-FAK [pY397] (Invitrogen), mouse anti α-SMA (Abcam), rabbit anti-procollagen I

(SP1.D8, Developmental Studies Hybridoma Bank, Univ. of Iowa), and rabbit anti-collagen I (Millipore). DAPI was used as a nuclear counterstain, Alexa Fluor 488 or 568 served as the secondary antibody, and Alexa Fluor 568 phalloidin enabled detection of the F-actin cytoskeleton (all from Invitrogen). Imaging was performed on a Zeiss Observer Z.1 microscope and AxioCam MRm camera unless otherwise noted. Cells cultured within collagen gels and stained with α-SMA primary and AlexaFluor 488 conjugated secondary antibody, phalloidin, and DAPI as described above were imaged on a Zeiss 710 Confocal Microscope.

Paraffin sections of *in vivo* samples were subjected to antigen retrieval treatments (proteinase K [Dako] for CD 31 staining, antigen retrieval system [Dako] for α-SMA, and 0.1M citrate buffer for alternate stains) prior to standard immunostaining procedures. Subsequently, samples were rinsed and blocked in 0.05% Tween-20 PBS (TBST) with SuperBlock (Thermo Fisher). An additional blocking treatment was required for α-SMA and procollagen I staining using M.O.M kit (Vector laboratories) and Vectastatin ABC kit (Vector laboratories), respectively. In addition to those previously listed, rat anti-CD31 (Pharmingen), mouse anti-α-SMA (Invitrogen), and rabbit anti-desmin (Abcam) were used. For CD 31 staining, the TSA biotin system (PerkinElmer) was used for signal amplification.

For DAB-based immunohistochemistry, sections were deparaffinized, rehydrated, and peroxidase activity was blocked using 3% hydrogen peroxide. An HRP-conjugated secondary antibody (Novus) and 3,3´-diaminobenzidine (DAB) substrate kit (Thermo Fisher) were used for color development. Samples were counter-stained with Gill's hematoxylin (EMD chemicals). IgG isotopes and primary antibody-lacking sections served as negative controls.

For picrosirius red staining, 4 μm thick sections of paraffin–embedded tissue were stained with 0.1% Sirius red F3B (Sigma) in saturated picric acid for two hours at room temperature followed by washes in 1% acetic acid and distilled water. Stained sections were imaged with a Nikon Eclipse TE2000-S

microscope equipped with a rotating filter for polarized light under 10x magnification. Microscope setting (light intensity, exposure time, condenser opening, gain, and gamma parameter) was identically applied to all samples.

Image analysis

For image analysis, raw data images of *in vitro* samples and histological cross-sections were utilized. Background staining was excluded from images of various samples prior to isolating positive pixels of interest using Adobe Photoshop. Isolated positive pixels were then quantified in ImageJ (NIH). Positive pixel density was averaged for 8-10 representative images per sample for 4 samples per *in vitr*condition and for 15-20 representative images per explant. Staining intensity was normalized to cell number as determined by semi-automated counting of DAPI-stained nuclei utilizing ImageJ. Alpha-SMA positive cells in *in vitro* samples were manually quantified. Cell alignment was determined by using ImageJ to measure the angle of lines drawn through the long axis of up to 20 randomly selected cells per image. The average cell angle was then calculated for each image, and the individual cell deviation from the average was computed and plotted. For all conditions, a total of 8-10 images were examined per sample with 4 samples per condition.

Collagen fiber maturity in picrosirus stained sections was analyzed by their birefringence color appearing as red/orange, green, or blue/white according to fiber thickness. The birefringence color pixels (red, green, and blue) of collagen fibers were segmented using RGD stacks in ImageJ and the separated pixels were quantified. Threshold was manually adjusted based on grayscale images, and kept constant throughout all samples. Five to six images were analyzed per tumor for a total of three tumors per condition.

Multiphoton Second Harmonic Generation (SHG) microscopic imaging and analysis

Multiphoton microscopy was accomplished on a previously described [141], custom-built multiphoton microscope. Tumor specimens were (placed in the tumor-size within biopsy foam pad), immersed in PBS and imaged with 780 nm illumination using an Olympus 20x/0.95W XLUMPlanFl objective. For each specimen, six Z-series (2 μm steps, from 60 μm to 100 μm deep) were acquired. Emissions were separated into SHG (360-405 nm, pseudocolored blue) and autofluorescence (420-550 nm, pseudocolored yellow) channels. Only the SHG channel was used for image quantification of collagen matrix properties. In order to analyze the mean structural characteristics of the collagen matrix, a 2D spatial autocorrelation was computed from the SHG channel image. An isocontour was fit to 1/e of the maximum value of each image autocorrelation. The mean radius of this isocontour (the mean correlation distance in the image) indicates the size scale of the collagen framework in any image. For the collagen fibril linearity (FL) assessment, individual fibrils were traced throughout each Z-stack. Specifically, both the full-length and the shortest distance between fibril ends were measured using Fiji (a packaged version of Image J). The ratio of the linear distance over the full fibril length was calculated to be the collagen FL. 30-50 fibrils per z-stack were measured, and the collagen FL of each condition was obtained by averaging the FL of 4 z-stacks in each tumor. A total 3 tumors per each condition were analyzed.

Dynamic Mechanical Thermal Analysis (DMTA) of tumor sections

Tumors were cut with a vibratome into sections ranging from 0.7 to 2.7 ± 0.1 mm in thickness as determined optically. These sections were punched into cylindrical thick sections of 2.6 ± 0.1 mm in diameter, fixed between the DMTA (Dynamic Mechanical Thermal Analyzer) parallel plates, and fully immersed in PBS in a standard submersion-compression clamp configuration at room temperature

(25°C). A controlled force was applied by the upper plate while the lower plate held the sample in a fixed position. Two series of compressive tests were then run on each tumor sample following an initial application of 9% pre-strain to ensure full sample engagement and homogeneous compression before measurement. In the first series, the maximum force applied was set at 0.01 N to exclusively probe the low-strain (9-14%) elastic regime, while it was set at 0.4 N in a second series to investigate the full elastic regime and the onset of material to plastic deformation (up to 30% strain). The rate of force application was kept constant at 0.025 N/min in all tests. The force F (force sensitivity of 0.001 N) and thickness L (distance resolution of 0.05 μm) were measured simultaneously and converted into engineering stress-strain plots as follows: strain, $\varepsilon=(L_o-L)/L_o$ (where L_o is the initial zero-strain sample thickness and L the thickness during compression) and stress, $\sigma=F/A_o$ (where F is the force during compression, and A_o the initial zero-strain sample cross-sectional area). The mean Young's modulus, E, was obtained for each sample from the slope of the stress-strain curve, $\sigma = E\,\varepsilon$ in the low-strain (9-14%) elastic regime.

Analysis of the effect of altered progenitor cell ECM

3T3-L1-derived matrices were prepared as previously described [142]. More specifically, 3T3-L1s were seeded in 12-well plates and cultured for 8 days in either TCM or control media supplemented with 50 μg/mL ascorbic acid (Sigma) with media changes every other day. On day 8,the matrix was incubated at 37°C for 15 minutes in extraction buffer (20 mM NH_4OH and 0.5% Triton-X in PBS). After washing in DI H_20 and PBS followed by blocking with 1% BSA, Vybrant DiO (Invitrogen) labeled MDA-MB231 cells were seeded atop the matrix. pROCK signaling was inhibited by supplementing culture media with 20 μg/mL Y-27632 (Tocris). The number of MDA-MB231 cells was assessed by counting 10 images per sample for 6 samples per condition.

2.5. Results and Discussion

Tumor-secreted soluble factors regulate the adipogenic and pro-angiogenic capability of ASCs

To evaluate the effects of tumor cell-secreted soluble factors on ASC behavior, human ASCs were cultured in conditioned media (TCM) from commonly used highly (MDA-MB231) or less (MCF-7) aggressive human breast cancer cell lines. Additionally, mouse 3T3-L1 preadipocytes – a well-characterized cell model for studies of adipogenesis [143] – were used to verify the broad implications from primary ASC studies. Analysis of cell numbers and BrdU incorporation suggested that tumor-secreted factors promoted ASC and 3T3-L1 proliferation (Figs. 2.1A and 2.2A). In contrast, these factors inhibited adipose differentiation of both cell types, as indicated by attenuated activity of the lipogenic enzyme glycerol-3-phosphate dehydrogenase (GPDH) (Fig. 2.1B), reduced activation of the key adipogenic transcription factor peroxisome proliferator-activated receptor gamma (PPARγ) (Fig. 2.1C), and inhibition of lipid droplet accumulation (Fig. 2.2B). An experiment in which ASCs and 3T3-L1s were first exposed to TCM and then evaluated for VEGF secretion further suggested that exposure to tumor-derived soluble factors enhances pro-angiogenic factor release by these cells (Fig. 2.1D). This increased pro-angiogenic potential is relevant to tumor angiogenesis as tumor-preconditioned ASCs and 3T3-L1s significantly enhanced VEGF-dependent migration of human umbilical vein endothelial cells (HUVECs) as compared to control cells (Fig. 2.1E). Notably, the magnitude of these changes directly correlated with tumor aggressiveness since MDA-MB231-TCM induced greater phenotypic changes than media collected from MCF-7 cultures (Figs. 2.1 and 2.2). Comparison of effects mediated by isogenically matched normal MCF10A, premalignant MCF10AT, and fully malignant MCF10ACA1a confirmed these results. Specifically, premalignant cells had no significant effect on ASC adipogenic differentiation and VEGF secretion, but promoted ASC proliferation, whereas MCF10ACA1 mediated similar outcomes as MDA-MB231 (Figs. 2.2). The described observations were broadly relevant as TCM collected from two murine

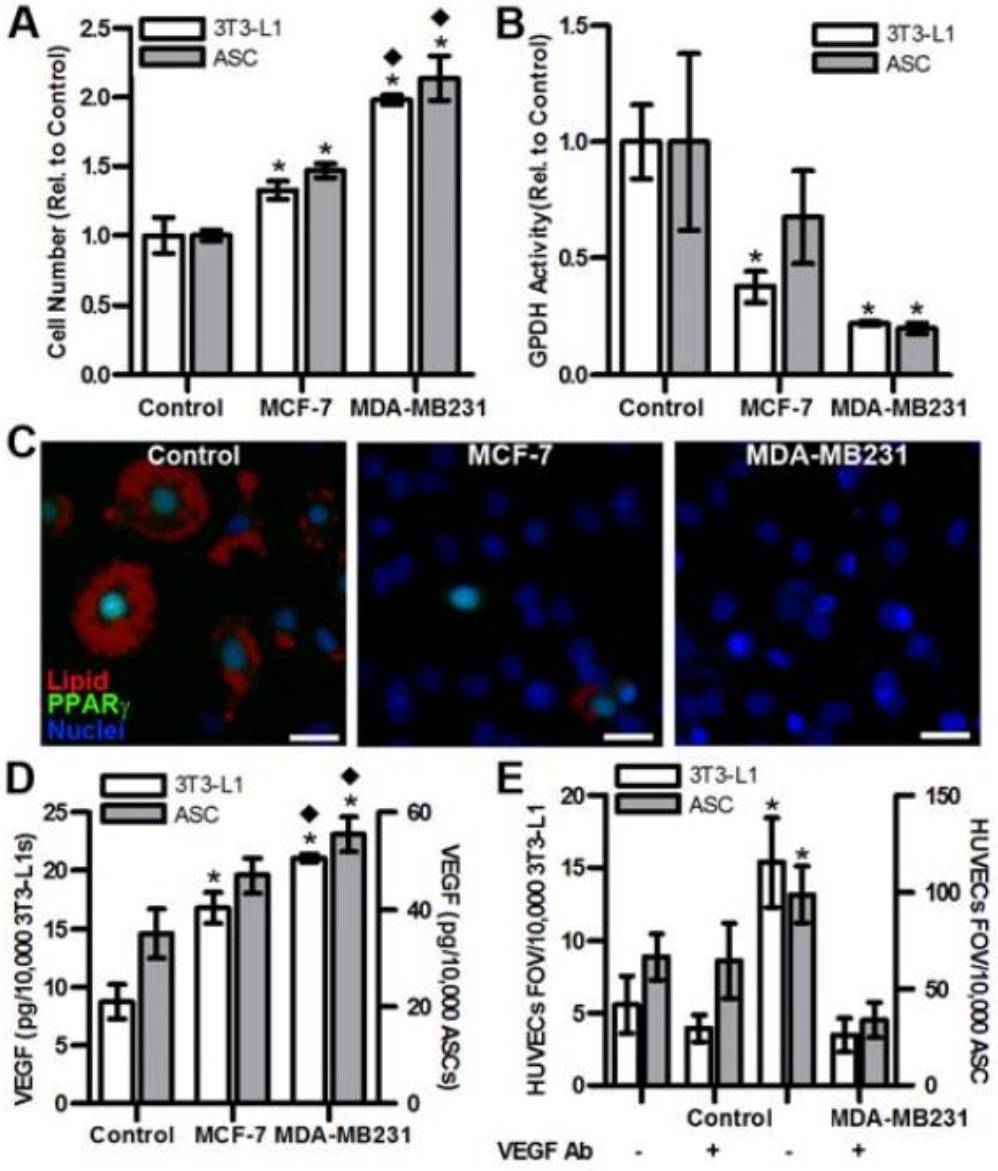

Fig. 2.1. Tumor-secreted soluble factors regulate ASC function. (A) TCM from MCF-7 and MDA-MB231 increases 3T3-L1 and ASC cell numbers relative to control (n = 4). (B) TCM treatment significantly decreases the adipogenic capability of 3T3-L1 and ASCs relative to control as determined by spectrophotometric analysis of GPDH activity (n = 4). (C) Immunofluorescence analysis of the transcription factor PPARγ in 3T3-L1s confirmed that TCM inhibits adipogenic differentiation (Scale bar = 20 μm). (D) ELISA suggested that ASCs and 3T3-L1s increase VEGF secretion when pre-conditioned with TCM from either MCF-7 or MDA-MB231 (n = 4). *$P < 0.05$ from control; ♦$P < 0.05$ from MCF-7 condition. (E) 3T3-L1s and ASCs that were previously pre-conditioned with TCM from MDA-MB231 enhanced HUVEC migration in a transwell assay as compared to 3T3-L1s and ASCs pre-conditioned with control media; addition of a VEGF neutralizing antibody decreased migration to control levels (n = 4). *$P < 0.05$ from all other conditions of the same cell type.

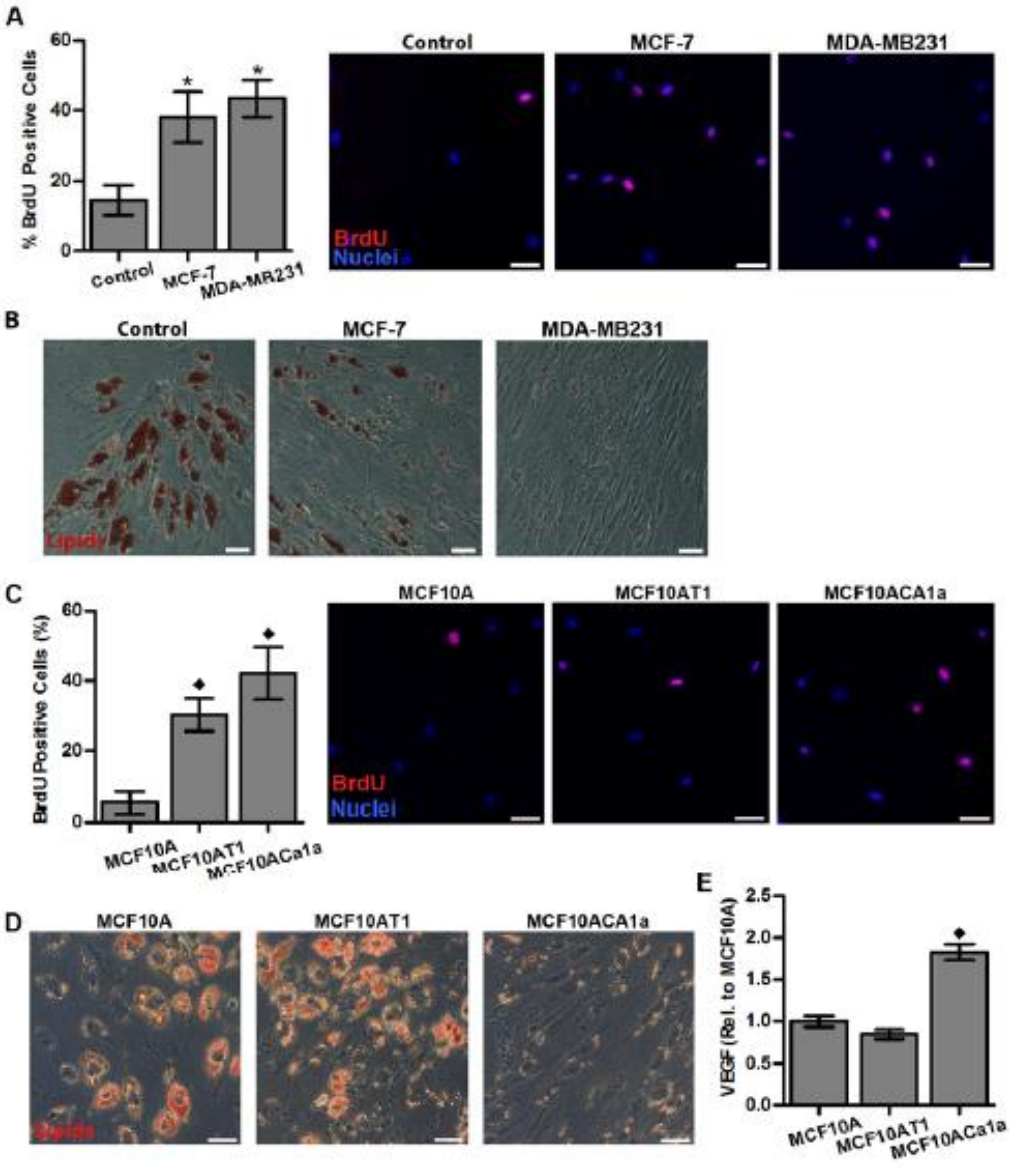

Fig. 2.2. Tumor-secreted soluble factors alter ASC functions. (A) TCM from MCF-7 and MDA-MB231 enhanced ASC proliferation as assessed by quantification of BrdU positive cells (Scale bar = 50 μm). (B) Differentiation of ASCs in control medium resulted in large lipid droplet formation, whereas ASCs cultured in TCM from MCF-7 or MDA-MB231 exhibited decreased lipogenesis, evidenced by diminished Oil Red O-staining (Scale bar = 50 μm). (C) Quantification of BrdU positive ASCs after culture in conditioned media of isogenically matched MCF10A (normal), MCF10AT1 (premalignant), and MCF10ACA1a (malignant) cells confirms that increased ASC proliferation represents a function of tumor malignancy (Scale bar = 50 μm). (D) Adipogenic differentiation of ASCs in conditioned medium from normal and premalignant cells resulted in lipid droplet formation, whereas ASCs cultured in TCM from MCF10ACA1a cells exhibited decreased lipogenesis, evidenced by diminished Oil Red O-staining (Scale bar = 100 μm). (E) MCF10ACA1a TCM also significantly increased VEGF secretion by ASCs as measured by ELISA (n = 4). *$P < 0.05$ from control condition; ♦$P < 0.05$ from MCF10A condition.

mammary tumor cell lines [128] also enhanced the proliferative and pro-angiogenic phenotype of adipose progenitor cells, and inhibited adipose differentiation (Figs. 2.3A-C).

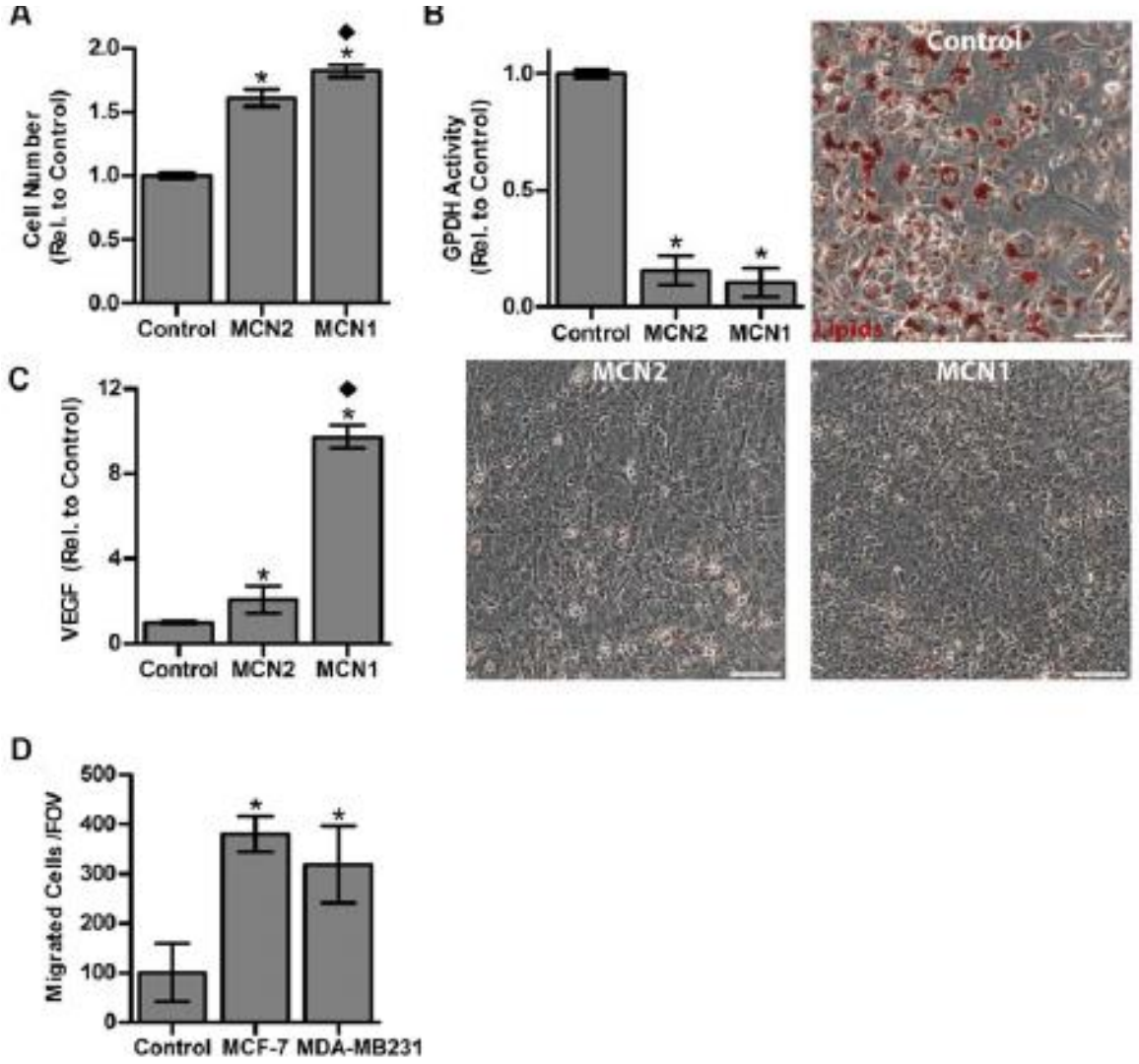

Fig. 2.3. Effect of tumor-derived soluble signals on 3T3-L1 cells. (A) Cell counting indicated enhanced 3T3-L1 cell numbers with TCM supplementation from two mouse breast cancer cell lines (MCN1, MCN2) as compared to control medium (n = 4). (B) Adipogenic differentiation significantly decreased with murine TCM treatment relative to control conditions as assessed by spectrophotometric analysis of GPDH activity and Oil Red O staining (n = 4) (Scale bar = 20 μm). (C) Murine TCM also significantly increased VEGF secretion by 3T3-L1s as measured by ELISA (n = 4). (D) Using a transwell assay, 3T3-L1 migration was enhanced towards TCM from MDA-MB231 and MCF-7 as compared to control medium (n = 3). **P* < 0.05 from control; ♦*P* < 0.05 from MCN2 condition.

To assess whether tumor cells actively recruit ASCs, we performed a transwell migration assay with TCM, which revealed that tumor cells attract adipose progenitor cells towards their respective location by enhancing their directed migration (Fig. 2.3D). Collectively, these data suggest that tumor cell-secreted soluble factors enhance the pro-angiogenic cell population in the tumor stroma by guiding ASC behavior. As TCM similarly modulated ASCs and 3T3-L1 behaviors, and because data generated with primary cells are typically more robust and generalizable the studies described in the following experiments were primarily performed with ASCs.

Tumor-secreted soluble factors enhance ASC differentiation into ECM-stiffening myofibroblasts

Myofibroblasts represent an abundant and pro-angiogenic cellular component of the tumor stroma whose differentiation is enhanced in the presence of reduced signaling by the adipogenic transcription factor PPARγ[144,145]. Accordingly, ASCs exposed to TCM exhibited increased expression of α-SMA relative to control conditions (Fig. 2.4A), whereby MDA-MB231 exerted a more pronounced effect than MCF-7 (Fig. 2.5A). Next, we evaluated whether tumor cell-derived transforming growth factor-beta (TGF-β) [146], which is pivotal to myofibroblast differentiation and secreted at higher levels by more malignant tumor cells [147] may be involved in inducing phenotypic changes of ASCs. Control media was supplemented with TGF-β at levels found in MDA-MB231-TCM, and this treatment induced ASC differentiation into myofibroblasts as suggested by immunofluorescence and Western Blot analysis (Figs. 2.4A, 2.5A, and 2.5B). Furthermore, addition of a TGF-β epitope-blocking antibody to TCM abrogated myofibroblast differentiation. While these data verify that tumor-secreted TGF-β functions as an upstream mediator of ASC differentiation into myofibroblasts (Fig. 2.4A) other molecules may also play a role. Comparison of control media as well as TCM from MCF-7 and MDA-MB231 via a cytokine antibody array revealed that interleukin-8 (IL-8), VEGF, tumor necrosis factor receptor 1 (TNFR1), and

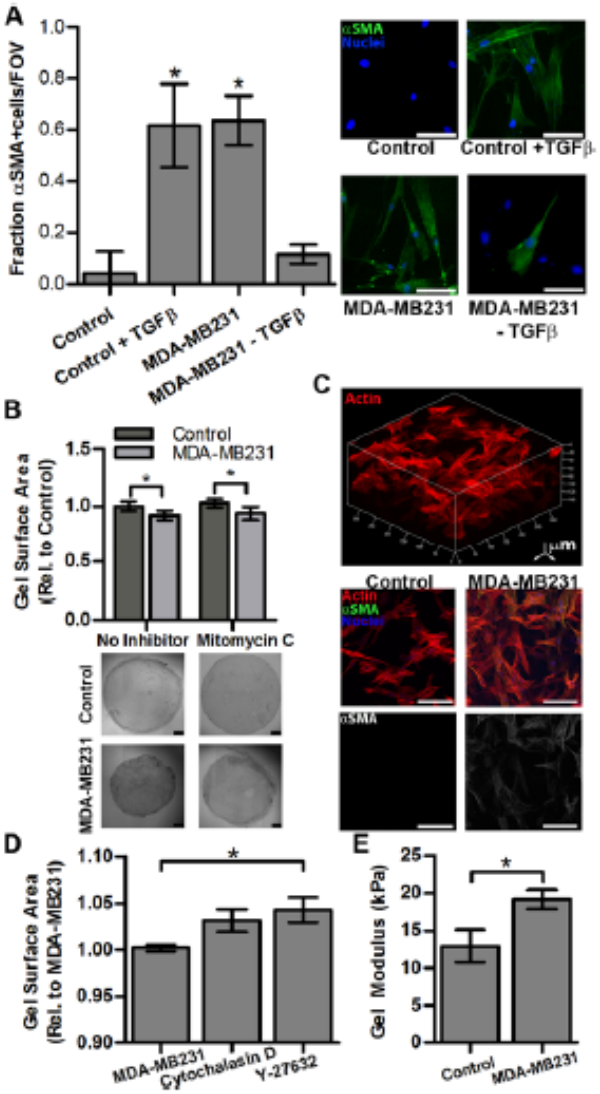

Fig. 2.4. Tumor-secreted soluble factors enhance ASC differentiation into myofibroblasts. (A) Treatment of ASCs with TCM from MDA-MB231 significantly increased the number of α-SMA (green) positive cells as quantified by immunofluorescence image analysis. Addition of TGF-β to control media (control + TGF-β) mimicked this effect, while blockade of TGF-β in TCM using a neutralizing antibody (MDA-MB231 - TGF-β) inhibited it (n = 4) (Scale bar = 100 μm) **P* < 0.05 from control and MDA-MB231-TGF-β conditions. (B) Collagen gels seeded with ASCs contracted significantly more when cultured in TCM as compared to control medium (n = 6), which occurred even in the presence of the proliferation inhibitor mitomycin C (Scale bar = 500 μm). (C) Confocal imaging revealed that ASCs within these gels developed stress fibers necessary to generate contractile tension, but only differentiated into α-SMA positive cells in the presence of TCM (Scale bar = 100 μm). (D) Pharmacological inhibition of cytoskeletal tension using cytochalasin D and Y-27632 contributed to the release of the contracted gels as determined via an increase in surface area (n = 3). (E) ASC-seeded collagen gels cultured in the presence of TCM were significantly stiffer relative to gels maintained in control media as determined by confocal-based stiffness measurements (n = 5) **P* < 0.05.

matrix metalloproteinase 3 (MMP3) were enhanced in the different TCM (Fig. 2.5C). As IL-8 has been related to myofibroblast differentiation in prostate cancer [148] and was enhanced in MDA-MB231 vs. MCF-7 TCM (Fig. 2.5D), we assessed its effect on ASC myofibroblast differentiation. Results from these studies elucidated that IL-8 regulates ASC differentiation into myofibroblasts in a dose-dependent manner (Fig. 2.5E). These findings are of particular interest as myofibroblasts themselves can up-regulate IL-8 [149], which may further promote ASC differentiation into myofibroblasts. Myofibroblasts mediate tissue stiffening by altering ECM composition and enhancing contraction. In particular, increased collagen I deposition has been associated with increased tumor stiffness and malignancy[33].

Our results support that ASC exposure to tumor-derived paracrine signals may contribute to this because ASCs produced significantly more procollagen I (6.0 ± 1.1-fold) and collagen I (4.2 ± 1.1-fold) when treated with TCM rather than control media (Fig. 2.6). Furthermore, ASCs seeded into microfabricated, free-floating 3-D collagen disks differentiated into myofibroblasts, developed stress fibers, and contracted significantly more when cultured in the presence of TCM as compared to control media (Figs. 2.4B and C). These variations in gel contraction were mediated by differences in TCM-mediated changes in myosin-mediated cell contractility rather than proliferation. Specifically, pharmacological inhibitors cytochalasin D (i.e., an agent preventing actin polymerization) or Y-27632 (i.e., an inhibitor of pROCK and thus RhoA signaling) added at levels not affecting cell viability restored the diameter of previously contracted gels (Fig. 2.4D), whereas disks cultured in TCM in the presence of mitomycin C contracted markedly more than similarly treated control disks (Fig. 2.4B). To more fully elucidate whether the integrated effects of varied ECM deposition and contraction indeed contribute to enhanced tissue rigidity, the mechanical properties of ASC-seeded disks were analyzed following culture in control or TCM. The shear modulus of these constructs was determined by applying a shear force to one side of a sandwiched gel while measuring the displacement of a photobleached line within the gel[136].

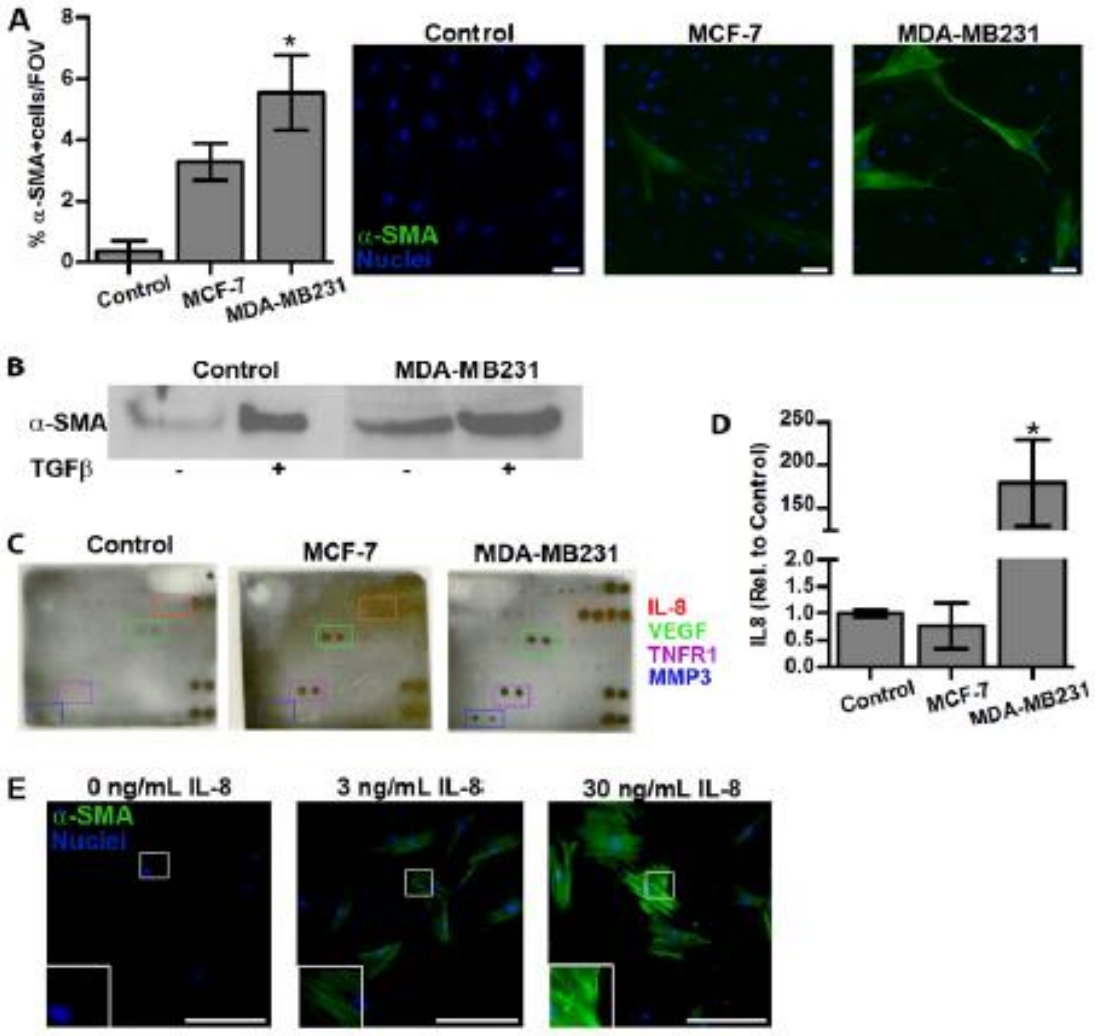

Fig. 2.5. Effect of tumor-derived soluble factors on ASC myofibroblast differentiation. (A) Immunofluorescence analysis indicates that ASCs up-regulate α-SMA more significantly with TCM from MDA-MB231 as compared to TCM from MCF-7 or control cells (n = 4) (Scale bar = 50 μm). (B) Western blot analysis of equally loaded samples shows elevated levels of α-SMA in ASCs treated with MDA-MB231 TCM, which were further enhanced by addition of TGF-β. (C) Cytokine array analysis indicates increased levels of noted cytokines within TCM as compared to control media. (D) ELISA of IL-8 detects greatest levels within MDA-MB231 TCM (n = 3). (E) Exposure of ASCs to relevant concentrations of IL-8 increased α-SMA and stress fiber formation (insets) in a dose-dependent manner (Scale bar = 200 μm). **P* < 0.05 from all other conditions.

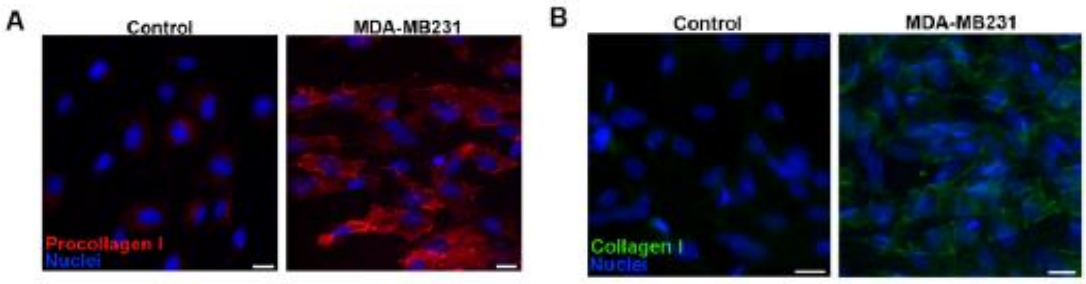

Fig 2.6. Effect of tumor-secreted soluble factors on ASC collagen deposition. (A) ASCs cultured in MDA-MB231 TCM exhibited increased collagen type I matrix assembly relative to ASCs maintained in control medium as indicated by positive staining for type I procollagen and (B) collagen. (Scale bar = 20 μm).

Our results indicate that TCM-treated collagen cultures were 1.5-fold stiffer than the control constructs (Fig. 2.4E), confirming the effect of tumor-derived soluble factors on ASC-mediated changes in tissue stiffness. These changes may be explained by varied matrix contraction and irreversible changes in ECM deposition mediated, for example, by increased collagen crosslinking due to enhanced lysyloxidase (LOX) expression by myofibroblasts [150] and/or deposition of additional fibrillar ECM components such as fibronectin[31].

ASCs respond to ECM mechanical properties in a tumor-dependent manner

Both normal and tumorigenic cells respond to increased matrix stiffness by adjusting integrin-dependent adhesion, traction forces, and subsequent downstream signaling [123,151] with effects on cell proliferation and differentiation [46]. To test the ability of ASCs to react to tumor-derived and/or self-imposed changes in matrix stiffness we evaluated their adhesion characteristics and corresponding activation of mechano-regulated signaling pathways using hydrogels of pathologically-relevant stiffness [122]. Specifically, use of collagen-coated polyacrylamide gels allowed control over mechanical properties of the culture substrates without affecting adhesion ligand density, which can independently affect cell behavior [152]. ASCs spread significantly more on substrates mimicking breast tumor rigidity (~10kPa [122])

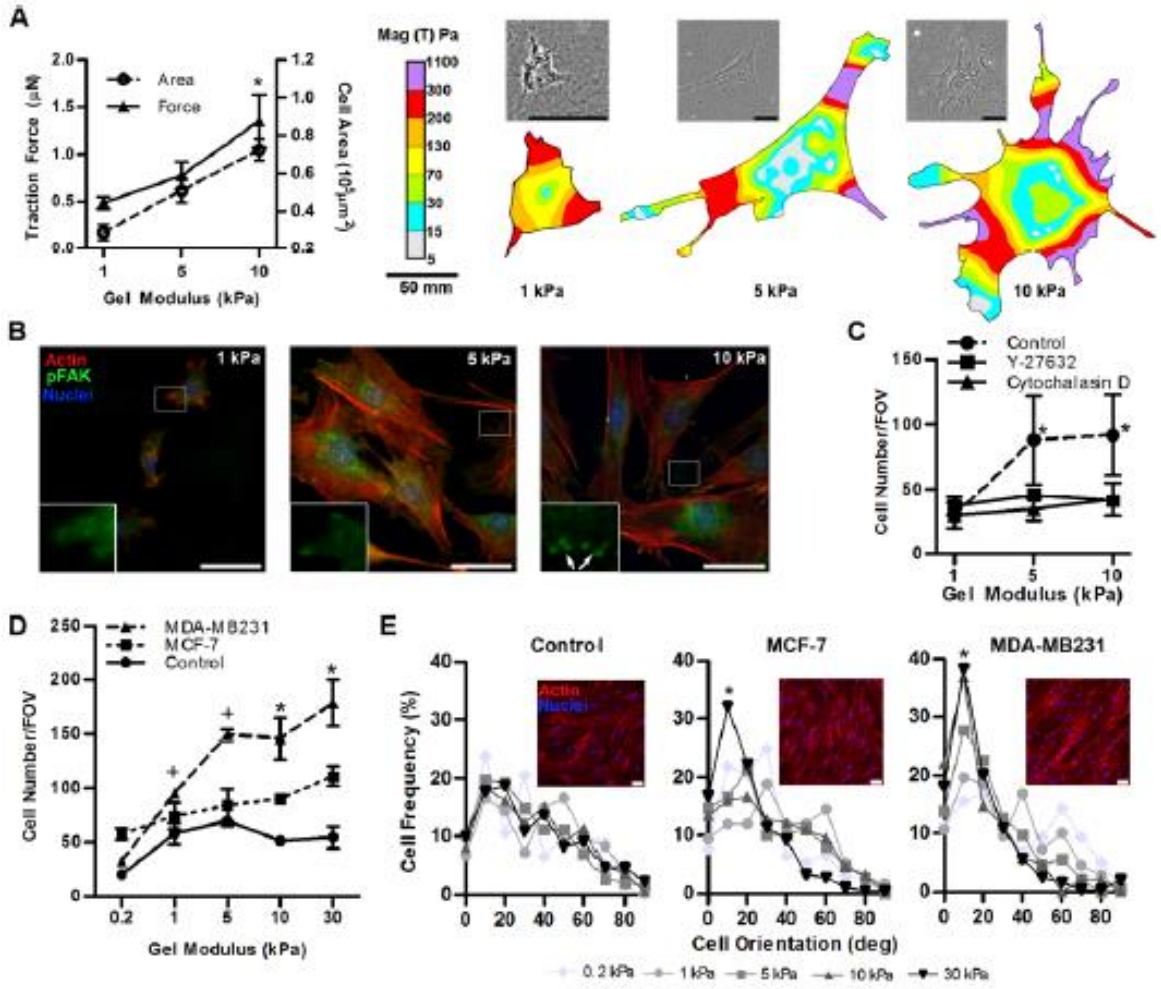

Fig. 2.7. ASC response to matrix mechanical properties. (A) Traction Force Microscopy indicated that ASCs cultured on hydrogels of increased stiffness spread significantly more and exert greater traction forces relative to cells cultured on soft matrices; representative ASC phase images with corresponding traction maps are shown (n = 13-32, error bars represent standard errors) (Scale bar = 50 μm) **P* < 0.05 from 1 kPa condition. (B) Immunofluorescence indicates increased recruitment of pFAK to ASC focal adhesions on stiffer matrices (white arrows) (Scale bar = 20 μm). (C) Cell counting suggested that increased matrix stiffness enhances ASC numbers and that pharmacological inhibition of cytoskeletal tension with Y-27632 or cytochalasin D inhibits this effect (n = 4). (D) ASC numbers on stiff matrices were further enhanced with culture in TCM whereby TCM from MDA-MB231 exerted a more pronounced effect than TCM from MCF-7 (n = 3) **P* < 0.05 between all conditions; +*P* < 0.05 between MDA-MB231 and control conditions. (E) Image analysis of the deviation from the average angle of phalloidin-stained cells revealed that ASC alignment represented an integrated effect of both substrate stiffness and tumor malignancy; 10 kPa represented a critical threshold of alignment in the presence of MDA-MB231 TCM, while 30 kPa were necessary with MCF-7 TCM (Scale bar = 50 μm) **P* < 0.05.

relative to substrates approximating premalignant (~5kPa) and adipose tissue (~1kPa [122]) stiffness (Fig. 2.7A). Traction force microscopy (TFM) confirmed that these morphological changes were accompanied by greater traction forces of ASCs on stiffer relative to more compliant matrices (Fig. 2.7A). These observations directly correlated with the recruitment of phosphorylated focal adhesion kinase (FAK) to focal adhesions (Fig. 3B, pFAK[Y397]), a result of activated Rho-ROCK signaling due to force-induced changes in adhesion dynamics [153]. Accordingly, ASC number was greater on stiffer matrices, and administration of cytochalasin D and Y-27632 inhibited this effect (Fig. 2.7C) confirming that Rho-ROCK mediated changes in cytoskeletal tension enable ASCs to respond to ECM stiffness.

To broadly assess stiffness-dependent cellular responses to a more relevant, biocompatible material that can be used for adipose tissue engineering and breast reconstruction applications[154,155], we cultured adipose progenitors on RGD-modified alginate disks similarly mimicking normal, premalignant, and cancerous breast tissue stiffness. Interestingly, increased stiffness recapitulated the effects of TCM and promoted the proliferative capacity and VEGF-secretion of these cells, while inhibiting their adipogenic differentiation (Fig. 2.8). These results are consistent with previous studies, which indicate elevated adipocyte conversion on more compliant matrices[46,156] and with less spread, rounder cell morphology[157].

To investigate whether tumor-secreted soluble factors enhance ASC response to ECM rigidity, ASCs were cultured on polyacrylamide substrates of a broad range of stiffnesses (0.2-30 kPa)), in the presence or absence of TCM from MCF-7 or MDA-MB231. Cell growth was commensurate with increasing stiffness whereby the level of tumor malignancy affected ASC stiffness response. More specifically, TCM from the more malignant MDA-MB231 cells increased cell growth on gels of lower stiffness relative to TCM of the less malignant MCF-7 (Fig. 2.7D). Furthermore, the combined effects of ECM stiffness and tumor-derived soluble factors promoted cellular alignment on stiffer, but not soft,

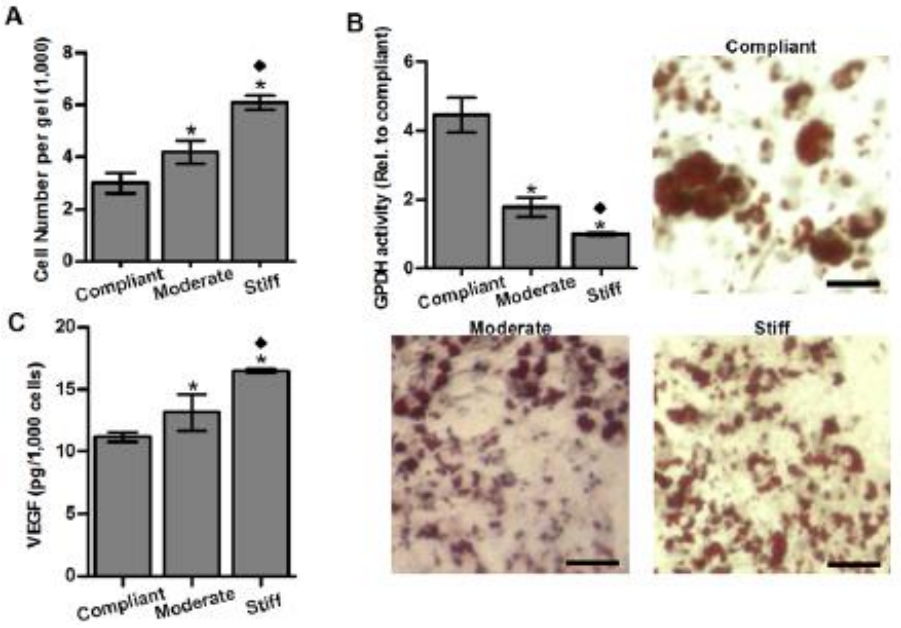

Fig. 2.8. Effect of matrix stiffness on adipose progenitors. Culture of 3T3-L1s on RGD-modified alginate hydrogels mimicking stiffness of normal (compliant, ~1.8 kPa), moderately diseased (~5.2 kPa) and malignant breast tissue (stiff, ~12 kPa) demonstrate that matrix mechanical properties mediate similar effects on adipose progenitors as tumor-derived soluble factors. (A) Enhanced matrix stiffness increased cell numbers (n = 8), (B) decreased adipogenesis as determined by GPDH analysis and Oil Red O-staining, (n = 3), and (C) enhanced VEGF secretion as measured by ELISA (n = 4). *$P < 0.05$ from compliant condition. ♦$P < 0.05$ from moderate condition. (Scale bar = 50 μm.)

matrices, and this effect was more pronounced with TCM from MDA-MB231 than MCF-7 (Fig. 2.7E). Collectively, these results suggest that tumor-secreted factors dramatically enhance adipose-derived cell responses to stiffness leading to (i) an increased contractile cell population, and (ii) directed force generation[158], which may ultimately exacerbate tumor rigidity and hence malignancy.

ASCs modulate tumor progression in vivo

To determine the relevance of our *in vitro* findings to tumor growth *in vivo*, ASCs and MDA-MB231 cells were injected individually or in combination into the cleared mammary fat pad of immunocompromised mice. Co-injection of MDA-MB231 with ASCs yielded larger tumors than delivery

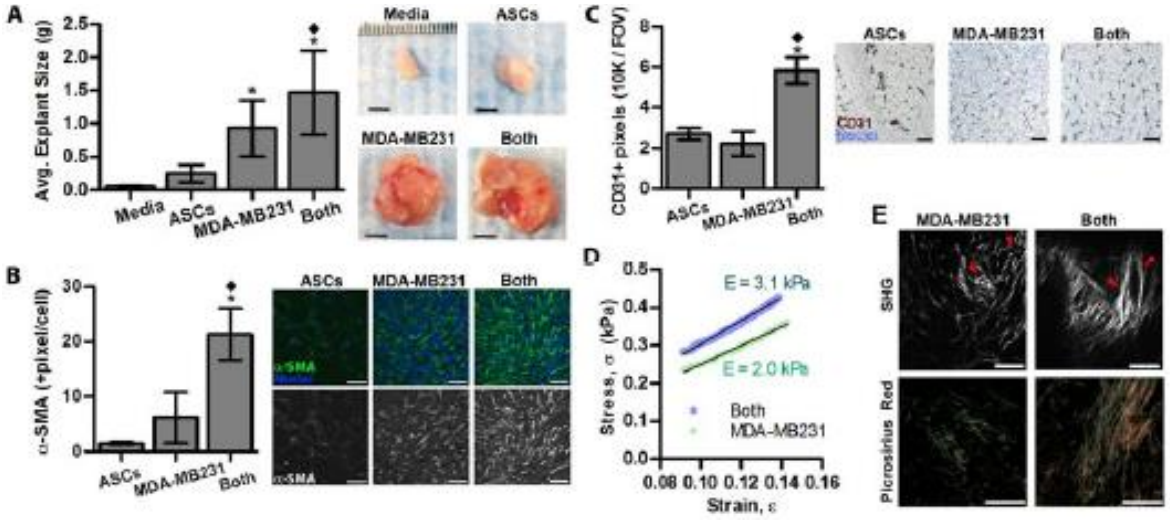

Fig. 2.9. ASCs modulate tumor progression *in vivo*. (A) Tumors resulting from the co-injection of ASCs and MDA-MB231 cells (Both) (n = 12) were significantly larger than tumors formed by MDA-MB231 cells alone (n = 12). Soft tissue explants generated from injected ASCs (n = 12) or Media (n = 2) are shown for a comparison (Scale bar = 5 mm). (B) Immunofluorescence analysis indicates that α-SMA levels were greatest in the explants resulting from co-implantation of ASCs and MDA-MB231 cells as compared to those from MDA-MB231 and ASCs alone (Scale bar = 50 μm). (C) Similarly, the density of CD31+ blood vessels was enhanced in explants from the co-implanted group (Scale bar = 20 μm). For α-SMA and CD31+ image analysis, ASC (n = 6), Both (n = 6), and MDA-MB231 (n = 12) explants were analyzed. (D) Mechanical analysis of tumor sections via DMTA. The mean stress-strain profile was measured in PBS at room temperature through the low-strain (9-14%) elastic regime. The engineering stress σ versus strain ε curve represents the average of 2 compressions per tumor section performed on 4 tumor sections from MDA-MB231 alone, and 9 tumor sections from the co-implantation group (see SI Materials and Methods). The mean Young's modulus, *E*, was extracted from the slope of the stress-strain curve, $\sigma = E\,\varepsilon$. (E) Compared to tumors from MDA-MB231, co-injected tumors contain more mature and linearized collagen fibers as revealed by second harmonic generation (SHG) imaging and picrosirius red staining of cross-sections, which is further quantified in Fig. S9. For (A-C) $^{*}P < 0.05$ from ASCs condition; $^{\blacklozenge}P < 0.05$ from MDA-MB231 condition.

of tumor cells alone in accordance with previous results [159,160] (Fig. 2.9A). In contrast, injected ASCs largely formed adipose tissue (Fig. 2.9C and 2.13A, B) that was similar in size to explants from sham-injected media suggesting that the different size of the tumors was caused by varied tumor malignancy rather than the additional volume assumed by the co-injected ASCs. Furthermore, tumors resulting from the mixture of ASCs and MDA-MB231 cells appeared more locally invasive upon explantation relative to MDA-MB231-borne tumors, which were easily demarcated for dissection. Pathological evaluation of H&E-stained cross-sections confirmed this assessment and revealed an enhanced degree of local invasion

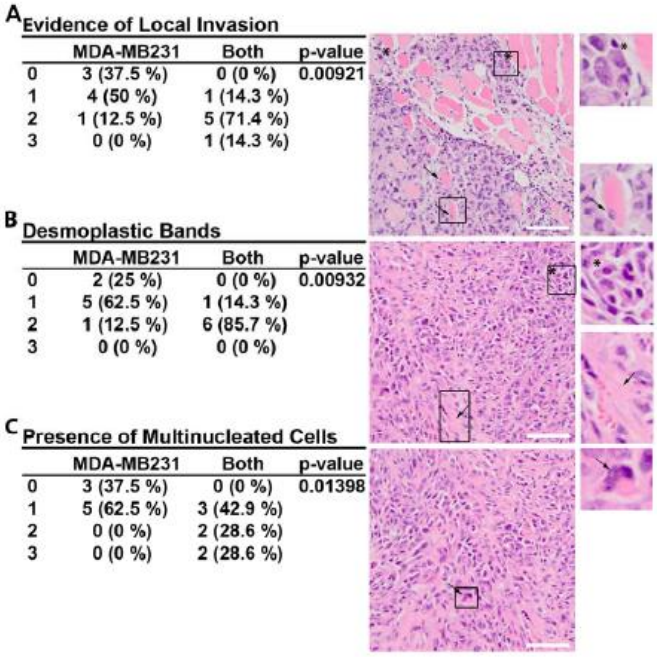

Fig. 2.10. ASCs modulate tumor progression *in vivo.* Representative H&E sections of tumors resulting from co-injection of ASCs and MDA-MB231 cells (Both) (n = 7) or MDA-MB231 cells alone (n = 8) scored for pathological features of malignancy are shown (Scale bar = 40 μm). (A) Co-implanted tumors exhibited enhanced local invasion relative to MDA-MB231 tumors as evidenced by indistinct tumor boarders. Tumor cells infiltrated and separated skeletal myofibers (*) and often surrounded atrophic skeletal myofibers (→). (B) Enhanced desmoplasia in the co-implanted group was evident as variably sized, pale to brightly eosinophilic, loose bands of connective tissue (→) scattered within the tumor. Additionally, rossettes (*) which indicate an anaplastic phenotype in tumors, were evident in the co-implanted tumors. (C) Multinucleated tumor cells (→), indicating the breakdown of cell division machinery, are also more evident in the co-implanted tumors as compared to MDA-MB231 tumors alone.

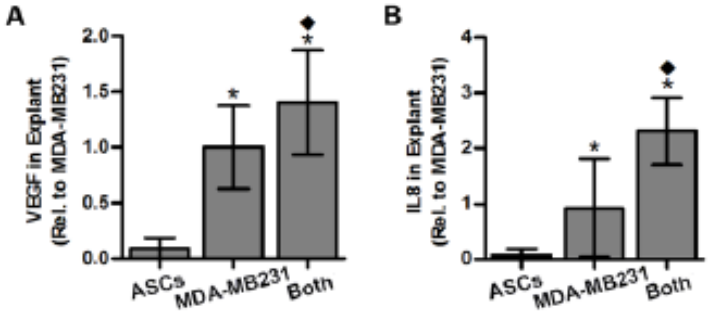

Fig. 2.11. ASCs increase pro-angiogenic factor levels in tumors. (A) VEGF and (B) IL-8 content was enhanced within tumors containing ASCs as compared to those from only MDA-MB231 cells as revealed by ELISA of lysates. *$P < 0.05$ from ASC condition; ♦$P < 0.05$ from MDA-MB231 condition. ASC (n = 6), ASC/MDA mixture (n = 6), and MDA (n = 12) implants were analyzed.

and desmoplasia for the co-implanted tumors versus the control tumors (Figs. 2.10A, B). Additionally, cytological features of malignancy (multinucleated cells and rosettes) were augmented in the co-implanted group as compared to the MDA-MB231 group (Fig. 2.10). To correlate variations in tumor growth with differences in myofibroblast differentiation, immunohistochemical analysis was performed, which confirmed that the density of α-SMA myofibroblastic cells (Fig. 2.9B) was increased in tumors originating from co-injection of both cell types rather than tumor cells alone. Circulating ASCs can be recruited to and associate with blood vessels in the form of α-SMA pericytes [161]. In our co-implantation studies, however, immunohistochemical analysis of desmin, a pericytes marker [162], verified that the majority of α-SMA positive cells were myofibroblasts rather than pericytes as desmin staining showed no significant difference ($p=0.33$) between co-implanted and control tumors. Nevertheless, blood vessel density was greater in the co-implantation group (Fig. 2.9C), and ELISA of tumor lysates suggested that ASC/myofibroblast secretion of pro-angiogenic VEGF and IL-8 [125,149] may have contributed to these differences (Fig. 2.11A, B).

To evaluate if varied myofibroblast content correlated with increased stiffness, we determined the mechanical properties of the different tumors via Dynamic Mechanical Thermal Analysis (DMTA) compression tests on 1 mm-thick tumor sections, in the elastic regime of deformations. The mean Young's modulus (*E)* was more than 50% higher in tumors generated by co-implantation of ASCs than in those generated in the absence of ASCs (3.1 ± 1.2 kPa vs. 2.0 ± 0.8 kPa) (Figs. 2.9D and 2.12). Data from the full elastic and plastic regime of deformations (Fig. 2.12) additionally indicated that tumors from the co-implanted group exhibit both higher stiffness and a smaller range of elastic (reversible) deformations than tumors grown without ASCs (Fig. 2.12B). Consistent with these results, tumors resulting from co-injection contained more procollagen I and collagen (Figs. 2.13A, B), were characterized by enhanced collagen fibril maturity and linearity (Figs. 2.13C, D), and likely also comprised increased fibronectin [31].

Such changes are indicative of enhanced desmoplasia and aggressiveness [33] and may further contribute to ASC-mediated changes in tumor growth; decellularized matrices of TCM-preconditioned adipose progenitors increased tumor cell growth relative to matrices from control cells in a manner dependent on generation of cytoskeletal tension (Fig. 2.13E). Nevertheless, additional conditions including paracrine signaling between ASC-derived cells and tumor cells may also contribute to the observed changes in tumor growth in our studies[159].

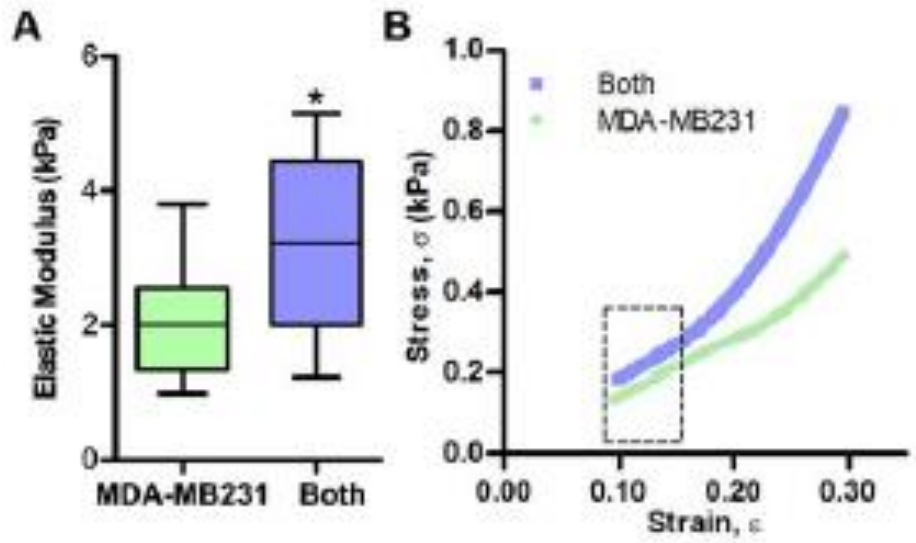

Figure 2.12. ASCs increase tumor stiffness. Tumors formed *in vivo* by MDA-MB231 alone (MDA-MB231) or MDA-MB231 in the presence of ASCs (Both) were analyzed for stiffness via DMTA of cross-sections in PBS at room temperature (n = 8-18). (A) The lines within the boxes indicate the mean Young's modulus for each condition, while the colored boxes span the 25th to 75th percentile. The whiskers correspond to the maximum and minimum measured Young's modulus values. The mean Young's modulus of the tumor sections from the co-implanted group (Both = 3.1 ± 1.2 kPa) is approximately 50% higher than that of the sections from the tumors grown without ASCs (MDA = 2.0 ± 0.8 kPa). (B) DMTA mean stress-strain profiles of tumor sections over the full regime of elastic and plastic deformation (n = 4-9). The boxed-in area corresponds to the low-strain (9-14%) regime from which the Young's moduli (shown in A) were extracted. Tumors from the co-implanted group (Both) exhibit not only higher moduli but also a smaller range of elastic deformations, i.e., earlier onset to plastic deformation than tumors grown without ASCs (17% versus 23%), and more pronounced stiffening prior to rupture, as indicated by the steeper stress-strain slope at high strains in the co-implanted group. *P < 0.05 from MDA-MB231.

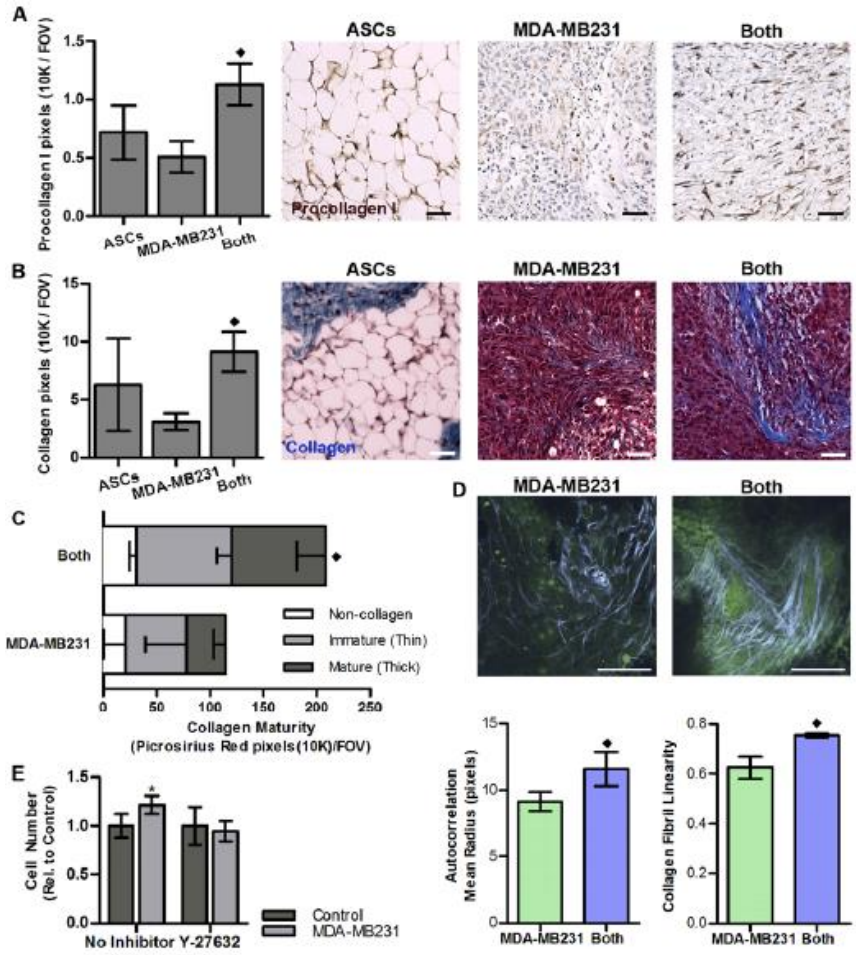

Fig. 2.13. ASCs modulate collagen deposition and structural changes in tumors, which, in turn, alters tumor cell behavior. (A) Immunohistochemical analysis of tissues subjected to co-injection of ASCs and MDA-MB231 cells (Both) or either cell type alone indicated increased collagen synthesis with co-injection, as indicated by greater levels of the precursor type I procollagen (brown). (B) Masson's Trichrome staining confirmed greater collagen deposition (blue) in tumors formed by both ASCs and MDA-MB231 cells as compared to tumors formed by MDA-MB231 only. **P* < 0.05 from ASC condition; ♦*P* < 0.05 from ASC condition from MDA-MB231 condition. For type I procollagen and collagen image analysis, ASC (n = 6), ASC/MDA mixture (n = 6), and MDA (n = 12) implants were analyzed. (Scale bar = 20 μm.) (C) Images captured from picrosirius red-stained cross-sections via polarized light microscopy (as shown in Figure 4e) were analyzed for non-collagen (white), immature/thin collagen (green), and mature/thick collagen content. Co-implanted tumors (Both) contain more mature collagen fibrils than control tumors. (D) A 2D spatial autocorrelation analysis based on SHG images shows that the average collagen framework size (autocorrelation mean radius) in the ASC-containing tumor explants (Both) is significantly greater than their counterparts (MDA-MB231). Additionally, analysis of fibril linearity (a ratio of the shortest distance to the full-length between fibril ends) indicate that collagen fibrils in tumors from the co-implantation group (Both) are straighter than those from control tumors. **P* < 0.05 from MDA-MB231. For picrosirius red and SHG image analysis, MDA-MB231/ASC (n = 3) and MDA-MB231 (n = 3) explants were analyzed. (E) MDA-MB231 grow more on decellularized matrices from MDA-MB231-conditioned 3T3-L1 than matrices from 3T3-L1 preconditioned with control media. These differences are related to varied cytoskeletal tension as treatment with the pROCK inhibitor Y-27632 inhibits this effect (n = 6). **P* < 0.05 from control.

2.6. Conclusions

Breast cancer cell signaling may undermine normal ASC function to form a physicochemical microenvironment that promotes tumorigenesis. Epidemiologically, controversy still exists as to whether fat grafting procedures contribute to recurrence of breast cancer[163]. Our findings suggest this possibility and long-term follow up studies will be needed in which not only the use of 'simple' fat, but implants concentrated with ASCs are evaluated. Additionally, the results presented herein provide a possible explanation for why obesity - associated with an increased pool of ASCs - represents a risk factor for breast cancer[164,165] and highlight novel design parameters for ASC-based breast reconstruction. Specifically, ASCs are frequently applied using relatively rigid biomaterial scaffolds or hydrogels[166,167], but vehicles mimicking the mechanical properties of adipose tissue and potentially co-delivery of morphogens are needed to ensure adipose tissue functionality. In particular, PPARγ agonists may represent attractive candidate molecules due to their ability to promote adipogenesis, while inhibiting myofibroblast differentiation[145]. Definition of whether tumor-related changes of ASC functions are due to selective mechanisms or cell fate instruction will also be needed to help increase the safety of such applications. Although the goal of the present study was to better define the physicochemical contributions of ASCs to breast cancer, a variety of other cancers may also depend on such phenomena. Because ASCs can be activated and released into the circulation to participate in tumor progression at spatially distinct sites they may, for example, impair the prognosis of prostate [168] and colorectal cancer patients [169]. Collectively, therapeutic application of ASCs independent of site should be carefully considered in patients previously treated for cancer, and the use of cell delivery vehicles accurately mimicking non-tumorigenic microenvironmental conditions should be a prerequisite.

CHAPTER 3

CANCER-ACTIVATED ADIPOCYTES AND THEIR ROLE IN EXTRACELLULAR MATRIX REMODELING AND ANGIOGENESIS

3.1. Contributors

Co-authors of this chapter made the following contributions: Jacqueline Gonzalez, undergraduate student in the Fischbach lab performed 2D experiments to analyze the phenotypic changes of adipocytes in response to tumor-derived factors. Seth Moore, undergraduate student in the Fischbach lab analyzed the contractile behaviors of adipocytes in response to tumor-derived factors. Manuel Gregoritza, visiting scholar in the Fischbach lab assessed the adipogenic activity of adipocytes cultured in a 3D system. Dr. L.T. Vahdat provided breast tumor specimens. Dr. Clifford A. Hudis provided human mammary tissue from cancer-free individuals. Prof. Claudia Fischbach guided the direction of project, assisted with experimental design and provided insight for data analysis.

3.2. Abstract

Due to the increasing socioeconomic impact of obesity and its associated diseases, both adipocytes and the metabolic and endocrinal roles of adipose tissue have recently been highlighted in the development and progression of obesity-associated diseases. Recent studies indicated the loss of adipogenic features in adipocytes adjacent to cancer cells as well as a high ratio of fibroblasts to adipocytes in tumor stroma, implying a possible contribution of adipocytes to the formation of cancer-activated fibroblasts, called myofibroblasts. Thus, we hypothesize that tumor-derived soluble factors induce conversion of adipocytes into myofibroblastic cells, and that the converted adipocytes stimulate ECM remodeling and pro-angiogenic signaling. First, we assessed the morphological changes of

adipocytes in tumor stroma, and then examined whether the changes were mediated by tumor-derived soluble factors through culturing adipocytes with tumor-derived soluble factors. Our findings indicate that adipocytes, both in 2D and 3D cultures, lost their adipogenic phenotype in response to tumor-derived soluble factors while gaining myofibroblastic features. TCM-treated adipocytes contained more α-SMA positive cells that exhibited increased contractility. Also, they produced more matrix protein such as fibronectin and collagen. Moreover, TCM-treated adipocytes stimulated pro-angiogenic signaling of vascular endothelial growth factor (VEGF) and interleukin-8 (IL-8), which ultimately promoted sprouting of human umbilical vascular endothelial cells (HUVECs) in our 3D co-culture system. Taken together, our study suggests the possible contribution of adipocytes to increasing myofibroblastic cell population and consequently tumor stroma remodeling. This study will aid in understanding the pro-tumorigenic potential of adipocytes and ultimately a link between obesity and cancer.

3.3. Introduction

Obesity and its associated diseases, such as type 2 diabetes, hypertension and cancer, have emerged as a public health concern, the metabolic functions of adipose tissue have received more attention[170]. Adipocytes serve as an energy depot as well as endocrine organ[171]. In health, adipocytes properly regulate lipid metabolism in concert with various adipokines and hormones such as leptin, adiponectin and insulin[172]. In addition, adipocytes also secrete inflammatory cytokines such as interleukin 6 (IL-6) and TNF-α[173]. However, during disease progression their well-controlled functions go awry through direct or indirect interactions with local inflammatory or cancer cells. Therefore, adipocytes potentially play a role promoting the development and progression of obesity-associated diseases[170,173].

In particular, an increasing number of studies highlight the metabolic and endocrinal dysfunction of adipocytes in exacerbating various types of cancer such as breast, prostate and ovarian cancer; all of

these cancer types have adipocytes in close proximity. For example, previous reports showed that crosstalk between adipocytes and ovarian cancer cells can upregulate the lipolysis of the adipocytes and consequently provide abundant fatty acid to fuel primary and metastatic ovarian tumor growth[174,175]. In addition, adipocytes at the invasive region of the tumor facilitated breast cancer cell invasion via stimulation of epithelial to mesenchymal transition of the cancer cells in an IL-6-dependent manner[176]. Interestingly, it was also noted that the cancer-activated adipocytes lost adipogenic features but acquired fibroblastic morphology in tumor stroma implying that adipocytes can be a source for cancer-activated fibroblasts (CAF)[173].

Our previous studies suggested that α-smooth muscle actin (α-SMA)-positive CAF can be derived from adipose-derived stem cells (ASCs) upon the regulation of tumor-derived factors such as transforming growth factor-β (TGF-β) and IL-8[177,178]. The myofibroblastic ASCs, in turn, construct a pro-tumorigenic microenvironment by participating in dynamic extracellular matrix (ECM) remodeling and stimulating pro-angiogenic signaling[177]. However, whether adipocytes can contribute to the myofibroblastic cell population upon the presence of tumor-derived stimuli remains unclear. Interestingly, recent studies highlighted plasticity of adipocytes into progenitor-like cells showing that dedifferentiated adipocytes exhibit similar characteristics of ASCs such as proliferative and multi-lineage potential[85]. Thus, the cancer-activated adipocytes may also similarly contribute to tumor stroma remodeling via changing their phenotype to myofibroblastic cells.

Therefore, we propose that tumor-derived factors induce the conversion of mature adipocytes into myofibroblastic cells and that the converted adipocytes contribute to both ECM remodeling and pro-angiogenic activity. In this study, we assessed the phenotypic changes of mouse and human progenitor cell-derived adipocytes in response to malignant cancer cell-derived factors leveraging both 2D and 3D

culture systems. This study suggests a role for adipocytes in remodeling tumor stroma and ultimately will aid in understanding an adipocyte-mediated link between obesity and cancer.

3.4. Materials and methods

Analysis of adipocyte size in mouse mammary tissue and tumors

Orthotopic mammary tumors were obtained as previously described[48]. Briefly, MDA-MB231 cells (1 x 10^6) were prepared in 20 μL of DMEM/ Ham's F-12 (Gibco) containing 10 % FBS (Tissue Culture Biologicals) and 1 % antibiotics (penicillin/streptomycin, Gibco). Immediately the cell suspension was injected into the cleared mammary fat pad of 3 week-old female SCID/NCr mice (Charles River Labs, 01S11). Tumors were harvested 6 weeks after implantation, and their control mammary fat was harvested from the age-matched cancer free- female mice (SCID/NCr). The explants were then formalin-fixed, paraffin-embedded, and cross-sectioned for haemotoxylin and eosin (H & E) staining. The stained sections were imaged on a Zeiss Observer Z.1 microscope and AxioCam MRm camera and subsequently the surface area of individual adipocyte was measured using Image J (NIH). 20 to 30 adipocytes from 10 representative images per tissue and tumors or tissues were analyzed, and averaged. The procedures required for *in vivo* models were performed in accordance with Cornell University animal care guidelines.

Analysis of patient-derived breast tumor specimens

H & E stained human breast tissue and breast tumor specimen were obtained from 16 breast cancer patients with BMI (an index of weight to height) less than 25. The sections were imaged and analyzed for the surface area of adipocytes as described above. Human specimens were obtained in collaboration with Dr. Linda T Vahdat under the approval of IRB Study 0408007390 in Cornell Weill

Medical College, and human mammary tissues were obtained in collaboration with Dr. Clifford A. Hudis under approval of the Institutional Review Boards of Memorial Sloan-Kettering Cancer Center (MSKCC) and Weill Cornell Medical College. The samples were collected as previously described[179].

In vitro adipocyte preparation and cell culture

Mouse preadipocytes cell line, 3T3L1 cells (ATCC) and human adipose derived stem cells (ASCs) (Lonza) were used to produce *in vitro* adipocytes. The adipogenic potential of 3T3L1 cells (3T3L1s) and pluripotency of ASCs were previously confirmed[180,181]. 3T3L1s or ASCs were cultured on 2D culture plate in MEM (α-modification [αMEM], Sigma) with 10% FBS and 1% antibiotic or ADSC-GM (Lonza), respectively until they were 90% confluent. Then adipogenic differentiation of 3T3L1s was initiated by a treatment of insulin (Sigma), dexamethasone (Sigma), indomethacine (Fischer Scientific), corticosterone (Fischer Scientific), and 3-isobutyl-1-methylxanthine (IBMX) and then completed by supplement of insulin every other day up-to 8 days. ASCs were differentiated into adipocytes by supplement of commercialized hormonal cocktails PGM-2 (Lonza) for 2 weeks.

Tumor Conditioned Media (TCM) preparation

Tumor conditioned media (TCM) was collected as previously described[48]. Briefly, breast cancer cell line, MDA-MB231 cells (MDA-MB231) were incubated in αMEM (1% FBS, 1% antibiotic) for 24 hours and the media containing tumor-derived factors was collected. For control medium, cell-free αMEM (1% FBS, 1% antibiotic) was collected in the same manner. Then the media was normalized to cell number, concentrated through Amicon centrifugal filter unit (Millipore, MWCO = 3kDa), and reconstituted with media containing 1% FBS, 1% antibiotic to make 2-fold concentration of tumor-derived factors as final concentration.

Analysis of adipogenic features

Lipid accumulation of (trans-) differentiated 3T3L1s and ASCs was visually assessed and quantified by Oil Red O staining and extraction assay as previously described [132]. Cells were formalin-fixed and stained with Oil Red O (0.33% w/v in isopropanol, Sigma) for 2 hours. After the excess Oil Red O from samples was washed with PBS, the samples were imaged with a bright field microscope (Zeiss Observer Z.1 microscope). For the quantification of lipid accumulation, Oil Red O incorporated into lipid was extracted in 100% isopropanol (J.T. Baker) and the absorbance of the extracted Oil Red O was measured at 510 nm. Also, DNA concentration was measured to normalize the obtained Oil Red O optical density. For DNA quantification, cell lysates were collected in DNA lysis buffer and then measured for DNA content by QuantiFluor® dsDNA System (Promega) following the manufacturer's protocols. In addition, adipogenic activity was assessed via measuring glycerol-3-phosphate dehydrogenase (GPDH) activity. The supernatants were collected from the cell lysates in a buffer containing 50mM Tris, 1mM EDTA, and 1mM β mercaptoethanol (all from J.T. Baker). Subsequently the supernatants kept in ice were quickly mixed with dihydroxyacetone phosphate and oxidized nicotinamide adenine dinucleotide (NADH). The decrease in NADH absorbance at 340 nm was measured on a spectrophotometer over a 7 min period. The GPDH activity was normalized to total protein content as measured by BCA kit as manufacturer's protocol suggested (Thermo Scientific).

Immunofluorescence imaging analysis

For immunofluorescence, TCM or control media-treated adipocytes were formalin-fixed, blocked in 1% BSA (Fischer Scientific) in Phosphate buffered saline (PBS), and then incubated with primary antibodies of Fn (Invitrogen) and collagen (Millipore) in PBS containing 0.05% triton-x (EMD) and 1% BSA overnight at 4°C. Next day, the samples were washed in PBS and labeled by AlexaFluor 488

conjugated secondary antibody for Fn and collagen, and 4',6-diamidino-2-phenylindole (DAPI) for nuclei (All from Invitrogen). Subsequently the stained samples were mounted with Prolong® Gold reagent (Invitrogen) and then imaged with fluorescent microscope (Zeiss).

Western Blot analysis

Cell lysates were prepared in RIPA buffer containing protease and phosphatase inhibitor cocktail (all from Thermo Scientific), and 1mM phenylmethylsulfonyl fluoride (Fischer Scientific) in isopropyl alcohol (VWR). The protein concentration was quantified by BCA kit and the equal amount of the proteins was loaded to SDS-PAGE. The loaded proteins were separated and subsequently transferred to a PDVF membrane (Bio-Rad). The membrane was blocked in 5% milk powder in PBST and then incubated with primary antibodies targeting the proteins of interest including Fn, and collagen as well as house keeping proteins such as HSP90 (Santa Cruz) in 5% milk powder in PBST overnight at 4°C. Next day the membranes were incubated with HRP-conjugated secondary antibody (Novus Bio) at room temperature for an hour. Chemiluminescence detection was performed to visualize the probed protein using ECL kit (Thermo Scientific) based on manufacturer's protocol. To quantify the resulting blots, densitometry was performed via Image J and Adobe Photoshop CS4.

Isolation of adipocytes

ASC-derived adipocytes in 2D culture plate were trypsinized and their extracellular matrix was digested by 1.5mg/ml collagenase Type 1 (Worthington Biochemical Corp.). Then the cells were filtered through a 250μm cell strainer (Pierce) and centrifuged in Histopaque-1077 solution (Sigma) to separate ASCs from floating adipocytes. Isolated ASCs were cultured in DMEM/F12 (Gibco) supplemented 10% FBS (Tissue Culture Biologicals), 1% antibiotic (penicillin/streptomycin).

3D Adipocyte dedifferentiation in vitro model fabrication

For analyzing dedifferentiation of adipocytes in 3D context, we micro-fabricated adipocyte-embedded 3D collagen gels. This 3D collagen scaffold fabrication procedure was adopted from our previously published protocol[182]. First, collagen was collected from rat-tail tendon (Pel-Freez Biologicals), solubilized in 0.1% [v/v] acetic acid, lyophilized and then reconstituted back in acetic acid at a concentration of 15mg/ml. Then, 4-mm-diameter and 250-μm-thick round shape of polydimethylsiloxane (PDMS) micro-wells were fabricated using Sylgard® 184 silicone elastomer kit (Dowcorning) and their surface was treated by 1% [v/v] poly-ethylenimine (Aldrich) and then 0.1% [v/v] glutaraldehyde (Fischer scientific) to crosslink collagen gels with PDMS mold. The reconstituted collagen in acetic acid was neutralized to pH 7.2 and then mixed with $1x10^6$ of adipocytes to produce a final concentration of 0.6% collagen suspension. Subsequently, adipocyte-embedded collagen scaffolds were polymerized in the PDMS micro-well at 37°C. The completely polymerized collagen scaffolds were cultured in either TCM or control media for 7 days.

Contraction assay

The contractility of the transdifferentiated adipocytes was measured using free-floating collagen gels. Collagen gel fabrication procedure was similar to the one for a 3D collagen scaffold in a micro-well as described above. 500 μm thick and 4 mm in diameter of circular collagen disks were fabricated using a Plexiglas® template. 15 mg/ml of collagen in 0.1% acetic acid was neutralized to pH 7.2 with 1N NaOH, 10x and 1x media (DMEM/F12), then slowly mixed with isolated adipocytes ($1x\ 10^6$ cells/ml), and finally casted in the Plexiglas® mold[134]. Subsequently gels were cross-linked at 37°C for 30mins, then transferred into 24 well plate (VWR), and treated with hormonal cocktails for adipogenic differentiation as previously described. After the 2 week-long-treatment of the hormonal cocktails, the adipocytes in the

gels were then cultured in TCM or control medium on an orbital shaker up-to 2 weeks, with media changes every other day. Lastly, gel contraction was determined by calculating the amount of the reduction in the surface area of each gel between Day 0 and final time point by image J.

Pro-angiogenic Factor Measurement

After treating adipocytes with TCM or control media for 7 days, DMEM/F12 with 1% FBS and 1% antibiotics were added to the adipocytes and incubated for 24 hours. Then the media was collected and analyzed for the levels of VEGF and IL-8 via VEGF and IL-8 ELISA duo set (R&D), respectively. Also, the DNA content of each sample was collected and measured as previously described for normalization.

Endothelial cell invasion assay in 3D collagen scaffolds

To evaluate functional impacts of the dedifferentiated adipocyte-mediated pro-angiogenic signaling, HUVEC invasion assay was performed after treating adipocytes in 3D scaffolds with and without TCM for 7 days. After the treatment of TCM or control media, a monolayer of HUVECs ($475x10^3$ cells/mL) was seeded atop the adipocyte-encapsulated collagen scaffolds. After one hour, HUVEC invasion media containing HUVEC-GM, 1% [v/v] L-ascorbic acid (50 μg/mL; Acros Organics, Morris Plains, NJ), and 0.16% [v/v] tetradecanoyl phorbol acetate (50 ng/mL; Cell Signaling Technology, Inc., Danvers, MA) was added, and cultured for 4 days. For VEGF, IL-8 and their cognate receptor inhibition study, 500ng/ml of VEGF and IL-8 neutralizing antibodies or 500ng/ml of VEGFR2 and CXCR1 antibodies (all from R&D) were supplemented in the invasion media and cultured for the same period of time. The HUVEC was immunofluorescently stained for their surface marker, CD31 (Sigma-Aldrich), and the resulting HUVEC sprouting was assessed by confocal microscopy analysis. 5 to 6 top-

to-bottom images per sample were obtained by Zeiss 710 confocal microscope with a 25×/0.8 water immersion objective at 5μm intervals. Sprouting HUVEC was determined by their length, which is equal or longer than 15μm, and the number of HUVEC sprouts was manually counted throughout the Z-stack images. The presented number of sprouts per condition was obtained averaging the counts of three samples in each experiment (n=3).

Statistical analysis

Statistical differences between two conditions or among multiple conditions were calculated by Student's t-tests or ANOVA, respectively. For ANOVA, post-hoc pairwise comparisons were performed by Tukey's test. When a P-value was less than 0.05 based on two-sided testing, the difference between or among conditions was considered statistically significant. All tests were performed on Microsoft Exel and GraphPad Prism 5©. Unless otherwise noted, values are reported as the mean with error bars to indicate standard deviations.

3.5. Results

Adipocyte size is reduced in mouse and human mammary tumors

To see if there were any morphological differences between adipocytes in mammary tumors vs. mammary fat, first we microscopically assessed the morphological changes of adipocytes in mammary tumors and mammary fat sections. Adipocyte size has been linked to their functional changes and has been used as an important indicator of adipocyte dynamics[183]. Fewer adipocytes were found in both mouse and human mammary tumors as compared to respective control mammary fat. In addition, the size of cancer-associated adipocytes was significantly reduced as compared to that of normal adipocytes (Figs.

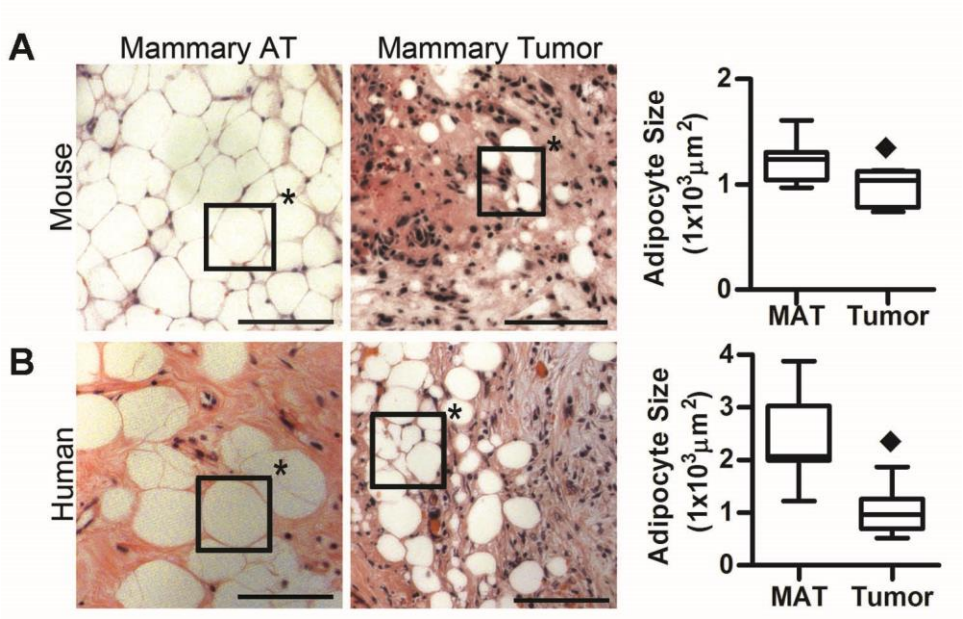

Fig. 3.1. Reduced size of adipocytes in mouse and human mammary tumors. (A) Microscopic assessment of H&E stained normal mouse mammary tissue and mammary tumor stroma showing that adipocytes in tumors were significantly smaller compared to those in tumor-free mammary fat. (B) Adipocytes in human mammary tumors became significantly smaller as compared to those in cancer-free mammary fat. (Scale bars = 100 μm). ♦$p < 0.05$.

3.1A and B). This finding substantiates previous findings showing a significant reduction of adipocyte size at the invasive edge of tumor stroma[176].

Tumor-derived soluble factors induce the loss of adipogenic features

To evaluate if loss of adipocyte features was mediated by tumor-derived soluble factors, we cultured adipocytes with tumor-derived soluble factors *in vitro*. First, adipocytes were obtained from mouse preadipocytes, 3T3L1 cells (3T3L1s) and human adipose-derived stem cells (ASCs). Then, adipocytes were cultured in 2D culture plate with or without tumor-conditioned media (TCM) containing soluble factors derived from the MDA-MB231 breast cancer cell line for 4 weeks (Fig. 3.2A). Subsequently, adipogenic features were assessed via Oil Red O staining for lipid staining and glycerol-3-

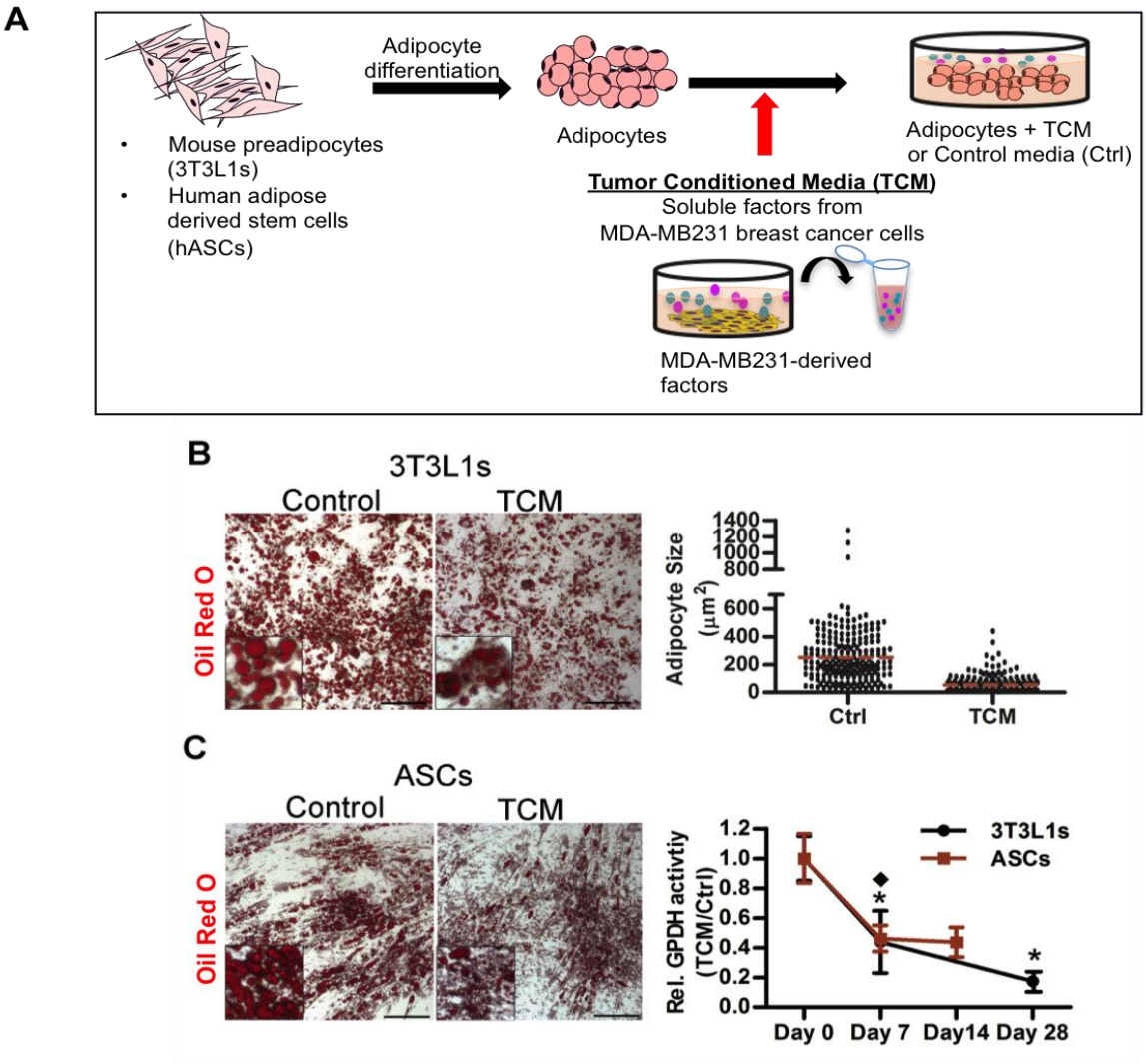

Fig. 3.2. Tumor-derived soluble factors induce loss of adipogenic features. (A) 3T3L1 and ASC-derived adipocytes were cultured in the presence and absence of TCM collected from MDA-MB231 breast cancer cells for 4 weeks. (B) After 4 weeks, the changes in the quantity of lipid, size of individual lipid droplets, and GPDH activity were recorded from 3T3Ll-derived adipocytes cultured in TCM relative to those cultured in control media. (C) ASC-derived adipocytes also lost adipogenic features as indicated by decreased lipid content and GPDH activity in response to TCM. (Scale bars = 200 μm). ♦$p < 0.05$.

phosphate-dehydrogenase (GPDH) activity, which has been used as an indicator of fat synthesis[184].

Microscopically, the quantity of Oil Red O stained lipid droplets in 3T3L1-derived adipocytes was robustly maintained up to 4 weeks in absence of TCM while the amount of lipid droplets dramatically decreased when they were cultured with TCM. Also, the size of individual lipid droplet within 3T3L1-derived adipocytes significantly decreased when the adipocytes were cultured in TCM as compared to those cultured in control media (Fig. 3.2B). In addition, to confirm whether the 3T3L1-derived adipocytes lost adipogenic activity, GPDH activity of 3T3L1-derived adipocytes were assessed. After one week, significant reduction of GPDH activity was observed in 3T3L1-derived adipocytes when the adipocytes were cultured in TCM, which mirrored the results from the Oil Red O image analysis. Also, the decreasing trend of GPDH activity was assessed up to 4 week (Fig. 3.2C).

Similarly, ASC-derived adipocytes cultured in control media maintained their lipid droplets for 2 weeks whereas most of the ASC-derived adipocytes were delipidated in the presence of TCM. In accordance with the microscopic assessment, GPDH activity of ASC-derived adipocytes significantly decreased in response to TCM after one week. In addition, GPDH activity of TCM-treated adipocytes continuously decreased as compared to adipocytes cultured in control media up to 2 weeks (Fig. 3.2C). Although TCM induced dramatic loss of adipogenic features from both adipocyte cell lines, ASC-derived adipocytes also spontaneously lost adipogenic characteristics on 2D culture in absence of TCM[85]. The adipogenic phenotypes of ASC-derived adipocytes were maintained up to 2 weeks, but after 4 weeks ASC-derived adipocytes cultured in control media also significantly delipidated (data not shown). This data suggests that the inherent capacities to develop and maintain adipogenic features might be different between 3T3L1- and ASC-derived adipocytes.

Tumor-derived soluble factors stimulate the conversion of adipocytes into myofibroblastic cells

Next, we assessed if the delipidated adipocytes developed different characteristics in response to TCM. First, the proliferative capacity of TCM-treated adipocytes was assessed. This was done as it has been noted that dedifferentiated adipocytes gain progenitor cell-like characteristics, including proliferative and multi-lineage potential, while terminally differentiated adipocytes rarely proliferate[185]. Our BrdU analysis indicated that ASC-derived adipocytes became actively proliferative after a 7-day culture with TCM and there was a much larger BrdU positive cell population among TCM-treated adipocytes (40.8 ± 0.2 %) as compared to adipocytes cultured in control media (20.9 ± 1.2 %) (Fig. 3.3A). However, approximately 20% of cells among the ASC-derived adipocytes were BrdU positive and this proliferating cell population might come from non-differentiated ASCs or spontaneously dedifferentiated adipocytes in response to a plastic culture plate[85].

Given the previous observation showing that dedifferentiated adipocytes share similar surface marker profiles as ASCs and that ASCs have the potential to develop myofibroblastic features in response to tumor-derived cues, we examined if ASC-derived adipocytes can develop a myofibroblastic phenotype in response to TCM[85,177]. First, we quantified extracellular matrix (ECM) components, including fibronectin (Fn) and type I collagen, since the primary role of myofibroblastic cells is excessive ECM deposition[186]. Our IF and western blot analysis indicated that TCM-treated adipocytes deposited abundant Fn matrices and only a few fat laden cells were observed after one week. However, adipocytes cultured in control media still contained relatively large lipid droplets while less fibronectin matrices were deposited over the time. Along with the enhanced Fn matrices, our western blot analysis indicated that a larger quantity of collagen was produced by TCM-treated adipocytes similar to myofibroblastic ASCs[177] (Fig.3.3B).

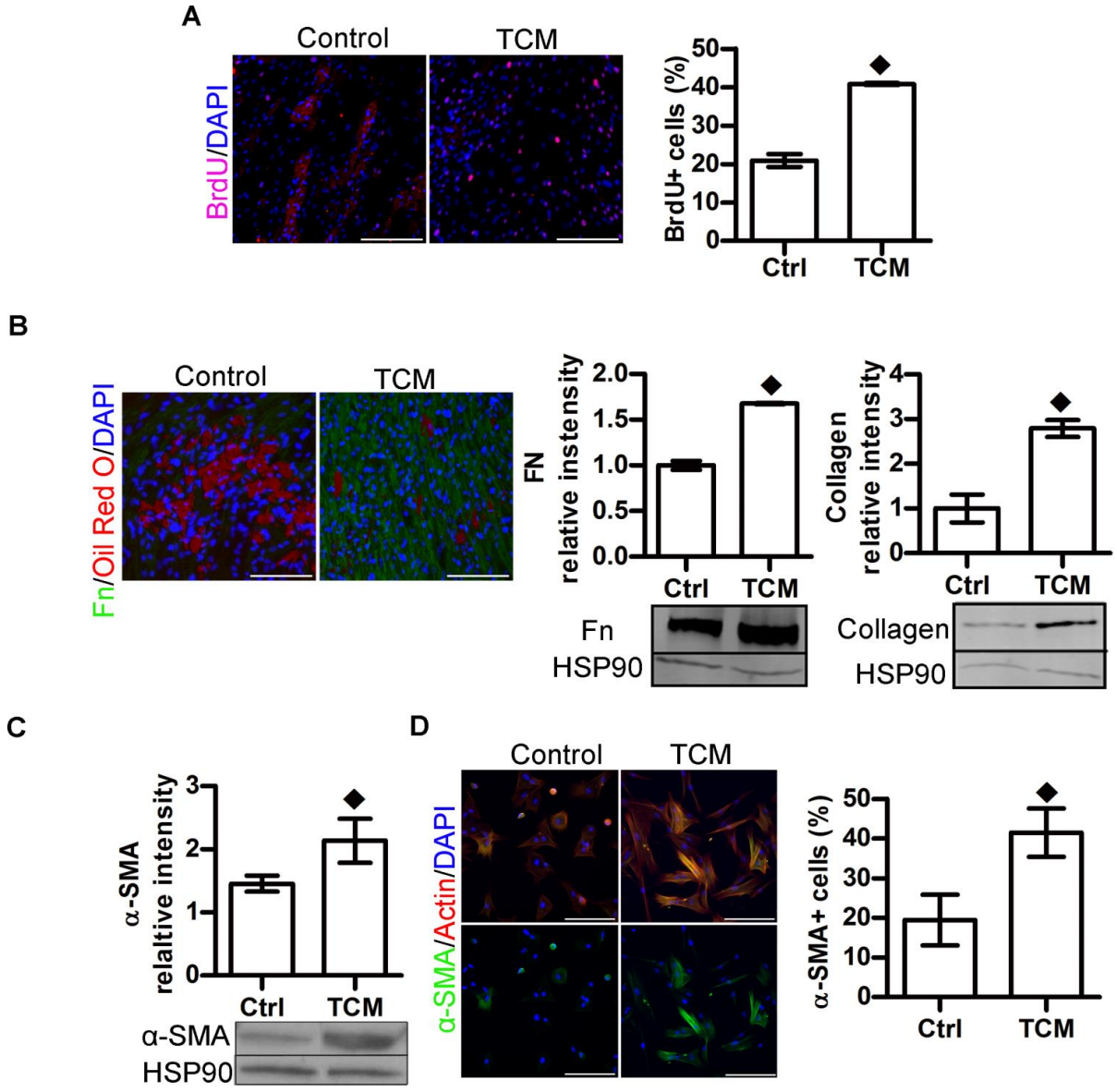

Fig. 3.3. Tumor-derived soluble factors stimulate the trans-differentiation of adipocytes. (A) BrdU analysis indicated that TCM-treated adipocytes were more proliferative than those cultured in control media. (B-C) IF and western blot data indicated that TCM-treated adipocytes deposited a denser ECM containing more Fn and collagen as compared to the matrices deposited by the control media-treated counterparts. (D-E) Western blot analysis indicated that α-SMA level was higher in TCM-treated adipocytes, and IF analysis also showed that the α-SMA positive cell population increased among the dedifferentiated (non-fat) cells. (Scale bars = 200 μm). ♦$p < 0.05$.

Next, to confirm if the enhanced production of ECM protein was due to the enlarged myofibroblastic cell make-up among cancer-activated adipocytes, we assessed the myofibroblastic cell marker, α-SMA, positive cell population among ASC-derived adipocytes cultured in either control media or TCM. First, we measured α-SMA protein expression from the total cell population via western blot. Our analysis indicated that the a-SMA level was significantly higher in TCM-treated adipocytes as compared to those from adipocytes cultured in control media (Fig. 3.3C). Then, we specifically assessed the a-SMA positive cell population among only non-fat-laden cells. For this, non-fat cells were isolated from the total population of cancer-activated adipocytes by centrifugation and removing floating fat cells, and then analyzed for the population of α-SMA positive cells via IF. As shown in Fig. 3.3D, the isolated non-fat cells from TCM-treated adipocytes exhibited a well-spread morphology with enhanced α-SMA stress fibers while those from the control group were poorly spread with only faint α-SMA positive immunoreactivity. In addition, the quantification of α-SMA positive cell population confirmed that non-fat cells among TCM-treated adipocytes contained a larger α-SMA positive cell population as compared to those cultured in the control media (41.5 ± 3.5 % and 19.4 ± 3.7 %, respectively).

TCM-treated adipocytes in 3D culture change their phenotype similarly as in 2D culture

Cell morphology is tightly linked to cell fate, and it has been widely accepted that dimensional difference (2D vs. 3D) induces morphological changes of cells and possibly phenotypical changes[187]. In addition, conventional 2D ceiling culture of mature adipocytes leads to spontaneous dedifferentiation of adipocytes over time[188]. Therefore, to confirm our findings in the 2D culture with a 3D culture model, we utilized 3D collagen scaffolds as fibrillar collagen is the most abundant ECM component in the interstitial area and provides biochemical and physical support to cells[93].

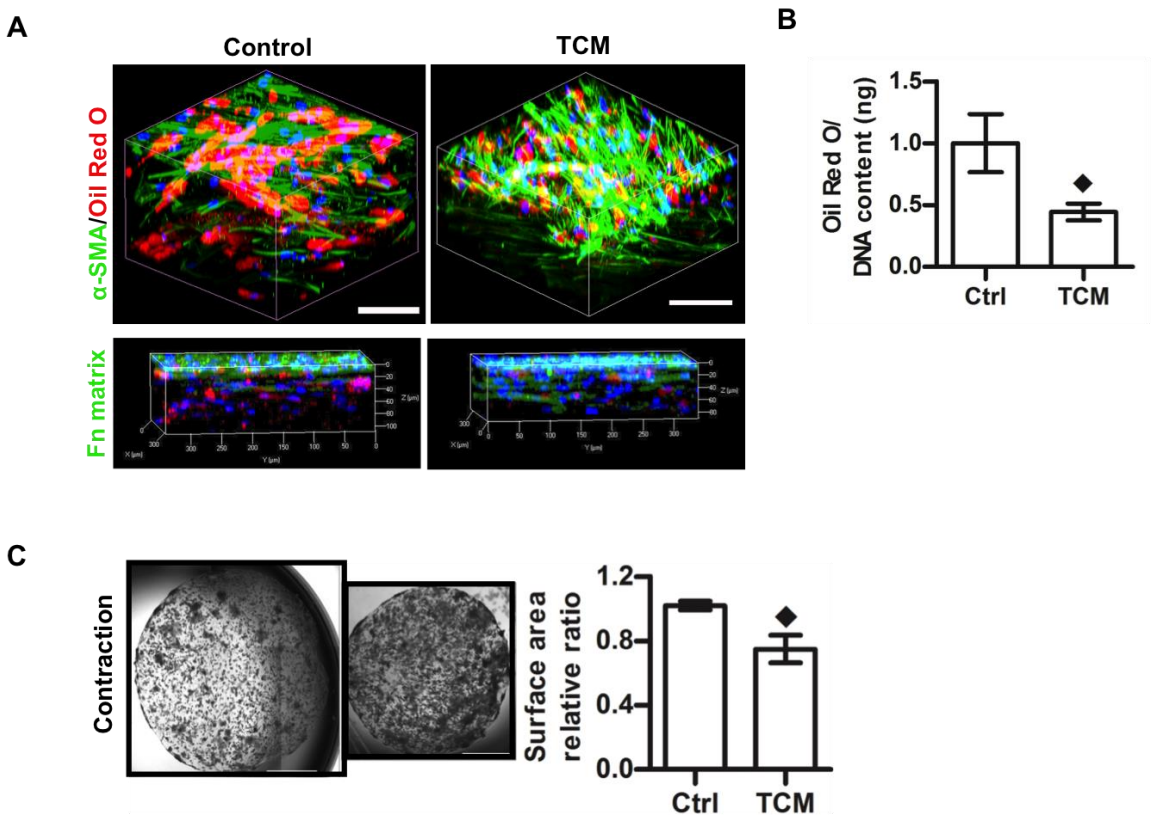

Fig. 3.4. TCM-treated adipocytes in 3D culture change their phenotype similarly as in 2D culture. (A) The adipogenic and myofibroblastic features of ASC-derived adipocytes were assessed via IF and confocal image analysis after culture in 3D collagen scaffolds with and without TCM for one week. Image analysis of the 3D construct indicated significant reduction in Oil Red O stained lipid droplets and an increase in α-SMA and Fn immunoreactivities in TCM-treated adipocytes relative to their control counterparts. (Scale bars = 50 μm). (B) An Oil Red O extraction assay confirmed the reduced fat content of TCM-treated adipocytes as compared to that of adipocytes cultured in control media. (C) A collagen gel contraction assay confirmed that the mean surface area of collagen gels containing TCM-treated adipocytes significantly decreased over time, implying the enhanced contractility of TCM-treated adipocytes. (Scale bars = 1000 μm). ♦$p < 0.05$.

Similar to our 2D studies, adipocytes were obtained through adipogenic differentiation of ASCs. Then, through centrifugation, only the floating adipocytes were collected and incorporated into collagen scaffolds, excluding undifferentiated ASCs during adipogenesis. After 7-days of treatment with TCM or control media, confocal imaging was performed on the scaffolds immunofluorescently stained for α-SMA or Fn with Oil Red O. Microscopically, significant delipidation but increased α-SMA immunoreactivity

were observed in ASC-derived adipocytes cultured in TCM as compared to the adipocytes cultured in control media (Fig. 3.4A). In addition, TCM-treated adipocytes deposited Fn matrices throughout the 3D construct while adipocytes cultured in control media deposited only a thin layer of Fn matrix on the very top of the scaffold. Also, the changes in fat content of dedifferentiated adipocytes were confirmed by quantification of Oil Red O uptake (Fig. 3.4B). In addition to the increased α-SMA stress fiber formation and ECM deposition, increased contractility is a key functional outcome of myofibroblastic cells[189]. The change in surface area of cell-embedded collagen scaffolds has been used as an indirect indicator of cell-mediated contractility[177]. Our data showed that TCM-treated adipocytes led to significantly decreasing the surface area of the collagen scaffolds where the adipocytes were embedded whereas a relatively small change was observed from the surface area of adipocyte-embedded scaffolds treated with control media, implying that TCM-treated adipocytes exhibited increased contractility (Fig. 3.4C). This enhanced contractility reflected the increased α-SMA stress fiber levels[184].

TCM-treated adipocytes exhibit enhanced *pro-angiogenic potential*

It has been widely accepted that myofibroblasts are highly pro-angiogenic, secreting multiple pro-angiogenic factors such as VEGF and IL-8[61]. Therefore, we tested if pro-angiogenic behaviors of adipocytes were modulated by tumor-derived cues, and if the pro-angiogenic potential was similarly regulated in 2D and 3D. Our ELISA analysis of VEGF and IL-8 from 2D culture suggested that ASC-derived adipocytes cultured with TCM secreted higher levels of VEGF and IL-8 as compared to adipocytes without any treatment and those cultured with control media (Fig. 3.5A). A similar trend was observed in 3D models. Interestingly, the differences of pro-angiogenic factor secretion between TCM-treated adipocytes and their control counterparts were greater in 3D as compared to 2D (Fig. 3.5B).

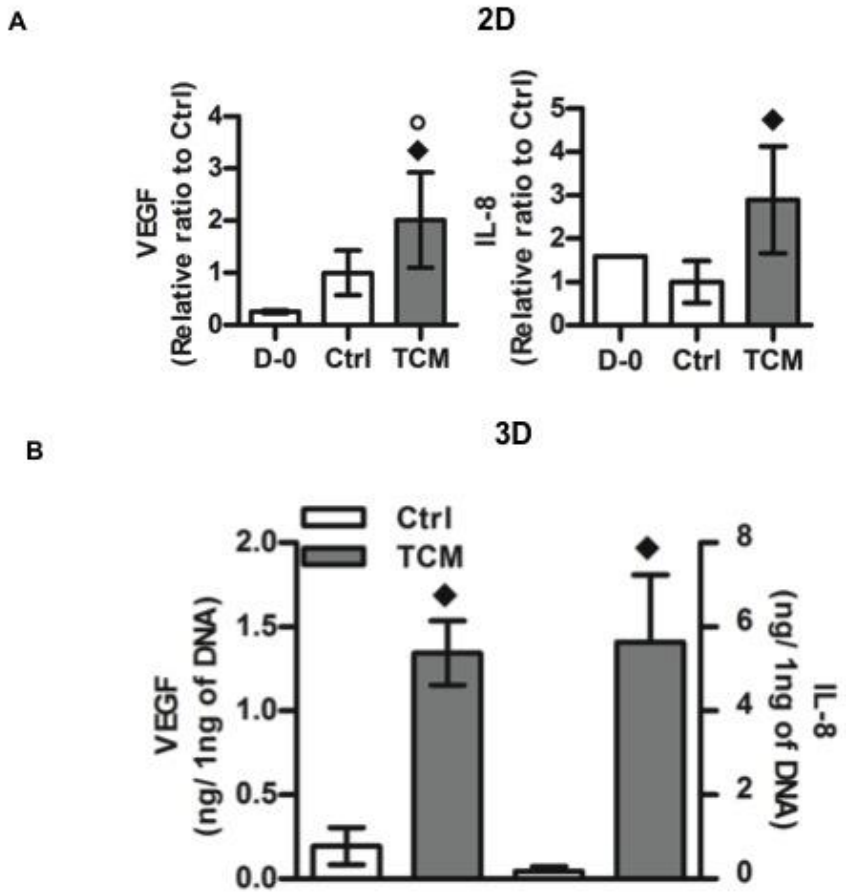

Fig. 3.5. TCM-treated adipocytes exhibit enhanced pro-angiogenic potential. (A) ELISA assessment indicated that TCM treated-adipocytes in 2D culture secreted a higher concentration of VEGF and IL-8 as compared to both adipocytes on Day 0 and those cultured in control media. (B) A similar but more pronounced trend was observed in 3D culture. ♦$p < 0.05$ and O$p < 0.05$ from control and D-0, respectively.

Enhanced pro-angiogenic signaling of TCM-treated adipocytes promotes HUVEC sprouting

To assess the functional impacts of the altered pro-angiogenic signaling from dedifferentiated adipocytes on the sprouting of Human umbilical vein endothelial cells (HUVECs), we cultured a monolayer of HUVECs atop TCM- or control media-treated adipocytes in the collagen scaffolds and quantified HUVEC sprouting via confocal immunofluorescence imaging (Fig. 3.6A). In accordance with

the enhanced pro-angiogenic signaling of TCM-treated adipocytes, the number of HUVEC sprouts co-cultured with TCM-treated adipocytes was significantly larger than that with adipocytes cultured in control media (Fig. 3.6B). To confirm these changes are primarily mediated by altered VEGF and IL-8 signaling, HUVEC sprouting was assessed in the presence and absence of VEGF and IL-8 neutralizing antibodies as well as their cognate receptor antibodies, VEGFR2 and CXCR1, respectively. The enhanced HUVEC sprouting with TCM-treated adipocytes was significantly reduced with the blockade of VEGF and IL-8 molecules as well as inhibitors of VEGFR2 and CXCR1 whereas no significant change was observed in adipocytes cultured in control media (Fig. 3.6C)

3.6. Discussion

Fibrotic tumor stroma often appears devoid of adipocytes or contains smaller adipocytes with a higher ratio of fibroblasts to adipocytes, suggesting the possibility of adipocyte-to-fibroblast trans-differentiation[176,190,191]. However, it remains unclear whether adipocytes developed myofibroblastic features in response to tumor-derived factors and therein participate in ECM remodeling and pro-angiogenic activities. In this study, our findings indicated that adipocytes decreased their adipogenic features in response to tumor-derived soluble factors both in 2D and 3D culture. On the other hand, TCM-treated adipocytes contained more a-SMA positive myofibroblastic cells, which deposited matrices enriched in Fn and collagen. In addition, TCM-treated adipocytes up-regulated VEGF and IL-8 signaling and consequently stimulated angiogenic-activities of HUVECs.

3T3L1s have been widely utilized as a model system of human pre-adipocytes, yet species-dependent discrepancies have been addressed indicating that there might be a difference in metabolic sensitivity of adipocytes between mice and humans[192]. In addition, 3T3L1s are committed pre-adipocytes, and might exhibit different gene and protein expression profiles, consequently leading to distinct

behaviors as compared to those of multi-potent ASCs[193]. In accordance with previous reports, we also recognized inherent differences of mouse and human adipocytes. For example, adipogenesis of 3T3L1s and their maintenance of adipogenic features were much robust than those of ASCs. In addition, a morphological difference was observed between mouse and human adipocytes both *in vitro* and *in vivo*, suggesting that there might be species-dependent adipogenic features. However, despite of the inherent differences between 3T3L1- and ASC-derived adipocytes, their responses to tumor-derived factors were still comparable. We observed decreased size of adipocyte in mammary tumor stroma from both mice and humans as compared to those in normal mouse and human mammary adipose tissue, respectively (Fig. 3.1A and B). In addition, our *in vitro* study confirmed that both mice and human adipocytes similarly decreased their adipogenic features in response to tumor-derived cues (Fig. 3.2).

Adipocyte differentiation is primarily governed by adipogenic transcription factors such as peroxisome proliferating-activated receptor-gamma (PPAR-γ) and CCAAT/enhancer binding protein-α (C/EBP-α) [194]. It has been shown that this process is modulated by multiple factors such as tumor-necrosis factor-alpha (TNF-α), TGF-β, and bone morphogenic proteins (BMPs)[114,194]. TNF-α has been known to regulate adipogenesis as well as lipolysis, implying TNF-α might participate in the process of adipocyte delipidation[195]. In addition, TGF-β is known as a molecular mediator of myofibroblastic differentiation and also inhibits adipocyte differentiation via repressing transcriptional activity of C/EBPs and subsequently PPAR-γ[196,197]. As previous studies, including ours, indicated, MDA-MB231 TCM contained higher levels of TNF-α and TGFβ, which might play a role in stimulating loss of adipogenic features and gain of myofibroblastic features, respectively. However, further studies are necessary to define a specific molecular mechanism underlying the conversion of adipocytes into myofibroblasts[177,198].

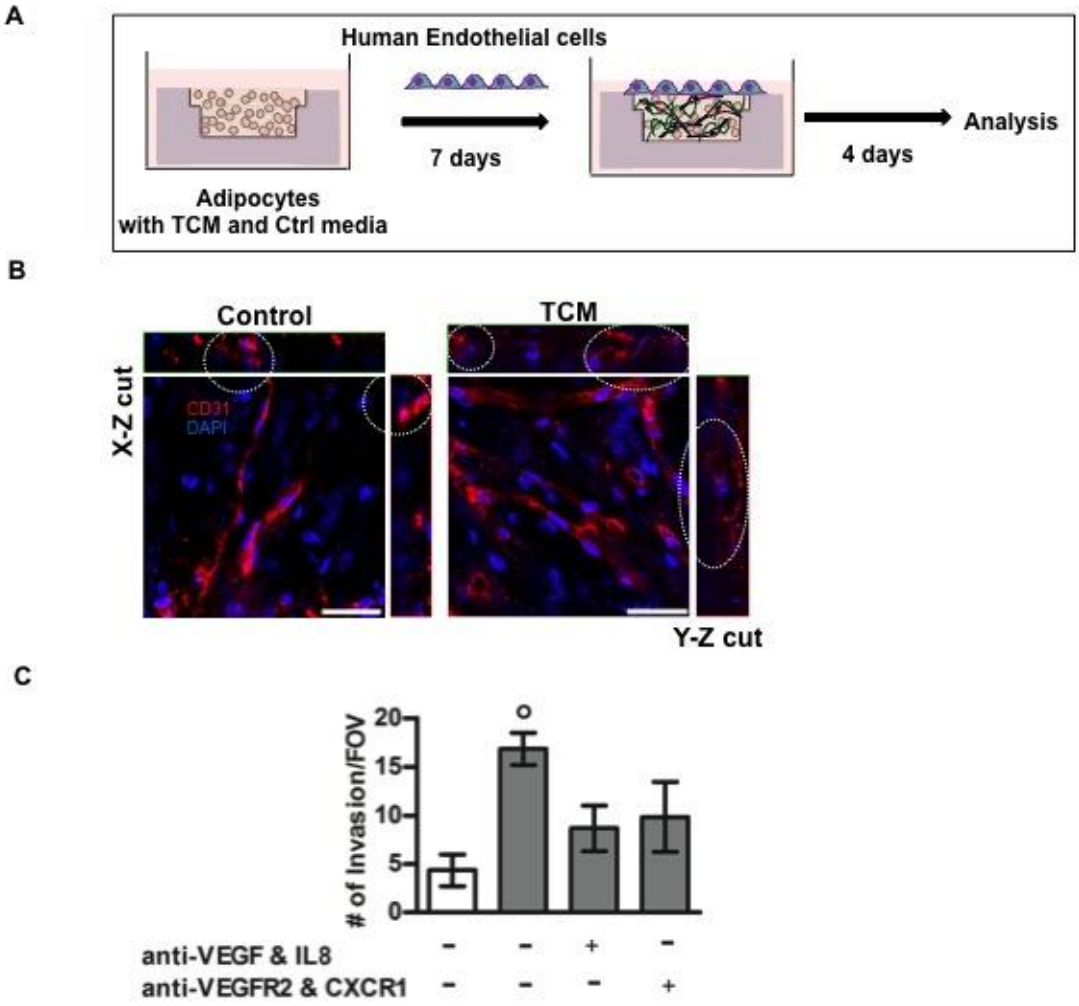

Fig. 3.6. Enhanced pro-angiogenic signaling of TCM-treated adipocytes promotes HUVEC sprouting. (A) As this schematic showed, a HUVEC invasion assay was performed to investigate the functional significance of the pro-angiogenic signaling mediated by dedifferentiated adipocytes. Adipocytes in 3D collagen scaffolds were treated with either TCM or control media for seven days, and then a monolayer of HUVECs was cultured atop the scaffolds to assess HUVEC sprouting through the collagen bulk. (B) HUVEC sprouting was enhanced in response to the increased VEGF and IL-8 secreted from TCM-treated adipocytes as compared to that with adipocytes cultured in control media. (C) Blockade of VEGF and IL-8 abrogated HUVEC sprouting associated with TCM-treatment whereas no pronounced effect on HUVEC invasion was observed in control media. Similarly, inhibition with VEGF and IL-8 receptors reduced HUVEC sprouting in the presence of TCM-treated adipocytes, implying that the changes in HUVEC sprouting were mediated by VEGF and IL-8 pro-angiogenic signaling. (Scale bars = 50 μm). **O**$p < 0.05$ from all other conditions.

In addition, 2D ceiling culture has been known to induce spontaneous dedifferentiation of adipocytes showing fibroblastic morphology, and the dedifferentiated adipocytes share similar features with ASCs such as surface markers and gene expression[85]. However, it was noted that the cell population from the dedifferentiated adipocytes was more homogenous in comparison to ASCs[85]. In particular, α-SMA positive cells were rare among dedifferentiated adipocytes versus ASCs, which contain about 15% of α-SMA positive cells at their first passage[199]. Thus, significantly enhanced α-SMA positive cell population among TCM-treated adipocytes from our study was a TCM-derived effect rather than a spontaneous conversion.

Moreover, our analysis indicated that TCM-treated adipocytes in 2D culture contained a larger population of myofibroblastic cells which exhibited enhanced proliferative, contractile and ECM depositing potential as compared to those cultured in control media (Fig. 3.3). As hormone-induced adipogenic differentiation of progenitor cells often was not 100% efficient[200], it is possible that a subset of un-differentiated progenitor cells within the culture contributed to enlarging a myofibroblastic cell population in response to TCM. Thus, our findings obtained through 2D culture were confirmed by performing similar studies in 3D culture exclusively incorporating adipocytes. Despite the concern that possible contamination of multiple cell types in 2D culture might result in different outcomes from those in 3D culture, our findings suggested that TCM-treated adipocytes in 3D culture reduced their adipogenic features and acquired myofibroblastic features, which mirrored TCM-treated adipocytes in 2D (Fig. 3.4).

Adipocytes primarily produced laminin, collagen IV, V and VI[201]. However, mammary tumor stroma consists of abundant fibrillar ECM components such as collagen I and Fn, which are deposited by non-fat stromal vascular cells[61,201]. However, previous reports indicated that dedifferentiated adipocytes were able to produce osteoid ECM in an implanted tissue construct upon osteogenic stimulation[85]. Our findings also suggested that adipocytes in tumor stroma could possibly contribute to deposition of an

ECM rich in collagen and Fn through cancer cell-derived paracrine signaling. The enhanced fibrillar ECM deposition and their remodeling have been positively correlated with tumor stiffening and tumor malignancy[202]. In addition, it is also possible that the changes in ECM composition, architecture and its resulting mechanical cues also give feedback to adipocyte fate. Fn has been known to inhibit adipogenic differentiation and various matrix metalloproteinases (MMPs); in particular, MMP 14 and MMP 11 are known to regulate adipocyte fate[203 191]. Moreover, previous studies indicated that stiff substrates and cyclic tensile force (stretching cells) repressed adipogenesis through modulating cell shape and actin cytoskeleton reorganization[204]. However, more studies are required to understand whether there were ECM-mediated effects on TCM-derived adipocyte conversion, and whether these aforementioned cues and their resulting mechanism for adipogenesis simply regulate the conversion of adipocyte to non-fat cells in a reversed signaling cascade or via completely different pathways.

Finally, we showed that TCM-treated adipocytes secreted higher levels of VEGF and IL-8, which consequently stimulated HUVEC sprouting. It has been known that adipocytes exhibit inherent pro-angiogenic potential, and this potential is enhanced under stresses such as hypoxia[205]. Our findings also suggested that the pro-angiogenic potential of TCM-treated adipocytes may surpass that of adipocytes since TCM-treated adipocytes secreted much higher concentrations of VEGF and IL-8 as compared to those of adipocytes and control-media treated adipocytes (Fig. 3.5A). Consequently, HUVEC sprouting was stimulated through VEGF and IL-8 signaling. In addition, adipocytes adjacent to cancer cells produce higher levels of MMPs, which may participate in regulating HUVEC sprouting[176]. Thus, to verify the pro-angiogenic factor-derived effects on HUVEC sprouting, we either neutralized VEGF and IL-8 or specifically blocked VEGFR2 and CXCR1. CXCR1 is highly specific for IL-8[38], and VEGFR2, one of the VEGF tyrosine kinase receptors, is known to stimulate angiogenesis[39]. In addition, VEGFR2 is known to be trans-activated by IL-8 interacting with its receptors[206,207]. Our inhibition study confirmed that

enhanced HUVEC sprouting in the presence of TCM-treated adipocytes was primarily modulated by VEGF and IL-8 signaling. This finding implies that adipocytes adjacent cancer cells might facilitate cancer cell growth and invasion via stimulating angiogenesis.

In conclusion, through this study we proposed several possible roles of adipocytes in modulating ECM deposition and pro-angiogenic activities upon exposure to tumor-derived soluble factors. The tumor and obesity-associated microenvironment share similar features such as hypoxia, chronic inflammation, and fibrosis, all of which may play a critical role in stimulating the pathogenic potential of adipocytes[208]. Therefore, this study suggests broad clinical implications, not only for cancer therapy but also obesity-associated diseases such as type 2 diabetes and atherosclerosis. However, certainly more studies are required to understand whether there is an organ- or depot-specific potential for adipocyte trans-differentiation since cancer (i.e. breast vs. prostate) interacts with organ-specific adipose tissue, and a majority of obesity-associate metabolic diseases are specifically associated with visceral fat depot over subcutaneous fat[171]. So far, many studies, including this study, utilized either a mouse cell line- or human ASC-derived adipocytes, which certainly cannot address potential regional differences in adipose tissue functions. Therefore, future studies testing primary adipocytes isolated from different anatomical locations are necessary.

In addition, as an increasing number of studies suggested, dedifferentiated adipocytes are certainly an attractive option for cell-based regenerative medicine for human as well as small animals due to difficulty to acquire adequate number of pure stem cell popluation[199]. However, our findings reiterate the importance of microenvironmental cues on regulating cell behaviors and pathological potential, suggesting a careful consideration of clinical use of adipocytes. Lastly, understanding the precise mechanism underlying adipocyte conversion will aid in developing better tissue engineering and therapeutic approaches.

CHAPTER 4

OBESITY-DEPENDENT CHANGES OF INTERSTITIAL ECM MECHANICS AND THEIR ROLE IN BREAST TUMORIGENESIS

4.1. Contributors

Co-authors of this chapter made the following contributions: Jacqueline Gonzalez, undergraduate student in the Fischbach lab analyzed pro-fibrotic features of mouse adipose tissue and human tumor specimens. Priya Bhardwaj, research assistant in the Dannenberg lab prepared mammary tissue from the mouse models of obesity. Roberto C. Andresen Eguiluz in the Gourdon lab performed ECM stiffness measurements via SFA and helped in writing the manuscript. Karin C. Wang in the Gourdon lab prepared FRET labeled Fn and aided in FRET analysis. Haibo Sha in the Ling Qi lab prepared adipose tissue from the mouse models of obesity. Sunish Mohanan performed histopathological analysis of tumor specimens. Rebecca M. Williams aided in SHG imaging and collagen image analysis. Prof. Ofer Reizes provided NANOG promoter (GFP+) MDA-MB231 and helped with their characterization. Dr. L.T. Vahdat provided breast tumor sections from obese and lean patients. Dr. A. J. Dannenberg provided human and mouse mammary tissue from obese and lean individuals as well as constructive advice on the direction of this project. Prof. Delphine Gourdon also provided scientific and technical advice on the data analysis and aided in writing the manuscript. Prof. Claudia Fischbach guided the direction of project, assisted with experimental design, provided insight for data analysis and wrote this manuscript.

4.2. Abstract

Obesity and extracellular matrix (ECM) stiffness are considered independent risk and prognostic factors for breast cancer. Whether they are functionally linked is uncertain. Here, we investigated the hypothesis that obesity enhances local myofibroblast content in mammary adipose tissue and that these stromal changes increase malignant potential via enhancing interstitial ECM stiffness. Indeed, mammary fat of both diet- and genetically-induced mouse models of obesity were enriched for myofibroblasts and stiffness-promoting ECM components. These differences were related to varied adipose stromal vascular cell (ASVC) characteristics as ASVCs isolated from obese mice contained more myofibroblasts and deposited denser and stiffer ECMs relative to ASVCs from lean control mice. Accordingly, decellularized matrices from obese ASVCs stimulated mechanosignaling and thereby the malignant potential of breast cancer cells. Finally, the clinical relevance and translational potential of our findings were supported by analysis of patient specimens and the observation that caloric restriction in a mouse model reduces myofibroblast content in mammary fat. Collectively, these findings suggest that obesity-induced interstitial fibrosis promotes breast tumorigenesis via altering mammary ECM mechanics with important implications for anti-cancer therapies and adipose tissue-based reconstructive approaches following mastectomy.

4.3. Introduction

Obesity, with increasing worldwide prevalence, is a key risk factor for the development and prognosis of breast cancer[209]. This correlation is commonly attributed to obesity-mediated differences in adipose endocrine functions[210]. However, given the critical role of contextual cues in tumorigenesis, obesity-mediated alterations to the local microenvironment may also be important. In particular, obesity induces fibrotic remodeling of adipose tissue[211,212] and these changes have been associated with malignant

potential[213]. Nevertheless, the exact mechanisms through which interstitial fibrosis in obese adipose tissue may impact the risk of and prognosis for breast cancer remain largely elusive.

Similar to obesity, tumors also feature fibrosis in the surrounding stroma, which is commonly referred to as desmoplasia. The concomitant changes in ECM density and rigidity not only enable detection by mammography and palpation, respectively, but also represent important risk factors for tumor development, progression, and response to therapy[27,47,214]. More specifically, enhanced stiffness changes cellular mechanosignaling[42], which, in turn, stimulates cancer aggressiveness through various mechanisms including perturbed epithelial morphogenesis[123], growth factor and cytokine signaling[124] and stem cell differentiation[46,48]. However, whether obesity-associated fibrotic remodeling alters local ECM mechanical properties and if these differences activate protumorigenic mechanotransduction remains to be elucidated.

Myofibroblasts are major cellular regulators of fibrotic and desmoplastic remodeling and thus, tissue mechanical properties[215]. Myofibroblasts are highly contractile and assemble a fibronectin (Fn) and collagen type I-rich ECM that is characterized by enhanced density, fibrillar architecture, crosslinking and partial unfolding: all parameters causally linked to increased ECM stiffness[32]. Various proinflammatory cytokines enhanced during obesity (e.g. transforming growth factor β1 [TGFβ1][216]) can initiate myofibroblast differentiation in mesenchymal cell types including adipose-derived stem cells (ASCs)[48,215]. Nevertheless, the impact of obesity on myofibroblast content of mammary adipose tissue remains elusive as most previous studies were performed with subcutaneous (s.c.) and visceral fat. Yet extrapolation of such results to mammary fat should be avoided because both global functions[217] and fibrotic remodeling[71] of adipose tissue can vary significantly between anatomic depots.

Here, our goal was to characterize the role of obesity in myofibroblast-mediated interstitial fibrosis in mammary fat, determine the impact of these variations on ECM mechanical properties, and

assess if these changes enhance the malignant potential of mammary tumor cells due to altered mechanotransduction. We have applied a multidisciplinary approach that integrates biological and physical sciences-based techniques ultimately extending our quantitative understanding of the functional relationship between obesity-induced alterations in ECM mechanics as it pertains to increased breast cancer pathogenesis.

4.4. Materials and methods

Animal models and tissue isolation

To characterize obesity-associated interstitial fibrosis mammary, subcutaneous (s.c.) or visceral fat was isolated from both dietary and genetic mouse models of obesity (n=10/group). For diet-induced obesity (DIO) model, female 5 week-old C57BL/6J mice (Jackson Laboratories) were randomized and fed low fat (LF) or high fat (HF) diets (Research Diets: D12492i, 10 kcal% fat and 12450Bi, 60 kcal% fat, respectively) *ad libitum* for 10 weeks as previously described (Fig. 1A)[218]. For the genetic model, 8 week-old B6.Cg-Lep^{ob}/J (*ob/ob*) and their age-matched C57BL/6J wild type controls (Jackson Laboratories) were fed PicoLab Rodent Diet 20, #5053 (W.F. Fisher & Son) *ad libitum* for 3 weeks until sacrifice (Fig. 1A). To mimic menopause, either ovariectomy or sham surgery was performed on C57BL/6J mice at 4 weeks of age. One week post-surgery, ovariectomized (OVX) and ovary intact mice were randomized for dietary intervention (LF or HF) (Fig. S1A). To study the effect of caloric restriction, OVX mice received 10 weeks of HF feeding and were subsequently subjected to 30% caloric restriction (CR) for 7 weeks using previously established protocols (Fig. 6E)[219]. Age-matched control mice were fed LF or HF diets for a total of 17 weeks (n=6/group). Isolated tissues were formalin fixed for immunohistochemical evaluation, or frozen and stored at -80°C for subsequent biochemical analysis. Animal protocols were

approved by the Institutional Animal Care and Use Committees at Weill Cornell Medical College and Cornell University.

Cell isolation and culture

ASVCs were isolated from the stromal vascular fraction of either s.c. or visceral white fat of both genetic (11 week-old) and dietary (14 week-old) mouse models (Jackson Laboratories) via collagenase digestion and density centrifugation (Fig. 2A)[220]. Briefly, isolated tissue was minced in Krebs-Ringer-HEPES (*KRBH*) *buffer* prepared as previously described[221] and digested with 1.5mg/mL collagenase type 1 buffer (Worthington Biochemical Corp.). Digested tissue was filtered through a 250μm cell strainer (Pierce) and centrifuged in Histopaque-1077 solution (Sigma) to separate ASVCs from adipocytes. Isolated ASVCs were cultured in media containing 1:1 Dulbecco's Modified Eagle Medium (DMEM)/F12 (Gibco) supplemented with 10% FBS (Tissue Culture Biologicals), 1% antibiotic (penicillin/streptomycin) (Gibco) up to passage 4. Human MDA-MB231 breast cancer cells (ATCC) were cultured in MEM (α-modification [αMEM], Sigma) containing 10% FBS and 1% antibiotic. MDA-MB231 cells transduced with a NANOG promoter GFP reporter construct were prepared as previously described[222] and cultured in MEM (Gibco) supplemented with 10% FBS and 1% antibiotic.

Mammary tissue immunostaining and image analysis

Cross-sections were prepared from paraffin-embedded mammary fat and immunofluorescently stained for Fn and α-SMA. Antigen retrieval was performed with 0.1 M citrate buffer, pH 6.0 (α-SMA) and additional proteinase K treatment (Fn) (Dako). Subsequently, tissue sections were permeabilized and blocked with SuperBlock (Thermo Fisher) in 0.05% Tween-20 PBS (PBST). For α-SMA staining, M.O.M kit blocking reagent (Vector laboratories) was used for an additional blocking. After overnight

incubation (4°C) with primary antibodies directed against Fn (Sigma-Aldrich) or α-SMA (Invitrogen), the sections were incubated with AlexaFluor 488-conjugated secondary antibody, counterstained with 4',6-diamidino-2-phenylindole (DAPI), and then mounted with Prolong® Gold reagent (all from Invitrogen). For each sample, 10 to 20 randomly selected areas were imaged with a Zeiss Observer Z.1 microscope and an AxioCam MRm camera, and average fluorescence intensity was calculated. To correct for background, all images were thresholded by subtracting fluorescence intensity of negative controls using Adobe Photoshop (n=10 samples/group). The isolated positive pixels of each image were quantified in ImageJ (NIH) and then normalized to the number of adipocytes.

Characterization of collagen fibers by SHG imaging analysis

Multiphoton SHG imaging was used to characterize collagen structure in fresh murine mammary tissue of genetic model and cross-sections of DIO mouse mammary tissue, human mammary tissue and tumors. Imaging was performed with a custom-built multiphoton microscope using 780 nm illumination and an Olympus 20x/0.95W XLUMPlanFl objective[141]. Emissions were separated into SHG (360-405 nm, pseudocolored purple) and autofluorescence (420-550 nm, pseudocolored green) channels. For murine samples, mammary tissue from 11 week-old *ob/ob* and lean mice (n=3 per condition) was isolated and immersed in PBS. Z-stacks (50-120 μm in depth) of areas adjacent to the mammary epithelium, as identified in transmitted light mode, were acquired at 2μm-intervals; 5 to 6 spots per tissue were imaged. For human specimens, 4μm cross-sections were deparaffinized, rehydrated, and immersed in PBS. Micrographs of 10 regions per sample were collected and a total of 10 specimens per condition were analyzed. SHG channel images were extracted and analyzed through Fiji (NIH) and a custom-built autocorrelation analysis algorithm as previously described[141]. To assess fibril linearity (FL) in murine samples, individual fibrils were tracked through the entire Z-stack and both ends identified via Fiji. The

distance between both ends (*D*) and full-length of the fibrils (*L*) was recorded and their ratio (*D/L*) represented as FL; 30 to 50 fibrils per Z-stack were analyzed. To analyze collagen structure in human tumor specimens, a 2D spatial autocorrelation was computed from the SHG channel image. An autocorrelation ellipse was generated by fitting to 1/e of the maximum value of each image autocorrelation; the mean radius of the ellipse (in pixels) indicates the length scale of the collagen framework. The minimum and maximum radius of the ellipse were obtained and presented as the correlation width and correlation length of the fibers, respectively.

Characterization of isolated ASVCs

ASVCs isolated from s.c. fat of both genetic and dietary mouse models were plated on glass coverslips, cultured for 3 to 5 days, fixed with 4% paraformaldehyde (PFA), and then immunofluorescently analyzed for α-SMA, proliferative capacity, and ECM deposition. To determine proliferation, ASVCs were incubated with 10μM bromodeoxyuridine (BrdU) (Sigma-Aldrich) for 20 hours. After fixation, cells were pretreated with ice-cold 1N HCl, 37°C 2N HCl, and 0.1 M borate buffer, incubated with biotinylated mouse anti-BrdU (Invitrogen), and finally fluorescently labeled with streptavidin-conjugated Alexa Fluor 555. For IF of α-SMA, Fn, and collagen, fixed cells were permeabilized with 0.05% Triton X-100 (VWR) in PBS (PBS-X), blocked in 1% BSA (Fischer Scientific) in PBS, and then incubated with primary antibodies directed against α-SMA, Fn, and collagen (Millipore) overnight at 4°C. Subsequently, samples were labeled with species-specific AlexaFluor 488-conjugated secondary antibodies. The percentage of BrdU and α-SMA positive cells was determined by manually counting 5 representative images for each sample for a total of 3 samples. Matrix thickness was determined by confocal analysis of Z-stack images (1 μm interval) captured with a Zeiss 710 confocal microscope. Differences in ASC secretion of SDF-1 were evaluated via SDF-1 ELISA duo set (R&D)

following 24 hours of incubation in serum-starved media and normalized to DNA content as measured from cell lysates by QuantiFluor® dsDNA System (Promega) (n=3/group). Also ASVCs isolated from visceral fat of *ob/ob* and wild type mice were similarly assessed as s.c. ASCs to evaluate the fat depot-dependent profibrotic characteristics.

Western Blot analysis

Tissue and cell lysates were prepared in RIPA buffer containing protease and phosphatase inhibitor cocktail (all from Thermo Scientific) as well as 1mM phenylmethylsulfonyl fluoride (Calbiochem). Protein concentrations were measured using a BCA kit (Thermo Scientific) and equal amounts of protein samples were loaded on gels (Bio-Rad), separated by reducing SDS-PAGE, and transferred to PVDF membranes (Bio-Rad). After blocking with 5% milk powder, membranes were incubated overnight (4°C) with primary antibodies raised against α-SMA, Fn, and p-FAK [397] (Invitrogen) as well as the house keeping proteins HSP90 (Santa Cruz), β-actin (Millipore), and GAPDH (Ambion). Following incubation with species-specific HRP-conjugated secondary antibodies (Novus Bio) chemiluminescence detection was performed using an ECL kit (Thermo Scientific). Finally, densitometric analysis was performed with Image J and Adobe Photoshop CS4.

Analysis of Fn conformation via FRET

Differences in Fn conformation were determined as previously described[31,223]. Briefly, $2x10^4$ ASVCs from *ob/ob* and wild type mice were seeded in Lab-Tek™ chamber slides (Thermo Scientific) pre-coated with 30 μg/mL unlabeled Fn (Invitrogen) in PBS (n=3 per condition). Subsequently, human plasma Fn (only 8% FRET-labeled Fn with an excess of 92% unlabeled-Fn to prevent intermolecular energy transfer between adjacent proteins in fibers[223]) was added to yield a final Fn concentration of 50

mg/mL necessary for FRET analysis. 24 hours post-incubation, cells were fixed with 4% PFA, washed with PBS and then imaged using a Zeiss 710 confocal microscope with a 40x water immersion objective under conditions that prevented photobleaching. Z-stack images (1μm interval) were captured at 6 randomly chosen areas following excitation with a 10% laser intensity through the 488 nm channel, and then the signals from both the donor (514-526 nm) and acceptor (566-578nm) channels were collected. Image processing of the acceptor and donor images was performed as previously described[224]. Briefly, MATLAB (MathWorks, Inc.) was used to compute the FRET intensity (ratio of acceptor and donor channels) images, to calculate the mean and standard deviation of the FRET intensities, and to compile FRET intensity data at each representative location for histogram plotting (n=3/group). The quantified FRET intensity was used to determine relative Fn conformation referencing pre-obtained calibration curves for the FRET intensity of chemically denatured dual-labeled Fn and its corresponding circular dichroism spectra[95,97].

Analysis of ECM stiffness via SFA

To measure the compressive elastic moduli of cell-free matrices deposited by *ob/ob* or wild type ASVCs, the SFA (SurForce LLC, CA) was utilized[225,226]. For measurements, mica surfaces holding the matrix were mounted on a double cantilever of known spring constant (k=980N/m) and compressed with a bare mica surface from the top. The force acting between the surfaces was then measured as a function of surface separation (Fig. 3C).

Briefly, two semi-cylindrical surfaces, which have previously been back-covered with silvered mica, build an optical interferometer. The surfaces were prepared in a laminar flow cabinet, keeping samples as clean as possible. Optical grade muscovite mica (S&J Trading, Australia) was hand-cleaved into thin and uniform sections, and further metallized with 55nm of silver on their back side, to obtain

semi reflective surfaces (used to build the optical interferometer). Equally thick mica sections, silver side down, were glued onto a pair of fused silica discs (diameter=10mm, radius of curvature=20mm) (ESCO Products, NJ) with UV curing glue for 45-50 minutes (61 Norlan, NJ). For each pair, the bare (upper) surface used for indentation was kept in a dessiccator until needed. The other (lower) surface was first coated with 30 µg/ml of Fn (Invitrogen) in PBS to facilitate cell adhesion then placed in a custom-made PDMS well containing culture media and cells (obesity-associated or control ASCs) during the 24 hour matrix deposition process. $2x10^4$ cells were seeded on the Fn-coated surfaces with 50 µg/mL of Fn supplemented (mimicking the FRET experiment) culture media for 24 hours. Next, matrices were decellularized using an extraction buffer (20mM $NHOH_4$ in 0.5% PBS-X) and subsequent multiple washing steps with PBS and distilled water[227]. Shortly after decellularization, the compressive Young modulus of the matrix was quantified via SFA without any chemical crosslinking.

Paired discs were mounted in a crossed cylinder axis configuration, to obtain a well-defined flat circular junction equivalent to a sphere-on-flat like contact. The SFA chamber was filled with PBS at 37°C, keeping both discs fully immersed during the SFA measurements. Before starting an experiment, the system was allowed to equilibrate to 37°C for 1 hour. Then, individual samples were probed at 4 different positions approximately 0.5mm apart. Each position was compressed at least 3 consecutive times with increasing normal force.

Compressive measurements were performed in the quasi-static regime, at the lowest speed achievable with our normal motor (V = 8-9nm/s) to prevent any viscous contribution. The system was allowed to equilibrate for 20 minutes between each compressive cycle. Measured force-distance profiles were further analyzed to extract the compressive elastic moduli using the Johnson contact mechanics model[228], in which the indentation under compression (d) between a sphere and a flat was related to normal force (F) by the following equation:

$$\frac{F}{R} = E\pi\frac{\delta^2}{D_0} \quad (1)$$

where R is the equivalent radius of curvature of the cylindrical discs, D_0 is the undistorted (prior to compression) thickness of the matrix and E the compressive Young's modulus of the ECM (Fig. 3C).

Analysis of tumor cell migration in response to obesity-dependent differences in SDF-1 levels

To investigate the effect of SDF-1 from *ob/ob* ASVCs on tumor cell recruitment, a transwell migration assay was used. MDA-MB231 cells were seeded on collagen-coated transwell inserts (Corning Inc.), which were subsequently placed in wells that contained ASVCs cultured in low serum media with or without SDF-1 antibody (50μg/mL) (R&D). After 18 hours, transwell membranes were fixed with formalin, stained with DAPI, and imaged from the bottom to the top with a Zeiss 710 confocal microscope. Subsequently, the number of migrated MDA-MB231 cells was quantified via manual counting of DAPI-stained nuclei at the bottom of the membrane. To further confirm the importance of the SDF-1/CXCR4 signaling axis to varied MDA-MB231 migration, SDF-1 signaling was inhibited by blocking its corresponding receptor with a CXCR-4 antibody (25μg/mL) (R&D) (n=3/group).

Analysis of tumor cell responses to obesity-mediated ECM changes

Variations in tumor cell behavior as a function of obesity-mediated differences in ECM assembly were assessed with decellularized matrices (Fig. 4B). Briefly, $3x10^4$ cells were seeded on Fn-coated Thermanox™ coverslips (Thermo Scientific) and cultured for 8 days after which cells were removed through detergent-based extraction as previously described[48,227]. Subsequently, MDA-MB231 cells were seeded on the decellularized matrices and cultured for 8 to 10 days (n=3 /condition). To assess tumor cell growth, MDA-MB231 were trypsinized and counted using a hemocytometer. Matrix-dependent differences in FAK phosphorylation were determined by IF and Western Blot analysis of pFAK[397] as

described above. The role of stiffness-dependent differences in tumor cell contractility and their effect on growth was tested by culturing tumor cells on the different decellularized matrices in the presence and absence of the ROCK inhibitor Y-27632 (10 μg/mL) (Tocris).

To determine the importance of obesity-mediated differences to NANOG expression, NANOG promoter GFP reporter MDA-MB231 cells[222] were cultured on the different matrices and the number of GFP positive cells was determined by image analysis with ImageJ (NIH). Correlation of GFP expression with ECM-dependent differences in integrin signaling was assessed by staining for pFAK[397] as per above and quantifying the number of MDA-MB231 doubly positive for GFP and pFAK[397]. To more directly test the effect of stiffness on NANOG transcription, PA gels of various Young's moduli were fabricated as described previously[229]. Briefly, the stiffness of PA gels was tuned by altering the ratio of 40% acrylamide and 2% bis-acrylamide (both from BioRad), and the surface of the polymerized gels was functionalized by a photo-initiated reaction with N6 (n-hydroxysuccinimidyl acrylamidohexanoic acid) (kindly provided by Valerie Weaver's lab, UCSF) and crosslinking with 30μg/mL of Fn. Cells were seeded on the different gels, cultured for 5 days, fixed with 4% PFA, and counterstained with DAPI. GFP-positive cells were evaluated as a percentage of the total number of cells using images captured with a Zeiss 710 confocal microscope. Five gels per stiffness were fabricated, 8-10 representative images per gel were analyzed (n=4/group).

ECM-dependent differences in cancer stem cell-like properties were evaluated by determining the capability of MDA-MB231 cells to form tumor spheres. To this end, NANOG promoter GFP reporter MDA-MB231 cells cultured on the decellularized matrices from control and obesity-associated ASVCs were trypsinized and suspended in serum-free DMEM/F12 containing basic FGF, EGF (20ng/ml each, both from Invitrogen), 1x B27, and 1x antibiotic/anti-mycotic (both from Gibco)[230]. Subsequently, a limiting dilution analysis was performed by serial dilution culture of MDA-MB231 cells in 96-well plates

under serum-free conditions for 7 days (n=12/group). The number and size of spheres were microscopically assessed. Stem cell frequency was assessed using the extreme limiting dilution algorithm[231].

The level of matrix-bound SDF-1 and its role in mechanoregulation of cancer stem cell-like properties of MDA-MB231 were analyzed. For the analysis of the matrix-bound SDF-1, decellularized matrices deposited by either *ob/ob* or wild type ASVCs were prepared as described above and then lysed in RIPA buffer. The level of SDF-1 from the lysate was measured by ELISA. In addition, to examine if there is any SDF-1/CXCR4 signaling-mediated effect on modulating FAK phosphorylation and cancer stem cell-like properties of MDA-MB231, SDF-1-CXCR4 signaling was inhibited by blocking CXCR4 of MDA-MB231. Prior to being seeded on decellularized matrices, MDA-MB231 were incubated with CXCR4 antibody (25ug/mL) in αMEM containing 1% FBS and 1% antibiotic for 2 hours, and cultured on the matrix with the CXCR4-contained media, which was replenished every other days. After 10days, pFAK[397] and Nanog positive cell populations were assessed similarly as described above.

Patient-derived tumor specimens and histopathological analysis

Paraffin-embedded breast tumor specimens were obtained from existing archived samples of 17 lean and 18 obese breast cancer patients under the approval of IRB Study 0408007390 at Weill Cornell Medical College. Tumor specimens were categorized by the patient's BMI whereby a BMI of <25 and >30 was considered lean and obese, respectively. The two cohorts were evenly matched for age (average age: 44.7 ± 9.7 [lean] vs. 44.8 ± 8.8 [obese]), menopausal status (premenopausal: 59% [lean] vs. 56% [obese]; postmenopausal: 41% [lean] vs. 44% [obese]), stage and subtype of breast cancer at the time of diagnosis. In both groups, the majority of patients (83%) had stage 3 breast cancer at diagnosis and the remainder (17%) had *de novo* stage 4 breast cancer as their initial diagnosis. Also the tumors from two

patient groups were found to be unbiased to any specific subtype of breast cancer as being impartially distributed among 8 types including Lumina A, B, A/B, HER2, and HER2 status not specified, HER2/neu enriched, triple negative, basal-like breast cancer. To assess the degree of desmoplasia, hematoxylin and eosin (H&E)-stained sections were scored by a pathologist in a blinded manner. Additionally, specimens were subjected to SHG imaging analysis of collagen as well as IF staining of α-SMA and Fn as described above. For the latter, images of 10 randomly selected areas were captured per sample and subjected to image analysis. Lastly, the level of NANOG protein on the specimens was assessed by immunohistochemical staining. The paraffin-embedded tumor sections were deparaffinized, rehydrated and treated by EDTA (pH 8) antigen retrieval solution. Subsequently endogenous peroxidase and then non-specific binding of antibodies were blocked by a 10 minute-treatment with 3% hydrogen peroxide and 1 hour-incubation with blocking solution from ImmPRESS Kit (Vector Lab), respectively. The blocked sections were incubated by NANOG antibody (Cell signaling) overnight at 4°C and then labeled by HRP-conjugated secondary antibody (Novus Bio). Finally HRP-tagged NANOG positive cells were visualized by the reaction with 3,3´-diaminobenzidine (DAB) and DAB substrate kit (Thermo scientific), counterstained by hematoxylin and mounted. The NANOG stained sections were imaged and graded by a histopathologist.

Statistical analysis

Microsoft Excel and GraphPad Prism 5© were utilized to perform statistical analysis. Student's t-tests and ANOVA were used to compare parametric data between two conditions and among multiple conditions, respectively. For ANOVA, post-hoc pairwise comparisons were determined by Tukey's test. Difference in stem cell frequency was evaluated by Chi-squared test and the log-dose slope obtained from the stem cell frequency was validated by goodness of fit tests. The statistical correlation between the non-

parametric variables of human breast tissue was assessed by Spearman's rank correlation and its coefficient was denoted as rho (ρ). The association between patients' body condition (obesity vs. lean) and other categories (age, breast cancer subtype, menopausal status) was tested by Fisher's exact test. In addition, non-parametric data from histopathological evaluation of human tumor specimens were analyzed via Mann-Whitney U test. Two-sided testing was performed for each analysis and a P-value less than 0.05 was considered statistically significant. Unless otherwise noted, values are reported as the mean with error bars to indicate standard deviations. *In vitro* results are shown for one representative study after similar results were replicated in three separate experiments.

4.5. Results

Obesity increases interstitial fibrosis in mouse mammary fat pads

To quantify fibrotic remodeling, myofibroblast content and related ECM changes were assessed in mammary adipose tissue harvested from two well-established mouse models of obesity. Diet-induced obesity was achieved by feeding high fat diet to female C57Bl/6 mice for 10 weeks starting at 5 weeks of age. Obesity was reflected by increased weight of these mice relative to lean control animals fed with low fat diet (29.74 ± 4.15 g vs. 21.07 ± 0.63 g) (Fig. 4.1A). Additionally, age-matched female *ob/ob* mice were used, which are morbidly obese compared to wild type mice (54.39 ± 2.93 g vs. 19.8 ± 1.46 g) due to a loss-of-function mutation in the gene encoding the satiety hormone leptin[232]. Immunofluorescence (IF) analysis suggested that both diet and genetically induced obesity enhances interstitial α-smooth muscle actin (α-SMA; i.e., a myofibroblast marker) levels relative to the respective control conditions (Fig. 4.1B). This was further confirmed by Western Blot analysis of mammary adipose tissue from diet-induced mouse models. Levels of Fn, an ECM component primarily deposited by myofibroblasts[32,233], were also enhanced in obese animals (Fig. 4.1C). Importantly, high fat diet equally increased α-SMA and

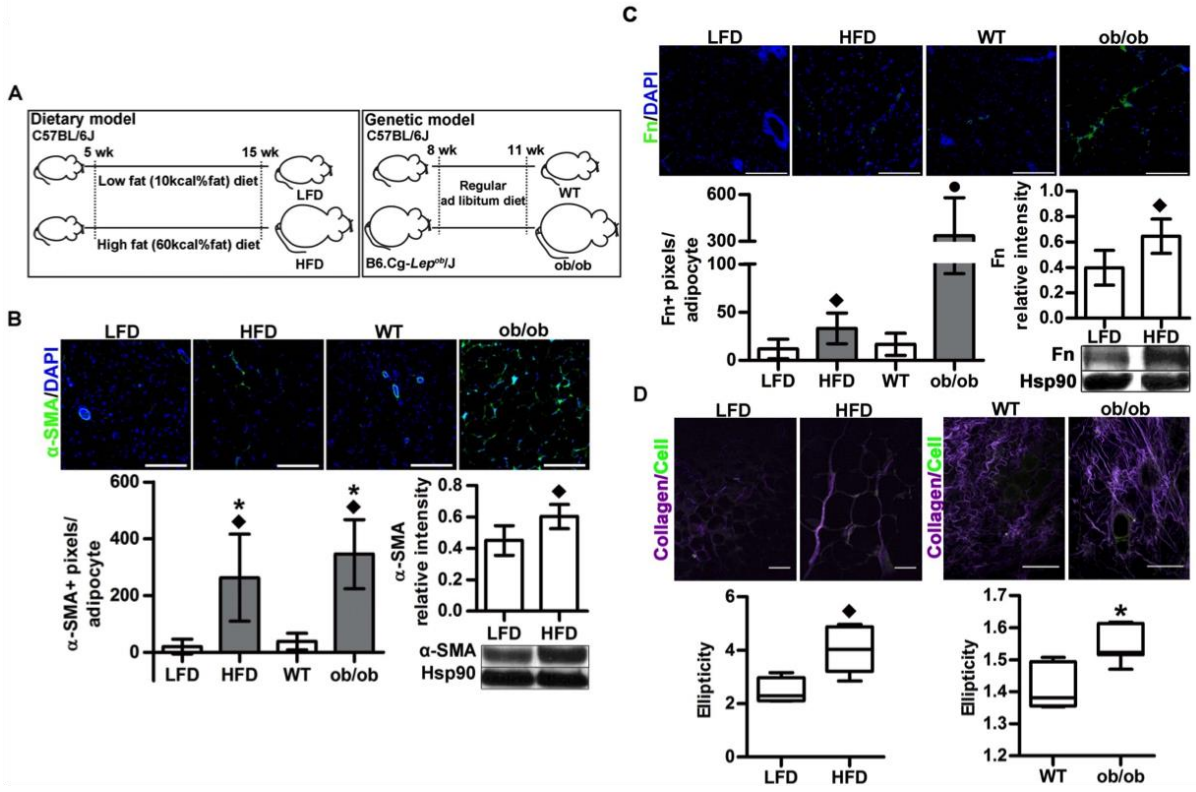

Fig. 4.1. Obesity increases interstitial fibrosis in mouse mammary fat pads. (A) Mammary fat harvested from both dietary and genetic models of obesity was compared to its lean counterpart harvested from age-matched (15 weeks and 11 weeks, respectively) mice. (B) IF and Western Blot analysis indicated that obesity-associated mammary fat (HFD, *ob/ob*) contains more α-SMA positive myofibroblasts than mammary fat from lean control animals (LFD, WT). (Scale bars = 200 μm) (C) Similarly, Fn levels were enhanced in mammary fat from *ob/ob* relative to wild type (WT) mice. (D) SHG imaging analysis suggested that collagen fibers in mammary fat from both HFD and *ob/ob* mice are more linearized as compared to those from, LFD and WT mice respectively. (Scale bar = 50 μm) ◆$p < 0.05$, *$p < 0.05$, and ●$p < 0.05$ indicate the difference from LFD, WT, and all others, respectively.

Fn content in mammary adipose tissue of ovariectomized mice (Fig. S1) suggesting that the above-described changes are relevant to postmenopausal breast cancer, the primary type of breast cancer whose risk increases with obesity[234]. Interestingly, ovariectomy did not further stimulate α-SMA in response to high fat diet (P=0.9706) (Fig. 4.2) although this regime increased mouse weight compared to high fat diet alone (mouse weights: 23.52 ± 2.09 g [ovariectomy/low fat diet]; 39.69 ± 2.72 g [ovariectomy/high fat diet]; 29.74 ± 4.15 g [high fat diet]). As this increase in weight is accompanied by elevated mammary

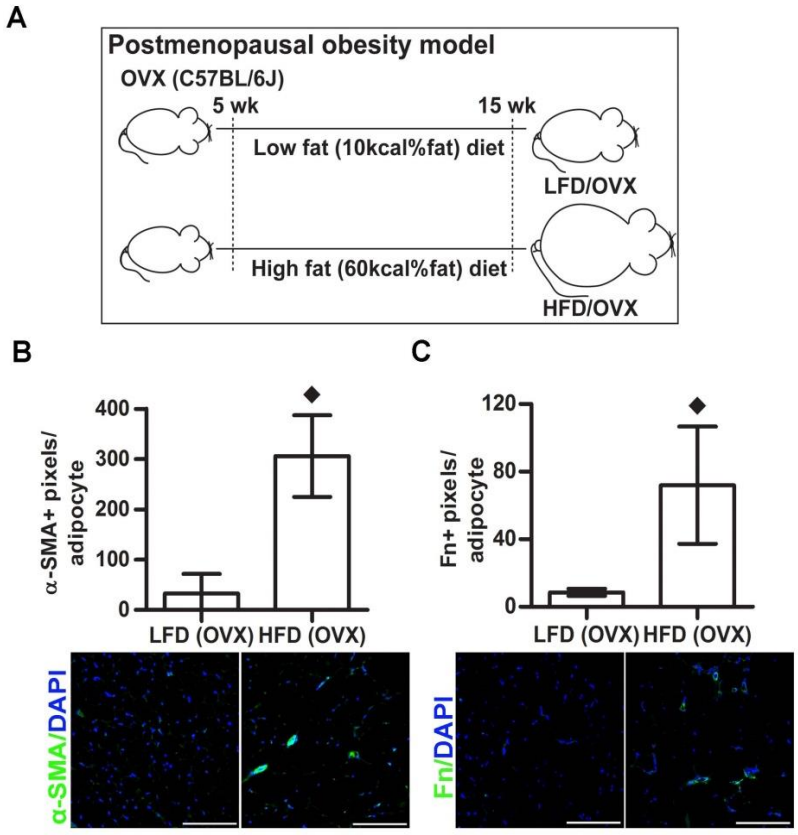

Fig. 4.2. Mammary fat of obese OVX-mice exhibits enhanced interstitial fibrosis. (A) Ovariectomized (OVX) mice subjected to high fat diet for 10 weeks were used as a postmenopausal obesity model; age-matched OVX mice fed with low fat diet served as controls. IF analysis of (B) α-SMA and (C) Fn content in mammary fat from OVX mice support that obesity promotes interstitial fibrosis in breast adipose tissue following menopause. (Scale bar = 200 μm) ◆$p < 0.05$

gland inflammation[218], our results imply that inflammation may not be the sole regulator of obesity-induced fibrosis.

In addition to these molecular and cellular characteristics of fibrosis, tissues were analyzed for the effect of obesity on ECM physical properties. More specifically, second harmonic generation (SHG) imaging analysis was utilized to quantify ECM structural changes and revealed that interstitial collagen was more linearized in mammary adipose tissue of *ob/ob* vs. wild type mice (Fig. 4.1D). Hence, obesity caused structural changes of collagen that were previously associated with enhanced stiffness,

malignancy, and ASVC-mediated ECM remodeling[33,48]. Consequently, obesity initiates fibrotic remodeling of mammary adipose tissue by triggering molecular, cellular, and ECM structural changes.

Obesity enhances the pro-fibrotic phenotype of ASVCs

To confirm that the detected cellular and molecular differences were functionally linked, we next performed *in vitro* experiments where we compared both the myofibroblast content and the ECM remodeling capacity of ASVCs isolated from the stromal vascular fraction of lean and obese adipose tissue (Fig. 4.3A). Given the small quantity of ASVCs that can be isolated from mammary adipose tissue and that differences observed in mammary fat were comparable to those present in s.c. depots from *ob/ob* mice (Fig. 4.4), ASVCs were isolated from the stromal vascular fraction of s.c. adipose tissue from age-matched lean (20.2 ± 1.4 g) and *ob/ob* (56.56 ± 3.33 g) mice. Indeed, IF and Western Blot analysis verified that ASVCs from obese mice were enriched for α-SMA positive, myofibroblastic cells (Fig. 4.3B). Furthermore, these cells also exhibited enhanced proliferative capacity as quantified by BrdU incorporation (Fig. 4.3C) and secreted greater levels of stromal vascular cell-derived factor 1 (SDF-1) (Fig. 4.3D), both additional markers of myofibroblasts[235,236,237]. Finally, compared to wild type ASVCs, *ob/ob*-derived ASVCs assembled thicker ECMs enriched with collagen and Fn as indicated by IF and additionally verified for Fn through Western Blotting (Figs. 4.3E and F), thus further confirming the profibrotic phenotype of these cells. Collectively, these results suggest that obesity promotes myofibroblast-mediated ECM remodeling via altering ASVC fate. In addition, similar changes were observed in ASVCs from diet-induced mouse model of obesity (Fig. 4.3G).

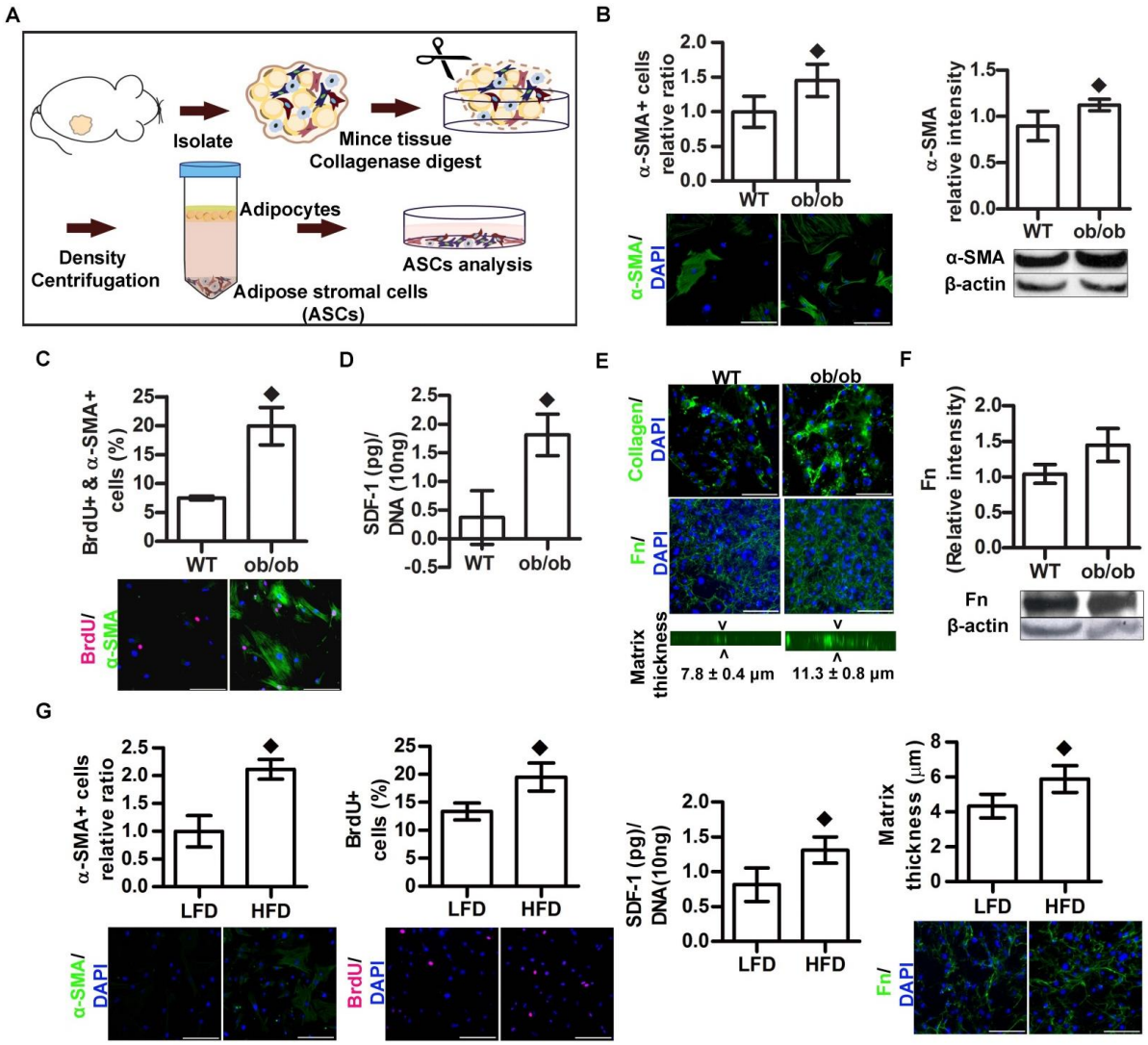

Fig. 4.3. Obesity enhances the profibrotic phenotype of ASVCs. (A) ASVCs were isolated from the stromal vascular fraction of subcutaneous fat from age-matched lean and obese (both genetically and diet-induced) mice, expanded, and their profibrotic characteristics analyzed. (B) IF and Western Blot analysis suggested that ASVCs from *ob/ob* mice contain more α-SMA positive myofibroblasts relative to ASVCs from lean mice. (Scale bars = 200 μm). (C) ASVCs from *ob/ob* mice exhibited enhanced proliferative capacity due in part to increased proliferation of myofibroblasts as indicated by an elevated percentage of α-SMA and BrdU double positive ASVCs in *ob/ob* vs. WT conditions. (Scale bars = 200 μm). (D) ASVCs from *ob/ob* mice secreted higher levels of SDF-1 as determined by ELISA followed by normalization to DNA content. (E) Confocal analysis of IF-stained samples indicated that ASVCs isolated from *ob/ob* mice deposit thicker ECMs, which are enriched in Fn and collagen type I. (Scale bars = 200 μm). (F) Western Blot analysis confirmed that ASVCs from *ob/ob* mice deposit more Fn relative to ASVCs from WT mice. (G) Similarly, ASVCs isolated from diet-induced obese mice (HFD contained more α-SMA positive cells relative to their lean counterparts (LFD) and were characterized by increased BrdU incorporation, SDF-1 secretion, and matrix deposition. (Scale bars = 200 μm). ◆$p < 0.05$.

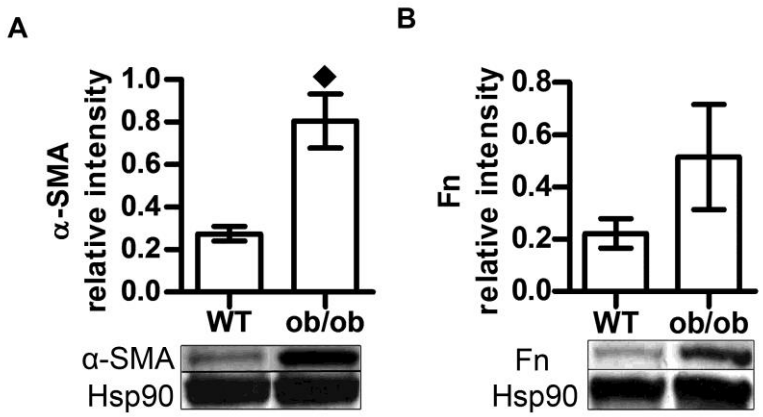

Fig. 4.4. Subcutaneous depots of adipose tissue feature markers of interstitial fibrosis. Western Blot analysis confirmed that (A) α-SMA and (B) Fn levels are enhanced in subcutaneous adipose tissue from *ob/ob* vs. WT mice in a manner comparable to mammary fat. ◆$p < 0.05$.

Obesity-associated ASVCs deposit partially unfolded and stiffer ECMs

Next, we tested whether obesity-mediated differences in ASVC fate translated to altered mechanical properties of the ECM. While increased rigidity of fibrotic and tumor tissue is typically believed to reflect alterations in collagen synthesis and crosslinking[33], variations in the Fn matrix structure and mechanics may be equally important. In fact, cellular deposition and remodeling of Fn is critical to the formation and turnover of collagen I-based ECMs[238-240], and both Fn conformational and mechanical changes may play an important role in this process[102,241]. Fluorescence Resonance Energy Transfer (FRET) analysis of Fn conformation suggests that ASVCs isolated from obese mice partially unfold Fn matrix fibers relative to ASVCs from lean control mice (Figs. 4.5A and B) thereby mimicking differences mediated by tumor-associated ASVCs[31]. Importantly, partial Fn unfolding may not only change cellular behavior via exposure of cryptic binding sites[91,242] or disruption of strain-sensitive binding sites such as the a5b1 integrin binding site[243], but also by directly elevating Fn fiber rigidity[95]. To confirm that obesity affects overall rigidity of ECM deposited by ASVCs at the cellular level, we performed measurements with the Surface Forces Apparatus (SFA) (Fig. 4.5C). The SFA is a force-sensing technique that uses

optical interferometry to determine the absolute surface separation between two reflecting atomically smooth mica surfaces. It allows studying normal (compressive and tensile) forces, and friction between surfaces and was initially established to measure mechanical properties of molecular-thin films under confinement and shear[244,245]. When applied to decellularized matrices, this technique confirmed that obesity elevates matrix rigidity to levels previously associated with enhanced malignancy (Fig. 4.5D)[123]. Consequently, obesity impacts the mechanical properties of the ECM deposited by ASVCs that may ultimately lead to interstitial stiffening.

Interestingly, ASVCs isolated from visceral fat of *ob/ob vs.* wild type mice similarly exhibit enhanced profibrotic potential as detected by elevated α-SMA and Fn content and partial unfolding of deposited Fn matrices. However, ASVCs from visceral fat deposited less ECM as compared to ASVCs from s.c. fat. These results suggest that our findings are broadly relevant and that obesity may alter the mechanical properties of adipose interstitial tissue at varying anatomical depots (Fig. 4.6).

Obesity-associated ASVCs stimulate MDA-MB231 migration and mechanosensitive growth

To evaluate whether the above-described changes affect the properties of tumor cells, the impact of obesity-mediated differences in ASVC paracrine signaling and matrix deposition on mammary tumor cell migration and growth were determined. Transwell migration assays showed that factors secreted by obese ASVCs stimulated MDA-MB231 migration compared to a similar number of lean ASVCs (Fig. 4.7A). Notably, these differences occurred in an SDF-1-dependent manner as antibody-based inhibition of both ASVC-secreted SDF-1 and the tumor cells' cognate CXCR4 receptor prevented the pro-migratory effect mediated by *ob/ob* ASVCs.

The effect of differential ECM properties on tumor cells was tested using decellularized matrices assembled by ASVCs from age-matched wild type and *ob/ob* subcutaneous adipose tissue (Fig. 4.7B).

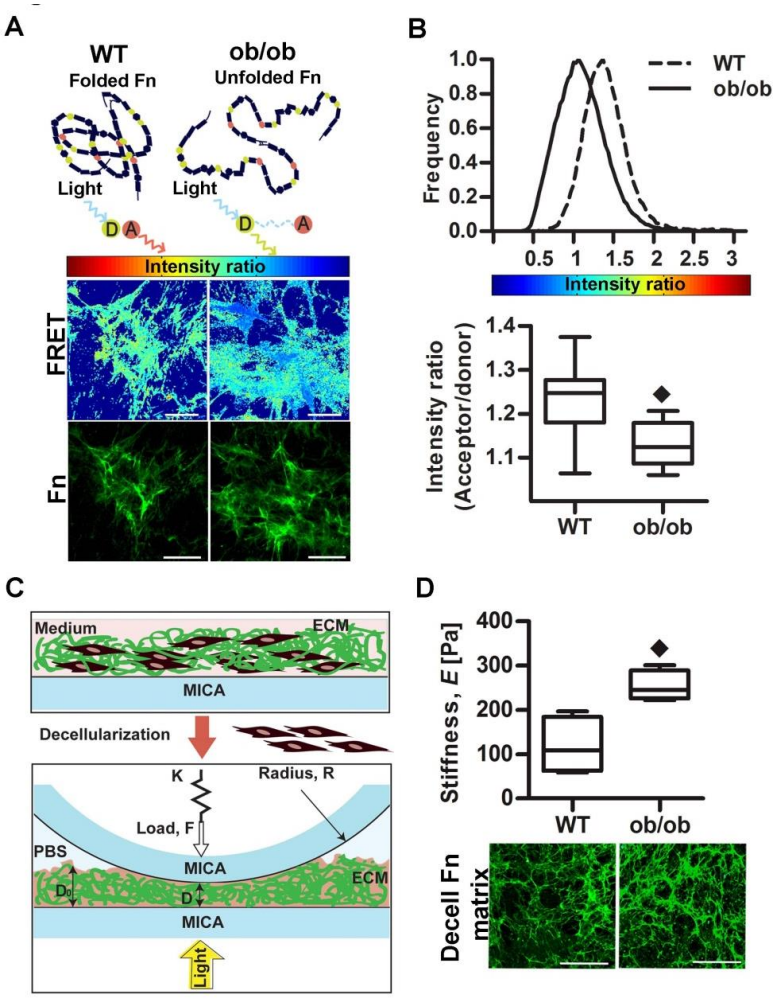

Fig. 4.5. Obesity-associated ASVCs deposit partially unfolded and stiffer ECMs. (A) Conformation of ASVC-assembled Fn matrices was determined by confocal analysis of FRET between donor [D] and acceptor [A] covalently coupled to Fn. Low FRET intensity due to separation of D and A indicates partial Fn unfolding, while enhanced FRET intensity suggests intact secondary/tertiary structure. Accordingly, Fn matrices deposited by obesity-associated ASVCs (*ob/ob*) contained more regions that were significantly unfolded (blue fibrils vs. green-yellow fibrils) relative to Fn matrices deposited by control ASVCs (WT). (Scale bars = 50 μm). (B) Analysis of FRET distribution confirmed that obesity-associated ASVCs induce elevated Fn fiber strain: Histogram of FRET intensities (i.e., acceptor intensity divided by the donor intensity [I_A/I_D]) derived from analysis of the fields of view shown in (A) and box and whiskers plots of the FRET intensity of 6-8 representative fields of view per condition. (C) Compressive elastic moduli of ECMs deposited by *ob/ob* and WT ASVCs was determined by indentation of decellularized ECMs between two silvered mica surfaces mounted on a cantilever spring of constant *k*. Surface separation was determined by optical interferometry and mathematically related to normal force (*F*) whereby *R* is the equivalent radius of curvature of the cylindrical discs, D_0 or *D* the undistorted or force-applied thickness of the matrix, respectively. (D) SFA analysis confirmed that ECMs deposited by obesity-associated ASVCs (*ob/ob*) on mica surfaces are stiffer than those deposited by their lean counterparts (WT); decellularization prior to analysis did not compromise the structural properties of Fn-rich matrices as indicated by IF. (Scale bars = 100 μm). ◆$p < 0.05$.

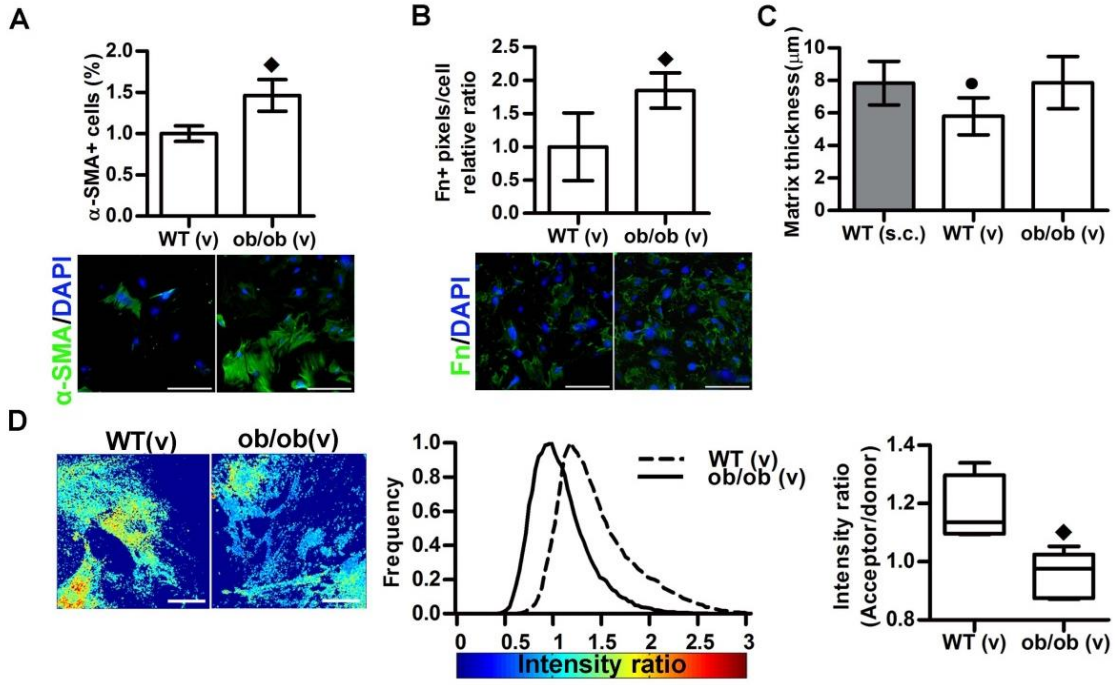

Fig. 4.6. Obesity-associated ASVCs promote fibrotic ECM remodeling in visceral fat. ASVCs isolated from visceral fat of *ob/ob* mice contained more myofibroblasts compared to their WT counterparts as identified by IF analysis of (A) α-SMA and (B) Fn. (C) Accordingly, confocal analysis of matrix thickness confirmed that matrices deposited by visceral ASVCs from *ob/ob* mice were thicker than those deposited by ASVCs from WT mice. Interestingly, ASVCs from visceral fat deposited less ECM as compared to ASVCs from s.c. fat. (Scale bar = 200 μm). (D) FRET analysis of Fn conformation suggested that ASVCs from visceral depots of *ob/ob* mice promote partial unfolding of Fn relative to the corresponding WT ASVCs resulting in decreased FRET intensity. Depicted here by more blue vs. green-yellow fibrils in ASVC-deposited, pseudocolored Fn matrices (left), histograms of the corresponding distribution of FRET intensity (middle), and box and whiskers plots of the FRET intensity of 6-8 representative fields of view per condition (right). ◆$p < 0.05$ and ●$p < 0.05$ indicate differences from WT (V) and all others, respectively.

Corresponding to our previous observation that stiffening of ASVC-derived ECMs promotes breast cancer cell proliferation[48], MDA-MB231 growth was enhanced on decellularized ECMs from *ob/ob* relative to wild type ASVCs (Fig. 4.7C). Increased stiffness stimulates cell growth by enhancing phosphorylation of focal adhesion kinase (pFAK), which, in turn, is caused by an elevation in RhoA/Rho-associated protein kinase (ROCK)-mediated cell contractility[90]. Accordingly, both IF and Western Blot analysis indicated that MDA-MB231 cells contained more pFAK when seeded onto ECMs deposited by

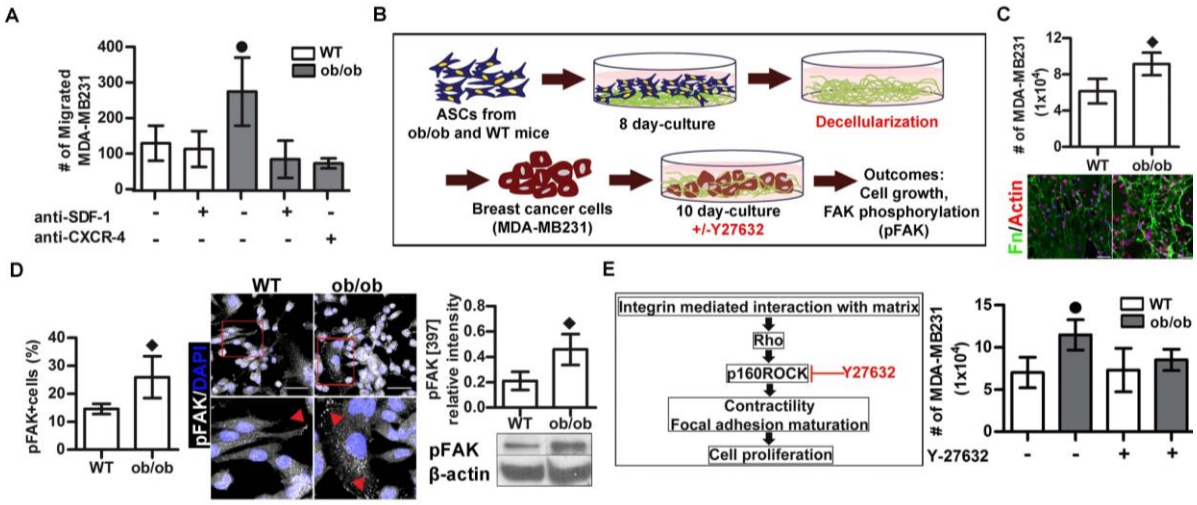

Fig. 4.7. ASVCs from obese mice stimulate MDA-MB231 migration and mechanosensitive growth. (A) Transwell assays revealed that ASVCs from *ob/ob* mice promote MDA-MB231 migration relative to ASVCs from WT mice. These differences were dependent on functional SDF-1/CXCR4-signaling because obesity-dependent promigratory effects were abrogated by inhibiting SDF-1 from ASVCs or blocking CXCR4 on MDA-MB231. (B) To determine the effect of obesity-mediated differences in ECM physicochemical properties on mammary tumor cells, decellularized ECMs were prepared from *ob/ob* and WT ASCs and reseeded with MDA-MB231. Subsequently, changes in tumor cell behavior were evaluated as a function of stiffness-dependent differences in cell contractility. (C) Cell counting suggested that MDA-MB231 (red for actin) grew more on decellularized ECMs (green for Fn) from *ob/ob* ASVCs than on ECMs from WT ASVCs. (Scale bar = 100 μm). (D) Image analysis of IF-stained cells and Western Blotting indicated that MDA-MB231 contained more pFAK[397] that was localized along the cell boundary when plated on decellularized matrices from obesity-associated ASVCs. (Scale bar = 50 μm). Red arrows indicate localized pFAK. (E) Enhanced pFAK levels suggested that elevated MDA-MB231 growth was related to ECM stiffness-dependent changes in cell contractility. Indeed, blocking the catalytic sites of Rho associated kinase p160ROCK with Y27632 decreased MDA-MB231 growth on *ob/ob*-derived ECMs to control levels. ◆$p < 0.05$ and ●$p < 0.05$ indicate the difference from WT and all others, respectively.

ob/ob vs. lean ASVCs (Fig. 4.7D). Moreover, inhibition of cell contractility using the ROCK inhibitor Y-27632 blocked the growth-promoting effect of ECMs deposited by *ob/ob* ASVCs (Fig. 4.7E), which further confirmed that obesity-induced interstitial ECM stiffness promotes tumor cell growth by altering cell contractility-dependent signal transduction (Fig. 4.8A).

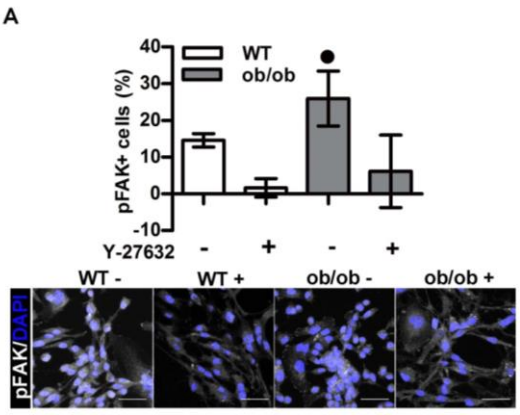

Fig. 4.8. Decellularized matrices from obesity-associated ASVCs promote pFAK and tumor sphere formation. (A) Analysis of IF images indicated that addition of the ROCK inhibitor Y-27632 reduced pFAK in MDA-MB231 cultured on decellularized matrices from *ob/ob*-ASVCs to levels comparable to culture on matrices deposited by WT ASVCs. Scale bar = 50 μm) ●$p < 0.05$ indicates the difference from all others.

Obesity-associated ASVCs promote MDA-MB231 expression of NANOG

As an additional measure of increased malignancy, we assessed whether obesity-mediated differences in ASVC matrix assembly enhance the expression of pro-carcinogenic molecules. We chose to test NANOG as a specific example given that this self-renewal transcription factor is a negative prognostic factor for breast cancer patients[246] and a promoter of cancer stem cell characteristics[247,248]. To monitor changes in NANOG expressing cells and thus cancer stem cells, MDA-MB231 cells were transduced with a reporter in which the NANOG promoter drives GFP expression as previously described[222]. GFP+ cells selectively express the stem cell markers NANOG, SOX2, and OCT4 compared to GFP- cells and have high stem cell frequency based on tumor sphere analysis[249]. Interestingly, the number of GFP+ cells was significantly increased on decellularized matrices deposited by *ob/ob* ASVCs relative to wild type ASVCs, suggesting that tumor cells enhanced NANOG transcription by interactions with obesity-associated ECM (Fig. 4.9A). Importantly, these differences correlated with altered mechanotransduction as IF and Western Blot analysis revealed that NANOG promoter (GFP+) - active cells contained enhanced levels of pFAK when cultured on *ob/ob* ASVC-derived ECMs (Fig. 4.9B). To

more directly determine the contribution of stiffness to NANOG promoter activity, cells were seeded onto polyacrylamide gels of stiffnesses relevant to normal and obesity-associated ECM rigidity. Culture on gels of increased elastic modulus elevated the number of NANOG promoter (GFP+) – active cells relative to softer gels (Fig. 4.9C).

Finally, to confirm a functional contribution of obesity-dependent ECM changes to NANOG-mediated differences in malignancy, tumor sphere formation of MDA-MB231 cells was evaluated following culture on decellularized ECMs deposited by *ob/ob* and wild type ASVCs. Indeed, tumor sphere formation of cells preconditioned on *ob/ob*-associated ECMs was increased suggesting enhanced self-renewal and stemness relative to cells preconditioned on control ECMs (Figs. 4.9D and 4.10). Collectively, these results suggest a contribution of obesity-mediated variations of ECM remodeling to NANOG-mediated tumorigenicity.

Obesity-associated ECM remodeling is clinically relevant

To determine the clinical relevance of our findings, we analyzed histological characteristics of desmoplastic remodeling in breast cancer specimens collected from lean and obese women. Pathological scoring of hematoxylin & eosin stained cross-sections revealed that tumors from obese patients exhibited more severe desmoplasia relative to tumors from lean patients (Fig. 4.11A, Table 1). Accordingly, IF analysis confirmed increased levels of α-SMA positive cells and Fn content in samples from obese vs. lean patients (Figs. 4.11B and C). Moreover, SHG analysis suggested that obesity leads to collagen-dependent structural changes contributing to enhanced mechanical rigidity because samples from obese patients not only exhibited increased collagen fiber linearity, but also fibril thickness (Fig. 4.11D). Together, these data suggest clinical relevance of our findings and that therapeutic interference with this process may prove valuable to improve patient outcome.

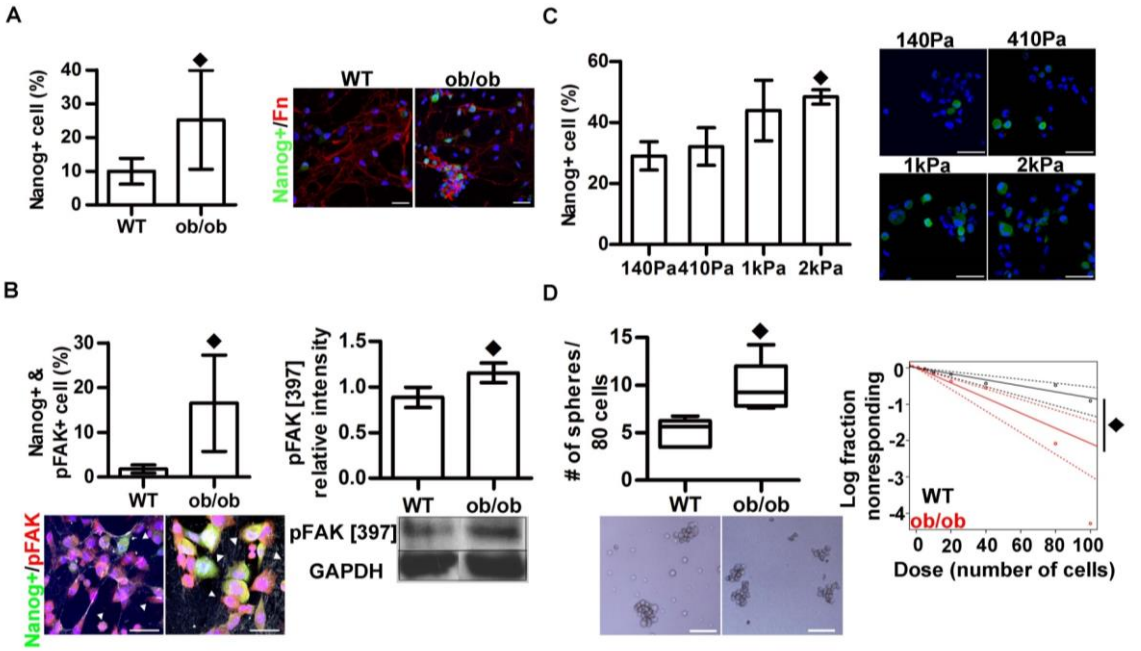

Fig. 4.9. Obesity-associated ASVCs promote MDA-MB231 expression of NANOG. (A) IF and Western Blot analysis of a reporter cell line in which the NANOG promoter drives GFP expression suggested that MDA-MB231 increased transcription of NANOG when cultured on decellularized matrices from *ob/ob* vs. WT-ASVCs. (Scale bar = 50 μm). (B) Enhanced NANOG transcription correlated with elevated pFAK[397] levels in this cell line as detected by IF and Western Blot analysis. White arrows indicate pFAK. (Scale bar = 50 μm). (C) Increased ECM stiffness promoted NANOG transcriptional activity because culture on polyacrylamide gels of elevated stiffness increased the number of GFP+ cells. (Scale bar = 50 μm). (D) Limited dilution assay indicated that the number of tumor spheres in a given population was increased when MDA-MB231 were cultured on decellularized matrices of *ob/ob* vs. WT-ASVCs. Left: number of tumor spheres formed from 80 cells per well; right: natural log fraction of negative responses as a function of seeding density. (Scale bar = 100 μm) ◆$p < 0.05$ indicates the difference of 140 Pa (C) and WT from all others.

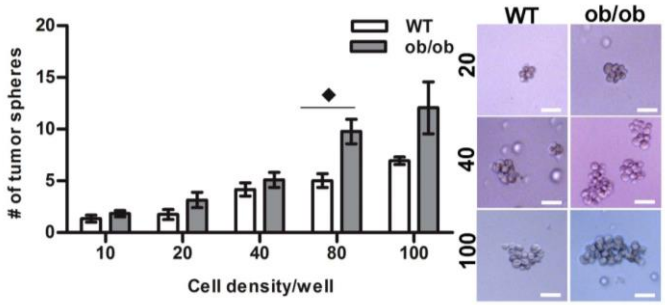

Fig. 4.10. Decellularized matrices from obesity-associated ASVCs enhance tumor sphere formation. MDA-MB231 increased tumor sphere formation when cultured on matrices deposited by *ob/ob*-ASVCs as compared to those assembled by WT ASVCs. (Scale bar = 50 μm). ◆$p < 0.05$.

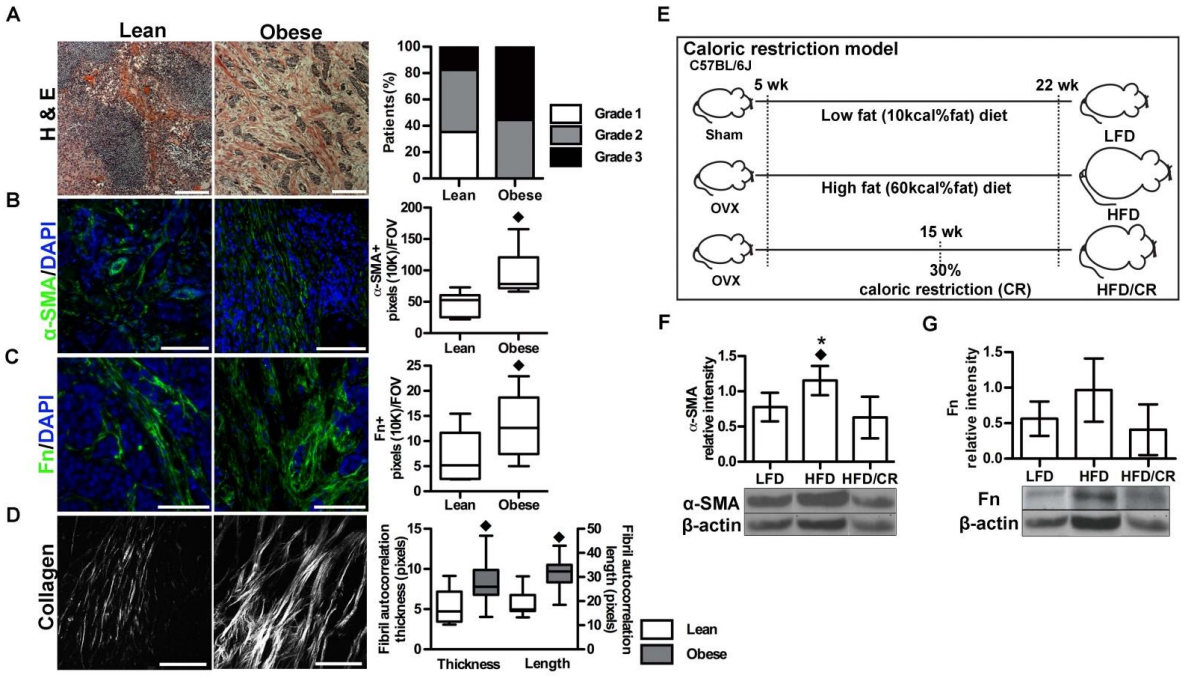

Fig. 4.11. Obesity-associated ECM remodeling is clinically relevant. (A) Histopathological scoring of clinical specimens indicated that breast cancers from obese patients exhibit a higher degree of desmoplasia. (Scale bar = 200 μm). Correspondingly, image analysis of IF-stained specimens suggested that breast cancers from obese patients were characterized by (B) enhanced α-SMA and (C) Fn content. (Scale bar = 100 μm) (D) SHG imaging analysis detected thicker and more linearized collagen fibers in tumors from obese patients. (Scale bar = 100 μm) (E) To investigate if caloric restriction can reverse obesity-mediated fibrosis, mice fed with HFD for 10 weeks were subsequently subjected to 30% of caloric restriction for 7 weeks. Western Blot analysis showed that reduced caloric intake (G) significantly lowered α-SMA levels, while (F) moderately decreasing Fn content. ◆ < 0.05, and *****p < 0.05 indicate differences from Lean (WT) and HFD/CR, respectively.

Nevertheless, controversy exists with regards to the therapeutic value of weight loss to the reversibility of adipose tissue interstitial fibrosis[250,251]. Therefore, we tested whether caloric restriction could reduce interstitial fibrosis in mammary fat. Ovariectomized mice were subjected to 10 weeks of high fat diet to mimic postmenopausal obesity followed by 7 weeks of caloric restriction to suppress further weight gain according to our previous reports (weights of mice: 22.10 ± 0. 58 g [low fat diet]; 38.93 ± 2.17 g [high fat diet], 30.12 ± 0.82 g [high fat diet/caloric restriction]) (Fig. 4.11E)[219]. Subsequently, mammary fat pads were excised and changes in interstitial fibrosis were assessed by

quantification of α-SMA and Fn levels. Western Blot analysis suggested that caloric restriction reduced the content of myofibroblasts in mammary fat interstitial tissue (Fig. 4.11F). A similar trend, but no statistical significance was noted for Fn (Fig. 4.11G). These results suggest that caloric restriction decreases features of fibrotic remodeling in mammary adipose tissue, but longer term follow up will be required to determine whether these cellular changes translate to differences in ECM physicochemical properties.

4.6. Discussion

Our results suggest that obesity leads to the formation of mechanical niches in adipose tissue that exhibit characteristics similar to tumor-associated stroma and promote carcinogenesis via altering mechanotransduction. More specifically, obesity increases the number of myofibroblasts in the stromal vascular fraction of mammary adipose tissue. These myofibroblasts not only deposit a more fibrillar, partially unfolded, and stiffer ECM, but also help recruit tumorigenic cells via increased secretion of SDF-1. Tumor cells interacting with the stiffer ECMs, in turn, exhibit varied mechanosignaling ultimately promoting mammary tumor cell growth and expression of malignancy markers.

The breast cancer-promoting capacity of obesity is widely recognized and mainly attributed to the altered paracrine and endocrine functions of adipose tissue[64], including elevated estrogen levels[252]. However, obesity not only worsens the clinical outcome of estrogen receptor (ER) positive, but also ER- and triple-negative breast cancer[253,254] suggesting that other, so far underappreciated, mechanisms play additional roles. According to the presented data, obesity-mediated differences of adipose interstitial mechanics may represent such a mechanism. Although our studies utilized ER-negative MDA-MB231

Tab. 1. Demographics and desmoplastic grade of lean and obese breast cancer samples Statistical examination of clinical specimens from 17 lean and 18 obese breast cancer patients confirmed the parity of age, cancer subtype, and menopausal status between the two cohorts. Histopathological analysis of desmoplasia indicated that the majority of tumors from lean patients was characterized by mild (grade 1) or moderate (grade 2) desmoplasia, while tumors from obese patients were characterized by moderate to severe (grade 3) desmoplasia. * indicates statistical difference between the two cohorts.

Variables		Body type		P-value
		Lean (17)	Obese (18)	
Age	Age < 30	1	0	
	30 ≤ age < 40	6	6	
	40 ≤ age < 50	3	3	
	50 ≤ age	7	9	
	Median age	43	43	1
Cancer type	Luminal (Her2 status not specified)	4 (23.5%)	4 (22.2%)	
	Luminal A	1 (5.9%)	3 (16.7%)	
	Luminal B	3 (17.7%)	2 (11.1%)	
	Luminal A/B	4 (23.5%)	2 (11.1%)	
	Luminal HER2	2 (11.8%)	3 (16.7%)	
	HER2/neu enriched	1 (5.9%)	0	
	HER2 negative	0	1 (5.6%)	
	ER/PR negative	1 (5.9%)	0	
	Triple negative	1 (5.9%)	1 (5.6%)	
	Basal-like	0	2 (11.1%)	0.782
Menopausal status	Pre-menopausal	10 (58.8%)	10 (55.6%)	
	Post-menopausal	7 (41.2%)	8 (44.4.%)	1
Desmoplastic grade	Grade 1	6 (35.3%)	0	
	Grade 2	9 (52.9%)	8 (44.4.%)	
	Grade 3	2 (11.8%)	10 (55.6%)	0.006*

Cancer subtype	Classification criteria
Luminal (Her2 status not specified)	ER+ and/or PR+, and HER2+/−
Luminal A	ER+ and/or PR+, HER2−, and low Ki67 (<14%)
Luminal B	ER+ and/or PR+, HER2−, and high Ki67 (>14%)
Luminal A/B	ER+ and/or PR+, HER2−, and no Ki67 available
Luminal HER2	ER+ and/or PR+, and HER2+
HER2/neu enriched	ER−, PR−, and HER2+
Triple negative	ER−, PR−, and HER2−
Basal-like	ER−, PR−, HER2−, and CK5/6 and/or EGFR+

.

breast cancer cells, increased ECM stiffness also promotes malignancy of other tumor subtypes[255,256] underscoring the broad relevance of our results.

While previous reports indicate that obesity stimulates fibrosis in subcutaneous and visceral adipose tissue[71], our results imply that similar changes occur in mammary adipose tissue. This observation is highly significant given that (i) the global functions and fibrotic remodeling of adipose tissue vary between anatomic depots[71,213,217] and (ii) the local microenvironment of the breast is indisputably relevant to mammary tumorigenesis[257-259]. Interestingly, obesity caused similar levels of fibrotic remodeling in mammary fat from ovariectomized and control mice further suggesting that obesity-associated stiffening of the ECM occurs independent of hormone status and thus, is pertinent to both pre- and postmenopausal breast cancer.

The described obesity-associated changes in ECM physicochemical characteristics were related to elevated myofibroblast population in the adipose stromal vascular fraction similar to tumor desmoplasia[48]. ASVCs isolated from obese adipose tissue were enriched for myofibroblasts and deposited a fibrillar, collagen type I- and Fn-rich ECM that was characterized by increased thickness, linearization, and partial unfolding. Importantly, these changes in ECM composition and structure elevated global matrix stiffness consistent with previous reports that increased ECM quantity[123], fibrosis-associated changes of collagen type I[260], as well as partial unfolding of Fn[95] all elevate ECM rigidity.

By combining both decellularized matrices and hydrogel-based artificial ECMs, we showed that the detected differences in ECM mechanical properties directly regulate the malignant capability of tumor cells. Our results confirmed that decellularized ECMs from obesity-associated ASVCs increased MDA-MB231 proliferation due in part to altered mechanosignaling. Importantly, elevated mechanosignaling is also correlated with the tumor cells' ability to up-regulate NANOG, a marker characteristic of increased malignancy and stem-like properties of tumor cells. This observation is important as cancer stem cells are

believed to promote cancer relapse and metastasis due to their self-renewal, differentiating capacity, and high resistance to chemo- and radiation therapy[261,262]. Together, our results suggest that the poor clinical prognosis of obese breast cancer patients may be related to ECM-mediated differences in cancer stem cell maintenance that may ultimately contribute to recurrence. Clearly, this is an exciting possibility, but future studies are needed to further evaluate this concept and assess the *in vivo* relevance of these changes.

Using specimens from lean and obese patients as well as testing the effect of caloric restriction on fibrotic remodeling of mammary fat, we provide experimental evidence supporting the clinical importance of our results. More specifically, we show that tumor desmoplasia and the related qualitative and quantitative ECM changes[257] worsen with obesity. Weight loss and exercise are routinely recommended to obese cancer patients as this regime may improve the clinical outcome of cancer patients[263]. A number of possibilities including altered metabolism[264] and reduction of local inflammation may contribute to this end[108]. Additionally, our data suggest that caloric restriction inhibits fibrotic remodeling because myofibroblast content in mammary fat of obese mice decreased with this condition; a similar trend was noted for ECM remodeling although the effect may be delayed relative to cellular change[265,266].

In addition to diet, a number of additional clinical scenarios could be impacted by our results. Mammography is a commonly-utilized modality for early detection of breast cancer and overall risk assessment because women with mammographically-dense breasts typically have a higher probability of developing breast cancer. However, radiographic breast density is inversely correlated with BMI. As fat is radiolucent, obese women appear to have non-dense breast tissue[267] although our data suggest that local, microscale density changes occur that may impact cancer risk. Therefore, alternative high-resolution imaging will be necessary in order to better localize and monitor regions that may stimulate tumorigenesis

in the obese. Furthermore, adipose tissue or ASVCs are increasingly being considered for regenerative approaches of mastectomy patients. Thus far, little attention is given to the body habitus of the patient from whom the ASVCs are isolated. Yet our data imply that ASVCs from obese individuals might promote recurrence of breast cancer relative to ASVCs from lean patients via changing the physicochemical properties at the implantation site. Stratification of patients based on BMI may help to better assess the potential risk, if any, associated with adipose tissue-based plastic and reconstructive approaches[268].

Based on our reported results a number of questions arise that provide ample opportunity for future studies. For example, what are the mechanisms contributing to obesity-associated differences in ECM mechanics and thus, mammary tumorigenesis? Is obesity-associated hypoxia an initiator of the detected changes due to its ability to upregulate the collagen-crosslinking, and thus, also increase the activity of the ECM stiffness-inducing enzyme lysyl oxidase[33,213,269] Alternatively, which role does obesity-associated chronic inflammation play in this process? Macrophages are enhanced in obese mammary tissue, but whether these differences indeed contribute to the elevated myofibroblast content in obese mammary fat remains to be confirmed. Moreover, obesity-associated fibrosis has been correlated with elevated levels of collagen type VI and its cleavage product endotrophin[213]. Nevertheless, the functional contributions of these molecules has only been tested at the biochemical level; whether their tumor-promoting effects[270] may also be related to altered ECM mechanics will need to be assessed. Finally, our study focused on the direct effect of obesity-mediated ECM differences on tumor cells. However, altered ECM mechanics can also promote tumorigenesis via indirect mechanisms; i.e., via influencing soluble factor (e.g. adipokines) signaling and by altering stromal cell responses[89]. Together, our results are of broad relevance to the field of obesity-induced cancer and inform a multitude of future studies in the arena of physical sciences oncology.

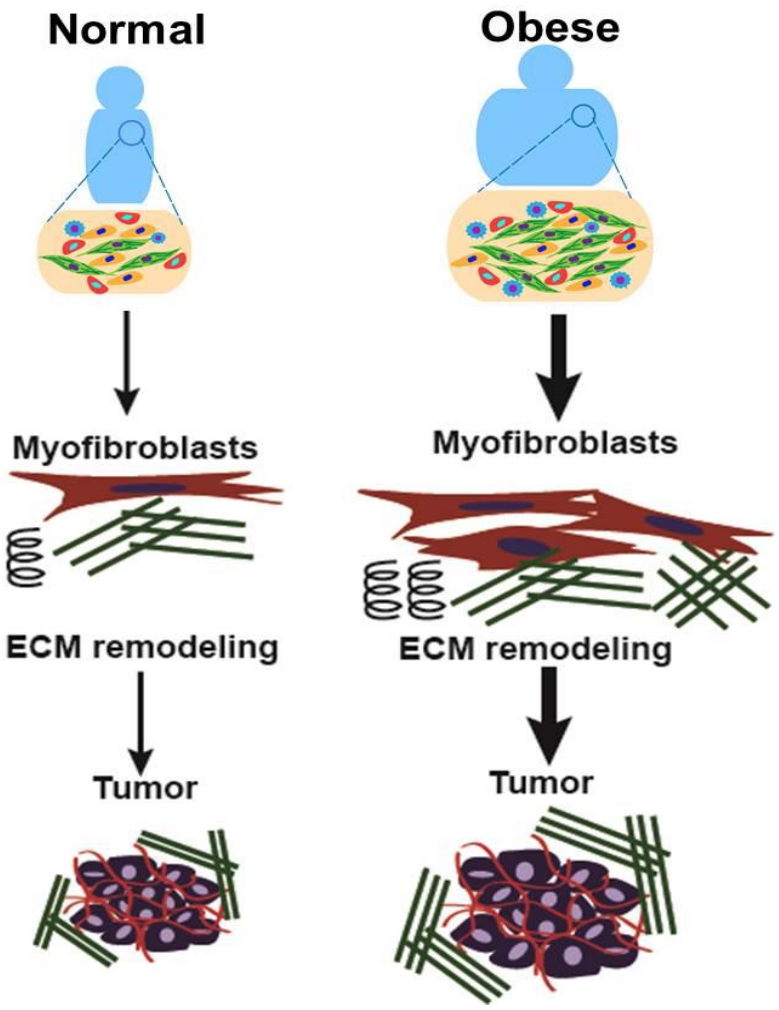

Fig. 4.12. Obesity-associated interstitial ECM remodeling promotes tumor growth.

CHAPTER 5

MICROSTRUCTURE OF COLLAGEN FIBERS REGULATES THE PRO-ANGIOGENIC POTENTIAL OF ADIPOSE-DERIVED STEM CELLS

5.1. Contributors

Co-authors of this chapter made the following contribution: Young Hye Song, Ph.D. graduate student in the Fischbach lab, aided in analyzing pro-angiogenic behaviors of adipose stromal cells and endothelial cells. Roberto C. Andresen Eguiluz, Ph.D. graduate student in the Gourdon lab and Jacqueline Gonzalez, undergraduate student in Fischbach lab at that time, measured the compressive moduli of collagen scaffolds and analyzed the results. Jiranuwat Sapudom, Ph.D. graduate student in the Pompe lab at Leipzig University, characterized interior architecture of collagen scaffolds. Siyoung Choi, a post-doctoral fellow in the Fischbach lab, aided in spinning electron microscopy (SEM) imaging. Prof. Denise Hocking at University of Rochester provided Fn-null mouse embryonic fibroblasts for the study. Prof. Tilo Pompe at University of Leipzig provided a custom-built algorithm for SEM image analysis. Prof. Delphine Gourdon provided resources for FRET analysis and advice on characterizing mechanical properties of collagen scaffolds. This project was completed under the guidance of Prof. Claudia Fischbach, who provided me with scientific and technical advice to complete this work.

5.2. Abstract

Angiogenesis is critical to normal (e.g. wound healing) and pathological (e.g. cancer) tissue remodeling and influenced by surrounding stromal cells. However, the effect of extracellular matrix (ECM) microarchitecture on endothelial-stromal cell interactions remains unclear. In particular, collagen is one of

the most abundant ECM proteins in the body and is enhanced during tumorigenesis. Here, we investigated the impact of collagen fiber morphology on the pro-angiogenic potential of adipose-derived stem cells (ASCs) and the functional consequences on human umbilical vein endothelial cells (HUVECs) sprouting. To this end, ASC-embedded 3D collagen scaffolds with thick and thin fibers were fabricated by cold- and warm-casting, respectively, and overlaid with a confluent HUVEC monolayer. Pore size was greater in cold-cast collagen gels relative to warm-cast scaffolds, while the opposite was true for fiber diameter. Accordingly, cold-cast collagen gels induced ASC differentiation into contractile alpha-smooth muscle actin (α-SMA)-positive myofibroblasts, which deposited partially unfolded fibronectin compared to cells in warm-cast gels. Furthermore, ASCs embedded in cold-cast collagen gels increased vascular endothelial growth factor (VEGF) and interleukin-8 (IL-8) secretion in a Rho-dependent manner, stimulating increased sprouting of HUVECs. Our study indicates that microstructural changes of collagen fibrils can modulate the pro-angiogenic potential of ASCs with implications for regenerative medicine and cancer research.

5.3. Introduction

Because adequate perfusion is essential for all living tissues, new vessel growth via angiogenesis is a critical aspect of wound healing, tissue regeneration, and therapeutic approaches for various disorders such as ischemic heart diseases and cancer[50,52]. The multistep process of angiogenesis requires coordinated efforts of peripheral stromal cells under the regulation of biochemical and physical cues[50,271]. Upon receiving the stimulation, stromal cells secrete angiogenic factors and remodel surrounding extracellular matrix (ECM), both of which collectively direct ECs' angiogenic behaviors[51,52,271]. Among the stromal cells, progenitor cells, such as bone-marrow mesenchymal stem cells (MSCs) have been highlighted by an increasing number of studies regarding their roles in the promotion of functional tissue

remodeling, showing that the presence of progenitor cells not only promotes EC sprouting but also blood vessel maturation[272,273].

Adipose-derived stem cells (ASCs) are considered a promising autologous cellular source for regenerative medicine due to their abundance and accessibility. More importantly, the pro-angiogenic potential of ASCs has been demonstrated by improved vascularization of ASC-implanted *in vitro* and *in vivo* models[274-276]. This may be due in part to the plasticity of ASCs, which can differentiate into various cell types involved in angiogenesis, including endothelial cells, smooth muscle cells, and myofibroblastic cells[83,277]. In particular, α-smooth muscle actin (α-SMA) positive myofibroblasts greatly contribute to tissue remodeling by secreting pro-angiogenic factors such as vascular endothelial growth factor (VEGF), basic fibroblast growth factor (bFGF), and interleukin-8 (IL-8), and by actively depositing thicker and aligned fibrillar ECM during wound healing, fibrosis, and tumor desmoplasia[61,186]. Thus, myofibroblastic differentiation of ASCs has been linked to tumor progression via enhanced angiogenesis and matrix remodeling[177,178]. Transforming growth factor-β (TGF-β) has been indicated as a primary molecular mediator of myofibroblast differentiation, but ECM-mediated physical cues are equally critical in determining cell fate[196].

Matrix properties have been known to regulate cellular behaviors such as proliferation, differentiation, and migration by modulating cytoskeleton organization and contractility[46,278,279]. ECM-derived biochemical and physical cues are modulated by changes in density, composition, conformation, and structure of ECM components at various spatial scales. Among interstitial ECM components, fibrillar collagen type I is the most abundant ECM protein and, together with fibronectin (Fn), plays a major role in regulating ECM integrity[280]. Changes in collagen microstructure, including collagen density, cross-linking, and alignment have been clinically correlated with disease stages[202,281-283]. Moreover, it has been shown that fibronectin conformational changes modulate cellular behaviors including angiogenic

potential via altered integrin engagement[284]. Nevertheless, little is known regarding the role of collagen fiber microstructure in the regulation of cellular behaviors. This is in part due to the difficulty of decoupling individual effect of fibrillar microstructure from other physical parameters of collagen matrix, which often concomitantly occur during tissue remodeling *in vivo*.

Engineered collagen scaffolds with varying mechanical property, interior architectures or fibrillar structures have been widely utilized for in vitro biological assays[133]. *In vitro*, collagen polymerization conditions such as pH, temperature, and ion strength modulate interior architecture (pore size) and microstructure of fibers (diameter, length, and alignment), which collectively alter the biochemical and mechanical properties of collagen matrix. These changes potentially regulate cellular behaviors such as proliferation and migration[93,285]. While engineered *in vitro* systems have aided in understanding the role of microarchitecture in the regulation of cell behaviors such as cancer cell invasion and blood vessel morphogenesis, there is still lack of understanding about whether fiber thickness influences mechanoregulation of cell behaviors[94,286]. In particular, the role of microstructure of collagen fiber in the regulation of ASC phenotype and its resulting effects on angiogenic activity of ECs remain elusive.

Here, we utilized 3D co-culture scaffold with varying microstructure of collagen fibers to investigate our hypothesis that thicker collagen fibrils mechanically stimulate pro-angiogenic potential of surrounding progenitor cells, thereby facilitating angiogenic activities of ECs. Our findings suggest that microstructural change of collagen fibers is a critical regulator of stem cell fate, providing significant implication in cancer, stem cell, and tissue engineering research.

5.4. Materials and methods

Cell culture

Human adipose derived stem cells (ASCs) were maintained in ADSC-GM supplemented by growth factors (both from Lonza). Human umbilical vein endothelial cells (HUVECs) (Lonza) were cultured in HUVEC-GM containing Bio-Whittaker® medium 199 (M199; Lonza) with Endothelial Cell Growth Supplement (Millipore), 2mM Glutamax, 5U/ml heparin, 20% Fetal Bovine Serum (FBS) (Tissue Culture Biologicals), 1% penicillin/streptomycin (Gibco). Fn-null mouse embryonic fibroblasts (FN-null MEFs) were generously provided by Prof. Denise Hocking, University of Rochester, Rochester, NY) were cultured on 50μg/ml of collagen I (Gibco)-coated culture plates under fibronectin- and serum-free media using a 1:1 mixture of Cellgro® (Mediatech) and Aim V (Invitrogen).

Fabrication of three-dimensional collagen scaffolds with varying microstructure

Three-dimensional collagen scaffold fabrication procedure was adopted from our previously published protocol[182]. First, 4-mm-diameter and 200-μm-thick round shape of polydimethylsiloxane (PDMS) molds were micro-fabricated using Sylgard® 184 silicone elastomer kit (Dow Corning) and their surface was treated by 1% [v/v] poly-ethylenimine (Aldrich) and then 0.1% [v/v] glutaraldehyde (Fischer Scientific) to aid the adhesion of collagen to the mold. After the surface treatment, the molds were kept in either ice-cold or 37°C to either delay or accelerate collagen fibrillogenesis, which ultimately modulates collagen fibril diameter. Collagen was obtained by acid extraction of rat-tail tendon (Pel-Freez Biologicals), lyophilized and then reconstituted in 0.1% [v/v] acetic acid at a concentration of 1.5mg/ml as previously described[287]. The reconstituted collagen was neutralized to pH 7.2 by an increment of 0.1N and 1N NaOH, and then mixed with ASCs at a density of 2 million cells/ml to produce a final concentration of 0.6% collagen suspension. Subsequently, the half of the ASCs-suspended collagen was injected to the pre-chilled molds and slowly polymerized by a series of gradual temperature change from ice-cold, room temperature to 37°C to create thicker collagen fibrils while the other half was abruptly

solidified in pre-warmed molds at 37°C for thinner fibrils. The completely polymerized collagen scaffolds containing ASCs were cultured in their growth media for 6 days.

Confocal reflectance microscopy (CRM) analysis of microstructure in collagen scaffold

To visualize the microarchitecture of collagen scaffolds with cells and its remodeling over time, ASCs-embedded collagen scaffolds cultured for 1, 6, and 10 days were briefly washed with ice-cold PBS and then fixed with 4% paraformaldehyde (PFA). Confocal reflectance imaging of collagen fibrils was performed using Zeiss 710 confocal microscope on a Zeiss Axio Observer Z1 inverted stand with 40x water immersion objective. The samples were illuminated by a low intensity of 488nm laser split through an 80/20 dichroic beam splitter, and the backscatter light reflected from collagen fibrils were collected by a photomultiplier tube. Z-stack images were captured from 5-6 random spots per each sample with 2μm intervals.

Scanning electron microscopy (SEM) imaging

For SEM analysis of the scaffold microarchitecture, ASCs-embedded collagen scaffolds were cultured for 1 and 6 days and briefly fixed by 2.5% glutaraldehyde in 0.05 M cacodylate buffer. The fixed scaffolds were sequentially dehydrated by a series of ethanol solution (25%, 50%, 75%, 95%, and 100%) and dried by a treatment with hexamethyldisilazane (Electron Microscopy Sciences). The dehydrated samples were mounted on the conductive carbon adhesive tab (Electron Microscopy Sciences), and then coated with gold/palladium alloy in sputter coater (Denton Vacuum, Desk II). Images were captured by scanning electron microscopy (Tescan, Mira3 LM) with 40000 magnification.

Image analysis of collagen scaffold microarchitecture

The pore size, mean diameter of fibril diameter of collagen and overall collagen content in cold- or warm-polymerized scaffolds were analyzed using a custom-built automated algorithm as described previously[288]. Briefly, the images taken by SEM were transformed to black and white binary images by a constant threshold throughout the conditions. The pore size was analyzed by an erosion algorithm where circular disks with varying size filled the pore areas, and the mean diameter of pore size was determined at 50% of total pore area. For fibril diameter, an autocorrelation method was utilized to evaluate the diameter of heterogeneously oriented collagen fibrils. 4 images per sample were analyzed. (n = 3)

Dynamic Mechanical Thermal Analysis (DMTA) of 3D collagen scaffolds

The compressive moduli of collagen scaffolds were measured by dynamic mechanical thermal analysis (DMTA) as previously described[177]. Collagen scaffolds were freshly prepared in PDMS micro-wells and kept submerged in PBS. For the test, gels were carefully taken out from the micro-well. Then the gels were placed between the DMTA parallel plates, and fully immersed in PBS in a standard submersion-compression clamp configuration at room temperature (25^{o}C). Given 10% pre-strain (0.001N), which prevented slippage of a sample during the test, the compressive tests were run on each sample under the controlled force up to 0.1N. The rate of force application was kept constant at 0.01 N/min in all tests. The force F (force sensitivity of 0.001 N) and thickness L (distance resolution of 0.05 μm) were measured simultaneously and converted into engineering stress-strain plots as follows: strain, $\varepsilon=(L_o-L)/L_o$ (where L_o is the initial thickness and L the thickness of compressed sample) and stress, $\sigma=F/A_o$ (where F is the applied force, and A_o the initial surface area). Young's modulus, E, was the slope of the stress-strain curve, $\sigma = E\,\varepsilon$ in the low-strain (5 - 20 %) elastic regime and the mean of Young's modulus [E] was obtained from four different samples. (n = 4)

Characterization of ASCs cultured in cold- vs. warm-cast collagen scaffolds

To investigate whether the micro-scale difference in collagen fibrils influence ASCs' phenotype, ASCs cultured in either cold- or warm-templated collagen scaffolds for 6 days were fixed and analyzed for myofibroblastic characteristics including alpha-smooth muscle actin (α-SMA) expression and fibronectin deposition by immunofluorescence and Western blot. For the fluorescent immunostaining, the fixed cells were permeabilized in 0.05% Triton X-100 (VWR) in PBS (PBS-X), blocked in 1% BSA (Fischer Scientific) in PBS, and then incubated with primary antibodies of α-SMA (Abcam) and Fn (Invitrogen) in 0.05% PBS-X overnight at 4°C. Then the samples were labeled by AlexaFluor 488 conjugated secondary antibody for α-SMA, and Fn, Alexa Fluor 568 Phalloidin for cytoskeleton, and counterstained with 4',6-diamidino-2-phenylindole (DAPI). For image analysis, 5 to 6 areas per stained sample were randomly selected and imaged by a Zeiss 710 confocal with 25x0.8 water immersion objective. The average positive pixel intensity above a constant threshold was calculated using Image J (NIH) and then normalized to the number of cells (n = 3).

Analysis of Fn conformation in 3D collagen scaffolds via FRET

ASCs in the cold- vs. warm-polymerized collagen scaffolds were pre-cultured for 3 days to render ASCs to deposit their own Fn matrix. 50 μg/mL of human plasma Fn consisting of 8% FRET-labeled and 92% unlabeled-Fn was supplemented and cultured for up-to 3 days[223]. Collagen scaffolds were fixed on day 1, 2, and 3 after FRET incorporation and then imaged using a Zeiss 710 confocal microscope with a 40x water immersion objective at 2μm intervals. FRET-labeled Fn in the matrices was excited by a low laser intensity (10%) through the 488 nm channel to prevent photobleaching, and the signals from both the donor (514-526 nm) and acceptor (566-578nm) channels were collected. For FRET image analysis, a strict threshold was set by averaging the highest signals from cell and fibronectin fibril-free areas in each

image to obtain concrete positive signals excluding autofluorescence from the underlying collagen. FRET intensity was obtained by calculating the ratio of acceptor to donor intensity through MATLAB (MathWorks, Inc.) as previously described[224]. 5 Z-stacks per sample, and three samples per condition were analyzed to determine the mean and standard deviation of the FRET intensities, and the histogram plots were generated to indicate FRET intensity at each representative location (n = 3). Finally, the obtained FRET intensity was compared to the pre-obtained calibration curves for the FRET intensity of chemically denatured dual-labeled Fn and its corresponding circular dichroism spectra [95,97]. Similarly, the strain of Fn fiber relative to the FRET intensity can be obtained by referencing a pre-obtained calibration curve of the FRET intensity as a function of real fiber strain[95].

Evaluation of pro-angiogenic factor secretion

To collect the pro-angiogenic factors secreted by ASCs in response to collagen fibrillar structure, ASCs cultured in collagen scaffolds for 6 days were incubated with DMEM/F12 (Gibco) with 1% FBS, and 1% penicillin/streptomycin for 24 hours. The media containing the ASCs secreted factors were collected, and the levels of vascular endothelial cell growth factor (VEGF) and interleukin-8 (IL-8) in the media were evaluated by VEGF and IL-8 ELISA duo set (R&D), respectively. The DNA content was extracted from the cells lysed in Caron's buffer (25mM Tris-HCl, 0.4M NaCl, 0.5% SDS), and measured by QuantiFluor® dsDNA System (Promega) following the manufacturer's protocols to normalize the VEGF and IL-8 levels. Each condition had three samples and each experiment was repeated three times to determine the statistical difference. (n = 3)

Endothelial cell sprouting assay

To evaluate the impact of the differences in VEGF and IL-8 concentration on the pro-angiogenic activity of endothelial cells, HUVECs were seeded on top of the ASCs-encapsulated cold vs. warm-templated collagen scaffolds. HUVECs were seeded on top of the collagen scaffolds at a density of 300 cells/mm^2 of the micro-well surface and were left to adhere for an hour. Subsequently, HUVEC invasion media containing HUVEC-GM, 1% [v/v] L-ascorbic acid (50 µg/mL; Acros Organics, Morris Plains, NJ), and 0.16% [v/v] tetradecanoyl phorbol acetate (50 ng/mL; Cell Signaling Technology, Inc., Danvers, MA) was added, and cultured for 4 days. For VEGF and IL-8 inhibition study, 1µg/ml of VEGF and IL-8 neutralizing antibodies (both from R&D) were supplemented in the invasion media and cultured for the same period of time. The resulting HUVEC sprouting in response to the ASC-derived pro-angiogenic factors were assessed by confocal microscope imaging the immunoflurescently labeled HUVECs by their surface marker, CD31 (Sigma-Aldrich). 5 to 6 top-to-bottom images per sample were obtained by Zeiss 710 confocal microscope with a 25×/0.8 water immersion objective at 5µm intervals. HUVEC sprouts, which exceed a length of 15µm, were manually counted throughout the Z-stack images. The average number of sprouts per condition was obtained from the counts of three samples in each experiment and the experiment was triplicated in a consistent manner. (n = 3)

Analysis of the stiffness-mediated effect on ASCs' pro-angiogenic factor secretion

To see whether the differences in the pro-angiogenic factor secretions from ASCs is mediated by the local scale of stiffness, ASCs in cold or warm-polymerized collagen scaffolds were cultured with Y27632 Rho/ROCK inhibitor (Tocris) which blocks Rho-mediated stress fiber formation and contraction (Ref). 30µM of Y27632-supplemented growth media (DMEM/F12 with 10% FBS and 1% antibiotics) were added to the cells every other day for 6 days. For the analysis of VEGF and IL-8 by ELISA, the media containing ASCs-derived factors was collected as explained above. To assess the response of

HUVECs to the Y27632-mediated changes of pro-angiogenic factors, HUVEC sprouting assay was performed after the Y27632 treatment for 6 days.

Statistical analysis

Student's t-tests and ANOVA were used to determine statistical difference between two conditions and among multiple conditions, respectively. For ANOVA, post-hoc pairwise comparisons were determined by Tukey's test. Two-sided testing was performed for each analysis and a P-value less than 0.05 was considered statistically significant. All tests were performed on Microsoft Exel and GraphPad Prism 5©. Unless otherwise noted, values are reported as the mean with error bars indicating standard deviations.

5.5. Results

Fabrication of collagen scaffolds with two different micro-architectures

To understand the impact of collagen fiber microstructures in a 3D scaffold on cellular behaviors, we utilized a previously-established micro-well model[289]. In this model, cell-suspended collagen solution was polymerized within each micro-scale cavity (4mm-diameter and 200μm in depth) patterned on a PDMS mold. This micro-well format aids in handling a compliant collagen scaffold and prevents contraction of the collagen scaffold, which binds to the walls of the micro-well during the culture period. To generate two different collagen fibrillar structures, we altered the polymerization temperature, which regulated lateral growth of collagen microfibrils and consequently fibrillar thickness[290,291]. As shown in Fig. 5.1A, solubilized collagen in acetic acid was first neutralized to pH 7.2-7.4 and mixed with the media containing $2x10^6$ ASCs. To ensure that other parameters (pH, salts and cell density) were kept identical, half of the prepared collagen solution was quickly polymerized in pre-warmed micro-wells at 37 ℃,

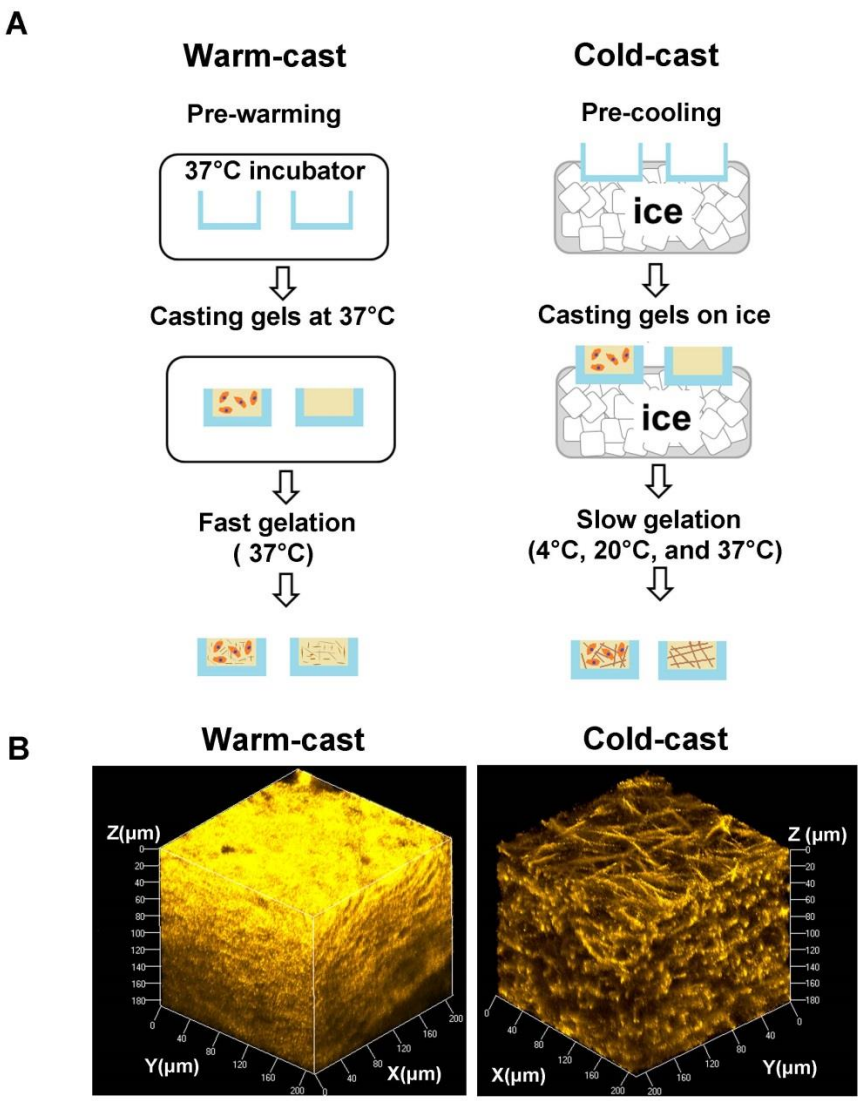

Fig. 5.1. Fabrication of collagen scaffolds with two different micro-architectures. (A) Cell-containing collagen suspension was prepared, and divided into half. The half of the suspension was injected to the pre-chilled molds and slowly polymerized by a gradual increase of temperature from ice-cold, room temperature to 37°C to create thicker collagen fibers. The other half was solidified in pre-warmed molds at 37°C to construct thinner collagen fibers. (B) After the polymerization, microarchitecture of a warm- (left) and cold-cast (right) collagen fibrils were visualized by confocal-microscope imaging.

while fibrillogensesis of the other half was prolonged by polymerizing collagen at initially cold temperature (4℃) for 20 minutes and gradually increasing the temperature to 20 ℃ for 20 minutes, and finally up to 37℃. The fully polymerized collagen scaffolds were then cultured in the growth media for the following analysis. Here we named a collagen scaffold casted at 37 ℃ as 'a warm-cast' scaffold and those casted initially at 4℃ as a 'cold-cast' scaffold. The 3D architectures of the collagen scaffolds were visualized by confocal reflectance microscope (CRM) to determine whether altered polymerization temperature changed the interior architecture of collagen scaffolds (Fig. 5.1B).

Characteristics of initial and remodeled collagen scaffold microarchitectures

Since ASCs actively remodel their ECM, we assessed structural features of the scaffolds at day 1 and day 6. For this, the cell-embedded scaffolds were cultured, harvested after each time point and imaged by CRM, as well as by scanning electron microscope (SEM) (Fig. 5.2A). For quantification, we utilized SEM images due to their higher resolution than CRM images at a nanometer scale as well as capacity to visualize collagen fibers at different angle[287,288]. Also, we quantified collagen fiber diameter and pore size from SEM using a custom-built algorithm[288]. In accordance with CRM observations and previously reported data, collagen fibrillar thickness changed as a function of cross-linking temperature[291]. The initial mean diameters of collagen fibrils (170.8 ± 5.9 nm) in the cold-cast scaffolds were significantly larger than those of warm cast scaffolds (129 ± 10.3 nm).

In addition, the pore size of cold-cast scaffolds was relatively larger (271.5 ± 16.4 nm) than that of warm-cast scaffolds (148.3 ± 10.8 nm). Finally, fiber linearity was assessed by calculating the ratio of the shortest length over the full length. Interestingly, collagen fibers in cold-cast scaffolds were more linear than those in warm-cast scaffolds on day 1. Therefore, cold-cast gels were characterized by

relatively thicker, straighter fibers and larger void spaces, whereas warm-cast gels exhibited smaller pores within a denser mesh of thinner, coiled/tortuous fibrils (148.3 ± 10.8 nm).

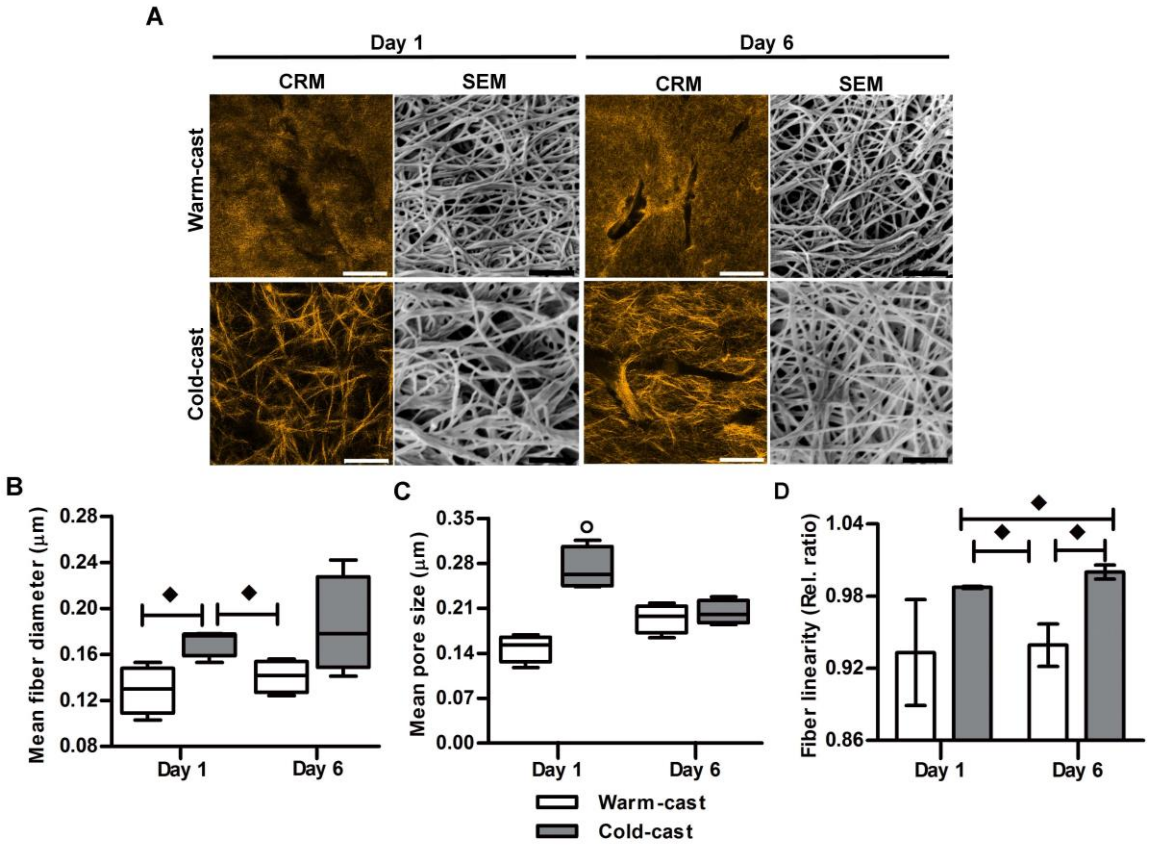

Fig. 5.2. Characteristics of initial and remodeled collagen scaffold microarchitectures. (A) The initial (day1) and ASC-remodeled (day6) interior architecture of warm- and cold-cast scaffolds were visualized by confocal reflectance microscope (CRM) and scanning electron microscope (SEM) imaging (Scale bars = 50 μm for CRM and 1 μm for SEM). (B) SEM image analysis indicated that the mean diameters of collagen fibers in cold-cast scaffolds remained greater than those of warm-cast scaffolds throughout the culture. (C) Larger pore size in cold-cast scaffolds significantly decreased, while the smaller size of pores in a warm-cast scaffold moderately increased over time. (D) Collagen fibrils in cold-cast scaffolds linearized over time, whereas only an insignificant change was noted in warm-cast scaffolds. ◆$p < 0.05$, and ❍$p < 0.05$ indicate the difference between two conditions and from all other conditions, respectively.

The trend to thicker fibers in cold-cast remained throughout the culture; however, the cold-cast conditions exhibited a broader range of fiber diameters (± 21.1 nm) on day 6 as compared to that on day 1 (± 6 nm) (Fig. 5.2B). Interestingly, after 6 days the pore size in cold-cast scaffolds significantly decreased, whereas it remained similar in a warm-cast scaffold (203.8 ± 9.2 nm and 194.5 ± 11.24 nm, respectively). Over this interval collagen fiber linearity increased in cold-cast scaffolds, whereas no significant difference was noted in warm-cast scaffolds (Figs. 3.2C and D). Since ASC-free collagen scaffolds maintained pore size and fibril linearity during the culture period (Fig. 5.3), our results suggest that these micro-structural changes were mediated by ASCs over time. These changes are considered indicators of increased cellular contractility[93,177], and has been seen in wound closure *in vivo* and fibroblast-embedded collagen scaffolds *in vitro*. Because the increased pulling force of cells is mediated in part by enhanced expression of α-SMA stress fibers[196,292], we next investigated changes in α-SMA levels of ASC in response to the different collagen fiber structure of the scaffolds.

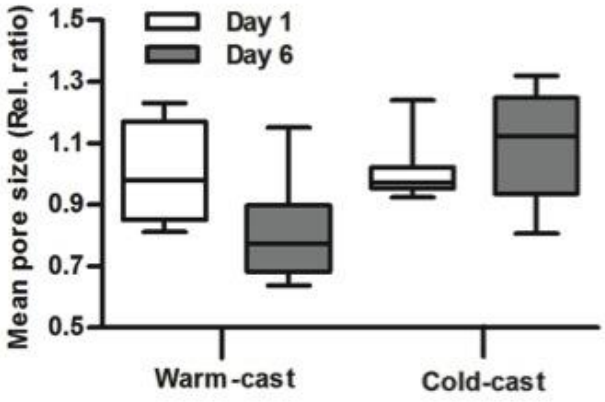

Fig. 5.3. Microarchitecture of collagen scaffolds in absence of ASCs. SEM image analysis indicated that the mean pore size of both warm and cold-cast scaffolds did not significantly change over time in the absence of ASCs.

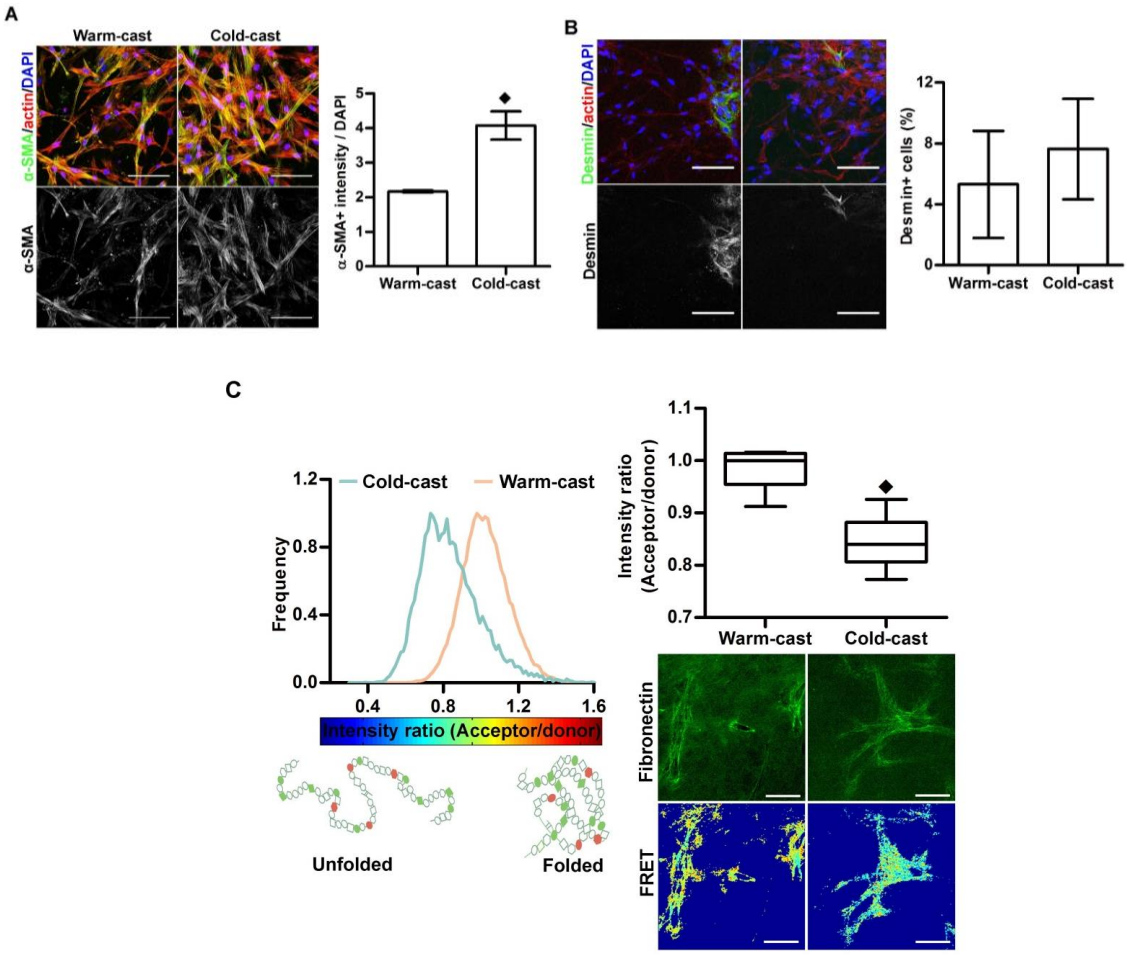

Fig. 5.4. Phenotypic changes of ASCs in response to collagen fiber thickness. (A) and (B) Immunofluorescence (IF) image analyses indicate that ASC-embedded cold-cast gels contained a larger population of α-SMA positive ASCs compared to those cultured in warm-cast scaffolds. Also, desmin positive cells were not associated with α-SMA positive cells. (C) A histogram and a box-and-whisker plot of FRET analysis show FRET intensity [Acceptor/Donor] obtained from a representative FRET image of each condition and the average of multiple FRET analysis per condition, respectively. Also, color-coded FRET image visualizes the relative conformational change of Fn by color spectrum from red (compact form) to blue (unfolded form). FRET analysis indicates that matrices deposited by ASCs cultured in cold-cast gels consisted of yellow to lighter blue-colored Fn fibers, which indicates a lower FRET intensity and thus, partially unfolded Fn. On the other hand, the matrices deposited by ASCs cultured in warm-cast gels contained red and orange colored Fn fibers indicating higher FRET intensity and thus, folded Fn. Scale bar =50 μm, ◆$p < 0.05$

Phenotypic changes of ASCs in response to the collagen fiber thickness

First, to evaluate ASC contractility, α-SMA expression level was assessed via immunofluorescence (IF) after 6-day culture either in cold-cast or warm-cast scaffolds. Because α-SMA is a marker of pericytes, smooth muscles cell, and myofibroblastic differentiation, we also stained for desmin, to identify the phenotype of the ASCs. Interestingly, our analysis indicates that ASCs cultured in a cold-cast scaffold exhibited increased expression of α-SMA protein while a pericytes marker, desmin positive cells were rare (Figs. 5.4A and B). This suggests that ASCs developed myofibroblastic phenotype in response to the thicker collagen fibers in cold-cast scaffolds, and this contractile cell population may further contribute to matrix remodeling by contraction, degradation, or deposition of ECM. This result is consistent with our previous study showed that ASCs develop a myofibroblastic phenotype in response to tumor-derived soluble factors[177].

In addition to collagen microarchitecture, fibronectin is another indicator of increased cellular contractility and Fn conformational change has been correlated with increased stiffness of Fn fiber, so we assessed fibronectin conformational change via FRET technique[31,97]. The histogram of FRET intensities obtained from a representative region of a cold-cast scaffold shifted to the left relative to that from a warm-cast scaffold, indicating that Fn fibers were more unfolded in cold-cast gels (Fig 5.4C). The corresponding FRET images visualize the Fn conformation of the representative region by a color spectrum, showing the matrix containing more low FRET Fn fibers in a cold-cast is colored by yellow to light blue while that with higher FRET Fn fibers in a warm-cast represents by orange and yellow. The whisker and box plot shows the compiled FRET intensities of Fn fibers in collagen scaffolds casted at cold temperature were significantly lower than those from warm-cast scaffolds, which implies that ASCs in cold-cast scaffolds deposited matrices containing partially unfolded and stiffer Fn fibers, whereas the Fn fibers in the matrices deposited by ASCs in warm-cast scaffolds were more compact and relaxed. In

addition, no differences were observed in FRET intensities of Fn fibers in the matrices deposited by ASCs cultured in cold- vs. warm-cast scaffolds when they were incubated with FRET-labeled Fn only for short periods of time (24 hours and 48 hours) (Figs. 5.5A and B), so we ensured that the difference of FRET intensities between two conditions in Fig. 5.4C was not associated with the auto-fluorescence of collagen fibers. These results altogether suggest that ASCs cultured in cold-cast scaffolds exhibit greater contractility and deposit stiffer fibers, thereby ultimately generating a stiffer microenvironment as compared to those cultured in warm-cast scaffolds.

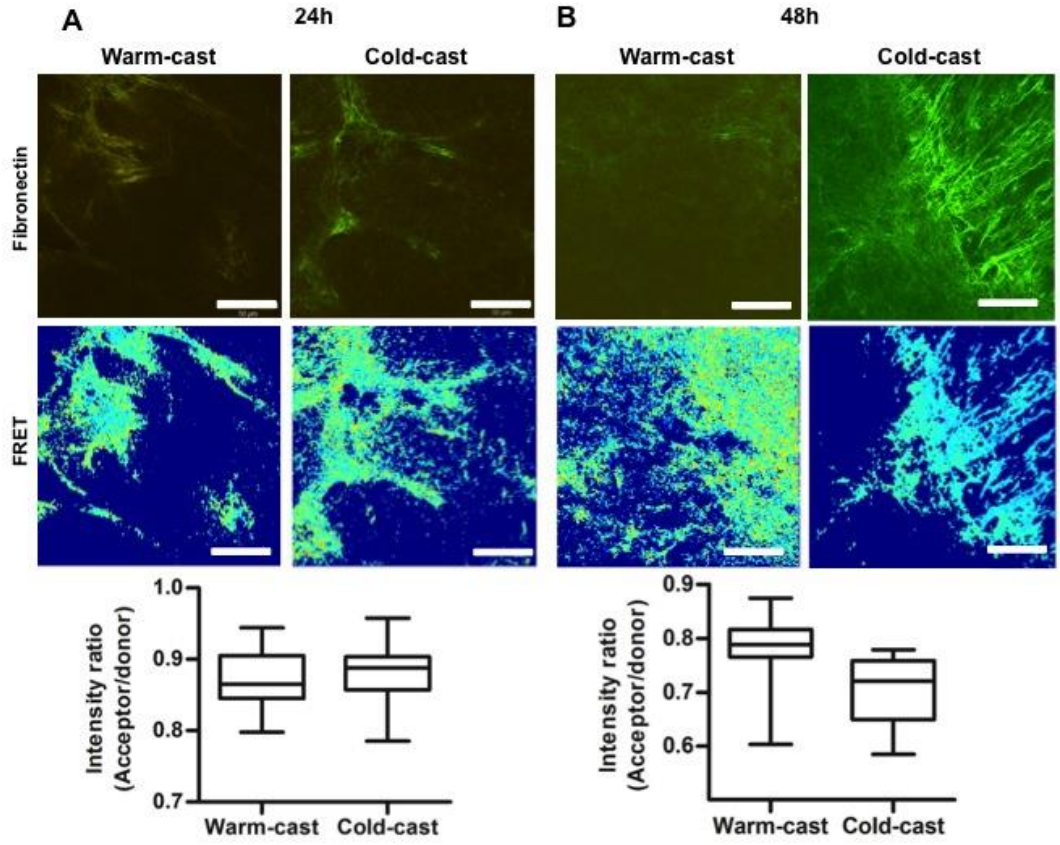

Fig. 5.5. FRET intensity of Fn in the matrices deposited by ASCs in response to collagen fibers. (A) and (B) FRET intensities of Fn in the matrices deposited by ASCs cultured in cold-cast scaffolds were not significantly different from those by ASCs cultured in warm-cast scaffolds when ASCs were incubated with FRET-labeled Fn for 24 hours and 48 hours. (Scale bar =50 μm).

Altered pro-angiogenic potential of ASCs by change in collagen fiber thickness

Next, we investigated if changes in fiber thickness of a collagen scaffold influence pro-angiogenic potential of ASCs. Media was collected from ASCs cultured in either a cold or a warm-cast scaffold for 6 days and their VEGF and IL-8 secretion levels were assessed by ELISA. In general, the levels of IL-8 secreted by ASCs cultured in collagen scaffolds are much greater than the levels of VEGF, which is similar to the previous study showing that IL-8 but not VEGF secretion was significantly up-regulated in 3D context as compared to 2D[294]. More interestingly, ASCs cultured in a cold-cast scaffold secreted greater amounts of VEGF and IL-8 in response to the thicker collagen fibers than those cultured in warm-cast scaffolds with thinner fibers and smaller pores (Fig. 5.6A).

To determine the functional consequences of altered pro-angiogenic signaling of ASCs in response to the collagen fiber structure, an endothelial cell invasion assay was performed using human umbilical vein endothelial cells (HUVECs). A monolayer of HUVECs was seeded on top of cold- or warm-cast scaffolds, which were pre-cultured with and without ASCs for 6 days. After 4 days, the number of HUVEC sprouts was quantified by confocal imaging analysis (Fig 5.6B). Our quantification revealed that the presence of ASCs significantly promoted HUVEC invasion in both cold- and warm-cast scaffolds.. However, the number of HUVEC invasions was much greater in cold-cast gels, in the presence or absence of ASCs, suggesting that matrix architecture may also play an important role in regulating angiogenic activities of HUVECs (Fig. 5.6C).

To distinguish ASC soluble factor signaling from matrix structural effects, we inhibited VEGF or/and IL-8 either alone or in combination while co-culturing a monolayer of HUVECs with embedded ASCs in the bulk of scaffolds. Our quantification of HUVEC sprouts showed that the presence of VEGF or/and IL-8 neutralizing antibody alone or together offset HUVEC sprouting in ASC-embedded cold-cast scaffolds, while there was no significant effect of VEGF and IL-8 neutralizing antibodies in ASC-embedded warm-

cast scaffolds (Fig. 5.7). Therefore, the increased angiogenic activity of HUVECs in cold-cast scaffolds was primarily mediated by enhanced pro-angiogenic signaling of ASC in response to thicker fibers. Since α-SMA-mediated contractility and pro-angiogenic behaviors of ASCs changed concomitantly in response to the changes in the architecture of collagen scaffolds, we examined whether the two behavioral changes (α-SMA-mediated contractility and pro-angiogenic behaviors of ASCs) were linked.

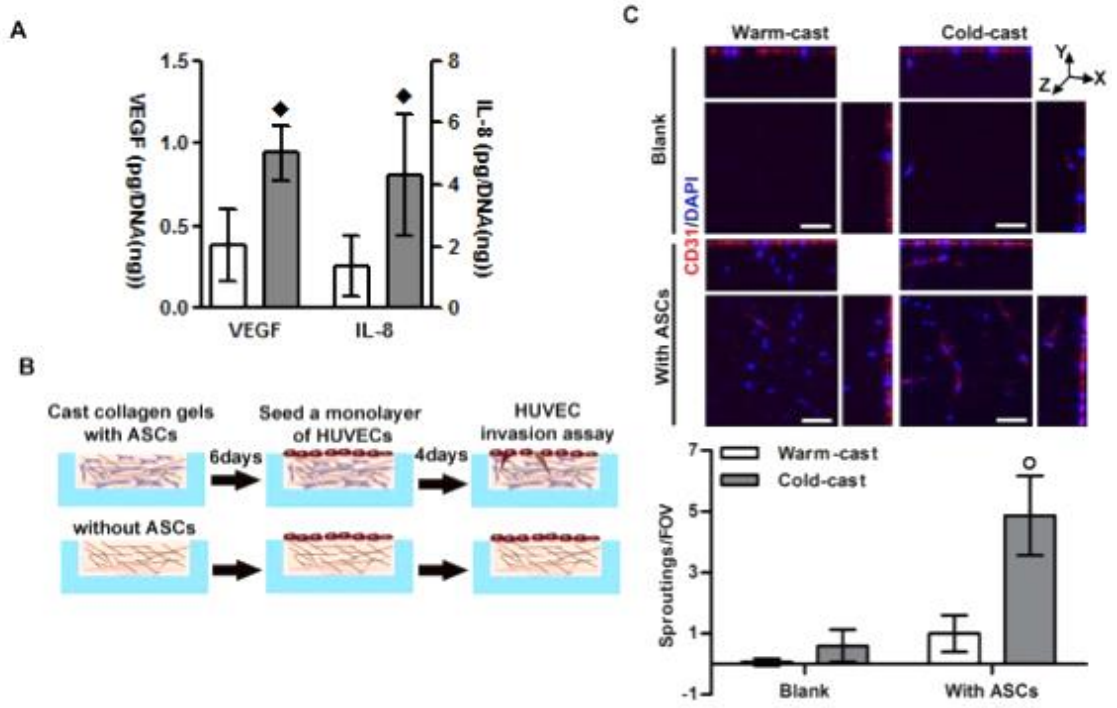

Fig. 5.6. Altered pro-angiogenic potential of ASCs by change in collagen fibrillar thickness. (A) ELISA analysis indicates that ASCs secreted higher amounts of VEGF and IL-8 in response to thicker fibrils in cold-cast gels. (B) To investigate the functional impact of the enhanced VEGF and IL-8 levels from ASCs cultured in cold-cast gels, an endothelial cell invasion assay was performed. Cold- and warm-cast gels were prepared with and without ASCs and cultured for 6 days and human umbilical vein endothelial cells (HUVECs) were seeded atop the gels. After 4 days, HUVECs were immunofluorescently labeled with antibody against CD31 and traced by confocal imaging analysis to quantify the number of HUVEC sprouts greater than 10 μm in length. (C) The presence of ASCs promoted HUVEC invasion in both cold- and warm-cast scaffolds, but to a greater extent in cold-cast scaffolds. In the absence of ASCs, HUVEC sprouting was still higher in cold-cast scaffolds than warm-cast scaffolds, yet the difference was insignificant. (Scale bar =50 μm), ◆$p < 0.05$, and ❍$p < 0.05$ indicate the difference from warm-cast and all other conditions, respectively.

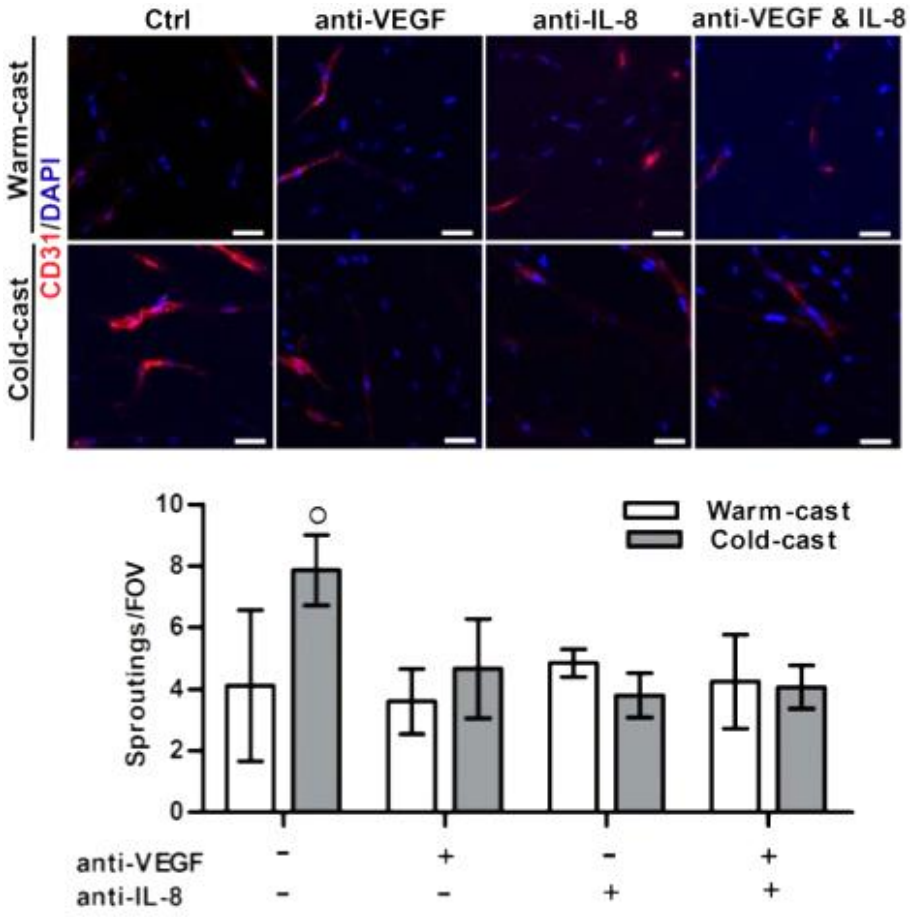

Fig 5.7. Effects of ASC-derived pro-angiogenic factors on HUVEC sprouting. (A) HUVECs were cultured on the top of both cold- and warm-cast collagen scaffolds with VEGF and/or IL-8 neutralizing antibodies for 4 days and analyzed for their invasion. In ASC-embedded cold-cast collagen scaffolds, HUVEC invasion was significantly inhibited with the addition of VEGF and IL-8 antibodies individually and together, whereas the inhibition of VEGF and IL-8 had no effect on HUVEC invasion in ASC-embedded warm-cast scaffolds. **O**$p < 0.05$ indicates significant difference from all other conditions, respectively.

ROCK-mediated changes in pro-angiogenic potential of ASCs in response to collagen fibers

To understand whether the pro-angiogenic potential of ASCs is regulated by actomyosin contractility in response to collagen fiber structure, angiogenic factor secretion was assessed after treating with Y27632, a Rho-associated protein kinase (ROCK) inhibitor in warm- and cold-cast gels. This inhibitor blocks actin polymerization, thereby constraining cellular contraction[295]. Our ELISA analysis indicates that the effect of matrix structure on VEGF and IL-8 secretion was abolished by the inhibition of

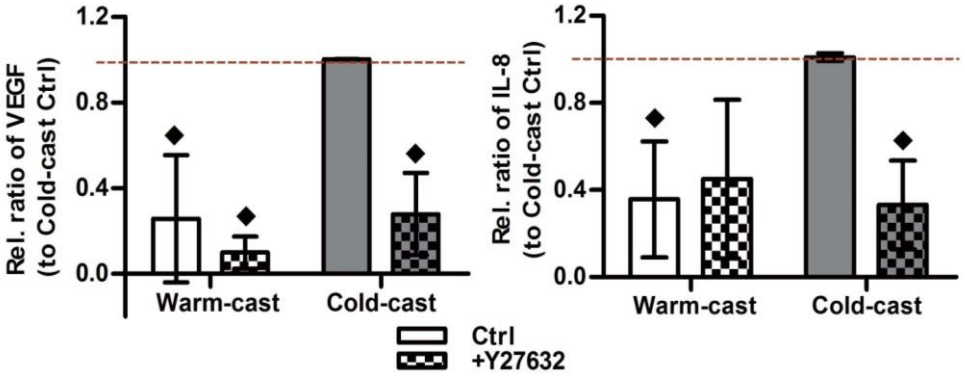

Fig. 5.8. ROCK-mediated changes in pro-angiogenic potential of ASCs in response to collagen fibers. (A) ELISA analysis of the media collected from ASCs cultured in both collagen scaffolds with and without Y-27632 indicates that VEGF and IL-8 secretion of ASCs cultured in cold-cast gels was significantly lowered with the disruption of ROCK-mediated cellular contractility. However, supplementing Y-27632 did not modulate the secretion of VEGF and IL-8 from ASCs cultured in warm-cast gels. ◆$p < 0.05$, and ○$p < 0.05$ indicate the difference from warm-cast and all other conditions, respectively.

ROCK-mediated contractility. In the presence of Y27632, the levels of VEGF and IL-8 from ASCs cultured in cold-cast scaffolds were not significantly different from warm-cast gels (Fig. 5.8). Therefore, increased ROCK-mediated contractility of ASCs in the cold-cast scaffolds contributed to enhancing pro-angiogenic potential of ASCs.

5.6. Discussion

Microstructure of collagen fiber has emerged as a critical regulator of tissue and cellular behavior, yet its role in modulating the pro-angiogenic potential of ASCs has not been explored. In this study, ASCs exhibited greater α-SMA-mediated contractility and enhanced pro-angiogenic behaviors in response to thicker collagen fibers and larger pore structures. The enhanced pro-angiogenic signaling of ASCs consequently promoted HUVEC sprouting, and this change was regulated by ROCK-mediated contractility of ASCs in response to tissue architecture.

For this study, we utilized 3D micro-sized collagen scaffolds with varying fiber thickness. Miniaturized tissue engineering models such as our micro-fabricated 3D scaffolds have great advantages with i) their efficacy to control homogeneity within the system, and ii) ability to recapitulate the cell-scale microenvironment[296,297]. For example, micro-scale hydrogels can prevent gradients of oxygen and nutrients that otherwise result from diffusion-limited transport in 3D, thereby controlling for confounding effects of hypoxia at the interior of the scaffold[134 298]. However, due to the efficient heat transfer rate in miniaturized systems, temperature-controlled cross-linking to tune the collagen fiber microstructure is challenging[299,300].

Temperature is a critical determinant of collagen assembly rate and consequently fiber microstructure[93]. In particular, the nucleation rate controls the lateral growth of collagen microfibrils and therefore fiber diameter[92]. Thus, we achieved thicker fibers in cold-cast scaffolds by delaying fiber nucleation at lower temperatures, while collagen was quickly polymerized for thinner fibers in a warm-cast scaffold (Fig. 5.1A). Although pH can also modify fiber length, diameter, and cross-linking, here we decided to use temperature-mediated method due to greater experimental precision[92].

We observed that ASCs exhibited an enhanced contractile phenotype, characterized by increased α-SMA stress fibers and increased Fn unfolding, when they were cultured in cold-cast gels as compared to those cultured in scaffolds of thinner fibers and smaller pores. In addition, previous reports indicated that actin stress fibers and cell viability of fibroblasts were enhanced when they were cultured in collagen scaffolds with thicker fibers, and a similar trend was also observed from fibroblasts cultured in fibronectin-coated synthetic polymer network with varying thickness[299,301]. Our findings including others imply that changes in fiber thickness from 10^{-2} (for ECM fibers) to 10 μm (for synthetic fibers) could alter biophysical signals to surrounding cells. The fiber diameter-mediated impact on cell contractility might not be ligand (i.e. collagen or fibronectin)-specific but more universal topological or physical cues.

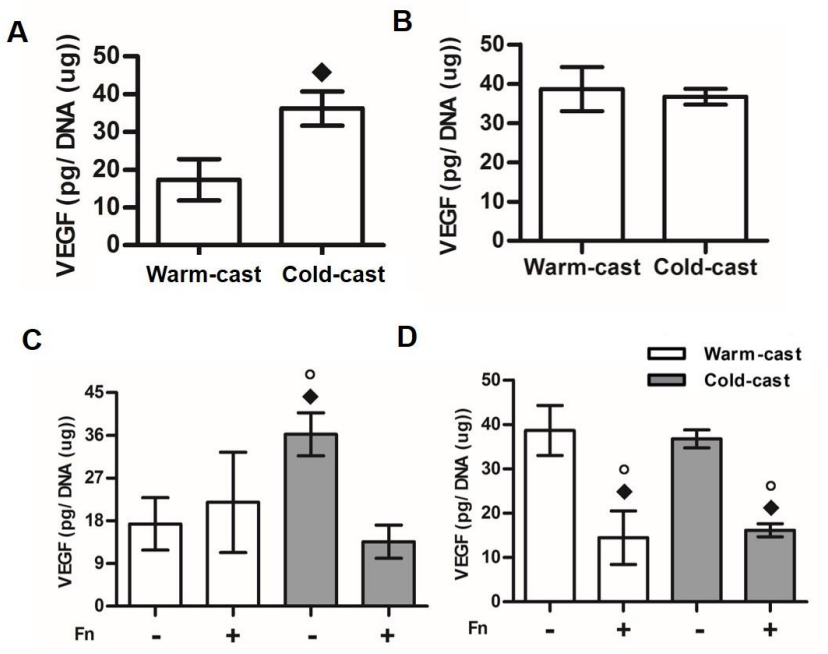

Fig. 5.9. VEGF secretion of Fn-null MEFs in absence and presence of Fn. (A) Fn-null MEFs secreted a higher level of VEGF in response to thicker collagen fibers as similar to ASCs cultured in cold-cast scaffolds. (B) The levels of matrix-bound VEGF were not significantly different. (C) The presence of Fn lowered the VEGF secretion of Fn-null MEFs cultured in cold-cast scaffolds while the levels of VEGF secreted from Fn-MEFs cultured in warm-cast scaffolds did not change by the supplemented Fn. (D) Matrix-bound VEGF was lowered by the supplemented Fn in Fn-MEFs cultured in both cold- and warm-cast scaffolds. ◆$p < 0.05$, and ❍$p < 0.05$ indicate the difference from warm-cast without Fn and cold-cast with Fn, respectively.

In addition, our studies using Fn-null mouse embryonic fibroblasts (MEFs) showed that MEFs which do not produce fibronectin similarly responded to thicker collagen fibers secreting a higher level of VEGF while the levels of matrix-bound VEGF were not significantly different (Figs. 5.9A and B). This data suggests that cells can response to the collagen-derived physical cues in the absence of Fn. However, in the presence of Fn, Fn-null MEFs cultured in cold-cast scaffolds secreted less VEGF, and their matrix-bound VEGF was also lowered. However, the secretion of VEGF from Fn-nul MEFs cultured in warm-cast scaffolds did not change much by the supplemented Fn, but their matrix-bound VEGF was similarly

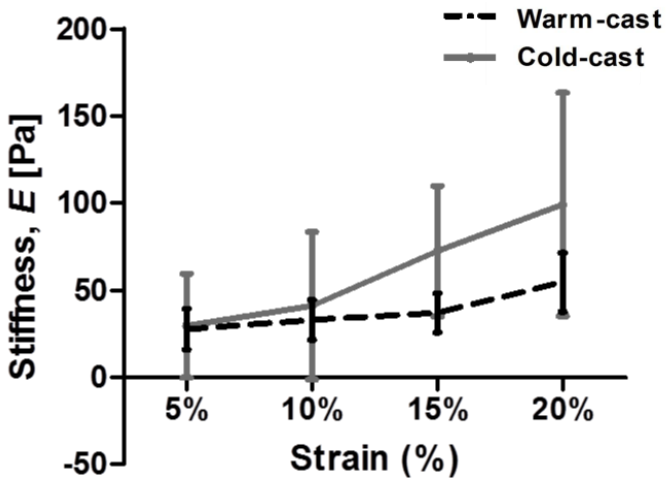

Fig. 5.10. Elastic moduli of ASC-free collagen scaffolds. Stress-strain profile of cell-free collagen scaffolds was measured via DMTA and Young's modulus (E) was calculated at low-strain (5–20%) elastic regime. The mean Young's modulus (E) of cold-cast scaffolds was not different from that of warm-cast scaffolds although it had a much broader range. Young's modulus (E) was calculated from the slope of the stress-strain curve, $\sigma = E\varepsilon$.

lowered as in the presence of Fn. Therefore, more studies are required to understand the response of Fn-null MEFs to the collagen fibers in presence of Fn.

In addition to matrix topography, increased cell contractility in cold-cast scaffolds might be a physical response against to the fibers with higher tensile strength. Increased actomyosin contractility is a typical response to maintain tensional balance against a stiff microenvironment[90], and previous reports correlate fiber thickness with increase tensile strength of collagen fiber at low strain rate[302,303]. In addition, at a cellular level, much smaller force might matter according to their size of cells and ECM fibers as previous studies stated single cell traction force and force required to deform ECM fibers range from pico- to nano-Newton[304,305]. Interestingly, our mechanical testing on the cell-free collagen scaffolds of thicker vs. thinner fibers on day 1 indicated that the average of Young's modulus [E] between cold-cast gels was moderately higher with a broader variation that warm-cast gels at low strain rate (5% - 20%), but

no significant difference was observed (Fig. 5.10). This might be because the concomitant changes in pore size and volume fraction of fibers in cold-cast scaffolds could mask fiber diameter-mediated effects[92], or because our apparatus detected bulk compression rather than localized compression on individual matrix components. However, as evidence from the FRET analysis suggests that scaffolds containing unfolded Fn may exhibit higher stiffness, as observed in matrix deposited by ASCs in cold-cast gels.

An increased expression of α-SMA in the absence of desmin suggests that ASCs adopted a contractile myofibroblastic phenotype in cold-cast scaffolds. This differentiation corresponded with increased collagen linearity, decreased pore size, and unfolded Fn conformation (Fig. 5.2C, 5.2D, and 5.3C), all typical of myofibroblast remodeling[186]. In addition, collagen fiber linearity and Fn elongation collectively contribute to matrix stiffening, which functions as a positive feedback loop of myofibroblastic differentiation[306,307]. Therefore, increased α-SMA positive cell population of ASCs might be initiated by predetermined thicker collagen fibers, but could be maintained or further enhanced by their own remodeled matrices later on.

In addition, the myofibroblastic ASCs in cold-cast scaffolds secreted higher levels of VEGF and IL-8 than ASCs in warm-cast gels[61], and this change was abrogated by ROCK-inhibition (Fig. 5.5A and 5.7A). Upon mechanical stimulation, cells develop a contractile phenotype and modulate the activity of small GTPase Rho and its effector ROCK. This signaling axis governs integrin-mediated focal adhesion maturation, actin cytoskeleton organization, and cell morphology[304]. In addition, other studies have shown that stiff substrates and high tensile stress stimulated VEGF and IL-8 signaling[308-310]. In our system, increased cellular contractility and matrix comprising the thicker and linearized collagen fibers with partially unfolded Fn collectively generated a tensional microenvironment, which could trigger VEGF and IL-8 signaling. This result might also be explained by Fn conformational changes, which might reduce the affinity of α5β1 integrin with the synergy site and downstream VEGF signaling[284].

Finally, our data confirmed that VEGF and IL-8 contributed to enhancing HUVEC sprouting in cold-cast scaffolds, showing that the enhanced HUVEC sprouting in cold-cast scaffolds was eliminated in presence of VEGF and IL-8 antibodies (Fig. 5.5 and 5.6A). As one of the most clinically and experimentally well-established angiogenic factors, VEGF aids in EC proliferation, migration, and organization[51]. Also, IL-8 stimulates EC actin polymerization, proliferation, and migration through CXCR-1/2 and epidermal growth factor receptor[311]. Moreover, a synergistic effect of VEGF and IL-8 has been noted as IL-8 stimulated autocrine VEGF signaling of ECs[312]. In addition, there might be a direct effect of matrix microarchitecture on EC sprouting[313,314], which might explain the enhanced HUVEC sprouting in cold-cast scaffolds even when ASCs were absent (Fig. 5.5C). However, in the presence of ASCs, despite the comparable pore sizes in both scaffolds, the difference of HUVEC sprouting between cold-cast and warm-cast gels was much greater relative to the difference in the absence of ASCs, which suggests the significant pro-angiogenic signaling of ASCs. Taken together, our study suggests the phenotypic change of ASCs to myofibroblastic cells and the resulting matrix remodeling and pro-angiogenic activities lead to the promotion of HUVEC sprouting.

Based on our findings, several future studies will be beneficial for i) understanding of mechanoregulation of angiogenic collaboration of stromal cells with ECs and ii) developing useful therapeutic and tissue engineering approaches. First, it has not been well understood if the microstructural changes of collagen fibers in 3D scaffolds regulate specific integrin engagement and clustering, thereby modulating cellular behaviors. Previous studies indicated that cells preferentially utilize $\alpha_2\beta_1$ to interact with fibrillar collagen and this preferential interaction regulates cell projection, thereby changing α-SMA expression and contractility[315]. In addition, it has been noted that cells cultured on the stiff substrate initially utilized $\alpha_2\beta_1$ but later switched to $\alpha_v\beta_3$ integrin while thickening collagen fibers and developing α-SMA stress fibers[316]. Also, increasing number of studies indicates that mechanical stimuli and spatial

presentation of ECM ligand are critical for integrin activation, clustering, and signaling[113,317]. Therefore, investigating whether microstructural changes of collagen fibers play a role in the preferential engagement and clustering of integrin, which ultimately influences cellular behaviors, will aid in understanding the mechanism underlying our findings. For this, high-resolution visualizing techniques are needed to detect the localized focal adhesion and integrin clustering in 3D constructs[113].

In addition, matrix metalloproteinases (MMPs) are important for blood vessel sprouting and morphogenesis[318]. Previous studies indicated that matrix mechanical cues can trigger progenitor cell-mediated matrix degradation via MMPs and facilitate blood vessel sprouting[272]. Thus, MMP-mediated effects may contribute to the observations in this study and should be explored further. Moreover, provisional ECM components other than type I collagen and fibronectin are involved in the angiogenic process[318]. For example, fibrin and proteoglycans (i.e. glycosaminoglycan) are known to modulate the biochemical and physical properties of matrix, which may trigger different cellular responses as compared to those cultured in only collagen I-based matrix[319,320]. Therefore, simplicity of our in vitro model might be a caveat to fully understanding the complex angiogenic process *in vivo*. However, since collagen fiber structure can be also modulated by the other ECM macromolecules, the optimization of this system is required to properly regulate the microstructure of collagen fibers[321].

In conclusion, we proposed that microstructural change of collagen fibrils is a critical regulator in governing the pro-angiogenic potential of ASCs with implications for stem cell, regenerative medicine, and cancer research.

CHAPTER 6

CONCLUSION

6.1. Summary

My doctoral research investigated the pro-tumorigenic potential of adipocytes and adipose stromal vascular cells (ASVCs), which include adipose-derived stem cells (ASCs). The pro-tumorigenic potential of these cells are significantly amplified during obesity, which is a risk factor for cancer. In particular, the four questions proposed in section 1.6 were examined utilizing various physical oncological approaches: 1) and 2) do ASCs and adipocytes in adipose tissue potentially acquire myofibroblastic features in response to tumor-derived cues, thereby consequently participating in ECM remodeling and angiogenesis, 3) does obesity, a risk factor for cancer, predetermine the pro-tumorigenic potential of adipose tissue, which potentially promotes tumor malignancy, and 4) do structural changes of collagen fibers as seen during tumorigenesis and obesity potentially regulate stromal cell behaviors. The following subsections will briefly revisit the answers to these questions, as discussed in each of the corresponding chapters. Following this, there will be a discussion on work that needs to be completed to fully draw the link between all of these various signals and then finally a discussion on how our findings can be utilized in practical therapies for breast cancer.

Cancer-activated ASCs promote breast tumor progression

It has been reported that the majority of myofibroblastic cells in tumor stroma are emanated primarily from peri-tumoral adipose tissue but not from bone-marrow mesenchymal stem cells[322].

However, whether ASCs in mammary adipose tissue contribute to enlarging the myofibroblast population during breast tumorigenesis was previously unknown.

The findings in chapter 2 showed that in the presence of soluble factors from MDA-MB231 breast cancer cell line, ASCs exhibited myofibroblastic features including highly contractile, proliferative, pro-fibrotic, and pro-angiogenic features while losing adipogenic potential (Figs. 2.1 and 2.2). The myofibroblastic ASCs then deposited and contracted abundant ECM components (collagen and fibronectin) with enhanced α-SMA-mediated contractility, which collectively contributed to increasing stiffness of their surrounding area (Fig. 2.4). The increased stiffness in turn provides positive feedback to enhance the myofibroblastic features of ASCs together with tumor-derived factors (TGF-β and IL-8) (Figs. 2.4 and 2.5). Interestingly, the growth and alignment of ASCs cultured on the stiffer substrates were progressively enhanced along the malignancy of cancer cells from which we collected tumor-derived factors. Finally, we showed that implanted ASCs with breast cancer cells *in vivo* indeed promote tumor desmoplasia, leading to increased tumor stiffness, angiogenesis, and ultimately tumor growth (Fig. 2.9). Although our studies show that tumor explants grown with co-implanted ASCs exhibited enhanced α-SMA levels and other desmoplastic features, further study will be helpful to confirm the origin of the enhanced α-SMA positive cells in the tumor explants. Since it is possible that circulating or host progenitor cells in mouse adipose tissue might be recruited and become a part of the myofibroblastic cell population by enhanced chemokine from both cancer cells and possibly extra human ASCs[323], further *in vivo* studies to support the concept of myofibroblastic differentiation of implanted human ASCs will complement our findings.

In addition, while other *in vivo* studies suggest that implanted adipose progenitor cells are more associated with blood vessels during tumorigenesis, our studies indicate the enhanced α-SMA levels are not associated with desmin levels, which are pericytic or smooth muscle cells[161]. To resolve this

discrepancy, it needs to be understood how the lineage commitment of ASCs between myofibroblastic and pericytic or smooth muscle cell lineage was precisely regulated *in vivo*. Understanding the ways to adequately control ASC fate will be beneficial for not only cancer therapeutic but also for tissue engineering approaches.

Lastly, while we reported that the phenotypic changes of ASCs into myofibroblastic cells from tumor-derived cues of a series of cancer cells, we have not shown whether this ASC-mediated tumor stroma remodeling can similarly modulate various subtypes of breast cancer. Since each subtype of breast cancer as we reviewed in section 1.2 exhibits quite unique characteristics, further studies to ensure whether these cancer-activated ASCs-mediated effects are also applicable to other subtypes will be beneficial.

Cancer-activated adipocytes increase the myofibroblastic cell population, thereby stimulating ECM remodeling and angiogenesis

Since we observed that the number and size of adipocytes are significantly reduced in mouse and human tumors (Fig. 3.1), we also assessed whether cancer-activated adipocytes could also contribute to tumor stroma remodeling in a way similar to that of ASCs, given their potential of dedifferentiating into ASC-like cells[85]. Our findings indicate that adipocytes cultured in both 2D and 3D *in vitro* systems lost their adipogenic features (Figs. 3.2 and 3.4) but acquired myofibroblastic features in response to tumor-derived factors from MDA-MB231 (Figs. 3.3 and 3.4). Similar to TCM-treated ASCs as seen in chapter 2, a larger quantity if α-SMA, Fn, and collagen proteins were detected in TCM-treated adipocytes. In addition, tumor-derived factors stimulated pro-angiogenic signaling of adipocytes, thereby promoting endothelial cell sprouting.

Although we observed the proportional change of adipocyte population (i.e. from adipogenic into myofibroblastic population), we have not specifically examined the trans-differentiation of a single adipocyte. One could think there might be a specific subset of adipocytes, which can be trans-differentiated into myofibroblastic cells and then proliferate while the majority of adipocytes might undergo apoptosis and consequently reduce lipid content in response to tumor-derived factors. Therefore, further investigation is required to confirm the trans-differentiating potential of adipocytes into myofibroblastic cells as well as to understand the specific molecular signaling responsible for adipocyte-myofibroblasts.

Obesity-associated interstitial ECM remodeling promotes tumor malignancy

In chapter 4, we assessed whether the functional significance of obesity-associated interstitial fibrosis predisposes adipose tissue to enhance mammary tumorigenesis. First, our histological analysis of clinical breast cancer samples suggests that obese patients exhibit an increased degree of desmoplasia. Also, our analysis of mammary fat tissue from both genetic and diet-induced mouse models of obesity showed that the fibrotic changes in mammary microenvironment occurred even before tumorigenesis, suggesting the fibrotic predisposition of obese mammary tissue is inherently greater than that of its lean counterpart (Fig. 4.1). Our findings also show that ASVCs isolated from the adipose tissue of obese mice contained more myofibroblastic cells, secreted a higher level of SDF-1, and deposited stiffer matrices containing thicker and aligned collagen and more unfolded Fn as compared to ASVCs from lean mice. This confirms that the enhanced interstitial fibrosis in mammary adipose tissue is due to the distinct cell composition in adipose tissue from obese mice (Figs. 4.3 and 4.5).

Collectively, it seems as if both biochemical and physical cues derived from obesity-mediated ASVCs promote breast tumorigenesis as our data shows that i) obesity-associated ASVCs potentially

stimulate the recruitment of MDA-MB231 breast cancer cells through SDF-1/CXCR4 signaling, and that ii) stiffer matrices deposited by obesity-associated ASVCs enhanced the cancer cell growth in a Rho/ROCK signaling-dependent manner (Figs. 4.7 and 4.8). Furthermore, cancer stem cell transcription factor NANOG activity, a poor prognostic marker of tumors, was also enhanced by the physicochemically active matrices deposited by obesity-associated ASVC (Fig. 4.9). Taken together, our findings imply that obesity-associated adipose tissue, which contains a larger population of myofibroblastic cells, can potentially generate a physicochemical microenvironment, which may favor breast tumorigenesis.

Our rigorous analysis of adipose tissues from different locations (mammary, subcutaneous, vs. visceral) as well as from ovary intact vs. ovariectomized mice suggests that enhanced interstitial fibrosis is a universal feature of obesity-associated adipose tissue (Figs. 4.2, 4.4 and 4.6), implying a possible link between obesity-associated fibrosis and other types of cancer (i.e. prostate and colorectal cancer) associated with different adipose depots.

In addition, our study also indicated that caloric restriction lowered interstitial fibrosis, suggesting that obesity indeed modulates interstitial fibrosis (Fig. 4.11). However, previous studies also indicate that caloric restriction concomitantly lowers inflammation level and estrogen synthesis in obese individuals[324]. Therefore, further studies need to be performed to understand the etiology of predisposition of interstitial fibrosis in obesity-associated mammary stroma. Conventional classification of obesity by body mass index might not accurately reflect the metabolic and inflammation status of individuals, which is more strongly correlated with enhanced pro-fibrotic features. Therefore, delicate stratification of obesity by the metabolic status and inflammation of individuals will aid in understanding the specific molecular mechanism underlying the enhanced pro-fibrotic potential of obesity-associated adipose tissue.

Collagen fiber microstructure regulates the pro-angiogenic potential of ASCs.

As we observed the dynamics in matrix remodeling during tumorigenesis and obesity (Chapters 1 and 3), we decided to further investigate whether the microstructural changes of collagen fibers provide a feedback mechanism for regulating the phenotype of ASCs in Chapter 5. For this study, we leveraged a tissue engineering model: ASC-incorporated 3D collagen scaffolds with varying fiber microstructures (Fig. 5.1). The findings of this study indicate that ASCs alter their behaviors in response to changes in the fiber microstructure thickness and in turn act to remodel their surrounding matrices. In addition, through the use of co-culture 3D models with human umbilical vein endothelial cells (HUVECs), we assessed the pro-angiogenic potential of the ASCs and found that they are also altered by the fiber microstructure. Finally, we investigated whether changes in the microstructure of collagen fibers regulate cell behaviors in a mechanoregulation-dependent manner.

It was observed that at an early point, the predetermined collagen matrix in scaffolds might dominantly affect the ASCs' behaviors. However, as ASCs begin to deposit more and more of their own Fn matrices in response to the microstructure of collagen fibers, these Fn matrices may play an increasing role in regulating the pro-angiogenic potential of ASCs while mediating the engagement with specific integrin of ASCs[91]. Thus, understanding the roles of the deposited Fn matrix in modulating the ASCs' behaviors will complement our findings.

We also attempted to assess changes in the mechanical properties of collagen scaffolds as a function of collagen fiber diameter yet the concomitant changes of pore size with fiber diameter in the collagen construct complicated this analysis. To overcome this limitation, computational modeling approaches have been utilized to dissect the role of each physical parameter in modulating mechanical properties of the biological construct, but experimental verification has not yet been presented. As such, it will be necessary to devise more effective and precise measurement methods to separately isolate the effects of collagen fiber diameter.

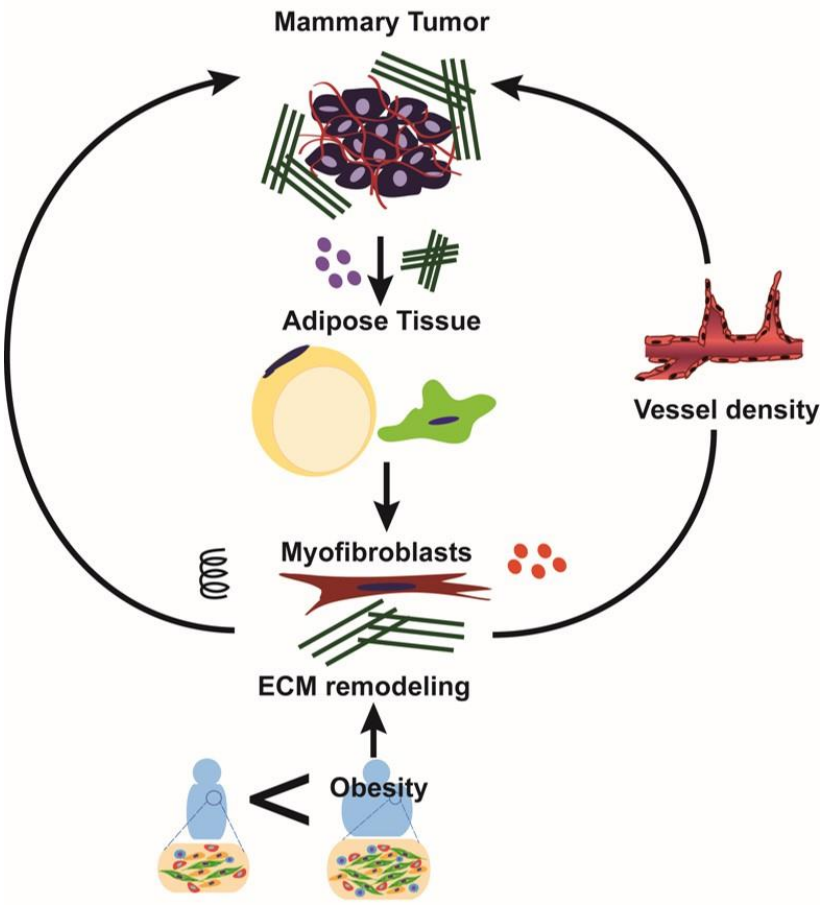

Fig. 6.1. Adipose tissue and its role in modulating the mammary microenvironment

In conclusion, the findings of my doctoral work suggest that during prolonged exposure of obesity and tumor development, host stromal cells lose their phenotypic and functional integrity while differentiating into myofibroblastic cells, which are the main cellular mediators to alter mammary stroma structure through ECM remodeling and pro-angiogenic activities. The ECM remodeling in turn provides positive feedback to increase the myofibroblastic cell population. Consequently, the perturbed mammary microenvironment favors tumor progression.

I believe our findings herein are broadly applicable for not only cancer and stem cell research but also for obesity-mediated metabolic diseases and tissue engineering. Our findings highlight that

maintaining phenotypic and functional integrity of host stromal cells is critical for preventing breast cancer progression and developing adequate cancer therapy. In addition, our findings call for exercising extra caution when considering the use of adipose tissue for tissue regenerative medicine, since the health conditions of both the tissue donor and recipients can possibly modulate the characteristics of adipose tissue. Moreover, our findings suggest that during obesity, the seemingly negligible interstitial fibrosis plays an equally significant role in promoting tumor malignancy as does dysfunctional adipocytes. Our studies also show that matrix changes at the micro-scale such as the microstructural changes of collagen fibers can also induce cellular phenotypic changes. As a side note, I believe other tissue engineers can benefit from our model system due to the difficulty to precisely control the microstructure of collagen fibers *in vivo*. However, as stated, several future studies will be beneficial for advancing our understanding of these diseases and consequently developing more nuanced and effective therapeutic approaches.

6.2. Future directions

This body of work suggests several causative factors for tumor progression, the understanding of which will aid in investigating specific mechanisms underlying the assessed links and ultimately developing better therapeutic approaches for cancer and other associated diseases. In addition, the combination of an appropriate *in vitro* platform as well as mouse models of human diseases presented in the course of this work are expected to guide the medical research community towards a comprehensive understanding of complex human diseases and ultimately aid in evaluating the therapeutic methods to tackle these diseases as well. In order to achieve these goals, however, there is still a significant amount of research that needs to be done. Some of these points were briefly outlined in the previous subsections of this chapter. The following subsection expands upon these aforementioned experiments with greater

detail and also introduces some other broader work that needs to be performed to translate these research findings to practical therapeutic methods.

Mechanism underlying possible trans-differentiation of adipocytes

Since the phenotypic and functional integrity of adipocytes are known to be responsible not only for cancer but also for a variety of other metabolic disease progressions, investigation of the specific molecular mechanism underlying adipocyte conversion is important in developing preventative care and treatments for such diseases[250]. Specifically, soluble factors responsible for adipogenesis and myofibroblast differentiation such as BMPs, IL-1β, TGF-β, and IL-8 may provides clues for adipocyte conversion, so they should be investigated in further detail[48,194]. Therefore, a first step is to develop an understanding of these aforementioned factors and their underlying signaling mechanisms will guide finding a potential regulator of adipocyte trans-differentiation. The next step would be to understand whether those signaling mechanisms regulate the conversion of adipocytes to myofibroblasts in a simply reversed-signaling cascade or via completely different routes.

In addition, ECM-mediated biophysical cues may also contribute to the adipocyte trans-differentiation as we have previously discussed in chapter 3. Previous studies indicate that mechanical stimuli (i.e. stretching) regulate adipogenesis through an ERK-mediated pathway as similar to biochemical cues (i.e. TNF-α)[195,204]. Also, morphological changes of adipocytes and subsequent actin cytoskeleton reorganization regulate cell fate via RhoA-mediated signaling[187]. However, how physical cues precisely regulate this process has not been well understood. In particular, similar to previous work indicating that collagen and adipocyte size are correlated[250], our microscopic image analysis on the picrosirius red stained tumor sections showed that the size of adipocytes is positively correlated with the proximity of collagen fibers (data not shown). The morphological changes of adipocytes in a close

proximity of collagen fibers suggest that the surrounding thicker collagen matrix might physically entrap the adipocytes and then reduce their size by mechanical stimuli[71]. Certainly more investigation on the link between ECM remodeling and adipocyte trans-differentiation needs to be done and this study will be also applicable for understanding of mechanism underlying obesity-associated fibrosis, which will be discussed in the following section.

Mechanism underlying the enhanced obesity-associated fibrosis

Although the process of fibrosis is relatively well understood, how obesity-associated interstitial fibrosis is stimulated remains unclear[250]. Fibrosis has been explained as a function of macrophage recruitment and the resulting high levels of inflammatory cytokine, but during obesity inflammation may not be an initiator of fibrosis since previous studies indicate that inflammatory cells are recruited at a later stage of obesity, so they may be responsible for progression rather than initiation of fibrosis[250]. Thus, other possibilities have been proposed in the literature including 1) hypoxia, and 2) a self-governing process of adipocytes to physically constrain their abnormal expansion by ECM fibers[71,265,269]. The proposed mechanisms may be linked and complement each other but even so, it still needs to be understood how these mechanisms (e.g., crosstalk between inflammatory cells and adipocytes, or adipocytes and surrounding stromal cell-mediated ECM deposition) are precisely regulated. Understanding this mechanism will aid in developing therapeutic approaches for obesity-associated cancer as well as other obesity-associated diseases given the strong association between fibrosis and adipocyte metabolic function.

Link between obesity-associated fibrosis and preferential development of breast cancer subtype

Based on our findings in chapter 4, understanding whether obesity preferentially encourages the development of a specific subtype of breast cancer and if the preferential development is mediated through fibrosis-mediated mechanosignaling will prove useful in diagnosing breast cancer subtype and predicting clinical outcomes. For this study, thorough classification is a prerequisite since all other risk factors such as age, menopausal status, family history, smoking, dense breast tissue, etc. could potentially influence the development of a specific subtype of breast cancer[325]. In addition, due to the heterogeneity of tumor, a large number of samples will be required to obtain a meaningful relationship.

Angiogenesis and blood vessel morphogenesis during obesity

Despite enhanced fibrosis during obesity, delayed wound healing in obese and diabetic patients has been problematic, and it is speculated that this might be partially due to formation of dysfunctional blood vessels, which also pose difficulties for cancer therapy[214,250]. In particular, obesity-associated adipose tissue has been observed to reduce capillary density as well as larger but dysfunctional vessels, which possibly prevent wound healing by inhibiting the adequate recruitment of inflammatory cells as well as delivery of their factors[71,250]. Therefore, how blood vessel morphogenesis is regulated during obesity and how the dysfunctional blood vessels also contribute to tumor progression needs to be understood.

In particular, it remains unclear whether ECM remodeling (i.e., collagen fiber structure) during obesity may influence blood vessel morphogenesis. For this study, the collagen scaffolds developed as a part of our work might be helpful in interrogating the role of collagen fiber microstructure in regulating vascular morphogenesis. Although we were not able to detect the morphogenic difference of HUVEC sprouting due to the short period of HUVEC culture in our system in chapter 5, understanding the role of

the collagen fiber microstructure on blood vessel morphogenesis will aid in developing effective therapies for cancer as well as obesity-associated wound healing and hypertension in multiple organs[326].

Molecular mechanism underlying the mechanoregulation of cancer stem cell

The cancer cell heterogeneity and cancer stem cell population have been recognized as key factors of the driving force necessary to maintain the heterogeneous cancer cell population[262]. Furthermore, clinical studies show that cancer stem cell populations have been correlated with high resistance to available cancer therapies, poor clinical outcomes, and recurrence of specific types of cancer[327]. Nevertheless, the mechanisms underlying the origin of cancer stem cells and the precise maintenance of their populations among the heterogeneous tumor mass are not well understood. However, since the maintenance of normal stem cells – which are also believed to be source of cancer stem cells – are known to be regulated by their surrounding microenvironment, it may be possible that the tumor microenvironment provides cancer stem cell with a favorable niche[257]. In particular, the mechanoregulation of cancer stem cell maintenance in fibrotic microenvironments might be one of the possible mechanisms, as our studies also suggest that obesity-associated fibrosis possibly contributes to cancer stem cell maintenance in chapter 4. More detailed studies, however, need to be performed to fully verify this mechanism.

Therapeutic approaches

Based on our understanding of partially successful cancer therapies that are currently being used, there may not be a single silver bullet therapy for treating cancer. It is more likely that a combination of targeting oncogenes as well as normalizing the unbalanced tumor microenvironment may be the optimal approach for cancer therapy. Based on our findings, several possible therapeutic approaches to normalize

the microenvironment can be suggested and precise control of the normalization will be a key factor in the effectiveness of these proposed therapeutic approaches to combat cancer.

First, the precise regulation of phenotypic and functional integrity of the implanted cells for tissue is a critical determining factor for safe tissue regeneration, in particular for breast reconstruction after mastectomy. Given that ASCs as well as adipocytes can be a source of pro-tumorigenic mediators, ways to control the undesirable differentiation of these cells after implantation will be essential. Therefore, incorporating specific factors to control their differentiation or accurate design of cell carriers for implantation might be an option.

Second, the findings from this dissertation emphasize that fibrosis and consequent tumor stiffness exacerbate tumor progression as previous studies suggested[123]. Accordingly, several therapeutic approaches to target matrix remodeling (i.e. heparanase inhibitor) or cancer-activated fibroblasts (i.e. FGF receptor inhibitor) were introduced[10]. Also, anti-fibrotic therapies using factors such as TGF-β and PPAR-γ might be considered[250]. However, a detailed investigation into the adequate treatment (i.e. timing and dosage) and the potential side effects of such treatments will need to be conducted.

As we have demonstrated through our studies, obesity-associated alteration in the mammary microenvironment is a critical factor for tumor progression. Thus, for obese cancer patients, weight loss through dietary intervention and exercise has been recommended since weight loss has been known to lead to lower chronic inflammation and estrogen synthesis[108,328]. However, a clear understanding of the impacts of acute weight loss on clinical outcomes of obese patients still needs to be established. Even still, the importance of proper homeostasis of our bodies including a well-regulated weight cannot be overstated.

Since current studies indicate that not only obesity but also lipodystrophy (i.e., loss of fat) may create a similar pathological microenvironment including chronic inflammation and the resulting fibrosis,

simple weight loss may not be the only solution for preventing breast cancer[328]. Rather, the effective control of chronic inflammation may play a critical role in regulating disease development. Therefore, pharmacological anti-inflammatory approaches such non-steroidal anti-inflammatory drugs, corticosteroids, and statins might be another option but careful timing of administration, dosage-control and regular medical check-ups for inflammation level are required[329].

Lastly, predisposed interstitial fibrosis might possibly be utilized as a diagnostic tool in the future, although much work is needed before it can be applied in practice. Specifically, it is not well understood if a specific risk factor for breast cancer (e.g., menopausal status, obesity, etc.) can be directly and uniquely mapped to a specific alteration to the tumor stroma structure in such a manner as to be used as a diagnostic marker. Certainly, more investigation is required to understand the characteristics of mammary tumor stroma in conjunction with breast cancer risk factors and the resulting impact on tumor malignancy and recurrence.

In conclusion, this dissertation emphasizes the significance of maintaining structural and functional integrity both at the cell and tissue levels since their compromised balance leads to the development and progression of breast cancer. More generally though, this work highlights that for any disease, it is important to discover ways to maintain this structural and functional integrity in healthy individuals for prevention and/or ways to recover it in sick patients for effective therapy. As such, it is my privilege to have completed the ground work in not only the field of cancer, but also in the broader spectrum of diseases closely linked to obesity. It is my hope that this work will continue to be pursued and applied for the successful treatment of many valuable lives.

REFERENCES

1 Global Cancer Statistics. (2011).

2 Society, A. C. Global Economic Cost of Cancer. 1 - 10 (2011).

3 Nowell, P. C. The Clonal Evolution of Tumor Cell Populations. *Science* **194**, 23-28 (1976).

4 Chang, Y. M. *et al.* Src family kinase oncogenic potential and pathways in prostate cancer as revealed by AZD0530. *Oncogene* **27**, 6365-6375, doi:Doi 10.1038/Onc.2008.250 (2008).

5 Hwang, C. I. *et al.* Wild-type p53 controls cell motility and invasion by dual regulation of MET expression. *Proceedings of the National Academy of Sciences of the United States of America* **108**, 14240-14245, doi:DOI 10.1073/pnas.1017536108 (2011).

6 Borgan, E. *et al.* Subtype-specific response to bevacizumab is reflected in the metabolome and transcriptome of breast cancer xenografts. *Molecular oncology* **7**, 130-142, doi:DOI 10.1016/j.molonc.2012.10.005 (2013).

7 Chin, L., Andersen, J. N. & Futreal, P. A. Cancer genomics: from discovery science to personalized medicine. *Nature medicine* **17**, 297-303, doi:10.1038/nm.2323nm.2323 [pii] (2011).

8 Correia, A. L. & Bissell, M. J. The tumor microenvironment is a dominant force in multidrug resistance. *Drug Resist Update* **15**, 39-49, doi:DOI 10.1016/j.drup.2012.01.006 (2012).

9 Seo, B. R., DelNero, P. & Fischbach, C. In vitro models of tumor vessels and matrix: Engineering approaches to investigate transport limitations and drug delivery in cancer. *Advanced drug delivery reviews* **69**, 205-216, doi:DOI 10.1016/j.addr.2013.11.011 (2014).

10 Bissell, M. J. & Hines, W. C. Why don't we get more cancer? A proposed role of the microenvironment in restraining cancer progression. *Nature medicine* **17**, 320-329, doi:Doi 10.1038/Nm.2328 (2011).

11 Fata, J. E., Werb, Z. & Bissell, M. J. Regulation of mammary gland branching morphogenesis by the extracellular matrix and its remodeling enzymes. *Breast Cancer Research* **6**, 1-11, doi:Doi 10.1186/Bcr634 (2004).

12 Provenzano, P. P. *et al.* Collagen reorganization at the tumor-stromal interface facilitates local invasion. *BMC medicine* **4**, 38, doi:10.1186/1741-7015-4-38 (2006).

13 Polyak, K. Breast cancer: origins and evolution. *Journal of Clinical Investigation* **117**, 3155-3163, doi:Doi 10.1172/Jci33295 (2007).

14 Sorlie, T. *et al.* Distinct molecular mechanisms underlying clinically relevant subtypes of breast cancer: gene expression analyses across three different platforms. *BMC genomics* **7**, doi:Artn 127 Doi 10.1186/1471-2164-7-127 (2006).

15 Reis-Filho, J. S. & Pusztai, L. Gene expression profiling in breast cancer: classification, prognostication, and prediction. *The Lancet* **378**, 1812-1823, doi:10.1016/s0140-6736(11)61539-0 (2011).

16 Malhotra, G. K., Zhao, X., Band, H. & Band, V. Histological, molecular and functional subtypes of breast cancers. *Cancer Biology & Therapy* **10**, 955-960, doi:10.4161/cbt.10.10.13879 (2010).

17 Buzdar, A. U. Role of biologic therapy and chemotherapy in hormone receptor- and HER2-positive breast cancer. *Ann Oncol* **20**, 993-999, doi:Doi 10.1093/Annonc/Mdn739 (2009).

18 Hudis, C. A. & Gianni, L. Triple-Negative Breast Cancer: An Unmet Medical Need. *Oncologist* **16**, 1-11, doi:Doi 10.1634/Theoncologist.2011-S1-01 (2011).

19 Guoren Deng, Y. L., Galina Zlotnikov, Ann D. Thor, Helene S. Smith. Loss of Heterozygosity in Normal Tissue Adjacent to Breast Carcinomas. *Science* **274**, 2057-2059 (1996).

20 Bissell, M. J. & Radisky, D. Putting tumours in context. *Nat. Rev. Cancer* **1**, 46-54, doi:10.1038/35094059 (2001).

21 Hanahan, D. & Weinberg, R. A. Hallmarks of Cancer: The Next Generation. *Cell* **144**, 646-674, doi:Doi 10.1016/J.Cell.2011.02.013 (2011).

22 Caino, M. C. *et al.* Metabolic stress regulates cytoskeletal dynamics and metastasis of cancer cells. *The Journal of clinical investigation* **123**, 2907-2920, doi:10.1172/JCI67841 (2013).

23 Pollard, J. W. Tumour-educated macrophages promote tumour progression and metastasis. *Nat. Rev. Cancer* **4**, 71-78 (2004).

24 Park, J., Euhus, D. M. & Scherer, P. E. Paracrine and endocrine effects of adipose tissue on cancer development and progression. *Endocr Rev* **32**, 550-570, doi:10.1210/er.2010-0030 (2011).

25 Khandekar, M. J., Cohen, P. & Spiegelman, B. M. Molecular mechanisms of cancer development in obesity. *Nature reviews. Cancer* **11**, 886-895, doi:10.1038/nrc3174 (2011).

26 De Wever, O., Demetter, P., Mareel, M. & Bracke, M. Stromal myofibroblasts are drivers of invasive cancer growth. *International journal of cancer. Journal international du cancer* **123**, 2229-2238, doi:10.1002/ijc.23925 (2008).

27 Egeblad, M., Rasch, M. G. & Weaver, V. M. Dynamic interplay between the collagen scaffold and tumor evolution. *Curr Opin Cell Biol* **22**, 697-706, doi:10.1016/j.ceb.2010.08.015 (2010).

28 Cox, T. R. & Erler, J. T. Remodeling and homeostasis of the extracellular matrix: implications for fibrotic diseases and cancer. *Dis Model Mech* **4**, 165-178, doi:10.1242/dmm.004077 (2011).

29 Butcher, D. T., Alliston, T. & Weaver, V. M. A tense situation: forcing tumour progression. *Nature reviews. Cancer* **9**, 108-122, doi:10.1038/nrc2544 (2009).

30 Baneyx, G., Baugh, L. & Vogel, V. Fibronectin extension and unfolding within cell matrix fibrils controlled by cytoskeletal tension. *Proceedings of the National Academy of Sciences of the United States of America* **99**, 5139-5143, doi:10.1073/pnas.072650799 (2002).

31 Chandler, E. M., Saunders, M. P., Yoon, C. J., Gourdon, D. & Fischbach, C. Adipose progenitor cells increase fibronectin matrix strain and unfolding in breast tumors. *Physical biology* **8**, 015008, doi:10.1088/1478-3975/8/1/015008 (2011).

32 Tomasek, J. J., Gabbiani, G., Hinz, B., Chaponnier, C. & Brown, R. A. Myofibroblasts and mechano-regulation of connective tissue remodelling. *Nature reviews. Molecular cell biology* **3**, 349-363, doi:10.1038/nrm809 (2002).

33 Levental, K. R. *et al.* Matrix crosslinking forces tumor progression by enhancing integrin signaling. *Cell* **139**, 891-906, doi:10.1016/j.cell.2009.10.027 (2009).

34 Erler, J. T. & Weaver, V. M. Three-dimensional context regulation of metastasis. *Clinical & experimental metastasis* **26**, 35-49, doi:10.1007/s10585-008-9209-8 (2009).

35 Kessenbrock, K., Plaks, V. & Werb, Z. Matrix metalloproteinases: regulators of the tumor microenvironment. *Cell* **141**, 52-67, doi:10.1016/j.cell.2010.03.015 (2010).

36 George E. Davis, K. J. B., Michael J. Davis, Gerald A. Meininger. Regulation of Tissue Injury Responses by the Exposure of Matricryptic Sites within Extracellular Matrix Molecules. *American Journal of Pathology* **156**, 1489-1498 (2000).

37 Wolf, K. *et al.* Multi-step pericellular proteolysis controls the transition from individual to collective cancer cell invasion. *Nature cell biology* **9**, 893-904, doi:10.1038/ncb1616 (2007).

38 Johnson, C. & Galis, Z. S. Matrix metalloproteinase-2 and -9 differentially regulate smooth muscle cell migration and cell-mediated collagen organization. *Arteriosclerosis, thrombosis, and vascular biology* **24**, 54-60, doi:10.1161/01.ATV.0000100402.69997.C3 (2004).

39 Defawe, O. D. *et al.* MMP-9 regulates both positively and negatively collagen gel contraction - A nonproteolytic function of MMP-9. *Cardiovasc Res* **66**, 402-409, doi:DOI 10.1016/j.cardiores.2004.11.025 (2005).

40 Egeblad, M. & Werb, Z. New functions for the matrix metalloproteinases in cancer progression. *Nat. Rev. Cancer* **2**, 161-174, doi:Doi 10.1038/Nrc745 (2002).

41 Page-McCaw, A., Ewald, A. J. & Werb, Z. Matrix metalloproteinases and the regulation of tissue remodelling. *Nat Rev Mol Cell Bio* **8**, 221-233, doi:Doi 10.1038/Nrm2125 (2007).

42 Provenzano, P. P., Inman, D. R., Eliceiri, K. W. & Keely, P. J. Matrix density-induced mechanoregulation of breast cell phenotype, signaling and gene expression through a FAK-ERK linkage. *Oncogene* **28**, 4326-4343, doi:10.1038/onc.2009.299 (2009).

43 Vogel, V. & Sheetz, M. Local force and geometry sensing regulate cell functions. *Nature reviews. Molecular cell biology* **7**, 265-275, doi:10.1038/nrm1890 (2006).

44 Guo, W. & Giancotti, F. G. Integrin signalling during tumour progression. *Nature reviews. Molecular cell biology* **5**, 816-826, doi:10.1038/nrm1490 (2004).

45 Fischbach, C. *et al.* Cancer cell angiogenic capability is regulated by 3D culture and integrin engagement. *Proceedings of the National Academy of Sciences of the United States of America* **106**, 399-404, doi:10.1073/pnas.0808932106 (2009).

46 Engler, A. J., Sen, S., Sweeney, H. L. & Discher, D. E. Matrix elasticity directs stem cell lineage specification. *Cell* **126**, 677-689, doi:10.1016/j.cell.2006.06.044 (2006).

47 Schrader, J. *et al.* Matrix stiffness modulates proliferation, chemotherapeutic response, and dormancy in hepatocellular carcinoma cells. *Hepatology* **53**, 1192-1205, doi:10.1002/hep.24108 (2011).

48 Chandler, E. M. *et al.* Implanted adipose progenitor cells as physicochemical regulators of breast cancer. *Proceedings of the National Academy of Sciences of the United States of America* **109**, 9786-9791, doi:10.1073/pnas.1121160109 (2012).

49 Castello-Cros, R., Khan, D. R., Simons, J., Valianou, M. & Cukierman, E. Staged stromal extracellular 3D matrices differentially regulate breast cancer cell responses through PI3K and beta1-integrins. *BMC cancer* **9**, 94, doi:10.1186/1471-2407-9-94 (2009).

50 Carmeliet, P. Angiogenesis in health and disease. *Nature Medicine* **9**, 653-660, doi:Doi 10.1038/Nm0603-653 (2003).

51 Carmeliet, P. & Jain, R. K. Angiogenesis in cancer and other diseases. *Nature* **407**, 249-257, doi:Doi 10.1038/35025220 (2000).

52 Laschke, M. W. *et al.* Angiogenesis in tissue engineering: Breathing life into constructed tissue substitutes. *Tissue Engineering* **12**, 2093-2104, doi:DOI 10.1089/ten.2006.12.2093 (2006).

53 Harris, A. L. Hypoxia - A key regulatory factor in tumour growth. *Nat. Rev. Cancer* **2**, 38-47, doi:10.1038/nrc704 (2002).

54 Hockel, M. & Vaupel, P. Tumor hypoxia: Definitions and current clinical, biologic, and molecular aspects. *Journal of the National Cancer Institute* **93**, 266-276, doi:10.1093/jnci/93.4.266 (2001).

55 Helmlinger, G., Yuan, F., Dellian, M. & Jain, R. K. Interstitial pH and pO(2) gradients in solid tumors in vivo: High-resolution measurements reveal a lack of correlation. *Nat Med* **3**, 177-182, doi:10.1038/nm0297-177 (1997).

56 Gatenby, R. A. & Gillies, R. J. Why do cancers have high aerobic glycolysis? *Nat. Rev. Cancer* **4**, 891-899, doi:10.1038/nrc1478 (2004).

57 Semenza, G. L. Targeting HIF-1 for cancer therapy. *Nat. Rev. Cancer* **3**, 721-732, doi:10.1038/nrc1187 (2003).

58 Fukumura, D. *et al.* Hypoxia and acidosis independently up-regulate vascular endothelial growth factor transcription in brain tumors in vivo. *Cancer Research* **61**, 6020-6024 (2001).

59 Forsythe, J. A. *et al.* Activation of vascular endothelial growth factor gene transcription by hypoxia-inducible factor 1. *Molecular and Cellular Biology* **16**, 4604-4613 (1996).

60 Hughes, C. C. W., Nakatsu, M. N. & Holderfield, M. T. Endothelial cell-stromal interactions during angiogenesis. *Faseb J* **21**, A35-A35 (2007).

61 Vong, S. & Kalluri, R. The role of stromal myofibroblast and extracellular matrix in tumor angiogenesis. *Genes Cancer* **2**, 1139-1145, doi:10.1177/1947601911423940 [pii] (2011).

62 Friedman, J. M. Obesity in the new millennium. *Nature* **404**, 632-634, doi:10.1038/35007504 (2000).

63 Kimm, S. Y. & Obarzanek, E. Childhood obesity: a new pandemic of the new millennium. *Pediatrics* **110**, 1003-1007 (2002).

64 Khandekar, M. J., Cohen, P. & Spiegelman, B. M. Molecular mechanisms of cancer development in obesity. *Nature Reviews Cancer* **11**, 886-895, doi:Doi 10.1038/Nrc3174 (2011).

65 Lloyd, L. J., Langley-Evans, S. C. & McMullen, S. Childhood obesity and adult cardiovascular disease risk: a systematic review. *Int J Obesity* **34**, 18-28, doi:Doi 10.1038/Ijo.2009.61 (2010).

66 Subbaramaiah, K. *et al.* Obesity is associated with inflammation and elevated aromatase expression in the mouse mammary gland. *Cancer prevention research* **4**, 329-346, doi:10.1158/1940-6207.CAPR-10-0381 (2011).

67 Aapro, M. & Wildiers, H. Triple-negative breast cancer: epidemiological considerations and recommendations. *Ann Oncol* **23**, 52-55, doi:DOI 10.1093/annonc/mds189 (2012).

68 Foulkes, W. D., Smith, I. E. & Reis-Filho, J. S. Triple-negative breast cancer. *N Engl J Med* **363**, 1938-1948, doi:10.1056/NEJMra1001389 (2010).

69 Jo, J. *et al.* Hypertrophy-Driven Adopocyte Death Overwhelms Recruitment under Prolonged Weight Gain. *Biophys J* **99**, 3535-3544, doi:Doi 10.1016/J.Bpj.010.10.009 (2010).

70 Fain, J. N. Release of inflammatory mediators by human adipose tissue is enhanced in obesity and primarily by the nonfat cells: a review. *Mediators of inflammation* **2010**, 513948, doi:10.1155/2010/513948 (2010).

71 Divoux, A. *et al.* Fibrosis in human adipose tissue: composition, distribution, and link with lipid metabolism and fat mass loss. *Diabetes* **59**, 2817-2825, doi:10.2337/db10-0585 (2010).

72 Otranto, M. *et al.* The role of the myofibroblast in tumor stroma remodeling. *Cell adhesion & migration* **6**, 203-219, doi:Doi 10.4161/Cam.20377 (2012).

73 Wajchenberg, B. L. Subcutaneous and visceral adipose tissue: Their relation to the metabolic syndrome. *Endocr Rev* **21**, 697-738, doi:Doi 10.1210/Er.21.6.697 (2000).

74 Lafontan, M. & Berlan, M. Do regional differences in adipocyte biology provide new pathophysiological insights? *Trends Pharmacol Sci* **24**, 276-283, doi:Doi 10.1016/S0165-6147(03)00132-9 (2003).

75 Bjorndal, B., Burri, L., Staalesen, V., Skorve, J. & Berge, R. K. Different adipose depots: their role in the development of metabolic syndrome and mitochondrial response to hypolipidemic agents. *Journal of obesity* **2011**, 490650, doi:10.1155/2011/490650 (2011).

76 Rosen, E. D. & Spiegelman, B. M. Adipocytes as regulators of energy balance and glucose homeostasis. *Nature* **444**, 847-853, doi:10.1038/nature05483 (2006).

77 Xu, R., Boudreau, A. & Bissell, M. Tissue architecture and function: dynamic reciprocity via extra- and intra-cellular matrices. *Cancer Metast Rev* **28**, 167-176, doi:Doi 10.1007/S10555-008-9178-Z (2009).

78 Muschler, J. & Streuli, C. H. Cell-Matrix Interactions in Mammary Gland Development and Breast Cancer. *Cold Spring Harbor perspectives in biology* **2**, doi:ARTN a003202 DOI 10.1101/cshperspect.a003202 (2010).

79 Cinti, S. The adipose organ at a glance. *Dis Model Mech* **5**, 588-594, doi:Doi 10.1242/Dmm.009662 (2012).

80 Robinson, S. D., Silberstein, G. B., Roberts, A. B., Flanders, K. C. & Daniel, C. W. Regulated Expression and Growth Inhibitory Effects of Transforming Growth-Factor-Beta Isoforms in Mouse Mammary-Gland Development. *Development* **113**, 867-& (1991).

81 Sakai, T., Larsen, M. & Yamada, K. M. Fibronectin requirement in branching morphogenesis. *Nature* **423**, 876-881, doi:10.1038/nature01712 (2003).

82 Russo J, R. I. H. in *Molecular Basis of Breast Cancer: Prevention and Treatment* 138 -176 (Springer, 2004).

83 Gimble, J. M., Katz, A. J. & Bunnell, B. A. Adipose-derived stem cells for regenerative medicine. *Circulation Research* **100**, 1249-1260, doi:Doi 10.1161/01.Res.0000265074.83288.09 (2007).

84 Moreno-Navarrete, J. M. & Fernández-Real, J. M. Adipocyte Differentiation. 17-38, doi:10.1007/978-1-4614-0965-6_2 (2012).

85 Matsumoto, T. *et al.* Mature adipocyte-derived dedifferentiated fat cells exhibit multilineage potential. *Journal of cellular physiology* **215**, 210-222, doi:10.1002/jcp.21304 (2008).

86 Petit, J. Y. *et al.* Locoregional recurrence risk after lipofilling in breast cancer patients. *Ann Oncol* **23**, 582-588, doi:DOI 10.1093/annonc/mdr158 (2012).

87 DuFort, C. C., Paszek, M. J. & Weaver, V. M. Balancing forces: architectural control of mechanotransduction. *Nature reviews. Molecular cell biology* **12**, 308-319, doi:10.1038/nrm3112 (2011).

88 Wozniak, M. A. & Chen, C. S. Mechanotransduction in development: a growing role for contractility. *Nat Rev Mol Cell Bio* **10**, 34-43, doi:Doi 10.1038/Nrm2592 (2009).

89 Mammoto, A., Mammoto, T. & Ingber, D. E. Mechanosensitive mechanisms in transcriptional regulation. *J Cell Sci* **125**, 3061-3073, doi:Doi 10.1242/Jcs.093005 (2012).

90 Provenzano, P. P. & Keely, P. J. Mechanical signaling through the cytoskeleton regulates cell proliferation by coordinated focal adhesion and Rho GTPase signaling. *J Cell Sci* **124**, 1195-1205, doi:Doi 10.1242/Jcs.067009 (2011).

91 Wan, A. M. *et al.* Fibronectin conformation regulates the proangiogenic capability of tumor-associated adipogenic stromal cells. *Biochimica et biophysica acta* **1830**, 4314-4320, doi:10.1016/j.bbagen.2013.03.033 (2013).

92 Achilli, M. & Mantovani, D. Tailoring Mechanical Properties of Collagen-Based Scaffolds for Vascular Tissue Engineering: The Effects of pH, Temperature and Ionic Strength on Gelation. *Polymers-Basel* **2**, 664-680, doi:Doi 10.3390/Polym2040664 (2010).

93 Hulmes, D. J. S. in *Collagen diversity, synthesis and assembly* (ed Peter Fratzl) 15-47 (Springer), 2008).

94 Provenzano, P. P. *et al.* Collagen reorganization at the tumor-stromal interface facilitates local invasion. *BMC medicine* **4**, doi:Artn 38Doi 10.1186/1741-7015-4-38 (2006).

95 Klotzsch, E. *et al.* Fibronectin forms the most extensible biological fibers displaying switchable force-exposed cryptic binding sites. *Proceedings of the National Academy of Sciences of the United States of America* **106**, 18267-18272, doi:Doi 10.1073/Pnas.0907518106 (2009).

96 Singh, P., Carraher, C. & Schwarzbauer, J. E. Assembly of Fibronectin Extracellular Matrix. *Annu Rev Cell Dev Bi* **26**, 397-419, doi:DOI 10.1146/annurev-cellbio-100109-104020 (2010).

97 Smith, M. L. *et al.* Force-induced unfolding of fibronectin in the extracellular matrix of living cells. *PLoS biology* **5**, e268, doi:10.1371/journal.pbio.0050268 (2007).

98 Smith, M. L. *et al.* Force-induced unfolding of fibronectin in the extracellular matrix of living cells. *Plos Biol* **5**, 2243-2254, doi:Doi 10.1371/Journal.Pbio.0050268 (2007).

99 Mott, J. D. & Werb, Z. Regulation of matrix biology by matrix metalloproteinases. *Curr Opin Cell Biol* **16**, 558-564, doi:10.1016/j.ceb.2004.07.010 (2004).

100 Akiyama, S. K., Olden, K. & Yamada, K. M. Fibronectin and integrins in invasion and metastasis. *Cancer Metastasis Rev* **14**, 173-189 (1995).

101 Chandler, E. M., Saunders, M. P., Yoon, C. J., Gourdon, D. & Fischbach, C. Adipose progenitor cells increase fibronectin matrix strain and unfolding in breast tumors. *Phys Biol* **8**, 015008, doi:10.1088/1478-3975/8/1/015008 (2011).

102 Kadler, K. E., Hill, A. & Canty-Laird, E. G. Collagen fibrillogenesis: fibronectin, integrins, and minor collagens as organizers and nucleators. *Current Opinion in Cell Biology* **20**, 495-501, doi:Doi 10.1016/J.Ceb.2008.06.008 (2008).

103 Guarnieri, D. *et al.* Effects of fibronectin and laminin on structural, mechanical and transport properties of 3D collageneous network. *J Mater Sci-Mater M* **18**, 245-253, doi:Doi 10.1007/S10856-006-0686-5 (2007).

104 HogenEsch, H. & Nikitin, A. Y. Challenges in pre-clinical testing of anti-cancer drugs in cell culture and in animal models. *J Control Release* **164**, 183-186, doi:10.1016/j.jconrel.2012.02.031 S0168-3659(12)00161-7 [pii] (2012).

105 Brill, B., Boecher, N., Groner, B. & Shemanko, C. S. A sparing procedure to clear the mouse mammary fat pad of epithelial components for transplantation analysis. *Lab Anim-Uk* **42**, 104-110, doi:DOI 10.1258/la.2007.06003e (2008).

106 Sharpless, N. E. & DePinho, R. A. Model organisms - The mighty mouse: genetically engineered mouse models in cancer drug development. *Nat Rev Drug Discov* **5**, 741-754, doi:Doi 10.1038/Nrd2110 (2006).

107 Carroll, L., Voisey, J. & van Daal, A. Mouse models of obesity. *Clinics in dermatology* **22**, 345-349, doi:10.1016/j.clindermatol.2004.01.004 (2004).

108 Bhardwaj, P. *et al.* Caloric Restriction Reverses Obesity-Induced Mammary Gland Inflammation in Mice. *Cancer prevention research* **6**, 282-289, doi:Doi 10.1158/1940-6207.Capr-12-0467 (2013).

109 Brightman, A. O. *et al.* Time-lapse confocal reflection microscopy of collagen fibrillogenesis and extracellular matrix assembly in vitro. *Biopolymers* **54**, 222-234 (2000).

110 Franke, K., Sapudom, J., Kalbitzer, L., Anderegg, U. & Pompe, T. Topologically defined composites of collagen types I and V as in vitro cell culture scaffolds. *Acta Biomater* **10**, 2693-2702, doi:Doi 10.1016/J.Actbio.2014.02.036 (2014).

111 Williams, R. M., Zipfel, W. R. & Webb, W. W. Interpreting second-harmonic generation images of collagen I fibrils. *Biophysical journal* **88**, 1377-1386, doi:DOI 10.1529/biophysj.104.047308 (2005).

112 Lattouf, R. *et al.* Picrosirius Red Staining, A Useful Tool to Appraise Collagen Network in Normal and Pathologic Tissues. *J Histochem Cytochem*, doi:0022155414545787 [pii]10.1369/0022155414545787 (2014).

113 Baker, B. M. & Chen, C. S. Deconstructing the third dimension - how 3D culture microenvironments alter cellular cues. *J Cell Sci* **125**, 3015-3024, doi:Doi 10.1242/Jcs.079509 (2012).

114 Moreno-Navarrete, J. M., Fernández-Real, J.M. in *Adipose Differentiation* (ed Symonds M.E.) 17 - 38 (Springer, 2012).

115 Cherubino, M. & Marra, K. G. Adipose-derived stem cells for soft tissue reconstruction. *Regen Med* **4**, 109-117, doi:10.2217/17460751.4.1.109 (2009).

116 Gimble, J. M., Katz, A. J. & Bunnell, B. A. Adipose-derived stem cells for regenerative medicine. *Circ Res* **100**, 1249-1260, doi:100/9/1249 [pii]10.1161/01.RES.0000265074.83288.09 (2007).

117 Surgeons, A. S. o. P. in http://www.plasticsurgery.org (2010).

118 Moioli, E. K. *et al.* Hybrid adipogenic implants from adipose stem cells for soft tissue reconstruction in vivo. *Tissue Eng Part A* **16**, 3299-3307, doi:10.1089/ten.TEA.2010.0157 (2010).

119 Yoshimura, K. *et al.* Cell-assisted lipotransfer for cosmetic breast augmentation: supportive use of adipose-derived stem/stromal cells. *Aesthetic Plast Surg* **32**, 48-55; discussion 56-47, doi:10.1007/s00266-007-9019-4 (2008).

120 Brewster, A. M. *et al.* Residual risk of breast cancer recurrence 5 years after adjuvant therapy. *J Natl Cancer Inst* **100**, 1179-1183, doi:djn233 [pii] 10.1093/jnci/djn233 (2008).

121 Janmey, P. A., Levental, I. & Georges, P. C. Soft biological materials and their impact on cell function. *Soft Matter* **3**, 299-306, doi:10.1039/b610522j (2007).

122 Samani, A., Bishop, J., Luginbuhl, C. & Plewes, D. B. Measuring the elastic modulus of ex vivo small tissue samples. *Phys Med Biol* **48**, 2183-2198 (2003).

123 Paszek, M. J. *et al.* Tensional homeostasis and the malignant phenotype. *Cancer cell* **8**, 241-254, doi:10.1016/j.ccr.2005.08.010 (2005).

124 Mammoto, A. *et al.* A mechanosensitive transcriptional mechanism that controls angiogenesis. *Nature* **457**, 1103-1108, doi:nature07765 [pii] 10.1038/nature07765 (2009).

125 Nakagawa, H. *et al.* Role of cancer-associated stromal fibroblasts in metastatic colon cancer to the liver and their expression profiles. *Oncogene* **23**, 7366-7377, doi:10.1038/sj.onc.1208013 1208013 [pii] (2004).

126 Kidd, S. *et al.* Origins of the tumor microenvironment: quantitative assessment of adipose-derived and bone marrow-derived stroma. *PLoS One* **7**, e30563, doi:10.1371/journal.pone.0030563PONE-D-11-19617 [pii] (2012).

127 Quante, M. *et al.* Bone marrow-derived myofibroblasts contribute to the mesenchymal stem cell niche and promote tumor growth. *Cancer Cell* **19**, 257-272, doi:S1535-6108(11)00042-0 [pii] 10.1016/j.ccr.2011.01.020 (2011).

128 Cheng, L. *et al.* Rb inactivation accelerates neoplastic growth and substitutes for recurrent amplification of cIAP1, cIAP2 and Yap1 in sporadic mammary carcinoma associated with p53 deficiency. *Oncogene* **29**, 5700-5711, doi:onc2010300 [pii]10.1038/onc.2010.300 (2010).

129 Santner, S. J. *et al.* Malignant MCF10CA1 cell lines derived from premalignant human breast epithelial MCF10AT cells. *Breast Cancer Res Treat* **65**, 101-110 (2001).

130 Debnath, J., Muthuswamy, S. K. & Brugge, J. S. Morphogenesis and oncogenesis of MCF-10A mammary epithelial acini grown in three-dimensional basement membrane cultures. *Methods* **30**, 256-268, doi:S104620230300032X [pii] (2003).

131 Lonza. (2011).

132 Fischbach, C. *et al.* Generation of mature fat pads in vitro and in vivo utilizing 3-D long-term culture of 3T3-L1 preadipocytes. *Exp Cell Res* **300**, 54-64 (2004).

133 Cross, V. L. *et al.* Dense type I collagen matrices that support cellular remodeling and microfabrication for studies of tumor angiogenesis and vasculogenesis in vitro. *Biomaterials* **31**, 8596-8607, doi:S0142-9612(10)00944-0 [pii]10.1016/j.biomaterials.2010.07.072 (2010).

134 Verbridge, S. S. *et al.* Oxygen-controlled three-dimensional cultures to analyze tumor angiogenesis. *Tissue Eng Part A* **16**, 2133-2141, doi:10.1089/ten.TEA.2009.0670 (2010).

135 Omoto, M. *et al.* The use of human mesenchymal stem cell-derived feeder cells for the cultivation of transplantable epithelial sheets. *Invest Ophthalmol Vis Sci* **50**, 2109-2115, doi:iovs.08-2262 [pii]10.1167/iovs.08-2262 (2009).

136 Buckley, M. R., Bergou, A. J., Fouchard, J., Bonassar, L. J. & Cohen, I. High-resolution spatial mapping of shear properties in cartilage. *J Biomech* **43**, 796-800, doi:S0021-9290(09)00586-7 [pii]10.1016/j.jbiomech.2009.10.012 (2010).

137 Califano, J. P. & Reinhart-King, C. A. Substrate Stiffness and Cell Area Predict Cellular Traction Stresses in Single Cells and Cells in Contact. *Cellular and Molecular Bioengineering* **3**, 68-75, doi:10.1007/s12195-010-0102-6 (2010).

138 Dembo, M., Oliver, T., Ishihara, A. & Jacobson, K. Imaging the traction stresses exerted by locomoting cells with the elastic substratum method. *Biophys J* **70**, 2008-2022, doi:S0006-3495(96)79767-9 [pii]10.1016/S0006-3495(96)79767-9 (1996).

139 Dembo, M. & Wang, Y. L. Stresses at the cell-to-substrate interface during locomotion of fibroblasts. *Biophys J* **76**, 2307-2316, doi:S0006-3495(99)77386-8 [pii]10.1016/S0006-3495(99)77386-8 (1999).

140 Wang, Y. L. & Pelham, R. J., Jr. Preparation of a flexible, porous polyacrylamide substrate for mechanical studies of cultured cells. *Methods Enzymol* **298**, 489-496 (1998).

141 Williams, R. M. *et al.* Strategies for high-resolution imaging of epithelial ovarian cancer by laparoscopic nonlinear microscopy. *Translational oncology* **3**, 181-194 (2010).

142 Cukierman, E. Preparation of Extracellular Matrices Produced by Cultured Fibroblasts. *Current Protocols in Cell Biology*, doi:10.1002/0471143030.cb1009s16 (2002).

143 Cornelius, P., MacDougald, O. A. & Lane, M. D. Regulation of adipocyte development. *Annu Rev Nutr* **14**, 99-129, doi:10.1146/annurev.nu.14.070194.000531 (1994).

144 Olaso, E. *et al.* Proangiogenic role of tumor-activated hepatic stellate cells in experimental melanoma metastasis. *Hepatology* **37**, 674-685, doi:10.1053/jhep.2003.50068S0270913902141115 [pii] (2003).

145 Hong, K. M., Belperio, J. A., Keane, M. P., Burdick, M. D. & Strieter, R. M. Differentiation of human circulating fibrocytes as mediated by transforming growth factor-beta and peroxisome proliferator-activated receptor gamma. *J Biol Chem* **282**, 22910-22920, doi:M703597200 [pii] 10.1074/jbc.M703597200 (2007).

146 De Wever, O. & Mareel, M. Role of tissue stroma in cancer cell invasion. *J Pathol* **200**, 429-447, doi:10.1002/path.1398 (2003).

147 Guerrero, J. *et al.* Soluble factors derived from tumor mammary cell lines induce a stromal mammary adipose reversion in human and mice adipose cells. Possible role of TGF-beta1 and TNF-alpha. *Breast Cancer Res Treat* **119**, 497-508, doi:10.1007/s10549-009-0491-1 (2010).

148 Schauer, I. G., Ressler, S. J., Tuxhorn, J. A., Dang, T. D. & Rowley, D. R. Elevated epithelial expression of interleukin-8 correlates with myofibroblast reactive stroma in benign prostatic hyperplasia. *Urology* **72**, 205-213, doi:S0090-4295(07)02466-1 [pii] 10.1016/j.urology.2007.11.083 (2008).

149 Yagi, Y., Andoh, A., Inatomi, O., Tsujikawa, T. & Fujiyama, Y. Inflammatory responses induced by interleukin-17 family members in human colonic subepithelial myofibroblasts. *J Gastroenterol* **42**, 746-753, doi:10.1007/s00535-007-2091-3 (2007).

150 Peyrol, S. *et al.* Lysyl oxidase gene expression in the stromal reaction to in situ and invasive ductal breast carcinoma. *Am J Pathol* **150**, 497-507 (1997).

151 Reinhart-King, C. A., Dembo, M. & Hammer, D. A. Endothelial cell traction forces on RGD-derivatized polyacrylamide substrata. *Langmuir* **19**, 1573-1579, doi:Doi 10.1021/La026142j (2003).

152 Shin, H., Zygourakis, K., Farach-Carson, M. C., Yaszemski, M. J. & Mikos, A. G. Modulation of differentiation and mineralization of marrow stromal cells cultured on biomimetic hydrogels modified with Arg-Gly-Asp containing peptides. *J Biomed Mater Res A* **69**, 535-543, doi:10.1002/jbm.a.30027 (2004).

153 McLean, G. W. *et al.* The role of focal-adhesion kinase in cancer - a new therapeutic opportunity. *Nat Rev Cancer* **5**, 505-515, doi:nrc1647 [pii]10.1038/nrc1647 (2005).

154 Cho, S. W. *et al.* Engineering of volume-stable adipose tissues. *Biomaterials* **26**, 3577-3585, doi:S0142-9612(04)00810-5 [pii] 10.1016/j.biomaterials.2004.09.013 (2005).

155 Davidenko, N., Campbell, J. J., Thian, E. S., Watson, C. J. & Cameron, R. E. Collagen-hyaluronic acid scaffolds for adipose tissue engineering. *Acta Biomater* **6**, 3957-3968, doi:S1742-7061(10)00232-1 [pii]10.1016/j.actbio.2010.05.005 (2010).

156 Chandler, E. M. *et al.* Stiffness of photocrosslinked RGD-alginate gels regulates adipose progenitor cell behavior. *Biotechnol Bioeng* **108**, 1683-1692, doi:10.1002/bit.23079 (2011).

157 McBeath, R., Pirone, D. M., Nelson, C. M., Bhadriraju, K. & Chen, C. S. Cell shape, cytoskeletal tension, and RhoA regulate stem cell lineage commitment. *Dev Cell* **6**, 483-495, doi:S1534580704000759 [pii] (2004).

158 Storm, C., Pastore, J. J., MacKintosh, F. C., Lubensky, T. C. & Janmey, P. A. Nonlinear elasticity in biological gels. *Nature* **435**, 191-194, doi:nature03521 [pii]10.1038/nature03521 (2005).

159 Muehlberg, F. L. *et al.* Tissue-resident stem cells promote breast cancer growth and metastasis. *Carcinogenesis* **30**, 589-597, doi:bgp036 [pii]10.1093/carcin/bgp036 (2009).

160 Prantl, L. *et al.* Adipose tissue-derived stem cells promote prostate tumor growth. *Prostate* **70**, 1709-1715, doi:10.1002/pros.21206 (2010).

161 Zhang, Y. *et al.* White adipose tissue cells are recruited by experimental tumors and promote cancer progression in mouse models. *Cancer Res* **69**, 5259-5266, doi:0008-5472.CAN-08-3444 [pii]10.1158/0008-5472.CAN-08-3444 (2009).

162 Kida, Y. & Duffield, J. S. Pivotal role of pericytes in kidney fibrosis. *Clin Exp Pharmacol Physiol* **38**, 417-423, doi:10.1111/j.1440-1681.2011.05531.x (2011).

163 Petit, J. Y. *et al.* Locoregional recurrence risk after lipofilling in breast cancer patients. *Ann Oncol*, doi:mdr158 [pii]10.1093/annonc/mdr158 (2011).

164 van Harmelen, V. *et al.* Effect of BMI and age on adipose tissue cellularity and differentiation capacity in women. *Int J Obes Relat Metab Disord* **27**, 889-895, doi:10.1038/sj.ijo.0802314 0802314 [pii] (2003).

165 Bianchini, F., Kaaks, R. & Vainio, H. Overweight, obesity, and cancer risk. *Lancet Oncol* **3**, 565-574, doi:S1470204502008495 [pii] (2002).

166 Moutos, F. T. & Guilak, F. Functional properties of cell-seeded three-dimensionally woven poly(epsilon-caprolactone) scaffolds for cartilage tissue engineering. *Tissue Eng Part A* **16**, 1291-1301, doi:10.1089/ten.TEA.2009.0480 (2010).

167 Ochoa, I. *et al.* Mechanical properties of cross-linked collagen meshes after human adipose derived stromal cells seeding. *J Biomed Mater Res A* **96**, 341-348, doi:10.1002/jbm.a.32988 (2011).

168 Lin, G. *et al.* Effects of transplantation of adipose tissue-derived stem cells on prostate tumor. *Prostate* **70**, 1066-1073, doi:10.1002/pros.21140 (2010).

169 Bellows, C. F., Zhang, Y., Chen, J., Frazier, M. L. & Kolonin, M. G. Circulation of progenitor cells in obese and lean colorectal cancer patients. *Cancer Epidemiol Biomarkers Prev* **20**, 2461-2468, doi:1055-9965.EPI-11-0556 [pii]10.1158/1055-9965.EPI-11-0556 (2011).

170 Hefetz-Sela, S. & Scherer, P. E. Adipocytes: impact on tumor growth and potential sites for therapeutic intervention. *Pharmacol Ther* **138**, 197-210, doi:10.1016/j.pharmthera.2013.01.008 S0163-7258(13)00020-X [pii] (2013).

171 Majka, S. M., Barak, Y. & Klemm, D. J. Concise Review: Adipocyte Origins: Weighing the Possibilities. *Stem Cells* **29**, 1034-1040, doi:Doi 10.1002/Stem.653 (2011).

172 Havel, P. J. Update on adipocyte hormones - Regulation of energy balance and carbohydrate/lipid metabolism. *Diabetes* **53**, S143-S151, doi:DOI 10.2337/diabetes.53.2007.S143 (2004).

173 Nieman, K. M., Romero, I. L., Van Houten, B. & Lengyel, E. Adipose tissue and adipocytes support tumorigenesis and metastasis. *Bba-Mol Cell Biol L* **1831**, 1533-1541, doi:DOI 10.1016/j.bbalip.2013.02.010 (2013).

174 Pavlides, S. *et al.* Transcriptional evidence for the "Reverse Warburg Effect" in human breast cancer tumor stroma and metastasis: Similarities with oxidative stress, inflammation, Alzheimer's disease, and "Neuron-Glia Metabolic Coupling". *Aging-Us* **2**, 185-199 (2010).

175 Nieman, K. M. *et al.* Adipocytes promote ovarian cancer metastasis and provide energy for rapid tumor growth. *Nature Medicine* **17**, 1498-U1207, doi:Doi 10.1038/Nm.2492 (2011).

176 Dirat, B. *et al.* Cancer-associated adipocytes exhibit an activated phenotype and contribute to breast cancer invasion. *Cancer research* **71**, 2455-2465, doi:10.1158/0008-5472.CAN-10-3323 (2011).

177 Chandler, E. M. *et al.* Implanted adipose progenitor cells as physicochemical regulators of breast cancer. *P Natl Acad Sci USA* **109**, 9786-9791, doi:DOI 10.1073/pnas.1121160109 (2012).

178 Jotzu, C. *et al.* Adipose tissue derived stem cells differentiate into carcinoma-associated fibroblast-like cells under the influence of tumor derived factors. *Cell Oncol* **34**, 55-67, doi:DOI 10.1007/s13402-011-0012-1 (2011).

179 Morris, P. G. *et al.* Inflammation and Increased Aromatase Expression Occur in the Breast Tissue of Obese Women with Breast Cancer. *Cancer Prev Res* **4**, 1021-1029, doi:Doi 10.1158/1940-6207.Capr-11-0110 (2011).

180 Fischbach, C. *et al.* Generation of mature fat pads in vitro and in vivo utilizing 3-D long-term culture of 3T3-L1 preadipocytes. *Exp Cell Res* **300**, 54-64, doi:Doi 10.1016/J.Yexcr.2004.05.036 (2004).

181 Lonza (2011) PoieticsTM human adipose derived stem cells (ADSC).

182 Scott S. Verbridge, N. W. C., Ying Zheng, Daniel J. Brooks, Abraham D. Stroock, and Claudia Fischbach. Oxygen-Controlled Three-Dimensional Cultures to Analyze Tumor Angiogenesis. *Tissue engineering. Part A* **16**, 2133-2141 (2010).

183 Garaulet, M. *et al.* Timing of food intake predicts weight loss effectiveness. *International Journal of Obesity* **37**, 604-611, doi:Doi 10.1038/Ijo.2012.229 (2013).

184 Hinz, B., Celetta, G., Tomasek, J. J., Gabbiani, G. & Chaponnier, C. Alpha-smooth muscle actin expression upregulates fibroblast contractile activity. *Mol Biol Cell* **12**, 2730-2741 (2001).

185 Poloni, A. *et al.* Human dedifferentiated adipocytes show similar properties to bone marrow-derived mesenchymal stem cells. *Stem Cells* **30**, 965-974, doi:10.1002/stem.1067 (2012).

186 Gabbiani, G. The myofibroblast in wound healing and fibrocontractive diseases. *J Pathol* **200**, 500-503, doi:Doi 10.1002/Path.1427 (2003).

187 McBeath, R., Pirone, D. M., Nelson, C. M., Bhadriraju, K. & Chen, C. S. Cell shape, cytoskeletal tension, and RhoA regulate stem cell lineage commitment. *Dev Cell* **6**, 483-495, doi:Doi 10.1016/S1534-5807(04)00075-9 (2004).

188 Sugihara, H., Yonemitsu, N., Miyabara, S. & Yun, K. Primary cultures of unilocular fat cells: characteristics of growth in vitro and changes in differentiation properties. *Differentiation* **31**, 42-49 (1986).

189 Hinz, B. Formation and function of the myofibroblast during tissue repair. *J Invest Dermatol* **127**, 526-537, doi:5700613 [pii]10.1038/sj.jid.5700613 (2007).

190 Tan, J. X., Buache, E., Chenard, M. P., Dali-Youcef, N. & Rio, M. C. Adipocyte is a non-trivial, dynamic partner of breast cancer cells. *Int J Dev Biol* **55**, 851-859, doi:DOI 10.1387/ijdb.113365jt (2011).

191 Andarawewa, K. L. *et al.* Stromelysin-3 is a potent negative regulator of adipogenesis participating to cancer cell-adipocyte interaction/crosstalk at the tumor invasive front. *Cancer Research* **65**, 10862-10871, doi:Doi 10.1158/0008-5472.Can-05.1231 (2005).

192 Murholm, M. *et al.* Retinoic acid has different effects on UCP1 expression in mouse and human adipocytes. *Bmc Cell Biol* **14**, doi:Artn 41Doi 10.1186/1471-2121-14-41 (2013).

193 DeLany, J. P. *et al.* Proteomic analysis of primary cultures of human adipose-derived stem cells: modulation by Adipogenesis. *Mol Cell Proteomics* **4**, 731-740, doi:M400198-MCP200 [pii] 10.1074/mcp.M400198-MCP200 (2005).

194 Rosen, E. D. & MacDougald, O. A. Adipocyte differentiation from the inside out. *Nat Rev Mol Cell Bio* **7**, 885-896, doi:Doi 10.1038/Nrm2066 (2006).

195 Zhang, H. H., Halbleib, M., Ahmad, F., Manganiello, V. C. & Greenberg, A. S. Tumor necrosis factor-alpha stimulates lipolysis in differentiated human adipocytes through activation of extracellular signal-related kinase and elevation of intracellular cAMP. *Diabetes* **51**, 2929-2935 (2002).

196 Hinz, B. Formation and function of the myofibroblast during tissue repair. *J Invest Dermatol* **127**, 526-537, doi:DOI 10.1038/sj.jid.5700613 (2007).

197 Choy, L. & Derynck, R. Transforming growth factor-beta inhibits adipocyte differentiation by Smad3 interacting with CCAAT/enhancer-binding protein (C/EBP) and repressing C/EBP transactivation function. *Journal of Biological Chemistry* **278**, 9609-9619, doi:DOI 10.1074/jbc.M212259200 (2003).

198 Pederson, L., Winding, B., Foged, N. T., Spelsberg, T. C. & Oursler, M. J. Identification of breast cancer cell line-derived paracrine factors that stimulate osteoclast activity. *Cancer Research* **59**, 5849-5855 (1999).

199 Kono, S. *et al.* Phenotypic and functional properties of feline dedifferentiated fat cells and adipose-derived stem cells. *Vet J* **199**, 88-96, doi:DOI 10.1016/j.tvjl.2013.10.033 (2014).

200 Sheng, X., Tucci, J., Malvar, J. & Mittelman, S. D. Adipocyte differentiation is affected by media height above the cell layer. *International Journal of Obesity* **38**, 315-320, doi:Doi 10.1038/Ijo.2013.96 (2014).

201 Mariman, E. C. M. & Wang, P. Adipocyte extracellular matrix composition, dynamics and role in obesity. *Cell Mol Life Sci* **67**, 1277-1292, doi:DOI 10.1007/s00018-010-0263-4 (2010).

202 Levental, K. R. *et al.* Matrix Crosslinking Forces Tumor Progression by Enhancing Integrin Signaling. *Cell* **139**, 891-906, doi:DOI 10.1016/j.cell.2009.10.027 (2009).

203 Spiegelman, B. M. & Ginty, C. A. Fibronectin Modulation of Cell-Shape and Lipogenic Gene-Expression in 3t3-Adipocytes. *Cell* **35**, 657-666, doi:Doi 10.1016/0092-8674(83)90098-3 (1983).

204 Tanabe, Y., Koga, M., Saito, M., Matsunaga, Y. & Nakayama, K. Inhibition of adipocyte differentiation by mechanical stretching through ERK-mediated downregulation of PPAR gamma(2). *J Cell Sci* **117**, 3605-3614, doi:Doi 10.1242/Jcs.01207 (2004).

205 Lolmede, K., de Saint Front, V. D., Galitzky, J., Lafontan, M. & Bouloumie, A. Effects of hypoxia on the expression of proangiogenic factors in differentiated 3T3-F442A adipocytes. *International Journal of Obesity* **27**, 1187-1195, doi:DOI 10.1038/sj.ijo.0802407 (2003).

206 Petreaca, M. L., Yao, M., Liu, Y., Defea, K. & Martins-Green, M. Transactivation of vascular endothelial growth factor receptor-2 by interleukin-8 (IL-8/CXCL8) is required for IL-8/CXCL8-induced endothelial permeability. *Mol Biol Cell* **18**, 5014-5023, doi:DOI 10.1091/mbc.E07-01-0004 (2007).

207 Smithson, A. *et al.* Expression of interleukin-8 receptors (CXCR1 and CXCR2) in premenopausal women with recurrent urinary tract infections. *Clin Diagn Lab Immunol* **12**, 1358-1363, doi:12/12/1358 [pii]10.1128/CDLI.12.12.1358-1363.2005 (2005).

208 van Kruijsdijk, R. C. M., van der Wall, E. & Visseren, F. L. J. Obesity and Cancer: The Role of Dysfunctional Adipose Tissue. *Cancer Epidem Biomar* **18**, 2569-2578, doi:Doi 10.1158/1055-9965.Epi-09-0372 (2009).

209 Hefetz-Sela, S. & Scherer, P. E. Adipocytes: Impact on tumor growth and potential sites for therapeutic intervention. *Pharmacol Therapeut* **138**, 197-210, doi:Doi 10.1016/J.Pharmthera.2013.01.008 (2013).

210 Park, J., Euhus, D. M. & Scherer, P. E. Paracrine and Endocrine Effects of Adipose Tissue on Cancer Development and Progression. *Endocr Rev* **32**, 550-570, doi:Doi 10.1210/Er.2010-0030 (2011).

211 Khan, T. *et al.* Metabolic Dysregulation and Adipose Tissue Fibrosis: Role of Collagen VI. *Mol Cell Biol* **29**, 1575-1591, doi:Doi 10.1128/Mcb.01300-08 (2009).

212 Divoux, A. & Clement, K. Architecture and the extracellular matrix: the still unappreciated components of the adipose tissue. *Obes Rev* **12**, e494-503, doi:10.1111/j.1467-789X.2010.00811.x (2011).

213 Park, J. & Scherer, P. E. Adipocyte-derived endotrophin promotes malignant tumor progression. *Journal of Clinical Investigation* **122**, 4243-4256, doi:10.1172/jci63930 (2012).

214 Seo, B. R., Delnero, P. & Fischbach, C. In vitro models of tumor vessels and matrix: Engineering approaches to investigate transport limitations and drug delivery in cancer. *Advanced drug delivery reviews*, doi:10.1016/j.addr.2013.11.011 (2013).

215 Hinz, B. *et al.* Recent Developments in Myofibroblast Biology: Paradigms for Connective Tissue Remodeling. *The American journal of pathology*, doi:10.1016/j.ajpath.2012.02.004 (2012).

216 Yadav, H. *et al.* Protection from obesity and diabetes by blockade of TGF-beta/Smad3 signaling. *Cell Metab* **14**, 67-79, doi:10.1016/j.cmet.2011.04.013 (2011).

217 Vohl, M. C. *et al.* A survey of genes differentially expressed in subcutaneous and visceral adipose tissue in men. *Obes Res* **12**, 1217-1222, doi:10.1038/oby.2004.153 (2004).

218 Subbaramaiah, K. *et al.* Obesity is associated with inflammation and elevated aromatase expression in the mouse mammary gland. *Cancer Prev Res (Phila)* **4**, 329-346, doi:10.1158/1940-6207.CAPR-10-0381 (2011).

219 Bhardwaj, P. *et al.* Caloric restriction reverses obesity-induced mammary gland inflammation in mice. *Cancer Prev Res (Phila)* **6**, 282-289, doi:10.1158/1940-6207.CAPR-12-0467 (2013).

220 Boquest, A. C., Shahdadfar, A., Brinchmann, J. E. & Collas, P. Isolation of stromal stem cells from human adipose tissue. *Methods Mol Biol* **325**, 35-46, doi:10.1385/1-59745-005-7:35 (2006).

221 Xia, S. *et al.* Gr-1+ CD11b+ myeloid-derived suppressor cells suppress inflammation and promote insulin sensitivity in obesity. *The Journal of biological chemistry* **286**, 23591-23599, doi:10.1074/jbc.M111.237123 (2011).

222 Zheng, Q. *et al.* Leptin receptor maintains cancer stem-like properties in triple negative breast cancer cells. *Endocr Relat Cancer* **20**, 797-808, doi:10.1530/ERC-13-0329 (2013).

223 Baneyx, G., Baugh, L. & Vogel, V. Coexisting conformations of fibronectin in cell culture imaged using fluorescence resonance energy transfer. *Proceedings of the National Academy of Sciences of the United States of America* **98**, 14464-14468, doi:Doi 10.1073/Pnas. 251422998 (2001).

224 Smith, M. L. *et al.* Force-induced unfolding of fibronectin in the extracellular matrix of living cells. *PLoS Biol* **5**, e268, doi:10.1371/journal.pbio.0050268 (2007).

225 Andresen Eguiluz, R. C., Wang, K. C., Benson, V., Seo, B. R., Fischbach, C. & Gourdon, D. Extracellular matrix morphology and mechanics in breast cancer. *Materials Research Society Fall Meeting Abstract* **C5.09**, 150 (2013).

226 Andresen Eguiluz, R. C., Wang, K. C., Wu, F., Seo, B. R., Benson, V., Brown, C. N., Fischbach, C. & Gourdon, D. Stiffening and unfolding of tumor-associated fibronectin activate proangiogenic secretion of adipogenic stromal cells. *In preparation* (2014).

227 Castello-Cros, R. & Cukierman, E. Stromagenesis during tumorigenesis: characterization of tumor-associated fibroblasts and stroma-derived 3D matrices. *Methods Mol Biol* **522**, 275-305, doi:10.1007/978-1-59745-413-1_19 (2009).

228 Johnson, K. L. Contact mechanics *Cambridge University Press* (1985).

229 Lakins, J. N., Chin, A. R. & Weaver, V. M. Exploring the link between human embryonic stem cell organization and fate using tension-calibrated extracellular matrix functionalized polyacrylamide gels. *Methods in molecular biology* **916**, 317-350, doi:10.1007/978-1-61779-980-8_24 (2012).

230 Infanger, D. W. *et al.* Glioblastoma Stem Cells Are Regulated by Interleukin-8 Signaling in a Tumoral Perivascular Niche. *Cancer research*, doi:10.1158/0008-5472.CAN-13-1355 (2013).

231 Hu, Y. & Smyth, G. K. ELDA: extreme limiting dilution analysis for comparing depleted and enriched populations in stem cell and other assays. *Journal of immunological methods* **347**, 70-78, doi:10.1016/j.jim.2009.06.008 (2009).

232 Zhang, Y. *et al.* Positional cloning of the mouse obese gene and its human homologue. *Nature* **372**, 425-432, doi:10.1038/372425a0 (1994).

233 Klingberg, F., Hinz, B. & White, E. S. The myofibroblast matrix: implications for tissue repair and fibrosis. *J Pathol* **229**, 298-309, doi:Doi 10.1002/Path.4104 (2013).

234 Renehan, A. G., Tyson, M., Egger, M., Heller, R. F. & Zwahlen, M. Body-mass index and incidence of cancer: a systematic review and meta-analysis of prospective observational studies. *Lancet* **371**, 569-578, doi:10.1016/S0140-6736(08)60269-X (2008).

235 Sheffer, Y. *et al.* Inhibition of fibroblast to myofibroblast transition by halofuginone contributes to the chemotherapy-mediated antitumoral effect. *Molecular cancer therapeutics* **6**, 570-577, doi:10.1158/1535-7163.MCT-06-0468 (2007).

236 Orimo, A. & Weinberg, R. A. Stromal fibroblasts in cancer - A novel tumor-promoting cell type. *Cell Cycle* **5**, 1597-1601, doi:Doi 10.4161/Cc.5.15.3112 (2006).

237 Ehrlich, H. P. & Krummel, T. M. Regulation of wound healing from a connective tissue perspective. *Wound repair and regeneration : official publication of the Wound Healing Society [and] the European Tissue Repair Society* **4**, 203-210, doi:10.1046/j.1524-475X.1996.40206.x (1996).

238 Anderson, J. M. Biological responses to materials. *Ann Rev Mater Res* **31**, 81-110, doi:Doi 10.1146/Annurev.Matsci.31.1.81 (2001).

239 Midwood, K. S., Williams, L. V. & Schwarzbauer, J. E. Tissue repair and the dynamics of the extracellular matrix. *Int J Biochem Cell B* **36**, 1031-1037, doi:Doi 10.1016/J.Biocel.2003.12.003 (2004).

240 Welch, M. P., Odland, G. F. & Clark, R. A. F. Temporal Relationships of F-Actin Bundle Formation, Collagen and Fibronectin Matrix Assembly, and Fibronectin Receptor Expression to Wound Contraction. *Journal of Cell Biology* **110**, 133-145, doi:Doi 10.1083/Jcb.110.1.133 (1990).

241 Erat, M. C. *et al.* Identification and structural analysis of type I collagen sites in complex with fibronectin fragments. *Proceedings of the National Academy of Sciences of the United States of America* **106**, 4195-4200, doi:Doi 10.1073/Pnas.0812516106 (2009).

242 Li, B. J., Moshfegh, C., Lin, Z., Albuschies, J. & Vogel, V. Mesenchymal Stem Cells Exploit Extracellular Matrix as Mechanotransducer. *Sci Rep-Uk* **3**, doi:Artn 2425 Doi 10.1038/Srep02425 (2013).

243 Krammer, A., Craig, D., Thomas, W. E., Schulten, K. & Vogel, V. A structural model for force regulated integrin binding to fibronectin's RGD-synergy site. *Matrix Biology* **21**, 139-147, doi:Pii S0945-053x(01)00197-4 Doi 10.1016/S0945-053x(01)00197-4 (2002).

244 Israelachvili, J. & Gourdon, D. Liquids - Putting liquids under molecular-scale confinement. *Science* **292**, 867-868, doi:Doi 10.1126/Science.1061206 (2001).

245 Israelachvilli, J. N. & Adams, G. E. Measurement of forces between two mica surfaces in aqueous electrolyte solutions in the range 0-100 nm. *J. Chem. Soc., Faraday Trans. 1* **74**, 975-1001 (1978).

246 Nagata, T. *et al.* Prognostic significance of NANOG and KLF4 for breast cancer. *Breast Cancer*, doi:10.1007/s12282-012-0357-y (2012).

247 Jeter, C. R. *et al.* Functional evidence that the self-renewal gene NANOG regulates human tumor development. *Stem Cells* **27**, 993-1005, doi:10.1002/stem.29 (2009).

248 Jeter, C. R. *et al.* NANOG promotes cancer stem cell characteristics and prostate cancer resistance to androgen deprivation. *Oncogene* **30**, 3833-3845, doi:10.1038/onc.2011.114 (2011).

249 Reizes, O. Personal communication. (2013).

250 Sun, K., Tordjman, J., Clement, K. & Scherer, P. E. Fibrosis and Adipose Tissue Dysfunction. *Cell Metab* **18**, 470-477, doi:Doi 10.1016/J.Cmet.2013.06.016 (2013).

251 Cancello, R. *et al.* Permanence of molecular features of obesity in subcutaneous adipose tissue of ex-obese subjects. *International journal of obesity* **37**, 867-873, doi:10.1038/ijo.2013.7 (2013).

252 Howe, L. R., Subbaramaiah, K., Hudis, C. A. & Dannenberg, A. J. Molecular pathways: adipose inflammation as a mediator of obesity-associated cancer. *Clinical cancer research : an official journal of the American Association for Cancer Research* **19**, 6074-6083, doi:10.1158/1078-0432.CCR-12-2603 (2013).

253 Pierobon, M. & Frankenfeld, C. L. Obesity as a risk factor for triple-negative breast cancers: a systematic review and meta-analysis. *Breast cancer research and treatment* **137**, 307-314, doi:10.1007/s10549-012-2339-3 (2013).

254 Petekkaya, I. *et al.* Association of breast cancer subtypes and body mass index. *Tumori* **99**, 129-133, doi:10.1700/1283.14180 (2013).

255 Xie, J. W. & Haslam, S. Z. Extracellular matrix, Rac1 signaling, and estrogen-induced proliferation in MCF-7 breast cancer cells. *Breast cancer research and treatment* **110**, 257-268, doi:10.1007/s10549-007-9719-0 (2008).

256 Barcus, C. E., Keely, P. J., Eliceiri, K. W. & Schuler, L. A. Stiff collagen matrices increase tumorigenic prolactin signaling in breast cancer cells. *The Journal of biological chemistry* **288**, 12722-12732, doi:10.1074/jbc.M112.447631 (2013).

257 Lu, P. F., Weaver, V. M. & Werb, Z. The extracellular matrix: A dynamic niche in cancer progression. *Journal of Cell Biology* **196**, 395-406, doi:Doi 10.1083/Jcb.201102147 (2012).

258 Bissell, M. J., Radisky, D. C., Rizki, A., Weaver, V. M. & Petersen, O. W. The organizing principle: microenvironmental influences in the normal and malignant breast. *Differentiation* **70**, 537-546, doi:Doi 10.1046/J.1432-0436.2002.700907.X (2002).

259 Cheng, G., Tse, J., Jain, R. K. & Munn, L. L. Micro-Environmental Mechanical Stress Controls Tumor Spheroid Size and Morphology by Suppressing Proliferation and Inducing Apoptosis in Cancer Cells. *Plos One* **4**, doi:ARTN e4632 DOI 10.1371/journal.pone.0004632 (2009).

260 Cox, T. R. *et al.* LOX-Mediated Collagen Crosslinking Is Responsible for Fibrosis-Enhanced Metastasis. *Cancer Res* **73**, 1721-1732, doi:Doi 10.1158/0008-5472.Can-12-2233 (2013).

261 O'Brien, C. S., Farnie, G., Howell, S. J. & Clarke, R. B. Breast cancer stem cells and their role in resistance to endocrine therapy. *Hormones & cancer* **2**, 91-103, doi:10.1007/s12672-011-0066-6 (2011).

262 Visvader, J. E. & Lindeman, G. J. Cancer stem cells in solid tumours: accumulating evidence and unresolved questions. *Nature reviews. Cancer* **8**, 755-768, doi:10.1038/nrc2499 (2008).

263 Wolin, K. Y., Carson, K. & Colditz, G. A. Obesity and Cancer. *Oncologist* **15**, 556-565, doi:Doi 10.1634/Theoncologist.2009-0285 (2010).

264 Longo, V. D. & Fontana, L. Calorie restriction and cancer prevention: metabolic and molecular mechanisms. *Trends Pharmacol Sci* **31**, 89-98, doi:10.1016/j.tips.2009.11.004 (2010).

265 Henegar, C. *et al.* Adipose tissue transcriptomic signature highlights the pathological relevance of extracellular matrix associated with inflammation in human obesity. *International journal of obesity* **32**, S57-S57 (2008).

266 Higami, Y. *et al.* Energy restriction lowers the expression of genes linked to inflammation, the cytoskeleton, the extracellular matrix, and angiogenesis in mouse adipose tissue. *J Nutr* **136**, 343-352 (2006).

267 Peres, J. Understanding Breast Density and Breast Cancer Risk. *Journal of the National Cancer Institute* **104**, 1345-1346, doi:Doi 10.1093/Jnci/Djs403 (2012).

268 Bertolini, F., Lohsiriwat, V., Petit, J. Y. & Kolonin, M. G. Adipose tissue cells, lipotransfer and cancer: A challenge for scientists, oncologists and surgeons. *Bba-Rev Cancer* **1826**, 209-214, doi:Doi 10.1016/J.Bbcan.2012.04.004 (2012).

269 Halberg, N. *et al.* Hypoxia-inducible factor 1alpha induces fibrosis and insulin resistance in white adipose tissue. *Molecular and cellular biology* **29**, 4467-4483, doi:10.1128/MCB.00192-09 (2009).

270 Park, J. & Scherer, P. E. Endotrophin in the tumor stroma: a new therapeutic target for breast cancer? *Expert review of anticancer therapy* **13**, 111-113, doi:10.1586/era.12.164 (2013).

271 Shpitz, B. *et al.* Angiogenic switch in earliest stages of human colonic tumorigenesis. *Anticancer Res* **23**, 5153-5157 (2003).

272 Ghajar, C. M., Blevins, K. S., Hughes, C. C., George, S. C. & Putnam, A. J. Mesenchymal stem cells enhance angiogenesis in mechanically viable prevascularized tissues via early matrix metalloproteinase upregulation. *Tissue Engineering* **12**, 2875-2888, doi:10.1089/ten.2006.12.2875 (2006).

273 Koike, N. *et al.* Creation of long-lasting blood vessels. *Nature* **428**, 138-139, doi:Doi 10.1038/428138a (2004).

274 Merfeld-Clauss, S., Gollahalli, N., March, K. L. & Traktuev, D. O. Adipose Tissue Progenitor Cells Directly Interact with Endothelial Cells to Induce Vascular Network Formation. *Tissue Engineering Part A* **16**, 2953-2966, doi:DOI 10.1089/ten.tea.2009.0635 (2010).

275 Matsuda, K. *et al.* Adipose-Derived Stem Cells Promote Angiogenesis and Tissue Formation for In Vivo Tissue Engineering. *Tissue Engineering Part A* **19**, 1327-1335, doi:DOI 10.1089/ten.tea.2012.0391 (2013).

276 Fumimoto, Y. *et al.* Creation of a Rich Subcutaneous Vascular Network with Implanted Adipose Tissue-Derived Stromal Cells and Adipose Tissue Enhances Subcutaneous Grafting of Islets in Diabetic Mice. *Tissue Eng Part C-Me* **15**, 437-444, doi:DOI 10.1089/ten.tec.2008.0555 (2009).

277 Desai, V. D., Hsia, H. C. & Schwarzbauer, J. E. Reversible Modulation of Myofibroblast Differentiation in Adipose-Derived Mesenchymal Stem Cells. *Plos One* **9**, doi:ARTN e86865 DOI 10.1371/journal.pone.0086865 (2014).

278 Mammoto, A. & Ingber, D. E. Cytoskeletal control of growth and cell fate switching. *Curr Opin Cell Biol* **21**, 864-870, doi:DOI 10.1016/j.ceb.2009.08.001 (2009).

279 Gardel, M. L. *et al.* Traction stress in focal adhesions correlates biphasically with actin retrograde flow speed. *J Cell Biol* **183**, 999-1005, doi:DOI 10.1083/jcb.200810060 (2008).

280 Cox, T. R. & Erler, J. T. Remodeling and homeostasis of the extracellular matrix: implications for fibrotic diseases and cancer. *Dis Model Mech* **4**, 165-178, doi:10.1242/dmm.004077 (2011).

281 Conklin, M. W. *et al.* Aligned Collagen Is a Prognostic Signature for Survival in Human Breast Carcinoma. *American Journal of Pathology* **178**, 1221-1232, doi:DOI 10.1016/j.ajpath.2010.11.076 (2011).

282 Ganganna, K., Shetty, P. & Shroff, S. E. Collagen in histologic stages of oral submucous fibrosis: A polarizing microscopic study. *J Oral Maxillofac Pathol* **16**, 162-166, doi:10.4103/0973-029X.98446
JOMFP-16-162 [pii] (2012).

283 Burke, R. M., Madden, K. S., Perry, S. W., Zettel, M. L. & Brown, E. B., 3rd. Tumor-associated macrophages and stromal TNF-alpha regulate collagen structure in a breast tumor model as visualized by second harmonic generation. *J Biomed Opt* **18**, 86003, doi:10.1117/1.JBO.18.8.0860031724146 [pii] (2013).

284 Wan, A. M. D. *et al.* Fibronectin conformation regulates the proangiogenic capability of tumor-associated adipogenic stromal cells. *Bba-Gen Subjects* **1830**, 4314-4320, doi:DOI 10.1016/j.bbagen.2013.03.033 (2013).

285 Xu, B., Chow, M. J. & Zhang, Y. Experimental and modeling study of collagen scaffolds with the effects of crosslinking and fiber alignment. *Int J Biomater* **2011**, 172389, doi:10.1155/2011/172389 (2011).

286 Gauvin, R. *et al.* Microfabrication of complex porous tissue engineering scaffolds using 3D projection stereolithography. *Biomaterials* **33**, 3824-3834, doi:DOI 10.1016/j.biomaterials.2012.01.048 (2012).

287 Cross, V. L. *et al.* Dense type I collagen matrices that support cellular remodeling and microfabrication for studies of tumor angiogenesis and vasculogenesis in vitro. *Biomaterials* **31**, 8596-8607, doi:DOI 10.1016/j.biomaterials.2010.07.072 (2010).

288 Franke, K., Sapudom, J., Kalbitzer, L., Anderegg, U. & Pompe, T. Topologically defined composites of collagen types I and V as in vitro cell culture scaffolds. *Acta biomaterialia* **10**, 2693-2702, doi:Doi 10.1016/J.Actbio.2014.02.036 (2014).

289 Verbridge, S. S. *et al.* Oxygen-Controlled Three-Dimensional Cultures to Analyze Tumor Angiogenesis. *Tissue Eng Pt A* **16**, 2133-2141, doi:DOI 10.1089/ten.tea.2009.0670 (2010).

290 Raub, C. B., Tromberg, B. J., George, S. C. in *Second-harmonic generation imaging* (ed F.S. Pavone, Campagnola, P. J.) 1-26 (CRC Press, 2013).

291 Humles, D. J. S. in *Collagen structure and mechanics* (ed P. Fratzl) 15-48(Springer, 2008).

292 Zhu, Y. K. *et al.* Contraction of fibroblast-containing collagen gels: Initial collagen concentration regulates the degree of contraction and cell survival. *In Vitro Cell Dev-An* **37**, 10-16 (2001).

293 Zhong, C. L. *et al.* Rho-mediated contractility exposes a cryptic site in fibronectin and induces fibronectin matrix assembly. *Journal of Cell Biology* **141**, 539-551, doi:DOI 10.1083/jcb.141.2.539 (1998).

294 Fischbach, C. *et al.* Engineering tumors with 3D scaffolds. *Nature Methods* **4**, 855-860, doi:Doi 10.1038/Nmeth1085 (2007).

295 Tomasek, J. J., Martin, M. D., Vaughan, M. B., Cowan, R. L. & Kropp, B. P. Myofibroblast contraction in granulation tissue is dependent on Rho kinase. *Mol Biol Cell* **11**, 88a-88a (2000).

296 Hakanson, M., Cukierman, E. & Charnley, M. Miniaturized pre-clinical cancer models as research and diagnostic tools. *Advanced Drug Delivery Reviews* **69**, 52-66, doi:Doi 10.1016/J.Addr.2013.11.010 (2014).

297 Khetani, S. R. & Bhatia, S. N. Microscale culture of human liver cells for drug development. *Nat Biotechnol* **26**, 120-126, doi:Doi 10.1038/Nbt1361 (2008).

298 Kim, J. W., Gao, P., Liu, Y. C., Semenza, G. L. & Dang, C. V. Hypoxia-inducible factor I and dysregulated c-myc cooperatively induce vascular endothelial growth factor and metabolic switches hexokinase 2 and pyruvate dehydrogenase kinase 1. *Molecular and Cellular Biology* **27**, 7381-7393, doi:Doi 10.1128/Mcb.00440-07 (2007).

299 Sung, K. E. *et al.* Control of 3-dimensional collagen matrix polymerization for reproducible human mammary fibroblast cell culture in microfluidic devices. *Biomaterials* **30**, 4833-4841, doi:Doi 10.1016/J.Biomaterials.2009.05.043 (2009).

300 Ghazanfarian, J. & Abbassi, A. Heat transfer and fluid flow in microchannels and nanochannels at high Knudsen number using thermal lattice-Boltzmann method. *Physical review. E, Statistical, nonlinear, and soft matter physics* **82**, 026307 (2010).

301 Bashur, C. A., Dahlgren, L. A. & Goldstein, A. S. Effect of fiber diameter and orientation on fibroblast morphology and proliferation on electrospun poly(D,L-lactic-co-glycolic acid) meshes. *Biomaterials* **27**, 5681-5688, doi:Doi 10.1016/J.Biomaterials.2006.07.005 (2006).

302 Parry, D. A. D. The Molecular and Fibrillar Structure of Collagen and Its Relationship to the Mechanical-Properties of Connective-Tissue. *Biophys Chem* **29**, 195-209, doi:Doi 10.1016/0301-4622(88)87039-X (1988).

303 Roeder, B. A., Kokini, K., Sturgis, J. E., Robinson, J. P. & Voytik-Harbin, S. L. Tensile mechanical properties of three-dimensional type I collagen extracellular matrices with varied microstructure. *J Biomech Eng-T Asme* **124**, 214-222, doi:Doi 10.1115/1.1449904 (2002).

304 Bukoreshtliev, N. V., Haase, K. & Pelling, A. E. Mechanical cues in cellular signalling and communication. *Cell Tissue Res* **352**, 77-94, doi:Doi 10.1007/S00441-012-1531-4 (2013).

305 Ventre, M., Causa, F. & Netti, P. A. Determinants of cell-material crosstalk at the interface: towards engineering of cell instructive materials. *J R Soc Interface* **9**, 2017-2032, doi:Doi 10.1098/Rsif.2012.0308 (2012).

306 Hinz, B. Formation and function of the myofibroblast during tissue repair. *J Invest Dermatol* **127**, 526-537, doi:5700613 [pii] 10.1038/sj.jid.5700613 (2007).

307 Baneyx, G., Baugh, L. & Vogel, V. Fibronectin extension and unfolding within cell matrix fibrils controlled by cytoskeletal tension. *P Natl Acad Sci USA* **99**, 5139-5143, doi:DOI 10.1073/pnas.072650799 (2002).

308 Chandler, E. M. *et al.* Stiffness of Photocrosslinked RGD-Alginate Gels Regulates Adipose Progenitor Cell Behavior. *Biotechnology and Bioengineering* **108**, 1683-1692, doi:Doi 10.1002/Bit.23079 (2011).

309 Muroi, Y., Kakudo, K. & Nakata, K. Effects of compressive loading on human synovium-derived cells. *J Dent Res* **86**, 786-791 (2007).

310 Quinn, T. P., Schlueter, M., Soifer, S. J. & Gutierrez, J. A. Mechanotransduction in the lung - Cyclic mechanical stretch induces VEGF and FGF-2 expression in pulmonary vascular smooth muscle cells. *Am J Physiol-Lung C* **282**, L897-L903, doi:Doi 10.1152/Ajplung.00044.2001 (2002).

311 Schraufstatter, I. U., Chung, J. & Burger, M. IL-8 activates endothelial cell CXCR1 and CXCR2 through Rho and Rac signaling pathways. *Am J Physiol-Lung C* **280**, L1094-L1103 (2001).

312 Martin, D., Galisteo, R. & Gutkind, J. S. CXCL8/IL8 Stimulates Vascular Endothelial Growth Factor (VEGF) Expression and the Autocrine Activation of VEGFR2 in Endothelial Cells by Activating NF kappa B through the CBM (Carma3/Bcl10/Malt1) Complex. *Journal of Biological Chemistry* **284**, 6038-6042, doi:DOI 10.1074/jbc.C800207200 (2009).

313 Friedl, P. & Wolf, K. Plasticity of cell migration: a multiscale tuning model. *J Cell Biol* **188**, 11-19, doi:DOI 10.1083/jcb.200909003 (2010).

314 Ulrich, T. A., Pardo, E. M. D. & Kumar, S. The Mechanical Rigidity of the Extracellular Matrix Regulates the Structure, Motility, and Proliferation of Glioma Cells. *Cancer Research* **69**, 4167-4174, doi:Doi 10.1158/0008-5472.Can-08-4859 (2009).

315 Jokinen, J. *et al.* Integrin-mediated cell adhesion to type I collagen fibrils. *Journal of Biological Chemistry* **279**, 31956-31963, doi:Doi 10.1074/Jbc.M401409200 (2004).

316 Christine Homcha, H. P. E. Fibroblast expression of α-smooth muscle actin, α2β1 integrin and αvβ3 integrin: Influence of surface rigidity. *Exp Mol Pathol* **91**, 394 - 399 (2011).

317 Katsumi, A., Matsushita, T., Naoe, T. & Schwartz, M. A. alpha v beta 3 integrin activation and matrix binding mediate cellular responses to mechanical stretch. *Blood* **106**, 1027A-1027A (2005).

318 Davis, G. E. & Senger, D. R. Endothelial extracellular matrix - Biosynthesis, remodeling, and functions during vascular morphogenesis and neovessel stabilization. *Circ Res* **97**, 1093-1107, doi:Doi 10.1161/01.Res.0000191547.64391.E3 (2005).

319 Griffith, L. G. & Swartz, M. A. Capturing complex 3D tissue physiology in vitro. *Nat Rev Mol Cell Bio* **7**, 211-224, doi:Doi 10.1038/Nrm1858 (2006).

320 Feng, X., Tonnesen, M. G., Mousa, S. A. & Clark, R. A. Fibrin and collagen differentially but synergistically regulate sprout angiogenesis of human dermal microvascular endothelial cells in 3-dimensional matrix. *International journal of cell biology* **2013**, 231279, doi:10.1155/2013/231279 (2013).

321 Cummings, C. L., Gawlitta, D., Nerem, R. M. & Stegemann, J. P. Properties of engineered vascular constructs made from collagen, fibrin, and collagen-fibrin mixtures. *Biomaterials* **25**, 3699-3706, doi:Doi 10.1016/J.Biomaterials.2003.10.073 (2004).

322 Scherberich, A., Di Maggio, N. D. & McNagny, K. M. A familiar stranger: CD34 expression and putative functions in SVF cells of adipose tissue. *World journal of stem cells* **5**, 1-8, doi:10.4252/wjsc.v5.i1.1 (2013).

323 Jung, Y. H. *et al.* Recruitment of mesenchymal stem cells into prostate tumours promotes metastasis. *Nature communications* **4**, doi:Artn 1795Doi 10.1038/Ncomms2766 (2013).

324 Bhardwaj, P. *et al.* Caloric restriction reverses obesity-induced mammary gland inflammation in mice. *Cancer prevention research* **6**, 282-289, doi:10.1158/1940-6207.CAPR-12-0467 (2013).

325 Yang, X. R. *et al.* Associations of breast cancer risk factors with tumor subtypes: a pooled analysis from the Breast Cancer Association Consortium studies. *Journal of the National Cancer Institute* **103**, 250-263, doi:10.1093/jnci/djq526 (2011).

326 Iruela-Arispe, M. L. & Davis, G. E. Cellular and Molecular Mechanisms of Vascular Lumen Formation. *Dev Cell* **16**, 222-231, doi:Doi 10.1016/J.Devcel.2009.01.013 (2009).

327 Park, S. Y. *et al.* Heterogeneity for Stem Cell-Related Markers According to Tumor Subtype and Histologic Stage in Breast Cancer. *Clinical Cancer Research* **16**, 876-887, doi:Doi 10.1158/1078-0432.Ccr-09-1532 (2010).

328 Herrero, L., Shapiro, H., Nayer, A., Lee, J. & Shoelson, S. E. Inflammation and adipose tissue macrophages in lipodystrophic mice. *Proceedings of the National Academy of Sciences of the United States of America* **107**, 240-245, doi:Doi 10.1073/Pnas.0905310107 (2010).

329 Roxburgh, C. S. D. & McMillan, D. C. Cancer and systemic inflammation: treat the tumour and treat the host. *Brit J Cancer* **110**, 1409-1412, doi:Doi 10.1038/Bjc.2014.90 (2014).